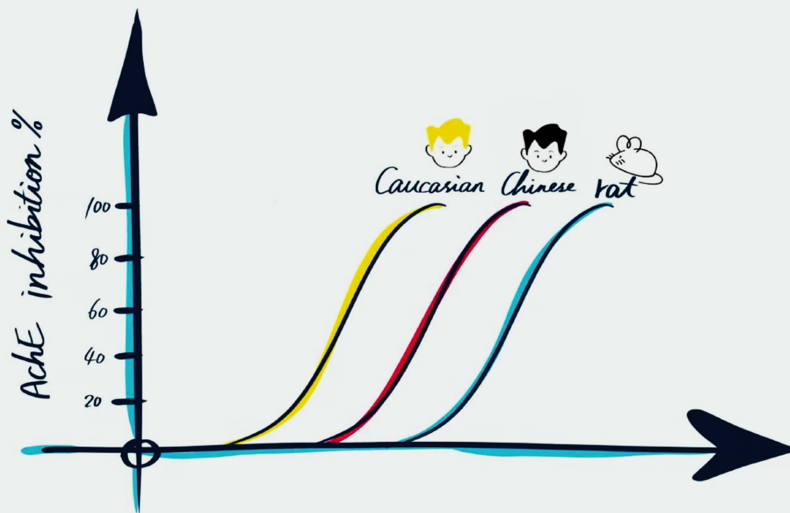


Consequences of kinetic variability for inter-species, inter-ethnic, and inter-individual differences in sensitivity towards organophosphate pesticides quantified by new approach methodologies



Shensheng Zhao

Propositions

1. Differences in toxicokinetics of organophosphate (OP) pesticides cause inter-species, inter-ethnic and inter-individual dissimilarity in their toxicity.
(this thesis)
2. The toxicity of the parent thionate OP pesticide cannot be systematically ignored.
(this thesis)
3. The impact of industrialization on gut microbiota is not negligible.
4. Organ-on-chip models provide important in vitro tools for drug development and characterization of disease mechanisms.
5. Starting is harder than finishing.
6. The Covid-19 pandemic does improve the efficiency of life.

Propositions belonging to the thesis, entitled

Consequences of kinetic variability for inter-species, inter-ethnic and inter-individual differences in sensitivity towards organophosphate pesticides quantified by new approach methodologies

Shensheng Zhao

Wageningen, 7 October 2021

**Consequences of kinetic variability for
inter-species, inter-ethnic and inter-individual
differences in sensitivity towards organophosphate
pesticides quantified by
new approach methodologies**

Shensheng Zhao

Thesis committee

Promotor

Prof. Dr I.M.C.M. Rietjens

Professor of Toxicology

Wageningen University & Research

Co-promotor

Dr M. Strikwold

Associate professor of Safety in the Food Chain

Van Hall Larenstein University of Applied Sciences

Other members

Prof. Dr P.J. (Paul) van den Brink, Wageningen University & Research

Prof. Dr Martin van den Berg, Utrecht University

Prof. Dr B.J. (Bas) Blaauboer, Utrecht University

Dr A. Punt, Wageningen Food Safety Research, Wageningen University & Research

This research was conducted under the auspices of the Graduate School VLAG (Advanced studies in Food Technology, Agrobiotechnology, Nutrition and Health Sciences)

**Consequences of kinetic variability for
inter-species, inter-ethnic and inter-individual
differences in sensitivity towards organophosphate
pesticides quantified by
new approach methodologies**

Shensheng Zhao

Thesis

submitted in fulfilment of the requirements for the degree of doctor

at Wageningen University

by the authority of the Rector Magnificus,

Prof. Dr A.P.J. Mol,

in the presence of the

Thesis Committee appointed by the Academic Board

to be defended in public

on Thursday 7 October 2021

at 11:00 a.m. in the Aula.

Shensheng Zhao

Consequences of kinetic variability for inter-species, inter-ethnic and inter-individual differences in sensitivity towards organophosphate pesticides quantified by new approach methodologies

264 pages

PhD thesis, Wageningen University, Wageningen, the Netherlands (2021)

With references, with summary in English

ISBN: 978-94-6395-941-4

DOI: <https://doi.org/10.18174/551737>

Table of content

Chapter 1	7
General introduction	
Chapter 2	43
Physiologically based kinetic modeling-facilitated reverse dosimetry to predict in vivo red blood cell acetylcholinesterase inhibition following exposure to chlorpyrifos in the Caucasian and Chinese population	
Chapter 3	83
Prediction of dose-dependent in vivo acetylcholinesterase inhibition by profenofos in rats and humans using physiologically based kinetic (PBK) modeling-facilitated reverse dosimetry	
Chapter 4	117
Physiologically based kinetic modelling based prediction of in vivo rat and human acetylcholinesterase (AChE) inhibition upon exposure to diazinon	
Chapter 5	165
Inter-individual variation in chlorpyrifos toxicokinetics characterized by physiologically based kinetic (PBK) and Monte Carlo simulation comparing human liver microsome and Supersome TM cytochromes P450 (CYP)-specific kinetic data as model input	
Chapter 6	219
General discussion and future perspectives	
Chapter 7	251
Summary	
Appendix	
Acknowledgements	256
About the author	261
List of publication	262
Overview of completed training activities	263

Chapter 1

General introduction

1.1 Background information on organophosphate (OP) pesticides

Organophosphate (OP) pesticides make up one of the main pesticide groups in addition to organochlorine, carbamate and pyrethroid pesticides (Saxena et al. 2020). OP pesticides have been widely used as insecticides in the last few decades as alternative to persistent organochlorine pesticides because of the rapid degradation of OP pesticides under natural conditions (Karasali and Maragou 2016). The general structure of OP pesticides includes either a P=S moiety or a P=O moiety, with the P=S moiety being bioactivated to a P=O moiety by cytochromes P450 (CYPs) (King and Aaron 2015). In the period from 2010 to 2015, 29,554 tons of OP pesticides were used in 17 Asian countries, 10,013 tons were used in 24 European countries, 342 tons were used in Caribbean and Central American countries, 13,404 tons were used in 6 South American countries and 1,145 tons were used in 13 African countries (Hertz-Picciotto et al. 2018). As a result of the worldwide use of OP pesticides, OP residues are often found in food. The latest European Union (EU) annual report on pesticide residues in food (EFSA 2020) reported that, for example in 2018, food samples from the European market were found to contain residue levels of different OP pesticides that exceeded their corresponding Maximum Residue Levels (MRLs), with 416 out of the 77,040 samples (0.54%) showing residue levels above the MRL for chlorpyrifos (CPF), 86 out of the 58253 samples (0.15%) for dimethoate, 78 out of the 55765 samples (0.14%) for omethoate, 60 out of the 72,875 samples (0.08%) for acephate, 43 out of the 76,742 samples (0.06%) for profenofos (PFF), 28 out of the 9,395 samples (0.30%) for ethephon and 12 out of the 9,573 samples (0.13%) for glyphosate. It should be noticed however, that exceedance of the MRL does not necessarily imply the exceedance of acute reference dose (ARfD) or acceptable daily intake (ADI) levels. Residues of OP pesticides in food have also been reported to occur in other countries including for example China, Thailand, Nigeria, Kenya, United States (Isegbe et al. 2016; Omwenga et al. 2020; Qin et al. 2016; Sapbamrer and Hongsoong 2014; USFDA 2020). Although dietary exposure is the major source for exposure of the general population, OP pesticides can also enter the human body by accidental (i.e. exposure of farmers or their bystanders) or intentional high-dose ingestion (i.e. suicide attempt), resulting in acute poisoning. This has been considered as an important cause of morbidity and mortality, especially in developing countries, due to easy access, misuse and the fact that in these countries, safety in use of these pesticides may not be well-regulated. For instance, Wang et al. (2019) reported that in the period from 2007 to 2016, a total of 30,789 pesticide poisonings (included self-poisoning cases) were reported in Jiangsu Province, China. Among all these pesticide poisoning cases, OP pesticides

appeared to be the type of pesticides responsible for the most of the poisoning cases (60.2% of all cases) (Wang et al. 2019). In addition, studies from Sri Lanka regarding self-poisoning revealed an acute pesticide poisoning incidence rate of approximately 180 per 100,000 individuals in the population (Thundiyl et al. 2008). Furthermore, an outbreak of food poisoning in India due to a cooking oil contaminated with the OP pesticide monocrotophos was reported, in which 23 children died and more than 48 individuals required medical treatment (Idrovo 2014).

To protect human health, numerous risk assessments for different OP pesticides have been performed by different organizations such as the European Food Safety Authority (EFSA), the United States Environmental Protection Agency (USEPA) and the Joint FAO/WHO Meeting on Pesticide Residues (JMPR). In these risk assessments, points of departure (PODs) such as a no observed adverse effect level (NOAEL) or a lower confidence limit of the benchmark dose (BMDL) are often obtained from dose-response data generated for the critical effect. The critical effect generally selected for the risk assessment of OP pesticides is the irreversible inhibition of acetylcholinesterase (AChE) in red blood cells (RBCs) observed in experimental animals upon both acute and repeated oral exposure (EFSA 2014; USEPA 2011; USEPA 2014; USEPA 2016b; USEPA 2016c). The POD obtained is subsequently used as the starting dose for the calculation of a health-based guidance value (HBGV) such as an ARfD or an ADI usually by incorporating a default 100-fold uncertainty factor (UF) to address inter- and intra-species differences. This default UF has been established as depicted in Figure 1 (IPCS 2005), indicating that the total UF of 100 consists of a UF of 10 for inter-species and a UF of 10 for inter-individual differences. These two UFs of 10 can be further subdivided into the UFs for kinetic differences and dynamic differences between species (AK_{UF} of 4 and AD_{UF} of 2.5, respectively) and within the human population (HK_{UF} of 3.16 and HD_{UF} of 3.16). However, one could question to what extent the POD derived based on an *in vivo* animal study using the default UF of 100 provides sufficient protection to the human population against OP pesticides. Applying the default UF values to establish a HBGV may for example turn out to be over- or under-protective when the potential metabolic, physiological and dynamic variation between different species, ethnic groups and individuals would be less/more than the default factor of 100. Given that the POD in risk assessment of OP pesticides is still mainly derived from animal data, and the fact that animal experiments are more and more considered unethical and not representative of humans, and that the HBGVs are obtained by using the default UF of 100, it is of importance to develop a new approach methodology (NAM) that can define HBGVs for

human safety following OP pesticides exposure. Such a NAM could be so-called physiologically based kinetic (PBK) model-facilitated reverse dosimetry, which is based on *in silico* and *in vitro* data. This method could allow definition of a POD based on human-specific metabolism, physiology and dynamics. The POD thus obtained, together with a chemical-specific adjustment factors (CSAF) for the test OP pesticide, would allow establishment of a chemical specific HBGV for the human situation without the need for studies in experimental animals.

The aim of the present PhD thesis was to investigate whether NAM and especially PBK model-based reverse dosimetry using *in vitro* and *in silico* data, in combination with Monte Carlo simulations or the toxic equivalency factor (TEF) methodology, can be used to derive PODs and CSAF values for characterizing inter-ethnic, inter-species and inter-individual differences in toxicokinetics and RBC AChE inhibition by OP pesticides upon single acute oral exposure. More detailed information on the toxicity endpoint, OP pesticide model compounds used in the present thesis, and the alternative testing strategy applied is provided in the following sections.

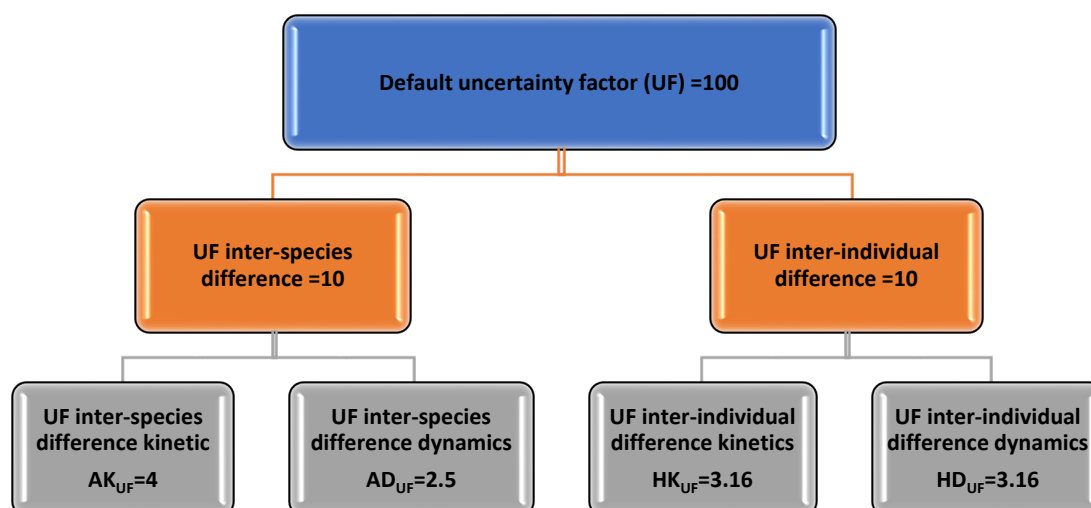


Fig 1. Subdivision of the default UF of 100 used in setting HBGVs in risk assessment, such as an ARfD or ADI (IPCS 2005).

1.2 Model OP pesticides studied in the present thesis: chemical characteristics, and occurrence in food

In the present thesis, the model OP pesticides were selected based on the following criteria: 1) The OP pesticide of interest is still widely used in some parts of the world; 2) A residue of the OP pesticide has been frequently found in food, in other words, the general population is exposed to the OP pesticide of interest; 3) In vivo data sets for the OP pesticide of interest are available for validation of the PBK model-based predictions and evaluation of the quantitative in vitro to in vivo extrapolations (QIVIVE) defining dose-response curves and a POD. Based on these criteria, CPF, diazinon (DZN) and PFF (Figure 2) were selected as OP model compounds in the present thesis. The chemical structure of the selected OP pesticides is presented in Figure 2, and the basic physico-chemical information of the model OP pesticides and their bioactive metabolites has been listed in Table 1.

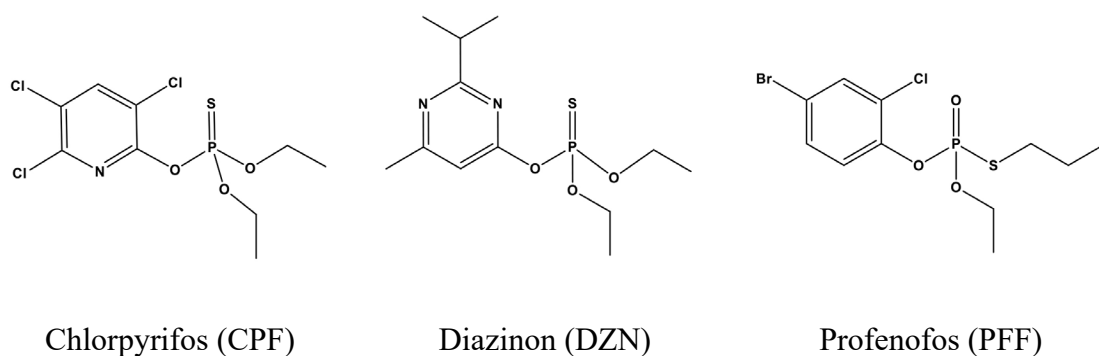


Fig 2. Chemical structures of the three OP pesticides studied in the present thesis

Table 1. Physico-chemical information on the three OP pesticides and their active metabolites studied in the present thesis

Substance	LogP value	pKa value	Reference
Chlorpyrifos (CPF)	4.78	No ionization	(ChemAxon)
Chlorpyrifos-oxon (CPO)	3.89	No ionization	(ChemAxon)
Diazinon (DZN)	4.19	Strongest base 4.19	(ChemAxon)
	3.81	2.6	(National Center for Biotechnology Information 2021a)
Diazoxon (DZO)	3.38	Strongest base 3.81	(ChemAxon)
	2.07	No detailed information is available	(National Center for Biotechnology Information 2021b)
Profenofos (PFF)	4.68	No ionization	(ChemAxon)

1.2.1 CPF

CPF (O,O-diethyl O-3,5,6-trichloropyridin-2-yl phosphorothioate) (Figure 2) is one of the OP pesticides with a P=S double bond, which has been used since 1965 (USEPA 2020). CPF has been registered in more than 100 countries (DOW 2017). It can be manufactured in different forms such as granular, liquid and powder forms (USEPA 2016a). Registered use of CPF includes agricultural and non-agricultural applications. In case of agricultural applications, CPF is mainly used as an insecticide to protect crops such as corn, soybeans, fruit and nut trees. CPF might also be used for non-agricultural applications, such as on golf courses, turf grass and in green houses to control insect pests. On 10 January 2020, the European Commission revoked the approval of CPF (European Commission 2020), due to uncertainties over its potential genotoxicity and developmental neurotoxicity (EFSA 2019c), and consequently the EU Member States had to revoke all authorisations of plant protection products that include CPF by 16 February 2020. In 2020, based on the evaluation from the Pest Management Regulatory Agency (PMRA), Health Canada is phasing out the outdoor uses of CPF except for a limited list of uses that require mitigation measures (PMRA 2020). In other countries, CPF is still allowed for use under some restrictions (e.g. it is not allowed for use on vegetables in China since 2016 and it is banned for residential use in the United States (US) since 2000 and in South Africa since 2010) (News 2010; Sang et al. 2020; USEPA 2020). This implies that in parts of the world there is still a chance that CPF may end up in food. Besides, it should be considered that banning the use of CPF in one country does not necessarily mean that this

country will be CPF free, as the general population can be exposed to CPF by consuming imported food items from a country where use of CPF is still allowed (EFSA 2020; Sang et al. 2020).

According to the 2018 European Union (EU) annual report on pesticide residues (EFSA 2020), CPF is among the pesticides for which the estimated intake resulting from residues in food most frequently exceeded the ARfD of 0.005 mg/kg bw (Table 2) (126 food samples out of 22,752 food samples = 0.55%). The exceedance of ARfD for CPF was mostly related to foods like grapefruit, apples, pears, peaches, peppers and quinces (EFSA 2020). Bertrand (2019) reported that CPF has been detected in tomato samples sold at the local market of Tanzania in 2016, with an average concentration of 7.528 mg/kg. Also, in a total diet study in Sub-Saharan Africa, of the 3,696 food stuffs, 46% contained pesticide residues and CPF contributed to 21% of all samples, with the highest concentration of 18.084 mg/kg being detected in smoked fish samples (Ingenbleek et al. 2019). A study on market foods in Shaanxi Province, China, reported that CPF was detected in 5 vegetable sample out of 285 food samples analysed, with a maximum concentration of 0.129 mg/kg (Wang et al. 2013). Besides, a study from Sapbamrer and Hongsibsong (2014) showed that CPF appeared to be the most common detected pesticide in the analysed samples from different sources in Thailand (being present in 50%, 33.9% and 33.3% of all samples from farms, markets, and supermarkets, respectively), with the highest CPF level found in lemon balm (farms, 2.423 mg/kg), garlic (market, 7.785 mg/kg), and parsley (supermarket, 0.027 mg/kg). Obviously, there are more studies that report on pesticide residues including CPF that have not been mentioned here (Hongsibsong et al. 2020; Qin et al. 2016; Skretteberg et al. 2015; Wanwimolruk et al. 2015), but the examples presented illustrate that CPF, in spite of a ban in several countries, still can be a pesticide residue detected in food. Apart from CPF residues in food, CPF residues have also been found in umbilical cord blood (Huen et al. 2012), and breast milk (Brahmand et al. 2019), which indicates maternal and fetal/infant exposure.

1.2.2 DZN

DZN (O,O-diethyl O-2-isopropyl-6-methylpyrimidin-4-yl phosphonothioate) (Figure 2) is another OP pesticide with a P=S double bond that is commonly used as an insecticide (control of insects on fruit, vegetables, nut and field crops), acaricide (against ticks and mites) and

nematicide (against nematodes or roundworms) (CAREX Canada 2020). DZN is also used as a drug in veterinary medicine for the treatment of external parasites, or applied on cattle as part of an insecticidal ear tag (Burgess et al. 2008; JMPR 2016). DZN is available in different formulations including dusts, granules, liquids, wettable powders, etc. (USEPA 2006a). The use of DZN was first registered in the US in 1956, but due to its high toxicity to avian and aquatic life, it has been classified as a restricted use pesticide (USEPA 2006a). Prior to cancellation of its residential uses in 2004, DZN was also used for indoor fly control or outdoors on lawns and in gardens. In 2006, the EU revoked approval for DZN because of concerns about occupational exposure and related risks to operators, and risks to insectivorous birds, mammals and its high toxicity to aquatic organisms (PAN Europe 2006; Watts 2013). Similarly, the PMRA in Canada has prohibited the domestic use of DZN since 2016 (CAREX Canada 2020). Although different restrictions have been applied on DZN by different countries, DZN is still used widely around the world. It was reported that DZN has been manufactured by 46 producers in 11 countries including China, India, US, Singapore, etc. (Humans 2017). There are 9 registered products that contain DZN as the active substance in Canada and around 60 DZN-related products are registered in China (CAREX Canada 2020; ICAMA 2021). This use of DZN can result in residues in food. Several studies reported detection of DZN residues in various foods, including fruits, vegetables, grains, meat, milk, and oils, in different countries (EFSA 2019a; Quintero et al. 2008; Srivastava et al. 2011; Zhang et al. 2008). EFSA (2020) reported that, in 2018, of 76,036 food samples on the European market, DZN was detected in 47 samples (0.06%). Saphamrer and Hongsibsong (2014) reported that, of 106 vegetable samples from the local market of Thailand, DZN was detected in 11 samples (18.6%). DZN residues were also found in Korea with the highest concentration of DZN in kale amounting to 3.8 mg/kg (Cho et al. 2009). As a result, it seems likely that the general population might be exposed to DZN via consumption of DZN-contaminated foods. Additionally, exposure of the fetus or infant may occur following maternal exposure, since DZN residues have been found in umbilical cord blood (Huen et al. 2012) and breast milk (Pedersen et al. 2020).

1.2.3 PFF

Another commonly used OP pesticide is PFF (O-4-bromo-2-chlorophenyl O-ethyl S-propyl phosphorothioate) (Figure 2), which was also introduced to replace chlorinated pesticides

(Chapalamadugu and Chaudhry 1992; Kushwaha et al. 2016). Different from CPF and DZN, PFF contains a P=O instead of a P=S double bond, so it does not require metabolic oxidation (bioactivation) of the P=S moiety to a P=O moiety to become more active (Fukuto 1990) (see detail in section “1.3 ADME (absorption, distribution, metabolism and excretion) of the selected OP pesticide model compounds”). PFF is a liquid with a garlic-like odor and a color between pale yellow and amber yellow. PFF was first registered in the US in 1982, where it has been solely used on cotton to control tobacco budworm, cotton bollworm, armyworm, cotton aphid, whiteflies, spider mites, plant bugs, and fleahoppers (USEPA 2006b). Yearly PFF use in the US has been estimated to be over 350 tons per year (Ma et al. 2019). In addition to use on cotton, PFF can also be used on vegetables and fruits. Although the approval of PFF was revoked by the European Commission under regulation (EC) 1107/2009 (based on the European Commission online pesticides database https://ec.europa.eu/food/plants/pesticides/eu-pesticides-database_en), it is still widely used in other countries around the world such as the US, China, Thailand, Vietnam, Pakistan, Australia, Japan, Egypt, Brazil, Australia, and India (Kushwaha et al. 2016; Latheef 1995; Li et al. 2010; Radwan et al. 2005; Swarnam and Velmurugan 2013; Van Toan et al. 2013). Due to extensive use of PFF, in 2018, of 76,742 food samples on the European market, PFF was detected in 103 samples (0.13%) with the level in 43 samples (41.7%) exceeding the MRL (EFSA 2020). Also, PFF has been found in the market of non-EU countries (in vegetables sample such as tomatoes, okra, gooseberries, green chili, curry leaves, mint leaves, kale and coriander leaves) (Karanja et al. 2012; Kushwaha et al. 2016; Omwenga et al. 2020; Qin et al. 2016), and the residue levels in kale have been reported to exceed EU MRLs (Karanja et al. 2012). Besides, PFF was found in umbilical cord blood (Wickerham et al. 2012), which results from maternal exposure.

1.3 ADME (absorption, distribution, metabolism and excretion) of the selected OP pesticide model compounds

In general, the absorption and distribution of OP pesticides are rapid with extensive metabolism and no accumulation in the tissues, and the majority (around or above 80%) of the formed water-soluble metabolites can be rapidly excreted mainly in the urine within 72 hours (Garfitt et al. 2002; USEPA 2011; USEPA 2016b; USEPA 2016c).

The general population is normally exposed to OP pesticides via oral ingestion (CDC 2017).

Upon exposure, CPF, DZN and PFF can be rapidly absorbed. However, the fraction absorbed appears to be dependent on the physical form of administration (Timchalk et al. 2002). This follows from two different human studies, reporting that the actual fraction of the dose absorbed varied with the formulation, with 70% and 20% to 35% of an orally administered dose of CPF being recovered as its water-soluble metabolites in urine when dosed in the form of a lactose tablet or a powder in a capsule, respectively (Nolan et al. 1984; Timchalk et al. 2002). In case of DZN, 66% of an oral dose was recovered as urinary metabolites in human upon dosing DZN in an ethanolic solution with further dilution in water (Garfitt et al. 2002). At the current state-of-the-art, there are no human absorption data available for PFF, but in rats, similar absorption values were found for PFF, CPF and DZN, with around 94% urinary metabolite recovery for PFF, 80% for CPF and 90% for DZN (EFSA 2006; Poet et al. 2004; Timchalk et al. 2002; WHO 2010).

Following absorption, CPF, DZN and PFF are distributed to the liver where biotransformation occurs. Figure 3 presents an overview of CPF, DZN and PFF metabolism. Both CPF and DZN can be initially bioactivated to their more toxic and potent “oxon” form metabolites, chlorpyrifos-oxon (CPO) and diazoxon (DZO), respectively. These reactive forms are not stable and can be inactivated via hydrolytic cleavage to the common metabolite diethyl phosphate (DEP), and the compound-specific metabolites 3,5,6-trichloro-2-pyridinol (TCPy) or 2-isopropyl-4-methyl-6-hydroxypyrimidine (IMHP) (Figure 3). CPF and DZN can also be detoxified to another common metabolite, diethyl thiophosphate (DETP), accompanied by formation of TCPy or IMHP (Figure 3). There are several enzymes involved in these metabolic conversions and thus the toxicity of CPF and DZN. CYP catalyze the bioactivation of CPF to CPO and of DZN to DZO. For CPF, this reaction is preferably performed by CYP1A2 CYP2B6, CYP3A4, and for DZN, it is mediated by CYP1A1, CYP2B6, CYP2C19 and CYP3A4 (Ellison et al. 2012; Foxenberg et al. 2011; Sams et al. 2004). Detoxification of CPF and DZN is also catalyzed by different CYP enzymes, with CYP1A2, CYP2B6, CYP2C19 and CYP3A4 catalyzing the conversion of CPF to TCPy, and CYP1A1, CYP1A2, CYP2B6, CYP2C19 and CYP3A4 catalyzing the conversion of DZN to IMHP (Ellison et al. 2012; Foxenberg et al. 2011). Differently, instead of to CYP enzymes, the detoxifications of CPO and DZO (Figure 3) are mainly ascribed to the activity of another enzyme called paraoxonase 1 (PON1), which has been found to occur not only in the liver but also in blood due to the release of PON1 from liver (Pyati et al. 2015). Unlike CPF and DZN, PFF does not undergo bioactivation because of the absence of the P=S moiety. However, PFF is a direct acting pesticide (oxon form) due to

the presence of its oxon moiety (P=O). So far, a complete PFF biotransformation pathway has not been reported, but available studies show that PFF can be detoxified to its specific metabolite 4-bromo-2-chlorophenol (BCP) by PON1-mediated detoxification in liver and plasma (Omwenga et al. 2021) and CYP enzymes (CYP3A4, CYP 2B6, and CYP 2C19)-mediated detoxification in liver (Dadson et al. 2013) (Figure 4).

To eliminate the metabolites from the body, the formed specific metabolites (TCPy, IMHP and BCP) will be directly excreted in urine or first conjugated to form glucuronide conjugates before their urinary excretion (EFSA 2006; Garfitt et al. 2002; Min et al. 2002; Nolan et al. 1984; Risher and Navarro 1997). These specific metabolites TCPy, IMHP and BCP have been frequently used as urinary biomarkers for assessing CPF, DZN and PFF exposure, respectively, in biomonitoring and epidemiology studies (Atabila et al. 2018; Barr et al. 2005; Garfitt et al. 2002; Min et al. 2002; Nolan et al. 1984). However, the common urinary metabolites DEP and DETP, which are generated as metabolites from many other OP pesticides, are normally used as biomarkers for assessing OP pesticide aggregate exposure (Quirós-Alcalá et al. 2012; Sudakin and Stone 2011).

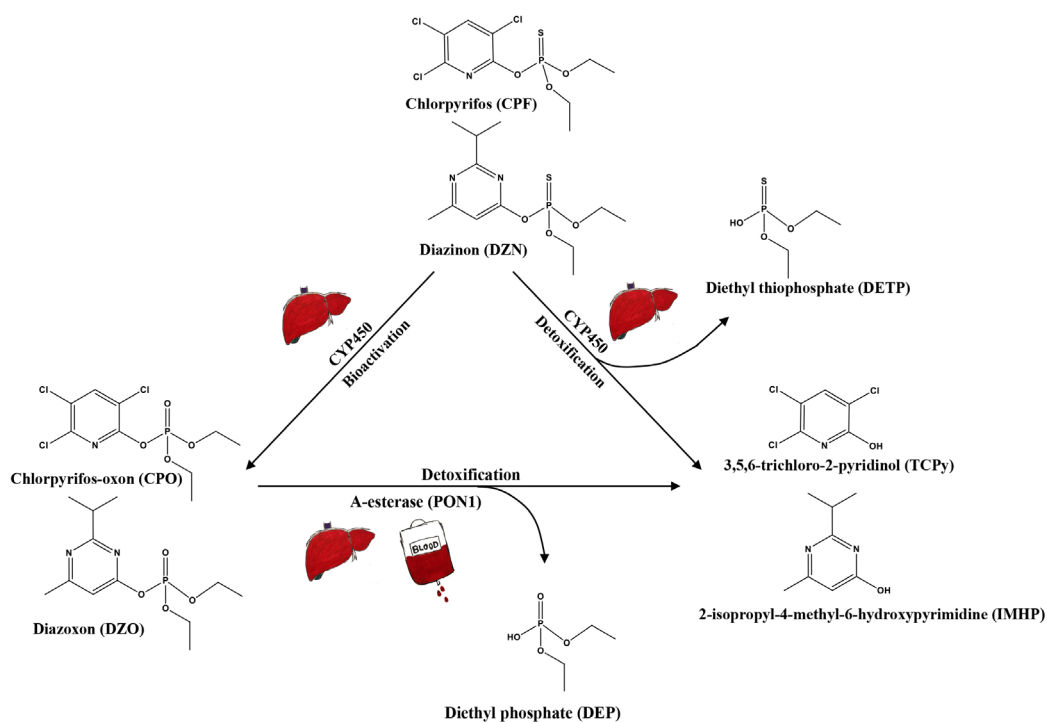


Fig 3. Metabolic pathways of chlorpyrifos and diazinon.

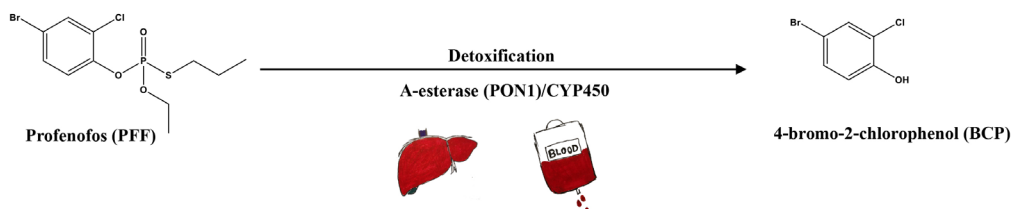


Fig 4. Schematic representation of the most prominent metabolic pathway of profenofos.

1.4 Toxicity of OP pesticides (including the selected OP model compounds) and the regulatory PODs

AChE inhibition has been identified as the mode of action (MOA) and molecular initiating event (MIE) in adverse outcome pathways (AOP) for the acute cholinergic toxicity (e.g. cholinergic syndrome) of OP pesticides (including CPF, DZN and PFF) and their resulting

mortality (USEPA 2015). The detailed AOP for AChE inhibition upon acute exposure is described in Figure 5. CPF, DZN and their oxon metabolites (CPO and DZO), as well as PFF are all primarily neurotoxicants, and act by inhibiting their primary target enzyme AChE via covalent binding, which has been identified as the MIE. AChE is in charge of breaking down the neurotransmitter acetylcholine (ACh) into acetic acid and choline by rapid hydrolysis in the central nervous system (CNS) and/or peripheral nervous system (PNS) (Costa 2018). Once AChE is inactivated by an inhibitor, this will result in accumulation of ACh at the synaptic cleft (key event 1 (KE1)), and continuous activation of the cholinergic receptors (nicotinic and muscarinic ACh receptors), leading to unregulated excitation (key event 2 (KE2)) at neuromuscular junctions of skeletal muscle, preganglionic and postganglionic nerve endings of the autonomic nervous system, in the CNS and/or PNS (Fukuto 1990; Mileson et al. 1998; Russom et al. 2014). As a result, upon acute single exposure, the OP pesticides can cause neurotoxic symptoms like cholinergic syndrome, which is manifested for example by increased sweating and salivation, profound bronchial secretion, bronchoconstriction, diarrhea, tremors, muscular twitching, and various CNS effects (dizziness, inhibition of central respiratory centers, convulsions, coma), respiratory failure, cardiovascular dysregulation and even death (adverse outcome (AO)) (Costa 2018; Roberts and Reigart 2013).

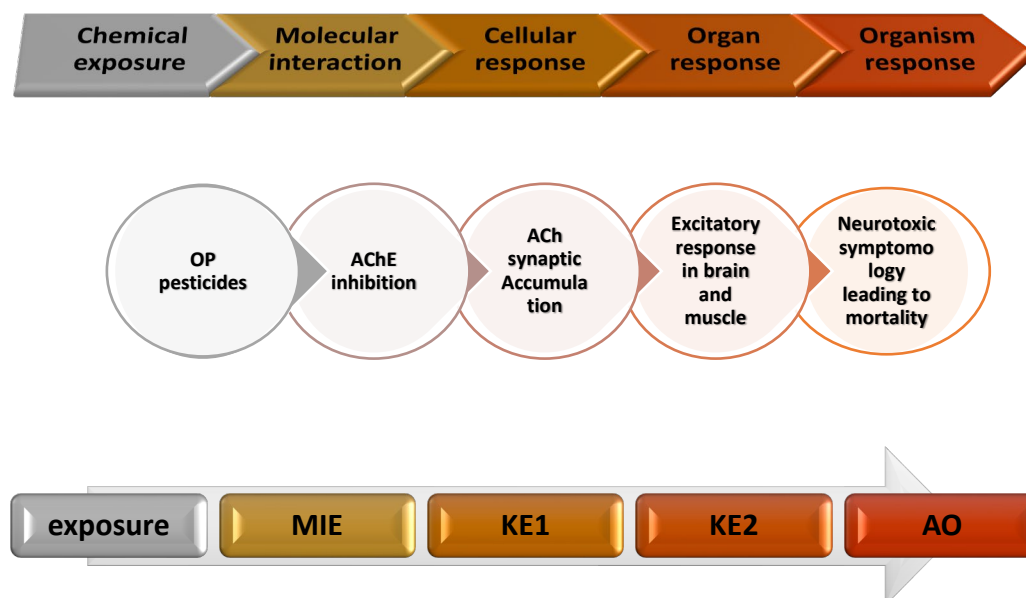


Fig 5. Adverse outcome pathway (AOP) for acetylcholinesterase (AChE) inhibition leading to acute lethality, as proposed by Russom et al. (2014). OP pesticides are organophosphate pesticides, AChE is acetylcholinesterase and ACh is acetylcholine. MIE represents the molecular initiating event, KE1 and KE2 represent different key events and AO is the adverse outcome.

In addition to acute cholinergic syndrome, an intermediate syndrome may also occur after resolution of the acute cholinergic syndrome (generally 24–96 hours after exposure), which may cause acute respiratory paresis and muscular weakness (USEPA 2013). Apart from that, a relatively rare toxicity known as organophosphorus ester-induced delayed neurotoxicity (OPIDN) may also occur, which is caused by some OP pesticides (e.g. diptalex) after single or short-term repeated exposures. This toxicity is associated with inhibition of neuropathy target esterase (NTE), leading to a delayed (8 to 15 days after exposure) effect like weakness or paralysis and paresthesia of the extremities (Lotti and Moretto 2005).

Except the adverse effects mentioned above, for the repeated exposure (longer than 21 days) of OP pesticides, generally, the related neurotoxicity is not well-defined, and the MIEs are not well established. However, available studies have shown that a stronger AChE inhibition may occur at a similar dose level compared to acute exposure (USEPA 2014). Moreover, a steady state AChE inhibition may occur within 2-3 weeks (time may vary among OP pesticides) as the result of the equilibrium between the degree of inhibition and the production of new enzymes (USEPA 2014; USEPA 2016b; USEPA 2016c), and possible prolonged neurological and neurobehavioral deficits (e.g. persistent cognitive impairment) and neurodevelopmental toxicity (e.g. cognitive deficits, behavioral deficits (related to attention, and motor deficits)

may occur (Muñoz-Quezada et al. 2013; Samsam et al. 2005).

Because AChE inhibition is the MIE, using AChE inhibition as a regulatory endpoint can provide protection for the downstream effects (USEPA 2015). However, it is not practically possible to determine AChE inhibition in brain especially in human, so that as an alternative, a surrogate endpoint consisting of AChE inhibition in RBC has been often used and considered as protective for other potential toxicities (EFSA 2014; USEPA 2011). RBC AChE inhibition has been considered to represent a more sensitive endpoint than inhibition of brain AChE, because RBC AChE was found to occur at dose levels below those that caused AChE inhibition in brain following both acute and repeated exposure (USEPA 2014). The USEPA has established POD values for the risk assessment of OP pesticides based on 10% RBC AChE inhibition for both acute and repeated exposure, resulting in for example (Table 2 and Table 3), POD values of 0.47 mg/kg bw (adult female, acute exposure) and 0.08 mg/kg bw (adult female, repeated exposure) for CPF, POD of 3 mg/kg bw (acute exposure) and 0.35 mg/kg bw (repeated exposure) for DZN, and POD of 1.99 mg/kg bw (acute exposure) and 0.12 mg/kg bw (repeated exposure) for PFF (USEPA 2014; USEPA 2015; USEPA 2016b; USEPA 2016c). However, more recently, a new concern has been highlighted by the USEPA, considering that using 10% RBC AChE inhibition as an endpoint may not be adequately protective for infants and youths, since for CPF, there are several epidemiological and toxicological studies suggesting that potential neurodevelopmental effects could occur even at lower dose levels than the dose causing 10% RBC AChE inhibition upon CPF prenatal exposure (USEPA 2016a). To further address this concern, USEPA used a CPF physiological based pharmacokinetic (PBPK) model to estimate the time weighted average (TWA) of CPF blood concentrations for women following an exposure scenario from an epidemiological study (USEPA 2016a). To this end, the predicted TWA of the blood CPF concentration was used as internal concentration to determine the specific external doses (POD) for fetuses, infants, and children following steady state (repeated 21 days) exposure by the PBPK model (USEPA 2016a). Given the fact that the present thesis is focusing on the adult general population and single acute exposure, RBC AChE inhibition is still considered as an appropriate endpoint for defining a POD for setting safe acute exposure levels.

An overview of available risk assessments of CPF, DZN, and PFF for both acute and repeated exposure and the critical effects used to define the PODs is provided in Table 2 and Table 3, respectively. This overview corroborates that RBC AChE inhibition is generally considered an adequate endpoint for defining a POD and HBGVs like an ARfD or ADI.

In the present thesis, the *in vitro* RBC AChE inhibition, which represents the surrogate endpoint underlying the acute toxicity of the OP pesticides and/or their potent metabolites (CPO, DZN, DZO and PFF) by AChE inhibition in CNS and/or PNS, were characterized by an *in vitro* AChE inhibition assay (Ellman et al. 1961; Li et al. 2019) using either recombinant human AChE (rhAChE) or rat AChE extracted from RBC.



1

Table 2. Overview of available risk assessments of CPF, DZN and PFF for acute oral exposure

Substance	Type of data from which POD originates	Critical effect for establishment of PODs	POD acute exposure (mg/kg bw/day)	Uncertainty factor	ARfD for different target group (mg/kg bw)	Organization	Year of publication	Reference
Chlorpyrifos (CPF)	In vivo dose-response curve (adult rats)	Significant (28-40%) plasma cholinesterase inhibition (Mendrala and Brzak 1998) and significant 30% RBC AChE inhibition (Zheng et al. 2000)	0.5 (NOAEL)	1000X for infants, children and females 13-50 years (10X=inter-species, 10X=intra-species, 10X=FQPA SF) or 100X for all other population groups (10X=inter-species, 10X=intra-species) 100X	0.0005 (infants, children and females 13-50 years) or 0.005 (for all other population groups)	USEPA	2000	(USEPA 2000)
	In vivo dose-response curve (rat pups)	10% RBC AChE inhibition	0.36 (BMDL ₁₀)	(10X=inter-species, 10X=intra-species, 1X=FQPA SF)	0.0036	USEPA	2011	(USEPA 2011)
	PBPK/PD predicted dose-response curve (human)	10% RBC AChE inhibition	Infants (< 1 yr): 0.60 (BMDL ₁₀) Children (1-2 yrs): 0.58 (BMDL ₁₀) Youths (6-12 yrs): 0.53 Adult (females 13-49 years): 0.47 (BMDL ₁₀)	40X for infants, children and youths (4X=inter-species, 10X=FQPA SF) or 100X for adult females 13-49 years (10X=intra-species factor, 10X=FQPA SF)	Infants (< 1 yr): 0.015 Children (1-2 yrs): 0.014 Youths (6-12 yrs): 0.013 Adult: 0.0047 (females 13-49 years)	USEPA	2014	(USEPA 2014)
	PBPK/PD predicted dose-response curve (human)	-	No POD value for acute exposure was established	-	-	USEPA	2016	(USEPA 2016a)
	No detailed information is available	Acute and delayed neurotoxicity in rats	No POD value was mentioned in report	100X (10X=inter-species, 10X=intra-species)	0.1	European Commission	2005	(European Commission 2005)
	In vivo dose-response curve (rat pups)	20% RBC AChE inhibition	0.5 (NOAEL)	100X (10X=inter-species, 10X=intra-species)	0.005	EFSA	2014	(EFSA 2014)



		In vivo dose-response curve (rats)	Acute (neuro)toxicity that brain/RBC/plasma AChE inhibition	2.5 (NOAEL)	100X (10X=inter-species, 10X=intra-species)	0.03	JMPR	2001, 2006, 2016	(JMPR 2001; JMPR 2006; JMPR 2016)
		In vivo dose-response curve (adult female rats)	10% RBC inhibition	1.99 (BMDL ₁₀)	100X for subgroup adults 50–99 years old (10X=inter-species, 10X=intra-species) or 1000X for all other population groups (10X=inter-species, 10X=intra-species 10X=FQPA SF)	0.0199 (for subgroup adults 50–99 years old) or 0.00199 (for all other population groups)	USEPA	2016	(USEPA 2016c)
Profenofos (PFF)		In vivo dose-response curve (dog)	The inhibition of brain (<20%) cholinesterase activity in 1 year study	No detailed information is available	100X (10X=inter-species, 10X=intra-species)	0.01	Germany as Rapporteur Member State (RMS)	2001	(EFSA 2012)
		In vivo dose-response curve (dog)	The inhibition of brain cholinesterase activity	No detailed information is available	No detailed information is available	0.005	German	2001	(EFSA 2019b)





	In vivo dose-response curve (rats)	The inhibition of brain cholinesterase activity	100 (NOAEL)	100X (10X=inter-species, 10X=intra-species)	1	JMPR	2007	(JMPR 2007)
	-	European Commission revoked approval for profenofos	Same as JMPR (2007)	Same as JMPR (2007)	Same as JMPR (2007)	European Commission, JMPR	No detailed information is available	(European Commission n.d.-b; JMPR 2007)

Note: POD is point of departure; RBC is red blood cell or erythrocyte; AChE is acetylcholinesterase; NOAEL is the no-observed-adverse-effect level; LOAEL is the lowest-observed-adverse-effect level; EFSA is the European Food Safety Authority; USEPA is the United States Environmental Protection Agency; JMPR is the Joint FAO/WHO Meeting on Pesticide Residues; PBPK/PD is physiologically based pharmacokinetic/pharmacodynamic; BMDL₁₀ is the benchmark dose lower confidence limit for 10% inhibition, ARFD is acute reference dose. FQPA SF is Food Quality Protection Act Safety Factor, applied because of the concern over uncertainty in the human dose-response relationship for potential neurodevelopmental effects on females 13-50 years and infants and children population subgroups that may arise from prenatal exposure to CPF, “-” represent no data is applied, “n.d.” represent no data is available.

Table 3. Overview of available risk assessments of CPF, DZN and PFF for repeated oral exposure

Substance	Type of data from which POD originates	Critical effect for establishment of PODs	POD repeated exposure (mg/kg bw/day)	Uncertainty factor	ADI for different target groups (mg/kg bw /day)	Organization	Year of publication	Reference
Chlorpyrifos (CPF)	In vivo dose-response curve (dog/rats)	Plasma and RBC AChE inhibition based on a weight of the evidence consideration of 5 toxicity studies	0.03 (NOAEL)	100X for infants, children, and females 13-50 Year (10X=inter-species, 10X=intra-species, 10X=FQPA SF or 100X (10X=inter-species, 10X=intra-species) 100X	0.00003 (infants, children, and females 13-50 Year) or 0.0003 (for all other population groups)	USEPA	2000	(USEPA 2000)
	In vivo dose-response curve (rat)	Chronic based on the inhibition of RBC AChE in pregnant rat in the developmental neurotoxicity study	0.03 (BMDL ₁₀)	(10X=inter-species, 10X=intra-species, 1X=FQPA SF)	0.0003	USEPA	2011	(USEPA 2011)
	PBPK/PD predicted dose-response curve (human)	10% RBC AChE inhibition	Infants (< 1 yr): 0.10 (BMDL ₁₀) Children (1-2 yrs): 0.10 (BMDL ₁₀) Youths (6-12 yrs): 0.09 (BMDL ₁₀) Adult (females 13-49 years): 0.08 (BMDL ₁₀)	40X for infants, children and youths (4X=intra-species, 10X=FQPA SF or 100X for Adult females 13-49 years (10X=intra-species factor, 10X=FQPA SF)	Infants (< 1 yr): 0.0026 Children (1-2 yrs): 0.0025 Youths (6-12 yrs): 0.0022 Adult (females 13-49 years): 0.00078	USEPA	2014	(USEPA 2014)
	PBPK/PD predicted chlorpyrifos concentrations in blood (human)	Time-Weighted Average of 0.004 µg/L Chlorpyrifos in blood	Infants (< 1 yr): 0.0002 Children (1-2 yrs): 0.00017 Youths (6-12 yrs): 0.00012 Adult (females 13-49 years): 0.00012	100X (10X=intra-species factor and 10X=LOAEL to NOAEL extrapolation factor)	- Infants (< 1 yr): 0.0000002 Children (1-2 yrs): 0.0000017 Youths (6-12 yrs): 0.0000012 Adult (females 13-49 years):	USEPA	2016	(USEPA 2016a)



				0-0.005 (for year of 2001,2006) and 0-0.003 (for year of 2016)	JMPR	2001, 2006, 2016	(JMPR 2001; JMPR 2006; JMPR 2016)
				0.5 (NOAEL for year of 2001 and 2006) 0.3 (NOAEL for year of 2016)			
				100X (10X=inter-species, 10X=intra-species)			
				100X for subgroup adults (for subgroup adults 50-99 years old) (10X=inter-species, 10X=intra-species) or 1000X for all other population groups (10X=inter-species, 10X=intra-species 10X=FQPA SF)			
				0.0012 (for subgroup adults 50-99 years old) or 0.00012 (for all other population groups)	USEPA	2016	(USEPA 2016c)
				1 (LOAEL)			
				200X (10X=inter-species, 10X=intra-species, 2X=LOAEL to NOAEL extrapolation factor)	Germany as Rapporteur Member State (RMS)	2001	(EFSA 2012)
				10% RBC inhibition in combined with chronic oral toxicity/carcinogenicity study			
				No detailed information is available			
				No detailed information is available	German	2001	(EFSA 2019b)
				200X No detailed information is available			
				Same as EFSA (2012)			
				No detailed information is available			
				No detailed information is available			
Profenofos (PFF)	In vivo dose-response curve (rats)	2001,2006: Inhibition of RBC AChE activity in a 92-day repeated-dose toxicity study 2016: Inhibition of AChE activity for all repeated-dose toxicity studies					
	In vivo dose-response curve (adult rats)	10% RBC inhibition in combined with chronic oral toxicity/carcinogenicity study					
	In vivo dose-response curve (dog)	No detailed information is available					
	In vivo dose-response curve (dog)	No detailed information is available					



1.5 Use of animal alternative testing strategies to define PODs for OP pesticides

As mentioned above, the HBGVs defined for the acute toxicity of the OP pesticides studied in the present thesis (Table 2) were based on the POD for the critical effect RBC AChE inhibition, which is usually determined in laboratory animal studies. At the present state-of-the-art, however, use of laboratory animals is considered unethical, expensive, time consuming and scientifically not always adequately presenting the situation in humans (Bailey et al. 2014; Hackam and Redelmeier 2006; Perel et al. 2007). To improve human risk assessment and replace, reduce and refine the use of experimental animals, the 3Rs concept was developed, firstly by Drs. William Russell and Rex Burch in 1959 (Russell and Burch 1959), and has been embedded in legislation and guidelines by different countries and/or regulatory bodies. The 3Rs refer to the Reduction, Refinement, and Replacement of animals used in research, testing, and education. To comply with the 3Rs concept, the development of animal alternative approaches is becoming increasingly important. The use of animal alternative approaches such as human-based in vitro methods (using human cells and/or (subcellular) tissue) and human-based in silico computer-model techniques enable a prediction directly applicable for the human situation without the need to introduce a UF of inter-species-differences. To translate the results from such in vitro models using human cells and/or (subcellular) tissue to the in vivo situation, PBK model-based reverse dosimetry gradually gains more and more interest as an important tool for the safety and risk assessment of compounds (EMA 2018; OECD 2021).

A PBK model contains a set of differential equations that together describe the kinetics including ADME of a selected chemical in an organism of interest. Three different types of parameters have to be obtained as input for the model, which are 1) physiological parameters (e.g. cardiac output, tissue volumes and tissue blood flows; 2) physico-chemical parameters (e.g. blood/tissue partition coefficients); 3) kinetic parameters (e.g. kinetic constants for metabolic reactions) (Louisse et al. 2017; Rietjens et al. 2011). These parameters are needed to define the equations that describe the kinetics in different tissue compartments in the PBK model as well as the fate and distribution of the chemical and its metabolites among these compartments. The PBK model can simulate the dose-dependent concentration of a chemical or its metabolites in the target organ or blood, by so called forward dosimetry. Alternatively, the PBK model allows translation of in vitro concentration-response curves (obtained using an in vitro toxicity model able to detect the MOA of the chemical studied) to in vivo dose-response

curves, by so called reverse dosimetry, thus enabling QIVIVE (Figure 6). From these predicted in vivo dose-response curves, POD values required in risk assessment can be derived. Similar animal alternative testing strategies have been successfully conducted by the USEPA to estimate POD values based on 10% RBC AChE inhibition for risk assessment of CPF for different human life stages. Though instead of using PBK model-based QIVIVE, the USEPA applied another PBK model-based approach, namely a physiologically based pharmacokinetic/pharmacodynamic (PBPK/PD) model in their risk assessment (USEPA 2014) (Table 2). This application provides support for the use of PBK models in the risk assessment of OP pesticides. At the same time, the PBK model-based reverse dosimetry approach enables to study possible inter-ethnic differences in more detail, which so far have not been addressed in risk assessments on OP pesticides. These inter-ethnic differences are generally considered to be covered by the default UF for inter-individual differences. However, it remains to be investigated whether such differences between ethnic groups exist and if so whether they are adequately covered by the default UF for inter-individual differences.

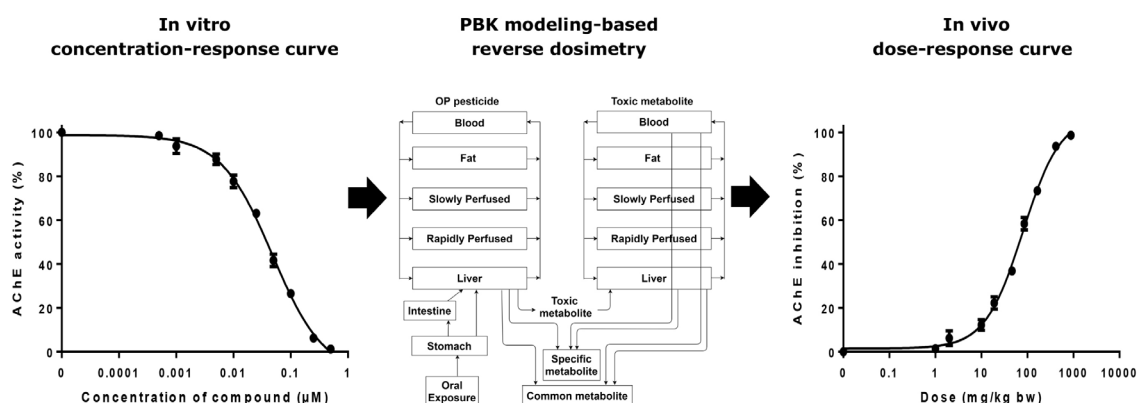


Fig 6. Schematic representation of the physiologically based kinetic (PBK) model-facilitated reverse dosimetry approach

In the current thesis, the animal alternative testing strategy applying PBK model-based reverse dosimetry for translation of in vitro concentration-response curves to in vivo dose-response curves was applied to predict PODs for in vivo RBC AChE inhibition for the different model OP pesticides of interest, and also to investigate inter-species and inter-ethnic human differences for this endpoint. To this end, the relevant species-specific (rat or human) and ethnic-specific (Caucasian and Chinese) parameters were collected directly from the literature,

or estimated based on physical and chemical properties of the target chemicals using different software such as Simcyp (Simcyp 2016) and pkCSM (pkCSM 2015), or obtained from in vitro metabolic incubations using species-specific or ethnic-specific pooled tissues (liver microsomes and plasma). The in vitro concentration-dependent RBC AChE inhibition following exposure to the OP pesticides and/or their potent metabolites (CPO, DZN, DZO and PFF) were obtained from reported data (Eyer et al. 2009) or experimentally derived using an in vitro AChE inhibition assay with either rhAChE enzyme or rat RBC AChE. Before extrapolating the in vitro concentration-response curve to an in vivo predicted dose-response curve, the free concentration used in vitro was set equal to the predicted free maximum concentration in vivo, to determine the dose that would result in this concentration, leading to the corresponding inhibition.

To further address inter-individual variation in toxicokinetics for the target population, experiment-derived and literature-obtained kinetic parameters for human liver microsome (HLM) and human plasma (HP) mediated metabolic conversion of the OP pesticides and the coefficients of variation for these parameters were used in the PBK model (HLM-based PBK model). In an additional approach, to address the inter-individual differences, enabling also studying differences with age, gender, and ethnicity, the metabolic variation in the adult population was characterized based on data obtained from incubations with Supersome™ CYP to generate the input parameters for the PBK model (Supersome™ CYP-based PBK model). Different with pooled HLMs, Supersome™ CYP only express one specific human CYP enzyme e.g. CYP1A2, CYP2B6, or CYP3A4 etc. Use of Supersome™ CYP enables quantification of the intrinsic activity of the respective CYP enzymes towards the OP pesticide of interest. By further correcting for the difference in the CYP activity between Supersome™ CYP and the relative activity in HLMs and applying individual CYP enzyme abundance values, CYP activities for (different) individuals can be quantified. Hence the Supersome™ CYP - based kinetic parameters can be scaled to the in vivo kinetic values. To describe inter-individual variation in toxicokinetics, the HLM-based and Supersome™ CYP -based PBK models were combined with Monte Carlo simulations, providing a computer-based approach to predict the variability of the model outcomes by running a large number of simulations, for which model parameters (e.g. kinetic parameters, CYP abundance) are randomly selected from their relevant distributions (Kenton 2020). In this way, the impact of variability of input parameters on the model output, for example the blood maximum concentrations (C_{max}) of CPO, can be characterized and quantified (Krishnan et al. 2013). The approach thus enables the description

of the effect of the variability in the model input parameters on the variability in the PBK model outcome. Together with reverse dosimetry, the inter-individual differences in susceptibilities for target chemical-related RBC AChE inhibition can be characterized, and a CSAF for describing inter-individual variation in toxicokinetics (HK_{AF}) can be established. Depending on the species and type of endpoint (kinetic and/or dynamic), it can be used to replace the relevant default UF for inter-species variation in kinetics or dynamics (AK_{UF} of 4.0 or AD_{UF} of 2.5) and for inter-individual variation in kinetics or dynamics (HK_{UF} of 3.16 or HD_{UF} of 3.16) (Figure 1) (IPCS 2005).

When applying alternative testing strategies to define PODs for OP pesticides, it is also important to note that for some OP pesticides, both the parent P=S compound as well as the oxon metabolite may have an AChE inhibiting potential. An example is DZN, for which in the present thesis a PBK model was developed that included the activity of both the parent OP pesticide and its oxon metabolite. To accommodate the activity of both compounds in the QIVIVE reverse dosimetry approach, the TEF methodology (Gao et al. 2016) was included in the model code in order to enable description of the combined effect of the OP pesticide of interest and its toxic metabolite at the target site. Use of the TEF concept is possible when i) the OP pesticide and its toxic metabolite act by the same MOA, ii) the combined toxicity is additive, and iii) the concentration-response curves for the induced *in vitro* AChE inhibition are parallel (Starr et al. 1999; Watt et al. 2016). Use of the TEF methodology allows the internal concentrations of the OP pesticide and its potent toxic metabolite present in the target site to be combined and expressed in term of equivalents of the potent toxic metabolite, by multiplying their effective internal concentration with the specific TEF values and adding up the resulting concentrations expressed in toxic equivalents using the equation presented below. The TEF values were defined as the inhibitory potency (based on the half maximal inhibitory concentrations (IC_{50})) of the OP pesticide relative to that of the potent toxic metabolite in terms of RBC AChE inhibition. The aforementioned total potent toxic metabolite equivalents and TEF values are calculated using the following equations (Delistraty 1997):

Total toxic metabolite concentration in toxic equivalents =

[OP pesticide] * $TEF_{OP\ pesticide}$ + [toxic metabolite] * $TEF_{toxic\ metabolite}$

$$TEF_{OP\ pesticide} = \frac{IC_{50\ toxic\ metabolite}}{IC_{50\ OP\ pesticide}} \quad TEF_{toxic\ metabolite} = \frac{IC_{50\ toxic\ metabolite}}{IC_{50\ toxic\ metabolite}} = 1.0$$

In the equation above, the Total toxic metabolite concentration in toxic equivalents represents the effective internal concentration of the OP pesticide plus its toxic metabolite expressed in toxic metabolite equivalents using the TEF values for the OP pesticide and its toxic metabolite, [OP pesticide] and [toxic metabolite] represent the effective internal concentration of the OP pesticide and the toxic metabolite at the target site, the $TEF_{OP\text{ pesticide}}$ and $TEF_{toxic\text{ metabolite}}$ are the toxic equivalency factors of the OP pesticide and its toxic metabolite with the $TEF_{toxic\text{ metabolite}}$ defined as equal to 1.0. The $IC_{50_{OP\text{ pesticide}}}$ and $IC_{50_{toxic\text{ metabolite}}}$ represent the half maximal inhibitory concentrations of the OP pesticide and its toxic metabolite that induced 50% inhibition of RBC AChE in vitro.

By combining the TEF methodology with the PBK model-facilitated reverse dosimetry approach, the combined effects induced by the parent compound and its bioactive metabolite at the target site can be characterized, and the resulting POD values can be established.

1.6 Outline of the thesis

Chapter 1 of this thesis, the current chapter, presents an overview of relevant background information, including an introduction of CPF, DZN and PFF as model compounds, their ADME and toxicity profiles, their POD and HBGVs, as well as an introduction to the alternative animal testing strategy applied in the thesis consisting of PBK model-based reverse dosimetry solely or in combination with Monte Carlo simulations for evaluation of inter-individual variation, or incorporating the TEF methodology to account for the RBC AChE inhibition potential of a parent OP pesticide and its oxon metabolite. Also, the aim and outline of the thesis are introduced.

Chapter 2 of this thesis defines a PBK model of CPF and its metabolites in the average Chinese and Caucasian population. The inter-ethnic differences in kinetics were characterized based on the comparison of metabolic biotransformation, in vivo predicted CPO concentrations at the target site, and dose-response curves. The resulting PODs for the two populations were compared to provide insight in the inter-ethnic differences in kinetics and the resulting sensitivity towards CPF exposure.

Chapter 3 of this thesis describes the development of a PBK model for PFF in human and rat. The inter-species differences in kinetics and the resulting RBC AChE inhibitory effects were characterized based on comparison of metabolic biotransformation and in vitro RBC AChE

inhibition, predicted PFF blood concentrations, dose-response curves, as well as the corresponding predicted POD values for the two species.

Chapter 4 of this thesis describes the development of TEF coded DZN PBK models for rat and human together with reverse dosimetry to predict the combined inhibitory effect of DZN and its active metabolite DZO on in vivo RBC AChE activity in these species. The inter-species differences were characterized based on the comparison of metabolic bioactivation and detoxification, in vitro RBC AChE inhibition, predicted dose-response curves, as well as derived POD values for the two species.

Chapter 5 of this thesis compared the applicability of using an HLM-based PBK model and a SupersomeTM CYP-based PBK model, combined with reverse dosimetry and Monte Carlo simulations to evaluate the inter-individual differences in toxicokinetics of CPF, allowing for the calculation of a CSAF for inter-individual differences in kinetics. Also, the consequences of these inter-individual differences in toxicokinetics for the inter-individual differences in predicted dose-response curves for CPF exposure induced RBC AChE inhibition were characterized, and the resulting POD values were established.

Finally, **Chapter 6** presents a discussion of the results obtained in this thesis, evaluating how the findings of the thesis can contribute to further research and risk assessment of OP pesticide exposure for different ethnic populations and individuals based on new approach in vitro and in silico testing strategies.

References

- Atabila A, Sadler R, Phung DT, Hogarh JN, Carswell S, Turner S, . . . Chu C (2018) Biomonitoring of chlorpyrifos exposure and health risk assessment among applicators on rice farms in Ghana *Environmental Science and Pollution Research* 25:20854-20867
- Bailey J, Thew M, Balls M (2014) An analysis of the use of animal models in predicting human toxicology and drug safety *Alternatives to Laboratory Animals* 42:181-199
- Barr DB, Allen R, Olsson AO, Bravo R, Caltabiano LM, Montesano A, . . . Walker RD (2005) Concentrations of selective metabolites of organophosphorus pesticides in the United States population *Environmental research* 99:314-326
- Bertrand PG (2019) Uses and misuses of agricultural pesticides in Africa: Neglected public health threats for workers and population *Pesticides–Use and Misuse and Their Impact in the Environment*
- Brahmand MB, Yunesian M, Nabizadeh R, Nasseri S, Alimohammadi M, Rastkari N (2019) Evaluation of chlorpyrifos residue in breast milk and its metabolite in urine of mothers and their infants feeding exclusively by breast milk in north of Iran *Journal of Environmental Health Science and Engineering* 17:817-825
- Burgess P, Harper C, Todd GD, Wohlers D (2008) Toxicological profile for diazinon. <https://www.atsdr.cdc.gov/toxprofiles/tp86.pdf>. Accessed 3rd March 2021
- CAREX Canada (2020) Diazinon Profile. <https://www.carexcanada.ca/profile/diazinon/>. Accessed 26th January 2021
- CDC (2017) Organophosphorus Insecticides: Dialkyl Phosphate Metabolites. https://www.cdc.gov/biomonitoring/OP-DPM_BiomonitoringSummary.html. Accessed 26 January 2021
- Chapalamadugu S, Chaudhry GR (1992) Microbiological and biotechnological aspects of metabolism of carbamates and organophosphates *Critical reviews in biotechnology* 12:357-389
- ChemAxon Chemicalize <https://chemaxon.com/products/chemicalize>. Accessed 25 May 2021
- Cho T, Kim B, Jo S, Kang H, Choi B, Kim M (2009) Pesticide residue monitoring in Korean agricultural products, 2003–05 *Food Additives and Contaminants: Part B* 2:27-37
- Costa LG (2018) Organophosphorus compounds at 80: some old and new issues *Toxicological Sciences* 162:24-35
- Dadson OA, Ellison CA, Singleton ST, Chi L-H, McGarrigle BP, Lein PJ, . . . Olson JR (2013) Metabolism of profenofos to 4-bromo-2-chlorophenol, a specific and sensitive exposure biomarker *Toxicology* 306:35-39
- Delistraty D (1997) Toxic equivalency factor approach for risk assessment of polycyclic aromatic hydrocarbons *Toxicological & environmental chemistry* 64:81-108
- DOW (2017) Dow Releases Statement about Chlorpyrifos. <https://corporate.dow.com/en-us/news/press-releases/dow-ap-chlorpyrifos.html>. Accessed 26 January 2021
- EFSA (2006) Conclusion regarding the peer review of the pesticide risk assessment of the active substance diazinon <https://efsa.onlinelibrary.wiley.com/doi/epdf/10.2903/j.efsa.2006.85r>. Accessed 27th January 2021
- EFSA (2012) Scientific support for preparing an EU position in the 44th Session of the Codex Committee on Pesticide Residues (CCPR). <https://efsa.onlinelibrary.wiley.com/doi/pdfdirect/10.2903/j.efsa.2012.2859>. Accessed 1st February 2021
- EFSA (2014) Conclusion on the peer review of the pesticide human health risk assessment of the active substance chlorpyrifos *EFSA Journal* 12:3640
- EFSA (2019a) The 2017 European Union report on pesticide residues in food *EFSA Journal* 17:e05743
- EFSA (2019b) Scientific support for preparing an EU position in the 51st Session of the Codex Committee on Pesticide Residues (CCPR) *EFSA Journal* 17:e05797
- EFSA (2019c) Statement on the available outcomes of the human health assessment in the context of the pesticides peer review of the active substance chlorpyrifos *EFSA Journal* 17:e05809
- EFSA (2020) The 2018 European Union report on pesticide residues in food *EFSA Journal* 18
- Ellison CA, Tian Y, Knaak JB, Kostyniak PJ, Olson JR (2012) Human hepatic cytochrome P450-

- specific metabolism of the organophosphorus pesticides methyl parathion and diazinon *Drug Metabolism and Disposition* 40:1-5
- Ellman GL, Courtney KD, Andres Jr V, Featherstone RM (1961) A new and rapid colorimetric determination of acetylcholinesterase activity *Biochemical pharmacology* 7:88-95
- EMA (2018) Guideline on the reporting of physiologically based pharmacokinetic (PBPK) modelling and simulation. https://www.ema.europa.eu/en/documents/scientific-guideline/guideline-reporting-physiologically-based-pharmacokinetic-pbpk-modelling-simulation_en.pdf. Accessed 25 May 2021
- European Commission (2005) Review report for the active substance chlorpyrifos. https://ec.europa.eu/food/plant/pesticides/eu-pesticides-database/active-substances/?event=as.details&as_id=548. Accessed 30th January 2021
- European Commission (2020) Chlorpyrifos & Chlorpyrifos-methyl. https://ec.europa.eu/food/plant/pesticides/approval_active_substances/chlorpyrifos_chlorpyrifos-methyl_en. Accessed 31st January 2021
- European Commission (n.d.-a) Diazinon -Pesticide database. https://ec.europa.eu/food/plant/pesticides/eu-pesticides-database/active-substances/?event=as.details&as_id=612. Accessed 31st January 2021
- European Commission (n.d.-b) Profenofos- Pesticide database. https://ec.europa.eu/food/plant/pesticides/eu-pesticides-database/active-substances/?event=as.details&as_id=61. Accessed 1st February 2021
- Eyer F, Roberts DM, Buckley NA, Eddleston M, Thiermann H, Worek F, Eyer P (2009) Extreme variability in the formation of chlorpyrifos oxon (CPO) in patients poisoned by chlorpyrifos (CPF) *Biochemical pharmacology* 78:531-537
- Foxenberg RJ, Ellison CA, Knaak JB, Ma C, Olson JR (2011) Cytochrome P450-specific human PBPK/PD models for the organophosphorus pesticides: chlorpyrifos and parathion *Toxicology* 285:57-66
- Fukuto TR (1990) Mechanism of action of organophosphorus and carbamate insecticides *Environmental health perspectives* 87:245-254
- Gao Y, Feng J, Han F, Zhu L (2016) Application of biotic ligand and toxicokinetic-toxicodynamic modeling to predict the accumulation and toxicity of metal mixtures to zebrafish larvae *Environmental Pollution* 213:16-29
- Garfitt S, Jones K, Mason H, Cocker J (2002) Exposure to the organophosphate diazinon: data from a human volunteer study with oral and dermal doses *Toxicology letters* 134:105-113
- Hackam DG, Redelmeier DA (2006) Translation of research evidence from animals to humans *Jama* 296:1727-1732
- Hertz-Picciotto I, Sass JB, Engel S, Bennett DH, Bradman A, Eskenazi B, . . . Whyatt R (2018) Organophosphate exposures during pregnancy and child neurodevelopment: recommendations for essential policy reforms *PLoS medicine* 15:e1002671
- Hongsibsong S, Prapamontol T, Xu T, Hammock BD, Wang H, Chen Z-J, Xu Z-L (2020) Monitoring of the organophosphate pesticide chlorpyrifos in vegetable samples from local markets in Northern Thailand by developed Immunoassay *International Journal of Environmental Research and Public Health* 17:4723
- Huen K, Bradman A, Harley K, Yousefi P, Barr DB, Eskenazi B, Holland N (2012) Organophosphate pesticide levels in blood and urine of women and newborns living in an agricultural community *Environmental research* 117:8-16
- Humans IWGotEoCRt (2017) Some organophosphate insecticides and herbicides
- Pesticide registration database (2021) <http://www.chinapesticide.org.cn/hysj/index.jhtml>. Accessed 26th January, 2021
- Idrovo AJ (2014) Food poisoned with pesticide in Bihar, India: new disaster, same story *Occupational and environmental medicine* 71:228-228
- Ingenbleek L, Hu R, Pereira LL, Paineau A, Colet I, Koné AZ, . . . Oyedele AD (2019) Sub-Saharan Africa total diet study in Benin, Cameroon, Mali and Nigeria: Pesticides occurrence in foods *Food chemistry: X* 2:100034
- IPCS (2005) Chemical-specific Adjustment Factors for Interspecies Differences and Human Variability: Guidance Document for Use of Data in Dose/concentrationResponse Assessment. International

- Programme on Chemical Safety. <https://archive.epa.gov/scipoly/sap/meetings/web/pdf/ipcs2005csaf.pdf>. Accessed 3rd February 2021
- Isegbe V, Habib M, Obaje J, Ekor S, Solomon S (2016) Organophosphate Pesticide Residues Analysis Sampled From Containerised Beans Repatriated from European Union International Journal of Innovative Food, Nutrition & Sustainable Agriculture 4 (4): 31-35
- JMPR (2001) Pesticide residues in food 2001. <http://www.inchem.org/documents/jmpr/jmpmono/2001pr03.htm>. Accessed 31st January 2021
- JMPR (2006) DIAZINON (addendum) Pesticide residues in food—2006:293
- JMPR (2007) Pesticide residue in food-2007. <http://www.inchem.org/documents/jmpr/jmpmono/v2007pr01.pdf>. Accessed 1st February 2021
- JMPR (2016) Pesticide residues in food 2016. <http://www.fao.org/3/a-i6585e.pdf>. Accessed 31st January 2021
- Karanja NN, Njenga M, Mutua G, Lagerkvist C, Okello J (2012) Concentrations of heavy metals and pesticide residues in leafy vegetables and implications for peri-urban farming in Nairobi, Kenya Journal of Agriculture, Food Systems, and Community Development 3:255–267
- Karasali H, Maragou N (2016) Pesticides and herbicides: Types of pesticide
- Kenton W (2020) Monte Carlo Simulation. <https://www.investopedia.com/terms/m/montecarlosimulation.asp#:~:text=A%20Monte%20Carlo%20simulation%20is,in%20prediction%20and%20forecasting%20models>. Accessed 3rd February 2021
- King AM, Aaron CK (2015) Organophosphate and carbamate poisoning Emergency Medicine Clinics 33:133-151
- Krishnan K, McPhail B, Chiu W, White P (2013) Modeling of Sensitive Subpopulations and Interindividual Variability in Pharmacokinetics for Health Risk Assessments. In: Computational Toxicology. Elsevier, pp 45-66
- Kushwaha M, Verma S, Chatterjee S (2016) Profenofos, an Acetylcholinesterase-Inhibiting Organophosphorus Pesticide: A Short Review of Its Usage, Toxicity, and Biodegradation Journal of environmental quality 45:1478-1489
- Latheef M (1995) Influence of spray mixture rate and nozzle size of sprayers on toxicity of profenofos and thiodicarb formulations against tobacco budworm on cotton Crop Protection 14:423-427
- Li S, Zhao J, Huang R, Santillo MF, Houck KA, Xia M (2019) Use of high-throughput enzyme-based assay with xenobiotic metabolic capability to evaluate the inhibition of acetylcholinesterase activity by organophosphorus pesticides Toxicology in Vitro 56:93-100
- Li X, Li S, Liu S, Zhu G (2010) Lethal effect and in vivo genotoxicity of profenofos to Chinese native amphibian (*Rana spinosa*) tadpoles Archives of environmental contamination and toxicology 59:478-483
- Lotti M, Moretto A (2005) Organophosphate-induced delayed polyneuropathy Toxicological reviews 24:37-49
- Louisse J, Beekmann K, Rietjens IMCM (2017) Use of physiologically based kinetic modeling-based reverse dosimetry to predict in vivo toxicity from in vitro data Chemical research in toxicology 30:114-125
- Ma M, Dong S, Jin W, Zhang C, Zhou W (2019) Fate of the organophosphorus pesticide profenofos in cotton fiber Journal of Environmental Science and Health 54:70-75
- Mendrala A, Brzak K (1998) Chlorpyrifos: Part A-concentration-time course of chlorpyrifos and chlorpyrifos-oxon in blood. Health and Environmental Research Laboratories. The Dow Chemical Co. Midland MI. Laboratory Project Study ID: 971187A. August 31, 1998. MRID No. 44648102 Unpublished Maxwell DM 1992a “The specificity of carboxylesterase protection against the toxicity of organophosphorus compounds” Toxicology and Applied Pharmacology Jun 114:306-312
- Mileson BE, Chambers JE, Chen W, Dettbarn W, Ehrich M, Eldefrawi AT, . . . Karczmar AG (1998) Common mechanism of toxicity: a case study of organophosphorus pesticides Toxicological sciences 41:8-20

- Min K-j, Lee I-s, Song D-h, Cho Y-j (2002) Determination of Urinary Metabolite of Profenofos after Oral Administration and Dermal Application to Rats Journal of the Korean Society of Food Hygiene and Safety 17:20-25
- Muñoz-Quezada MT, Lucero BA, Barr DB, Steenland K, Levy K, Ryan PB, . . . Rojas E (2013) Neurodevelopmental effects in children associated with exposure to organophosphate pesticides: a systematic review Neurotoxicology 39:158-168
- National Center for Biotechnology Information (2021a) PubChem Compound Summary for CID 3017, Diazinon. <https://pubchem.ncbi.nlm.nih.gov/compound/Diazinon>. Accessed 25 May 2021
- National Center for Biotechnology Information (2021b) PubChem Compound Summary for CID 13754, Diazoxon. <https://pubchem.ncbi.nlm.nih.gov/compound/Diazoxon>. Accessed 25 May 2021
- News I (2010) Harmful pesticide banned in SA. <https://www.iol.co.za/news/south-africa/harmful-pesticide-banned-in-sa-485733#.U-VBFPldV9w>. Accessed 26 January 2021
- Nolan R, Rick D, Freshour N, Saunders J (1984) Chlorpyrifos: pharmacokinetics in human volunteers Toxicology and applied pharmacology 73:8-15
- OECD (2021) Guidance document on the characterisation, validation and reporting of Physiologically Based Kinetic (PBK) models for regulatory purposes. <https://www.oecd.org/chemicalsafety/risk-assessment/guidance-document-on-the-characterisation-validation-and-reporting-of-physiologically-based-kinetic-models-for-regulatory-purposes.pdf>. Accessed 25 May 2021
- Omwenga I, Kanja L, Zomer P, Louisse J, Rietjens IMCM, Mol H (2020) Organophosphate and carbamate pesticide residues and accompanying risks in commonly consumed vegetables in Kenya Food Additives & Contaminants: Part B:1-11
- Omwenga I, Zhao S, Kanja L, Mol H, Rietjens IMCM, Louisse J (2021) Prediction of dose-dependent in vivo acetylcholinesterase inhibition by profenofos in rats and humans using physiologically based kinetic (PBK) modeling-facilitated reverse dosimetry Archives of toxicology 95:1287-1301
- PAN Europe (2006) What substances are banned and authorised in the EU market ? <https://www.pan-europe.info/old/Archive/About%20pesticides/Banned%20and%20authorised.htm#banned>. Accessed 26th January 2021
- Pedersen TL, Smilowitz JT, Winter CK, Emami S, Schmidt RJ, Bennett DH, . . . Taha AY (2020) Quantification of non-persistent pesticides in small volumes of human breast milk with ultra-high performance liquid chromatography coupled to tandem mass-spectrometry medRxiv
- Perel P, Roberts I, Sena E, Wheble P, Briscoe C, Sandercock P, . . . Khan KS (2007) Comparison of treatment effects between animal experiments and clinical trials: systematic review Bmj 334:197
- pkCSM (2015). <http://biosig.unimelb.edu.au/pkcsml/>. Accessed 18 June 2021
- PMRA (2020) Re-evaluation Decision RVD2020-14, Chlorpyrifos and Its Associated End-use Products (Environment). <https://www.canada.ca/en/health-canada/services/consumer-product-safety/reports-publications/pesticides-pest-management/decisions-updates/reevaluation-decision/2020/chlorpyrifos.html>. Accessed 17 May 2021
- Poet TS, Kousba AA, Dennison SL, Timchalk C (2004) Physiologically based pharmacokinetic/pharmacodynamic model for the organophosphorus pesticide diazinon Neurotoxicology 25:1013-1030
- Pyati AK, Halappa CK, Pyati SA (2015) Serum basal paraoxonase 1 activity as an additional liver function test for the evaluation of patients with chronic hepatitis Journal of clinical and diagnostic research: JCDR 9:BC12
- Qin G, Zou K, Li Y, Chen Y, He F, Ding G (2016) Pesticide residue determination in vegetables from western China applying gas chromatography with mass spectrometry Biomedical Chromatography 30:1430-1440
- Quintero A, Caselles MJ, Ettiene G, De Colmenares NG, Ramírez T, Medina D (2008) Monitoring of organophosphorus pesticide residues in vegetables of agricultural area in Venezuela Bulletin of environmental contamination and toxicology 81:393-396
- Quirós-Alcalá L, Bradman A, Smith K, Weerasekera G, Odetokun M, Barr DB, . . . Nicas M (2012) Organophosphorous pesticide breakdown products in house dust and children's urine Journal of exposure science & environmental epidemiology 22:559-568

- Radwan M, Abu-Elamayem M, Shiboob M, Abdel-Aal A (2005) Residual behaviour of profenofos on some field-grown vegetables and its removal using various washing solutions and household processing *Food and Chemical Toxicology* 43:553-557
- Rietjens IMCM, Lousse J, Punt A (2011) Tutorial on physiologically based kinetic modeling in molecular nutrition and food research *Molecular nutrition & food research* 55:941-956
- Risher J, Navarro HA (1997) Toxicological profile for chlorpyrifos
- Roberts JR, Reigart JR (2013) Recognition and management of pesticide poisonings
- Russell WMS, Burch RL (1959) The principles of humane experimental technique. Methuen,
- Russum CL, LaLone CA, Villeneuve DL, Ankley GT (2014) Development of an adverse outcome pathway for acetylcholinesterase inhibition leading to acute mortality *Environmental toxicology and chemistry* 33:2157-2169
- Sams C, Cocker J, Lennard M (2004) Biotransformation of chlorpyrifos and diazinon by human liver microsomes and recombinant human cytochrome P450s (CYP) *Xenobiotica* 34:861-873
- Samsam TE, Hunter DL, Bushnell PJ (2005) Effects of chronic dietary and repeated acute exposure to chlorpyrifos on learning and sustained attention in rats *Toxicological Sciences* 87:460-468
- Sang C, Sørensen PB, An W, Andersen JH, Yang M (2020) Chronic health risk comparison between China and Denmark on dietary exposure to chlorpyrifos *Environmental Pollution* 257:113590
- Sapbamrer R, Hongsihsong S (2014) Organophosphorus pesticide residues in vegetables from farms, markets, and a supermarket around Kwan Phayao Lake of Northern Thailand *Archives of environmental contamination and toxicology* 67:60-67
- Saxena G, Kishor R, Bharagava R (2020) Bioremediation of industrial waste for environmental safety. Springer,
- Simcyp (2016) Blood to Plasma Partition Ratio (B/P). <https://members.simcyp.com/account/tools/BP/>. Accessed 27 March 2021
- Skretteberg L, Lyrån B, Holen B, Jansson A, Fohgelberg P, Siivinen K, . . . Jensen BH (2015) Pesticide residues in food of plant origin from Southeast Asia—A Nordic project *Food Control* 51:225-235
- Srivastava AK, Trivedi P, Srivastava M, Lohani M, Srivastava LP (2011) Monitoring of pesticide residues in market basket samples of vegetable from Lucknow City, India: QuEChERS method *Environmental Monitoring and Assessment* 176:465-472
- Starr TB, Greenlee WF, Neal RA, Poland A, Sutter TR (1999) The trouble with TEFs *Environmental health perspectives* 107:A492-A493
- Sudakin DL, Stone DL (2011) Dialkyl phosphates as biomarkers of organophosphates: the current divide between epidemiology and clinical toxicology *Clinical Toxicology* 49:771-781
- Swarnam T, Velmurugan A (2013) Pesticide residues in vegetable samples from the Andaman Islands, India *Environmental monitoring and assessment* 185:6119-6127
- Thundiyil JG, Stober J, Besbelli N, Pronczuk J (2008) Acute pesticide poisoning: a proposed classification tool *Bulletin of the World Health Organization* 86:205-209
- Timchalk C, Nolan R, Mendrala A, Dittenber D, Brzak K, Mattsson J (2002) A physiologically based pharmacokinetic and pharmacodynamic (PBPK/PD) model for the organophosphate insecticide chlorpyrifos in rats and humans *Toxicological Sciences* 66:34-53
- USEPA (2000) Human Health Risk Assessment for Chlorpyrifos. https://archive.epa.gov/scipoly/sap/meetings/web/pdf/hed_ra.pdf. Accessed 29th January 2021
- USEPA (2006a) Reregistration Eligibility Decision for Diazinon https://www3.epa.gov/pesticides/chem_search/reg_actions/reregistration/red_PC-057801_31-Jul-06.pdf. Accessed 26 January 2021
- USEPA (2006b) Reregistration Eligibility Decision for Profenofos
- USEPA (2011) Preliminary Human Health Risk Assessment. <https://www.regulations.gov/document?D=EPA-HQ-OPP-2008-0850-0025>. Accessed 29th January 2021
- USEPA (2013) Recognition and Management of Pesticide Poisonings. https://www.epa.gov/sites/production/files/2015-01/documents/rmpp_6thed_final_lowresopt.pdf. Accessed 25 May 2021
- USEPA (2014) Chlorpyrifos: Revised Human Health Risk Assessment for Registration Review. <https://www.regulations.gov/document?D=EPA-HQ-OPP-2008-0850-0195>. Accessed 30th

- January 2021
- USEPA (2015) Chlorpyrifos; Tolerance Revocations. <https://www.federalregister.gov/documents/2015/11/06/2015-28083/chlorpyrifos-tolerance-revocations>. Accessed 29th January 2021
- USEPA (2016a) Chlorpyrifos Revised Human Health Risk Assessment (2016). <https://www.regulations.gov/document?D=EPA-HQ-OPP-2015-0653-0454>. Accessed 30th January 2021
- USEPA (2016b) Diazinon Draft Human Health Risk Assessment for Registration Review. <https://www.regulations.gov/document?D=EPA-HQ-OPP-2008-0351-0093>. Accessed 31th January 2021
- USEPA (2016c) Profenofos: Human Health Draft Risk Assessment (ORA) for Registration Review. https://www3.epa.gov/pesticides/chem_search/cleared_reviews/csr_PC-111401_19-Oct-16.pdf. Accessed 1st February 2021
- USEPA (2020) Chlorpyrifos. <https://www.epa.gov/ingredients-used-pesticide-products/chlorpyrifos#:~:text=Chlorpyrifos%20has%20been%20used%20as,of%20active%20ingredient%20is%20corn>. Accessed 26 January 2021
- USFDA (2020) Pesticide Residue Monitoring Program Fiscal Year 2018 Pesticide Report.
- Van Toan P, Sebesvari Z, Bläsing M, Rosendahl I, Renaud FG (2013) Pesticide management and their residues in sediments and surface and drinking water in the Mekong Delta, Vietnam *Science of the Total Environment* 452:28-39
- Wang N, Jiang Q, Han L, Zhang H, Zhu B, Liu X (2019) Epidemiological characteristics of pesticide poisoning in Jiangsu Province, China, from 2007 to 2016 *Scientific reports* 9:1-8
- Wang S, Wang Z, Zhang Y, Wang J, Guo R (2013) Pesticide residues in market foods in Shaanxi Province of China in 2010 *Food Chemistry* 138:2016-2025
- Wanwimolruk S, Kanchanamayoon O, Phopin K, Prachayasittikul V (2015) Food safety in Thailand 2: Pesticide residues found in Chinese kale (*Brassica oleracea*), a commonly consumed vegetable in Asian countries *Science of the Total Environment* 532:447-455
- Watt J, Webster TF, Schlezinger JJ (2016) Generalized concentration addition modeling predicts mixture effects of environmental PPAR γ agonists *Toxicological Sciences* 153:18-27
- Watts M (2013) Reassessment of organophosphate and carbamate insecticides. <https://www.epa.govt.nz/assets/FileAPI/hsno-ar/APP201045/cbd61fbc75/APP201045-Submission-102658-M-Watts-PAN-ANZ.pdf>. Accessed 31th January 2021
- WHO (2010) Pesticide Residues in Food 2007: Toxicological Evaluations vol 184. World Health Organization,
- Wickerham EL, Lozoff B, Shao J, Kaciroti N, Xia Y, Meeker JD (2012) Reduced birth weight in relation to pesticide mixtures detected in cord blood of full-term infants *Environment international* 47:80-85
- Zhang X, Driver JH, Li Y, Ross JH, Krieger RI (2008) Dialkylphosphates (DAPs) in fruits and vegetables may confound biomonitoring in organophosphorus insecticide exposure and risk assessment *Journal of agricultural and food chemistry* 56:10638-10645
- Zheng Q, Olivier K, Won YK, Pope CN (2000) Comparative cholinergic neurotoxicity of oral chlorpyrifos exposures in preweanling and adult rats *Toxicological Sciences* 55:124-132

Chapter 2

Physiologically based kinetic modeling-facilitated reverse dosimetry to predict in vivo red blood cell acetylcholinesterase inhibition following exposure to chlorpyrifos in the Caucasian and Chinese population

Shensheng Zhao, Lenny Kamelia, Rungnapa Boonpawa, Sebastiaan Wesseling, Bert Spenkelink, and Ivonne. M.C.M Rietjens

Published in Toxicological sciences 2019; 171(1): 69-83

Abstract

Organophosphates have a long history of use as insecticides over the world. The aim of the present study was to investigate the interethnic differences in kinetics, biomarker formation, and *in vivo* red blood cell acetylcholinesterase inhibition of chlorpyrifos (CPF) in the Chinese and the Caucasian population. To this purpose, physiologically based kinetic models for CPF in both the Chinese and Caucasian population were developed, and used to study time- and dose-dependent interethnic variation in urinary biomarkers and to convert concentration-response curves for red blood cell acetylcholinesterase inhibition to *in vivo* dose-response curves in these 2 populations by reverse dosimetry. The results obtained revealed a marked interethnic difference in toxicokinetics of CPF, with lower urinary biomarker levels at similar dose levels and slower CPF bioactivation and faster chlorpyrifos-oxon detoxification in the Chinese compared with the Caucasian population, resulting in 5- to 6-fold higher CPF sensitivity of the Caucasian than the Chinese population. These differences might be related to variation in the frequency of single-nucleotide polymorphisms for the major biotransformation enzymes involved. To conclude, the interethnic variation in kinetics of CPF may affect both its biomarker-based exposure assessment and its toxicity and risk assessment and physiologically based kinetic modeling facilitates the characterization and quantification of these interethnic variations.

1. Introduction

Organophosphate pesticides (OPs) are an important class of crop protection agents used worldwide (Stauber et al., 2016). OPs and their metabolites have been detected in human urine, blood, serum, and breast milk (Drevenkar et al., 1994; Hardt and Angerer, 2000; Liu et al., 2014; Naksen et al., 2016; Zhang et al., 2014), reflecting human exposure to these pesticides. Upon acute exposure, the activated form of OPs can covalently bind to and inhibit acetylcholinesterase (AChE), the enzyme responsible for hydrolysis of the neurotransmitter acetylcholine (ACh) (Flaskos, 2014). This inhibition causes accumulation of ACh in the synaptic cleft, resulting in overstimulation of the ACh receptor ultimately causing cholinergic dysfunction, paralysis, and respiratory failure (Eaton et al., 2008; Hung et al., 2015). Chronic low dose exposure to OPs has been associated with poorer neurobehavioral development in infants/school children and poorer intellectual development in 7-year-old children (Bouchard et al., 2011; González-Alzaga et al., 2014; Wang et al., 2012).

In the past decades, physiologically based kinetic (PBK) models have been developed for a few OPs, i.e. chlorpyrifos (CPF) (Bouchard et al., 2005; Lu et al., 2009; Mosquin et al., 2009; Timchalk et al., 2002) and diazinon (Poet et al., 2004), in order to better predict the internal exposure level and risk upon exposure to OPs (Bouchard et al., 2005; Foxenberg et al., 2011; Lu et al., 2009; Mosquin et al., 2009; Nolan et al., 1984; Timchalk et al., 2002). These PBK models can be used for reverse dosimetry, enabling translation of urinary biomarker data to internal or external exposure levels, whereas in theory, also enabling conversion of in vitro concentration-response curves for AChE inhibition to in vivo dose-response curves for AChE inhibition. However, when developing these PBK models, interethnic differences have not yet been taken into account. Biomonitoring studies have reported OP metabolite levels in maternal urine in China to be higher than those in maternal urine in developed countries (Wang et al., 2012), and interethnic differences in bioactivation and detoxification have already been reported for other compounds than OPs (Ning et al., 2017; Zhang et al., 1990). Hence, it is of importance to include the interethnic differences in kinetics when developing PBK models for CPF in human. To date, several PBK models have been developed for CPF in the Caucasian population (Bouchard et al., 2005; Lu et al., 2009; Mosquin et al., 2009; Timchalk et al., 2002). Knowing that there is no PBK model available that is specifically defined for the Chinese population, the aim of the present study was to investigate, via PBK modeling, the interethnic differences between the Chinese and the Caucasian population in kinetics, biomarkers of

exposure, and predicted in vivo red blood cell (RBC) AChE inhibition using CPF as the model OP compound.

In present study, CPF was used as model OP because there are available kinetic data for evaluating the performance of the PBK models (Eaton et al., 2008; Griffin et al., 1999; Nolan et al., 1984; Brzak et al., 2000; Timchalk et al., 2002; Bouchard et al., 2005). In humans, CPF will be either detoxified to 3,5,6-trichloro-2-pyridinol (TCPy) and diethyl thiophosphate (DETP) or activated to the corresponding active oxon form chlorpyrifos-oxon (CPO), which inhibits AChE (Figure 1). These 2 pathways have been demonstrated to occur mainly in the liver (Timchalk et al., 2002). Conversion of CPF is catalyzed by cytochromes P450 (CYP450), with CYP2B6 being the most active CYP450 for conversion of CPF into CPO, and CYP2C19 being the most active CYP for conversion of CPF into TCPy and DETP, whereas CYP3A4 is involved in both pathways (Foxenberg et al., 2007; Tang et al., 2001). The detoxification of CPO is catalyzed by A-esterases, with paraoxonase (PON 1) as the major A-esterase involved, resulting in formation of TCPy and diethyl phosphate (DEP) (Figure 1) (Furlong et al., 1989; Timchalk et al., 2002). B-esterase in for example liver, blood, and brain including AChE, butyrylcholinesterase (BChE) and carboxylesterase (CaE) can be bound and inhibited by CPO (Timchalk et al., 2002; Wagner, 1999).

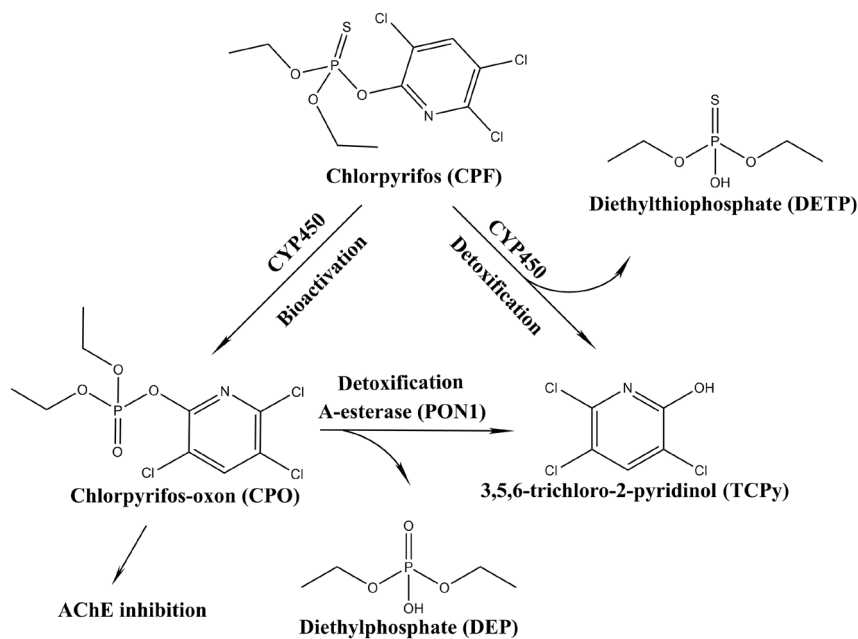


Fig 1. Metabolic pathways for bioactivation and detoxification of CPF (Smith et al., 2011). AChE, acetylcholinesterase; CYP450, cytochrome P450.

The inhibition of RBC AChE activity has been used as the surrogate endpoint for deriving points of departure (POD) in risk assessment of CPF, such as a benchmark dose (BMD) or a no observed adverse effect level (NOAEL). The rationale for using RBC AChE inhibition as indicator of CPF exposure is based on the fact that RBC AChE is more sensitive and easier to sample compared with AChE in other target organs like brain, spinal cord, and the peripheral nervous system (EPA, 2011). Moreover, it is also known that there is less variation among individuals in the enzyme activity of RBC AChE than plasma BChE (Brock and Brock, 1990; Lefkowitz et al., 2007). Thus, in the present study, the concentration-dependent RBC AChE inhibition by CPO (Eyer et al., 2009) was used as the surrogate endpoint to define the in vivo dose-response curves for RBC AChE inhibition in the 2 populations, Chinese and Caucasian, upon CPF exposure.

2. Materials and methods

2.1 Materials

2.1.1 Chemicals

Chlorpyrifos and TCPy were purchased from Sigma-Aldrich (Zwijndrecht, The Netherlands). Chlorpyrifos-oxon was purchased from TRC-Canada (Toronto, Ontario, Canada). Tetraisopropyl pyrophosphoramidate (iso-OMPA) and diisopropyl ether (DIPE) were purchased from Sigma-Aldrich (Zwijndrecht, The Netherlands). Magnesium chloride hexahydrate ($MgCl_2 \cdot 6H_2O$), ethylenediaminetetraacetic acid disodium salt dihydrate (EDTA), dipotassium hydrogen phosphate (K_2HPO_4), trifluoroacetic acid (TFA), hydrochloric acid (HCl), perchloric acid ($HClO_4$), dimethylsulfoxide (DMSO), and calcium chloride dihydrate ($CaCl_2 \cdot 2H_2O$) were purchased from VWR International (Amsterdam, The Netherlands). Acetonitrile (ACN, UPLC/MS grade) and methanol (UPLC/MS grade) were purchased from Biosolve (Valkenswaard, The Netherlands). Reduced nicotinamide adenine dinucleotide phosphate (NADPH) was obtained from Sigma-Aldrich (Zwijndrecht, The Netherlands).

2.1.2 Human liver microsomes

Caucasian liver microsomes (pooled from 20 donors, mixed gender) were purchased from Corning (Amsterdam, The Netherlands) and Chinese liver microsomes (pooled from 20 donors, mixed gender) were purchased from Pre-TOX (Wuhan, China).

2.2 In Vitro Incubations to Derive the Kinetic Parameters for the PBK Model

2

Human liver microsomal incubations for bioactivation and detoxification of CPF by CYP450 were optimized to be linear in metabolite formation with time and amount of microsomal protein (data not shown). The incubations were carried out in 50 mM phosphate buffer (pH 7.4) containing (final concentrations) 5 mM MgCl₂, 1 mM EDTA (A-esterase PON1 inhibitor), 50 μM iso-OMPA (B-esterase inhibitor), 1 mM NADPH (CYP450 cofactor), and CPF (at final concentrations ranging from 5 to 100 μM, added from 100 times concentrated stock solutions in DMSO). Control incubations were performed without the addition of NADPH. After 1 min preincubation, the reaction was initiated by adding 5 μl of either Caucasian or Chinese liver microsomes (final concentration 0.5 mg/ml) and incubated for 15 min (Caucasian) or 30 min (Chinese) in a 37°C water bath. The total volume of the incubation mixtures was 200 μl. The reaction was terminated by the addition of 20 μl ice cold 10% (vol/vol) HClO₄.

The PON1-catalyzed metabolism of CPO was measured in the in vitro liver microsomal incubations as follows. Preliminary experiments were conducted to define the optimal incubation conditions that are linear in time and with the liver microsomal concentration (data not shown). The kinetic incubations were carried out in 50 mM Tris-HCl (pH 7.4) containing 2 mM CaCl₂ (to stimulate the PON1 activity) (Carr et al., 2015), and CPO (at a final concentration range of 25–1500 μM, added from 100 times concentrated stock solutions in DMSO). After 1 min preincubation, the reaction was initiated by adding either 5 μl of Caucasian (final concentration 0.5 mg/ml) or 2.5 μl of Chinese liver microsomes (final concentration 0.25 mg/ml) and incubated for 5 min in a 37°C water bath. Incubations in the absence of microsomes were performed as control. The total volume of the incubation mixtures was 200 μl. The reaction was terminated by the addition of 20 μl ice cold 10% (vol/vol) HClO₄ and samples were kept on ice.

Extraction of metabolites was conducted prior to UPLC analysis. To this end, the organic solvent DIPE was added to the ice-cold incubation mixtures. Afterwards, the incubation mixtures were mixed well by vortexing and the upper layer that contained CPF and its metabolites was collected and transferred into a glass tube. The extraction process was conducted 3 times, and the collected DIPE fractions were combined. The extracts were then evaporated to dryness under a stream of nitrogen (N₂). Finally, the extracts containing CPF and its metabolites were redissolved in 100 µl methanol and subsequently used for the UPLC analysis.

It is worth to note that microsomal incubations are well accepted and also validated to define kinetic parameters for metabolism and clearance in PBK model (Al-Subeihi et al., 2012; Lu et al., 2009; Mosquin et al., 2009; Ning et al., 2017; Punt et al., 2008,, 2009; Timchalk et al., 2002). Furthermore, experimental data shown that kinetic data derived from microsomal incubations and hepatocyte incubations are comparable as Di et al. (2012) reported that the intrinsic clearance for compounds predominantly mediated by CYP450 obtained from microsomal incubations are comparable with that obtained from hepatocyte incubations.

2

2.3 UPLC Analysis

All redissolved extracts from microsomal incubations of CPF were analyzed by a Waters Acquity UPLC H₂ class system that consisted of a quaternary solvent manager, a sample manager, and a photodiode array detector, equipped with a Water Acquity UPLC BEH C18 column (1.7 µM, 2.1 × 50 mm) and Waters Xbridge UPLC BEH C18 precolumn (1.7 µM, 2.1 × 5 mm). The temperature of the column was set at 40°C and the auto-sampler at 10°C during the UPLC analysis. The mobile phases used for the analysis consisted of (A) 0.1% TFA in nanopure water and (B) 100% ACN. A gradient elution at a flow rate of 0.6 ml/min was applied for the analysis with the initial condition of 90% A:10% B (vol/vol). The gradient program was set as follows: the starting condition was 90:10 (A:B), changing to 0:100 (A:B) from 0 to 6 min and was maintained for 30 s, and then changed to 100:0 (A:B) in 30 s and was maintained for 1 min. After which, the starting condition were reset from 8 to 8.1 min, and the column was equilibrated at the starting condition of 90:10 (A:B) until 9.5 min. The injection volume for each sample was 3.5 µl. Under these conditions, the retention times of CPF, CPO, and TCPy were 4.8, 3.6, and 2.5 min, respectively. The amount of CPF, CPO, and TCPy was

quantified by integrating the peak areas at 299 nm using calibration curves that were prepared using the commercially available standards.

2.4 Data Analysis

Kinetic parameters including the apparent maximum velocity (V_{max} ; expressed in nmol/min/mg microsomal protein) and the apparent Michaelis–Menten constant (K_m ; in μM) for bioactivation of CPF and detoxification of CPF and CPO were obtained by fitting the data using GraphPad Prism 5 software for Windows, version 5.04 (San Diego, California) to the standard Michaelis–Menten equation:

$$v = \frac{V_{max} * [S]}{(K_m + [S])}$$

in which the S represents the concentration of substrate in μM .

2.5 Physiologically based kinetic (PBK) model

2.5.1 Model structure

Figure 2 illustrates the structure of the CPF PBK model for both the Chinese and Caucasian population. The model was developed based on the model reported by Timchalk et al. (2002) with some modifications. The model contained separated compartments for the gastrointestinal tract (GI-tract), blood, fat, liver, slowly perfused tissue (muscle, skin, and bone), and rapidly perfused tissue. The bioavailability of CPF upon oral exposure was included by taking the fractional absorption (f_a) into account. This f_a was found to vary across human volunteer studies, amounting to 0.22 (22% of the oral dose being absorbed) (Bouchard et al., 2005), 0.224 (Timchalk et al., 2002), 0.70 (Nolan et al., 1984), and 0.93 (Bouchard et al., 2005; Griffin et al., 1999), respectively, in part depending on the form of CPF administration (Timchalk et al., 2002). When modeling the data, the f_a values reported by Timchalk et al. (2002; $f_a = 0.224$) and Nolan et al. (1984; $f_a = 0.70$) were used, and the mean of those 2 f_a values, which is 0.462, was also included. First-order kinetics was used to describe the absorption of CPF by the GI tract with an absorption rate constant of 0.46/h (Bouchard et al., 2005). The absorbed CPF was assumed to be transferred to the liver compartment without intestinal biotransformation based on the fact that intestinal CPF biotransformation was reported to be limited compared with that in the liver (Leoni et al., 2012). Furthermore,

CYP450-mediated conversion of CPF was assumed to occur only in the liver because liver is known to be the main organ for CYP450-mediated biotransformation of CPF (Leoni et al., 2012). This metabolism resulted in formation of TCPy and DETP, and of CPO (Figure 1). Based on a preliminary experiment (data not shown), the conversion of CPF by A-esterase (PON1) appeared to be negligible compared with the CYP450-catalyzed reaction and thus was not included in the model. The PBK model also contained a sub-model describing the kinetics of CPO. The formation of CPO from CYP450-mediated conversion of CPF in the liver compartment provided the input of CPO for this CPO sub-model, in which CPO was predicted to be further converted to TCPy and DEP in both the liver and blood compartment mediated by A-esterase (PON1). The cumulative urinary excretion of TCPy and of the dialkylphosphate (defined as the sum of DEP and DETP) was described by applying first-order rate equations with the first-order rate constants amounting to 0.026/h and 0.199/h, respectively (Bouchard et al., 2005). The Rosenbrock's algorithm for stiff systems was used to code the differential equations and the mass balance in Berkeley Madonna software (Macey and Oster, UC Berkeley, California). The PBK model differential equations are provided in the Supplementary Data I.

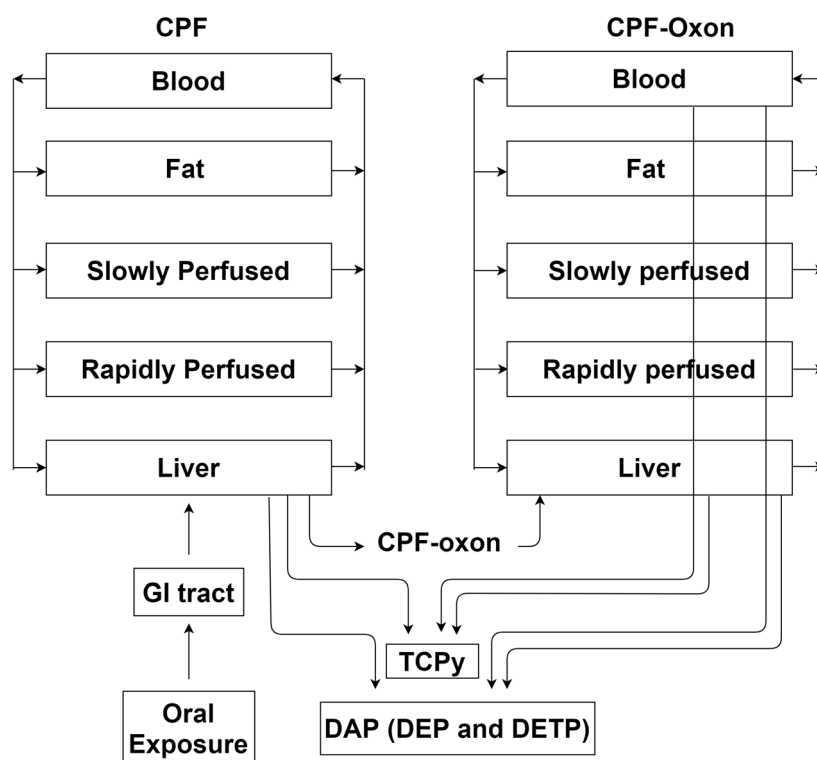


Fig 2. Schematic diagram of the PBK model for CPF (Timchalk et al., 2002) in the Chinese and Caucasian population, consisting of 2 models including one for CPF (left) and one submodel for CPO (right). GI tract, gastrointestinal tract.

2.5.2 Model parameters

The physiological parameters for both the Chinese and Caucasian population were collected from the literature (Brown et al., 1997; NHFPC, 2007a,b, 2014) and are presented in Table 1. The physico-chemical parameters (tissue:blood partition coefficients) for CPF and CPO, also presented in Table 1, were determined based on clogP using ChemDraw Professional 16.0 software (CambridgeSoft), using the method described by DeJongh et al. (1997). The kinetic parameters for conversion of CPF and CPO in the liver were determined in the present study and are summarized in Table 2 and presented in some more details in the Results section. For PON1-mediated detoxification of CPO to TCPy in blood, the V_{max} expressed in $\mu\text{mol/h/kg bw}^{0.75}$ for the Caucasian population, obtained from plasma enzymatic incubations (Furlong et al., 1989; Mosquin et al., 2009), was multiplied by the $\text{bw}^{0.75}$ of the Chinese and Caucasian, respectively, to obtain the corresponding value for both populations expressed in $\mu\text{mol/h}$. A hepatic microsomal protein scaling factor of 32 mg microsomal protein/g liver (Al-Malahmeh et al., 2017; Barter et al., 2007) was applied to scale the apparent V_{maxc} from $\mu\text{mol/min/mg}$ microsomal protein to the V_{max} expressed in $\mu\text{mol/min/g}$ liver. Furthermore, the V_{max} was expressed in $\mu\text{mol/h/kg}$ liver.

Table 1. Summary of physiological and physico-chemical parameters for the PBK models for CPF and its metabolites in the Caucasian and Chinese population (Brown et al., 1997; DeJongh et al., 1997; NHFPC, 2007 a,b, 2014)

Model parameters	Caucasian	Chinese
Physiological parameters		
Body weight (kg)	70	58.5
Percentage of body weight		
Liver	2.6	2.3
Fat	21.4	18.4
Rapidly perfused	5.4	6.9
Slowly perfused	58	57.3
Blood	7.9	7.9
Flow(l/h)		

Inter-ethnic differences in red blood cell acetylcholinesterase inhibition of chlorpyrifos

Cardiac output	347.9	327
Percentage of cardiac output		
Liver	22.7	26.3
Fat	5.2	6.8
Rapidly perfused	43	42.4
Slowly perfused	29.1	24.5
Tissue: blood partition coefficients for CPF		
Liver	8.1	8.1
Fat	142	142
Rapidly perfused	8.1	8.1
Slowly perfused	5.2	5.2
Tissue: blood partition coefficients for CPO		
Liver	4.9	4.9
Fat	119.3	119.3
Rapidly perfused	4.9	4.9
Slowly perfused	3.3	3.3

2

Table 2. Summary of kinetic parameters (K_m , unscaled/scaled V_{max}) and catalytic efficiency (V_{max}/K_m), for metabolism of CPF and CPO (Barter et al., 2007; Brown et al., 1997; Furlong et al., 1989; Mosquin et al., 2009; NHFPC, 2007a)

Pathways	Caucasian	Chinese
CPF to CPO (Liver)		
K_{m1} (μM)	28.59 ± 6.60	44.91 ± 34.90
In vitro V_{max1c} (nmol / min / mg microsomal protein)	0.156 ± 0.014	0.055 ± 0.019
In vitro Catalytic efficiency (V_{max1c} / K_{m1}) ^{a,b}	5.5	1.2
In vivo scaled V_{max1} ($\mu\text{mol} / \text{h} / \text{kg liver}$) ^c	300 ± 27	106 ± 36
In vivo scaled Catalytic efficiency (V_{max1} / K_{m1}) ^d	10.49	2.36
CPF to TCPy (Liver)		

Km2 (μM)	4.33 ± 0.56	3.16 ± 0.745
In vitro Vmax2c (nmol / min / mg microsomal protein)	0.234 ± 0.006	0.093 ± 0.004
In vitro Catalytic efficiency (Vmax2c / Km2) ^{a b}	54.0	29.4
In vivo scaled Vmax2 ($\mu\text{mol} / \text{h} / \text{kg liver}$) ^c	449 ± 12	179 ± 8
In vivo scaled Catalytic efficiency (Vmax2 / Km2) ^d	103.7	56.6

CPO to TCPy (Liver)

Km3 (μM)	627.90 ± 165.00	660.70 ± 167.00
In vitro Vmax3c (nmol / min / mg microsomal protein)	37.98 ± 4.33	111.90 ± 12.51
In vitro Catalytic efficiency (Vmax3c / Km3) ^{a b}	60.5	169.4
In vivo scaled Vmax3 ($\mu\text{mol} / \text{h} / \text{kg liver}$) ^c	72922 ± 8314	214848 ± 24019
In vivo scaled Catalytic efficiency (Vmax3 / Km3) ^d	116.1	325.2

CPO to TCPy (Blood)

Km4 (μM)	75	75
Vmax4c ($\mu\text{mol} / \text{h} / \text{kg}^{0.75}$ body weight)	4.4	4.4
Catalytic efficiency (Vmax4c / Km4) ^e	0.05867	0.05867
Vmax4 ($\mu\text{mol} / \text{h}$) ^f	106.48	93.28
Catalytic efficiency (Vmax4 / Km4) ^g	1.41973	1.24373

^a $\mu\text{l} / \text{min} / \text{mg}$ microsomal protein

^b $\text{Vmaxc} / \text{Km} * 1000$

^c $\text{Vmax} = \text{Vmaxc} / 1000 * 60 * 32 * 1000$, where the 32 is the scaling factor to scale the Vmaxc from nmol/min/mg microsomal protein to nmol/min/g liver, 1000 is for changing unit from nmol to μmol , the 60 is for changing the unit from min to h and 1000 is for changing the unit from g to kg (liver)

^d $1 / \text{h} / \text{kg liver}$

^e $1 / \text{h} / \text{kg}^{0.75}$ body weight

^f $\text{Vmax4} (\mu\text{mol}/\text{h}/\text{kg liver}) = \text{Vmax4c} * \text{body weight}^{0.75}$, the body weight could be either the Caucasian body weight (70 kg) or the Chinese body weight (58.5kg)

^g $1 / \text{h}$

2.5.3 Model validation

To validate the model, the PBK model-predicted blood concentration of TCPy and the cumulative urinary amount of TCPy were compared with reported in vivo data (Bouchard et al., 2005; Nolan et al., 1984; Timchalk et al., 2002).

2.5.4 Sensitivity analysis

The impact of each parameter on the model output (in this study especially the blood concentrations of CPO) was estimated by performing a sensitivity analysis. Normalized sensitivity coefficient (SC) was determined based on the following equation:

$$SC = \frac{(C' - C)}{(P' - P)} * \left(\frac{P}{C}\right)$$

in which P represents the parameter value in the PBK model and P' represents the parameter value with a 5% increase (Evans and Andersen, 2000). Similarly, C is the output of the model with the original model parameter value and C' the model output with 5% increase in the model parameter value. Only parameters with SC > 0.15 (absolute value) are presented in the current manuscript (Figure 7).

2

2.6 Reverse Dosimetry

2.6.1 Derivation of a concentration-response curve for RBC AChE inhibition

In the present study, the concentration-response curve for CPO-mediated RBC AChE inhibition reported by Eyer et al. (2009) was used, who quantified the level of AChE inhibition upon incubating plasma samples from CPF-poisoned patients (with quantified level of CPO) with RBC from an unexposed donor to determine the level of AChE inhibition (Eyer et al., 2009).

2.6.2 Conversion of concentration-response curves to in vivo dose-response curves for RBC AChE inhibition

The concentration-response curve for RBC AChE inhibition by CPO in human was obtained from Eyer et al. (2009), and used as input to quantify the maximum blood concentration (C_{max}) of CPO in the PBK models for calculating the corresponding dose levels. By performing this calculation for all the concentrations, the concentration-response curve for RBC AChE inhibition was converted to an in vivo dose-response curve for CPF-induced RBC AChE inhibition. Given that the concentrations in the concentration-response curve represented the total concentration of CPO (Eyer et al., 2009; Heilmair et al., 2008), the concentration values

of the concentration-response curve could be directly used as input in the PBK models. By performing the reverse dosimetry using the PBK model for the Caucasian and Chinese population, *in vivo* dose-response curves for both ethnic groups were predicted.

2.6.3 Validation of predicted dose-response curves for RBC AChE inhibition

To validate the performance of the PBK model-facilitated reverse dosimetry approach, the predicted dose-response curve for RBC AChE inhibition upon exposure to CPF for the Caucasian population was compared with available *in vivo* data (EPA, 1999; Timchalk et al., 2002). Evaluation of the Chinese PBK model was based on the evaluation of the Caucasian model combined with the fact that both models were defined in the same way.

2

2.7 Derivation of BMD and BMDL

The predicted dose-response curves were used to derive PODs for CPF risk assessment for these 2 populations. Because the data were not suitable for BMD modeling, the effective dose (ED)_{10/20} value for CPF in the Chinese and Caucasian was defined at 10% or 20% inhibition of RBC AChE. Subsequently, taking into account that a BMDL should not be more than a factor 3 below a BMD value to provide an adequate POD, the obtained ED_{10/20} values were divided by 3 to obtain POD values that could be compared with the PODs reported by The European Food Safety Authority (EFSA, 2014) and EPA (BfR, 2012; Fan, 2014; Koshlukova and Reed, 2014).

3. Results

3.1 In Vitro Metabolism of CPF and CPO

The CYP450-mediated conversion of CPF to CPO and TCPy was measured in incubations with both Chinese and Caucasian liver microsomes. No metabolites were detected in control incubation performed in the absence of NADPH. The PON1-mediated conversion of CPO to TCPy was detected in both population, Chinese and Caucasian, of liver microsomal incubations, whereas in the absence of liver microsomes, some TCPy was detected, mainly ascribed to an impurity in the CPO starting material (data not shown). Thus, results obtained in the presence

of liver microsomes were corrected for the TCPy detected in control incubation without microsomes.

The concentration-dependent increase in metabolite formation following incubations of CPF and CPO with both Chinese and Caucasian liver microsomes is depicted in Figure 3. The kinetic parameters K_m and V_{max} derived from these results as well as the catalytic efficiency, calculated as V_{max}/K_m , are presented in Table 2.

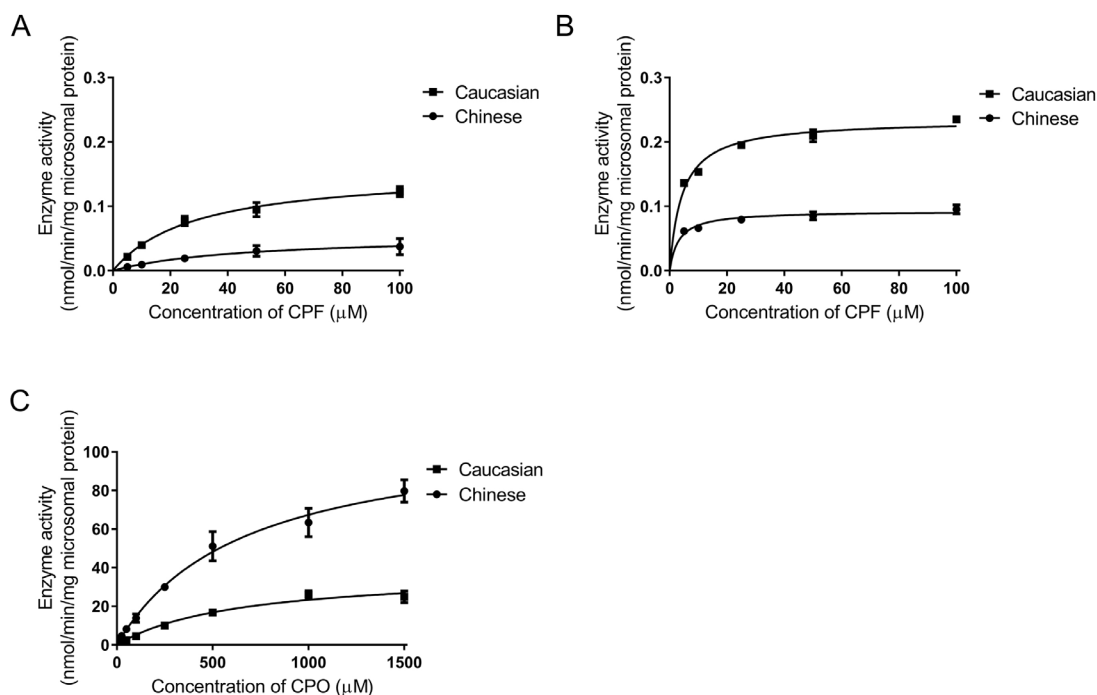


Fig 3. Comparison of the concentration-dependent rate of conversion of (A) CPF to CPO, (B) CPF to TCPy, and (C) CPO to TCPy, in incubations with Caucasian (solid squares) and Chinese (solid circles) liver microsomes. Results represent data from 3 independent experiments and are presented as mean \pm SEM.

The results presented in Figure 3 and Table 2 indicate that there is a difference in the catalytic efficiency for conversion of CPF and CPO by the Chinese and Caucasian population. The catalytic efficiency for bioactivation of CPF to CPO was around 4.5-fold less efficient in incubations with Chinese than with Caucasian liver microsomes, due to a 2.8-fold lower V_{max} and a 1.6-fold higher K_m (Table 2). However, Chinese liver microsomes were only 2 times less efficient than Caucasian liver microsomes in detoxification of CPF to TCPy. In addition, Chinese liver microsomes appeared to be 2.8 times more efficient in the detoxification of CPO into TCPy than Caucasian liver microsomes.

3.2 PBK Model Validation

The developed PBK model of CPF was evaluated against in vivo data from human volunteer studies in the Caucasian population (Bouchard et al., 2005; Nolan et al., 1984; Timchalk et al., 2002). The model was first evaluated using the data from Nolan et al. (1984). Figure 4A presents the model-predicted and reported amount of TCPy eliminated in urine using a f_a of 0.70, as reported by Nolan et al. (1984). In addition, Figure 4B compares the model-predicted blood concentration of TCPy and the reported data. These results indicate that the predictions made by the newly developed PBK model match the reported data quite well, and in a manner comparable with the model reported before by Lu et al. (2009). However, a best fit between model-predicted TCPy blood concentration and in vivo data could be achieved (Figure 4) by increasing the volume of distribution for TCPy (V_d) from 5.53 l (setting the V_d equal to the average human blood volume (V_B ; Brown et al., 1997)) to 15 l. This 15 l was obtained by fitting the model to in vivo data (Nolan et al., 1984) similar as done by others (Mosquin et al., 2009; Timchalk et al. 2002). Together these data illustrate how the currently developed PBK model can adequately match the reported in vivo data.

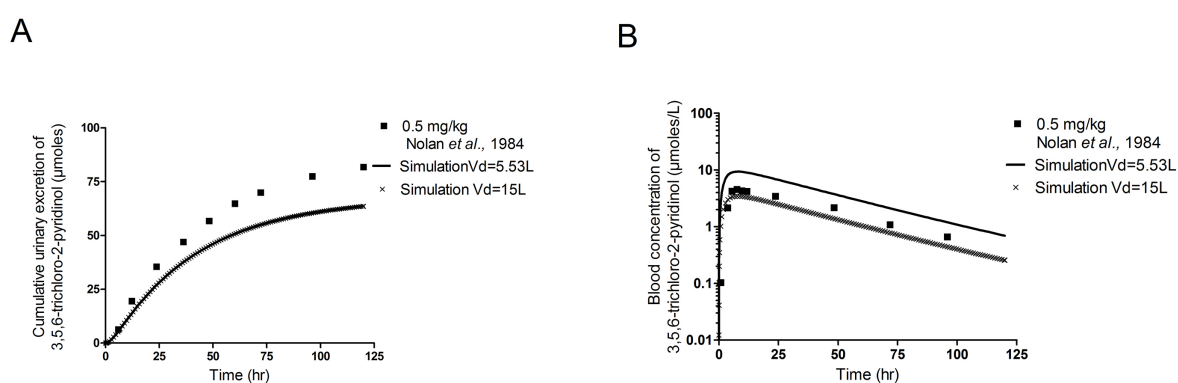


Fig 4. Comparison of PBK model-predicted and experimentally determined time-dependent (A) cumulative urinary excretion of TCPy and (B) blood concentrations of TCPy in Caucasian volunteers upon oral administration of 0.5 mg CPF/kg bw (Nolan et al., 1984). The simulations were performed using a f_a equal to 0.70, and either $V_d = 5.53$ l (solid line) or $V_d = 15$ l (cross line), whereas the squares represent the values from the human volunteer study (Nolan et al., 1984).

In a next step, a comparison was made to the data reported by Timchalk et al. (2002) and Lu et al. (2009) to further evaluate the developed-PBK model (Figure 5). The application of $f_a = 0.224$, as reported by this literature, was set in the defined PBK model for the Caucasian population, resulting in a good match between predicted and experimental human in vivo data (Lu et al., 2009; Timchalk et al., 2002). Also, the model adequately predicted the blood

concentration of TCPy with 3-fold deviation from the data reported by Timchalk et al. (2002). Using a Vd of 15 l, fitting this model parameter Vd to the in vivo data as done by Timchalk et al. (2002) and Mosquin et al. (2009), a better fit was even obtained (see Figure 5).

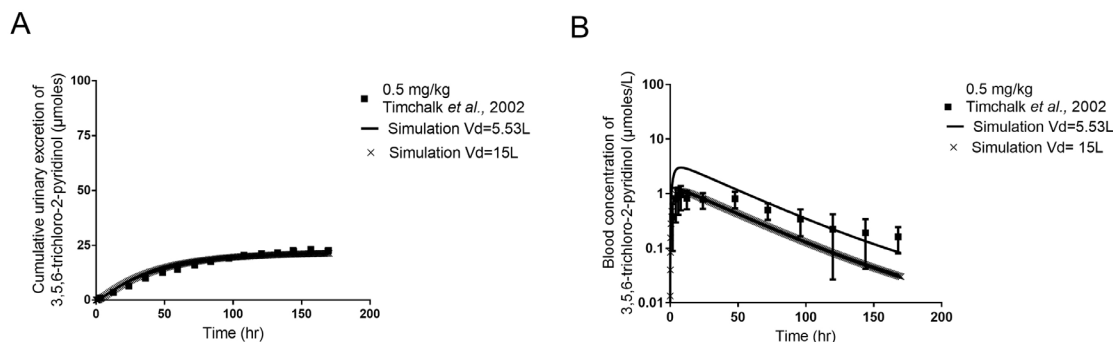


Fig 5. Comparison of PBK model-predicted and experimentally determined time-dependent (A) cumulative urinary excretion of TCPy (Lu et al., 2009; Timchalk et al., 2002) and (B) blood concentrations of TCPy in Caucasian volunteers upon oral administration of 0.5 mg CPF/kg bw (Timchalk et al., 2002). The simulations were performed using $fa = 0.224$, and either $Vd = 5.53$ l (solid line) or $Vd = 15$ l (cross line), whereas the squares symbols represent the values from the human volunteer study (Timchalk et al., 2002).

Finally, the performance of the model was evaluated based on the experimental data originally from Brzak (2000) but reported by Bouchard et al. (2005) using a fa of 0.22 (Bouchard et al., 2005) (Figure 6). The results reveal that also for this data set, the newly developed PBK model closely predicted both the cumulative amount of TCPy eliminated in urine and the blood concentration of TCPy at all 3 dose levels tested. The predicted TCPy concentration in blood were around 3-fold higher than what was actually observed in vivo. As observed from the other data sets, these matches could be further improved by changing the value of Vd to 15 l, based on fitting this model parameter to the in vivo data as done by others (Mosquin et al., 2009; Timchalk et al. 2002) (see Figure 6).

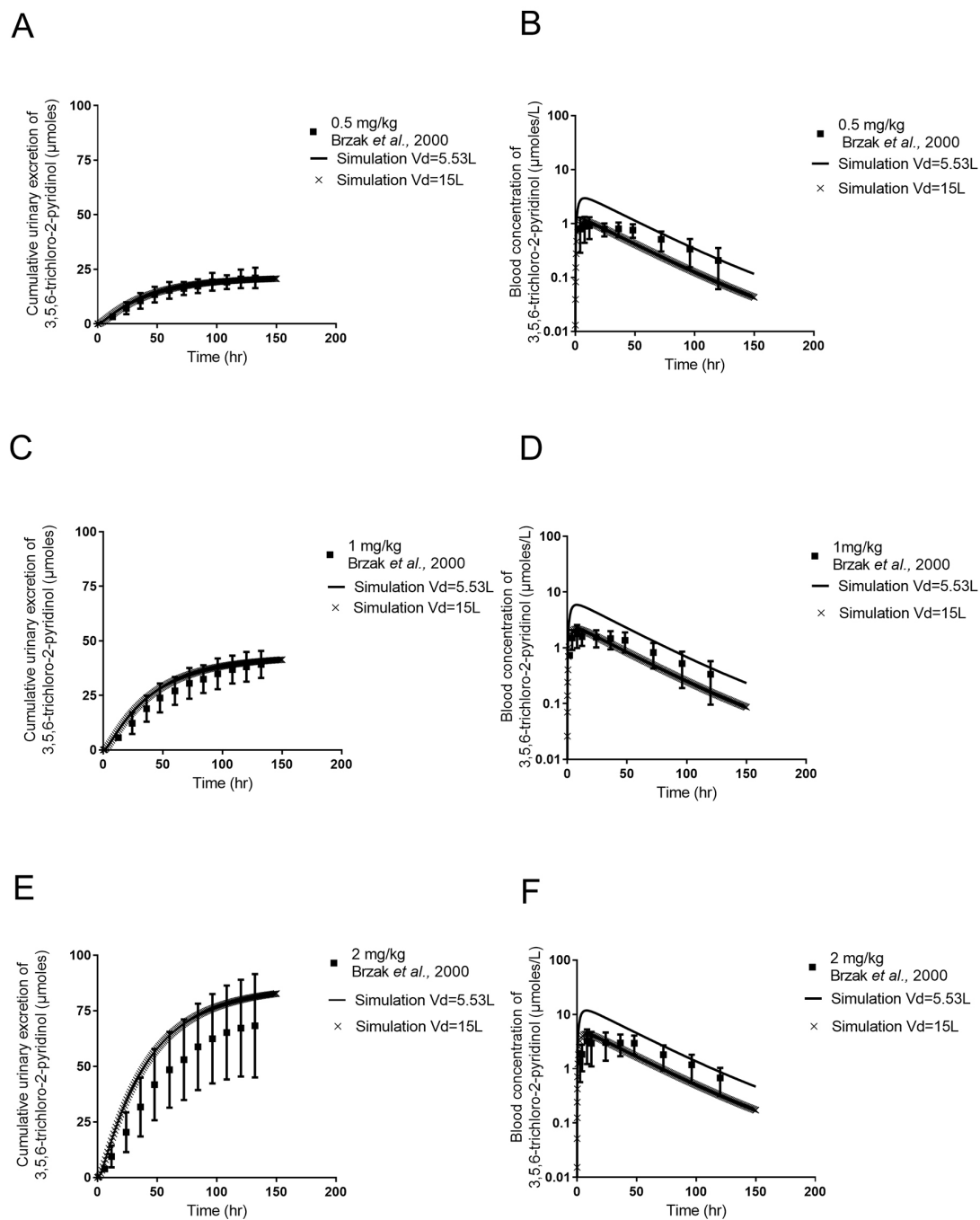


Fig 6. Comparison of PBK model-predicted and experimentally determined time-dependent cumulative urinary excretion of TCPy at an oral dose of (A) 0.5 mg CPF/kg bw, (C) 1.0 mg CPF/kg bw, and (E) 2 mg CPF/kg bw, and of PBK model predicted and experimentally determined blood concentration of TCPy at an oral dose of (B) 0.5 mg CPF/kg bw, (D) 1 mg CPF/kg bw, and (F) 2 mg CPF/kg bw. The simulations were performed using $f_a = 0.22$, and either $V_d = 5.53$ l (solid line) or $V_d = 15$ l (cross line), whereas the squares represent the values taken from Bouchard et al. (2005) which originally from Brzak (2000).

Although some underestimation is still observed at later time points after reaching the maximum TCPy blood concentration when comparing our prediction with the in vivo data from Timchalk et al. (2002) as well as with the data from Brzak (2000) after changing the Vd to 15 l. These inter-study differences are mainly caused by the TCPy elimination rate constant (Ke) that we used because the value of Ke (0.026/h) that we used in our model was obtained from Nolan et al. (1984) but not obtained by fitting model to data from Nolan et al. (1984) as what others did (Ke = 0.017/h in Timchalk et al., 2002 and Ke = 0.03820/h in Mosquin et al., 2009). Thus, these fits can be improved even further if we fit Ke (0.019/h) in the model to in vivo data Nolan et al. (1984) in line with what others did (Mosquin et al., 2009; Timchalk et al., 2002) (Supplementary Data V and VI).

In our later prediction, we assumed the Vd for TCPy to be equal to human blood volume (5.53 l, Brown et al., 1997), which has physiological meaning, and Ke equal to 0.026/h. Nevertheless, a better match between the model prediction and in vivo data for the blood concentration of TCPy could be obtained when the Vd value was increased to 15 l. The match between the model prediction and in vivo data sets from Timchalk et al. (2002) and Brzak (2000) can be further improved by changing Ke to 0.019/h (both of these 2 parameters were obtained by fitting the model to the in vivo data Nolan et al. (1984) as done by others (Mosquin et al., 2009; Timchalk et al. 2002). However, it is important to note as well that changing the value of Vd and value of Ke did not affect the prediction of the CPO concentration in blood, and thus also did not affect the resulting prediction for AChE inhibition (data not shown).

Due to a lack of kinetic data for Chinese subjects, evaluation of the performance of the PBK model for CPF in the Chinese population was based on this validation of the Caucasian model.

3.3 Sensitivity Analysis

A sensitivity analysis was performed at a dose of 0.5 mg CPF/kg bw and of 180 mg CPF/kg bw (Timchalk et al., 2002) to determine the impact of each parameter on the predicted blood Cmax of CPO in the Chinese and the Caucasian PBK models. Figure 7 presents the values for which the SC was higher than 0.15 (absolute value). Comparing the results of the sensitivity analysis for the Chinese PBK model with that of the Caucasian PBK model, a similar result was obtained at both dose levels. For both the Chinese and the Caucasian model, the prediction of the Cmax of CPO appeared to be mainly affected by the kinetic parameters for hepatic CPO

formation as well as the kinetic parameters for hepatic detoxification of CPO to TCPy, although the f_a also significantly affected the C_{max} of CPO (Figure 7A). In addition, the C_{max} of CPO was also influenced by blood flow from various compartments (liver to blood, rapidly perfused tissue to blood and slowly perfused tissue to blood). For physiological parameters, volume of liver was found to have the largest impact in both the Caucasian and the Chinese model. At the higher dose of 180 mg/kg bw, similar results were obtained except for a somewhat lower impact of the kinetic parameters for conversion of CPF to TCPy.

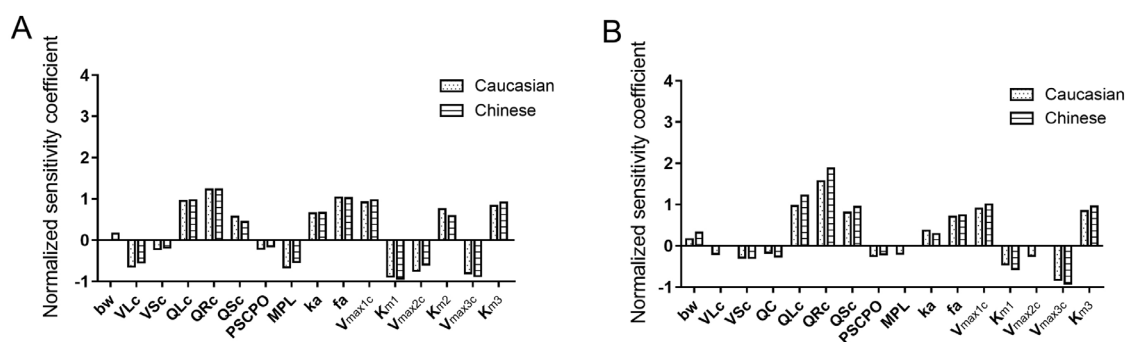


Fig 7. Sensitivity analysis representing the influence of model parameters on the predicted blood C_{max} of CPO in the Caucasian and the Chinese population at a dose of (A) 0.5 mg CPF/kg bw and (B) 180 mg CPF/kg bw. The parameters are stand for bw = body weight, VLc = fraction of liver tissue, VSc = fraction of slowly perfused tissue (bone, skin, and muscle), QC = cardiac output, QLc = fraction of blood flow to liver, QRc = fraction of blood flow to richly perfused tissue, QSc = fraction of blood flow to slowly perfused tissue (bone, skin, and muscle), PSCPO = slowly perfused tissue/blood partition coefficient of CPO, MPL = scaling factor of human liver microsome, ka = absorption constant, f_a = fractional absorption, V_{max1c} = maximum rate of conversion from CPF to CPO, K_{m1} = kinetic constant for conversion from CPF to CPO, V_{max2c} = maximum rate of conversion from CPF to TCPy, K_{m2} = kinetic constant for conversion from CPF to TCPy, V_{max3c} = maximum rate of conversion from CPO to TCPy, K_{m3} = kinetic constant for conversion from CPO to TCPy.

3.4 PBK Model Predictions

3.4.1 Dose-dependent blood concentrations of CPO

After PBK model validation, the defined models were used to quantify the dose-dependent blood C_{max} of CPO in both populations using not only $f_a = 0.224$ (Figure 8A) but also $f_a = 0.462$ and $f_a = 0.70$ (presented in Supplementary Data II) in order to take into account the different values reported in the literature of CPF bioavailability. Comparison of the blood C_{max} of CPO at increasing dose levels in the Chinese and the Caucasian population, reveals a 5- to 8-fold difference in the C_{max} values between the Caucasian and the Chinese population,

with the C_{max} values for the Caucasian population being higher (Figure 8A). This difference originates from the less efficient bioactivation of CFP to CPO and the more efficient detoxification of CPO in the Chinese as compared with the Caucasian population, which already noted above. Clearly, the PBK model integrates the kinetic data for the individual reactions enabling prediction of the overall effect on the C_{max} for CPO.

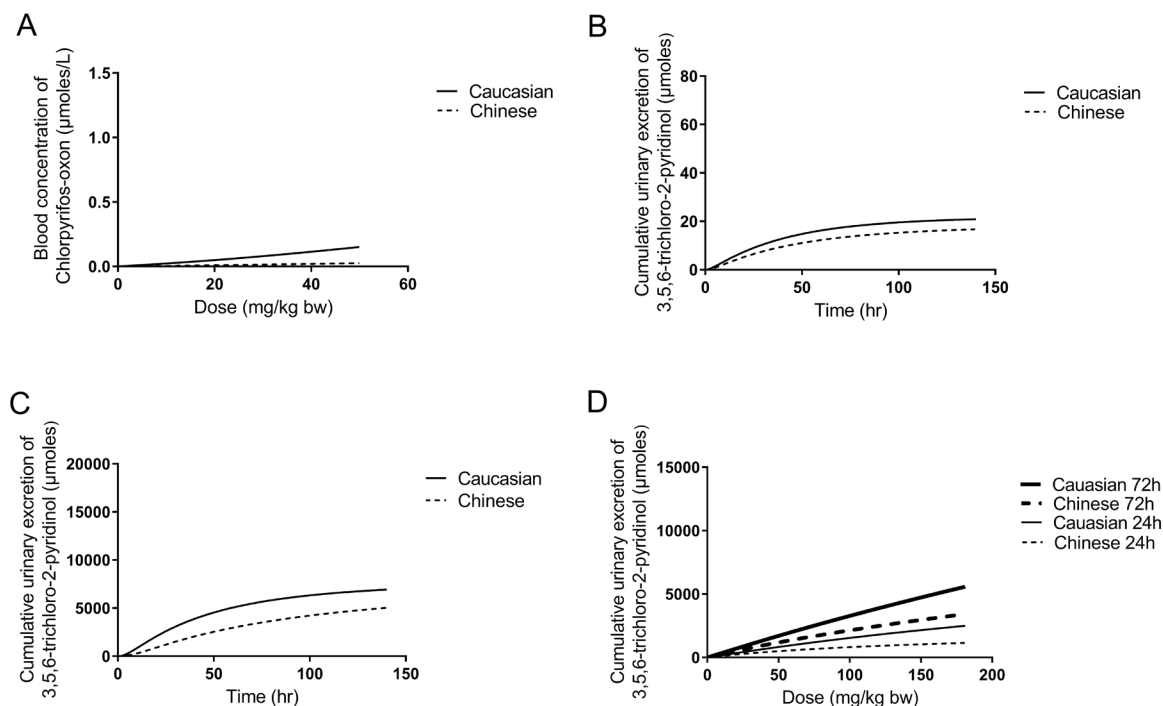


Fig 8. Predicted (A) dose-dependent C_{max} of CPO (B) time-dependent cumulative urinary excretion of TCPy at a dose of 0.5 mg CPF/kg bw, (C) time-dependent cumulative urinary excretion of TCPy at a dose of 180 mg CPF/kg bw, and (D) dose-dependent cumulative urinary excretion of TCPy. All presented for both the Caucasian (solid line) and Chinese (dash line) population, with $f_a = 0.224$ at 24 h (thin solid/dashed line, for (D) only) and 72 h (thick solid/dashed line, for (D) only), respectively (Timchalk et al., 2002).

3.4.2 Time- and dose-dependent cumulative urinary excretion of TCPy

The defined PBK models were also used to predict the time- and dose-dependent cumulative urinary excretion of TCPy in both ethnic groups, in order to capture the possible ethnic differences when using urinary TCPy as a biomarker for exposure assessment. The time-dependent cumulative excretion was predicted to increase especially over the first 72 h. The time-dependent urinary TCPy excretion at a dose level of 0.5 mg/kg was predicted to be 1- to 2-fold higher in the Caucasian than in the Chinese population, and a similar pattern was observed at a higher CPF dose of 180 mg/kg bw (data for $f_a = 0.224$ presented in Figs. 8B and



8C, data for $f_a = 0.46$ and $f_a = 0.70$ presented in Supplementary Data II). The CPF dose-dependent urinary excretion of TCPy (data for $f_a = 0.224$ are presented in Figure 8D, data for $f_a = 0.46$ and $f_a = 0.70$ are presented in Supplementary Data II) reveals a difference in urinary TCPy levels at similar dose levels at both 24 and 72 h, with the levels in Caucasians being higher than those in Chinese (Figure 8D). The curves also indicate that to reach a similar urinary TCPy elimination as in the Caucasian, the corresponding dose level of CPF exposure may vary from 1.3- to 5-fold higher in the Chinese, depending on the duration for urinary collection, the CPF dose and the f_a (Figure 8D).

2

3.5 Interethnic differences in CPF dose-dependent inhibition of AChE

In a next step, the CPO concentration-dependent AChE inhibition curve reported by Eyer et al. (2009) was converted into CPF dose-dependent curves for AChE inhibition in the Caucasian and Chinese population using PBK model-facilitated reverse dosimetry to calculate the dose levels required to generate the respective CPO C_{max} values. Figure 9 presents the predicted in vivo dose-response curves for CPF-mediated AChE inhibition in the Caucasian and Chinese population using the 3 different values for f_a . Figure 9 also presents available experimental data for in vivo CPF dose-dependent inhibition of AChE (solid circle/unfilled square). These results reveal that predicted in vivo dose-response curves for RBC AChE inhibition in the Caucasian population were comparable with reported in vivo data (EPA, 1999; Timchalk et al., 2002), with the best fit obtained for a f_a of 0.462. Data for Chinese subjects for further evaluation of the predicted dose-response curves were not available.

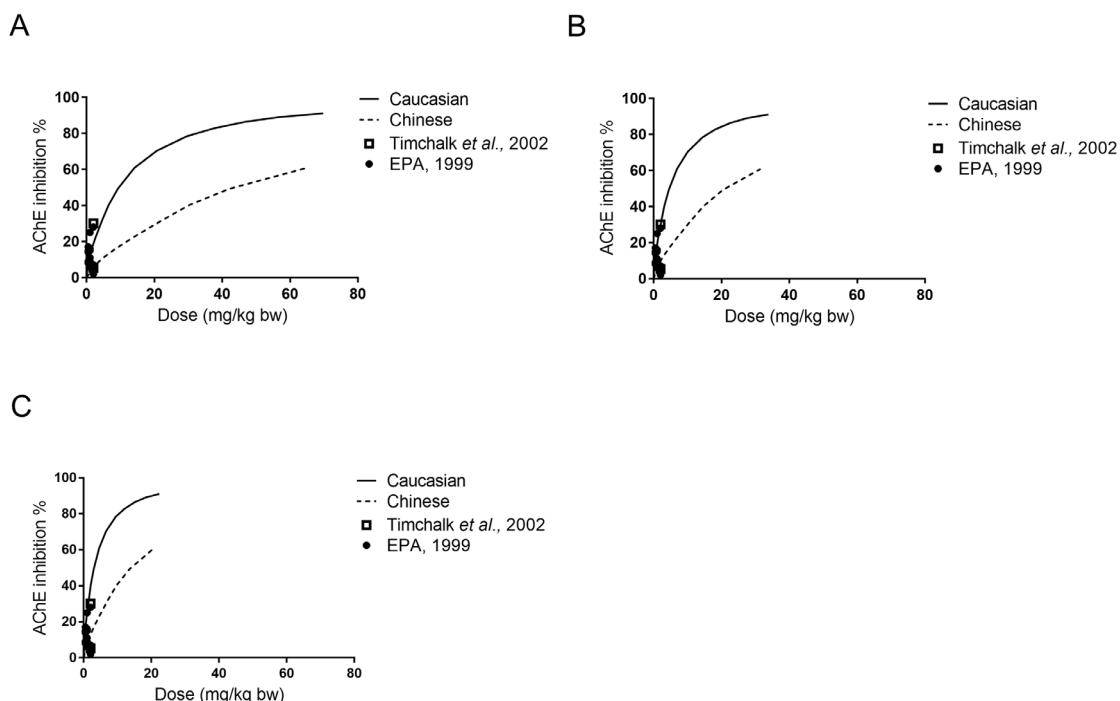


Fig 9. Predicted in vivo dose-dependent RBC AChE inhibition upon CPF exposure for the Caucasian (solid line) and Chinese (dash line) population as well as reported data (solid circles/unfilled squares) (EPA, 1999; Timchalk et al., 2002) using (A) $fa = 0.224$ (Timchalk et al., 2002), (B) $fa = 0.46$, and (C) $fa = 0.70$ (Nolan et al., 1984). The solid circles represent the in vivo data from humans upon oral administration of 0.5 mg CPF/kg bw, 1 mg CPF/kg bw, and 2 mg CPF/kg bw (EPA, 1999), and the black unfilled square represents in vivo data from Timchalk et al. (2002) in human exposed to 2 mg CPF/kg bw.

From the results presented in Figure 9, it follows that in the Chinese population similar AChE inhibition is reached at a 4- to 7-fold higher dose than in the Caucasian population. This indicates that the Chinese population is less sensitive to CPF-mediated AChE inhibition and CPF-related adverse effects than the Caucasian population. Analysis of the differences in the kinetics reveals that this is mainly due to an approximately 4.5-fold less efficient bioactivation of CPF to CPO combined with a 2.8-fold more efficient detoxification of CPO (Table 2).

3.6 Defining a point of departure for risk assessment

In a final step, the predicted dose-response curves were used to derive a POD for risk and safety assessment of CPF. To this end, the ED resulting from 10% or 20% inhibition of RBC AChE was derived from the dose-response curves for both the Caucasian and Chinese population, and was divided by 3 to obtain PODs that would be comparable with BMDL or NOAEL values



used as PODs in previous risk assessments (BfR, 2012; EFSA, 2014; Fan, 2014; Koshlukova and Reed, 2014). A 20% inhibition of AChE has been defined before by EFSA to obtain a suitable POD to define the acute reference dose for CPF (EFSA, 2014) whereas EPA in its risk assessment of CPF established a BMDL10 resulting in 10% RBC AChE inhibition as POD (BfR, 2012; Fan, 2014; Koshlukova and Reed, 2014). More recently, EPA indicated that 10% RBC AChE inhibition may not be adequately protective for human health because several studies suggested that adverse effects could occur even at lower levels of RBC AChE inhibition (EPA, 2016).

2

In Figure 10, the obtained PODs for CPF are compared with the POD established by EFSA based on 20% RBC AChE inhibition in pups (EFSA, 2014) and the BMDL10 defined by EPA (BfR, 2012; Fan, 2014; Koshlukova and Reed, 2014). The values are summarized in Supplementary Data III to also specify the influence of the *fa* on the values obtained. The comparison reveals that the predicted PODs derived in the present study using the PBK model-based reverse dosimetry are comparable with the PODs defined by EFSA and EPA. The reported reference value of 0.5 mg/kg bw reported by EFSA (2014) is (depending on the *fa* value) 0.6 to 1.8-fold higher compared with the predicted ED_{20/3} value for Caucasians and is 0.1 to 0.3-fold higher compared with the predicted ED_{20/3} value for the Chinese population. When compared with the EPA reported BMDL10 of 0.36 mg/kg bw (BfR, 2012; Fan, 2014; Koshlukova and Reed, 2014), the predicted ED_{10/3} values for the Caucasian and the Chinese population are 1.3 to 4.3-fold lower and 0.2 to 0.8-fold higher, respectively, indicating an interethnic variation, with values for the Chinese population being approximately 5- to 6-fold higher than those for the Caucasians, reflecting the lower sensitivity of the Chinese population.

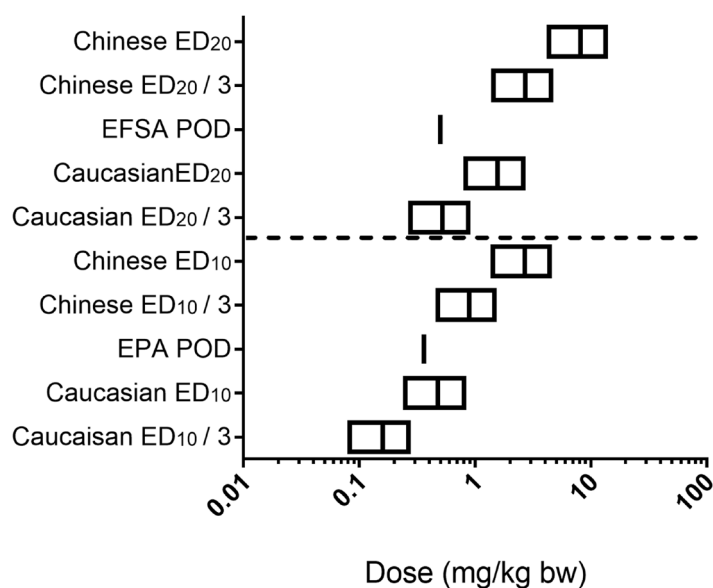


Fig 10. Comparison of the predicted and reported POD values by EFSA (2014) and EPA (BfR, 2012; Fan, 2014; Koshlukova and Reed, 2014) for CPF risk assessment in human. The Y-axis represents the label for the corresponding box plot on the right. The ED₁₀ or ED₂₀ values represent the predicted effective dose (ED) resulting in 10% or 20% RBC AChE inhibition for the respective populations. The left, middle, and right line in each box plot presents the ED value derived from fa equal to 0.7, 0.462, and 0.224, respectively. The ED_{10/3} or ED_{20/3} values represent PODs derived from these ED values, acknowledging that a BMDL (a lower confidence bound of the BMD) would be accepted as the POD for setting safe levels of exposure when it would be not more than 3-fold lower than the BMD, the dose level resulting in 10% or 20% effect above background level, and thus comparable to the ED. Both ED₁₀ and ED₂₀ are presented because the cutoff value to set the POD for AChE may be higher than the default of 10%. In this way the predicted values can be compared with the EFSA POD (set at 20% effect level) and EPA POD (set at 10% effect level) (BfR, 2012; Fan, 2014; Koshlukova and Reed, 2014). The dashed line in the plot is separating the results for 20% and 10% effect for RBC AChE inhibition.

4. Discussion

The aim of the present study was to investigate the interethnic differences in kinetics, biomarker formation, and in vivo RBC AChE inhibition for CPF in the Chinese and the Caucasian population. To this end, CPF PBK models were developed for the Chinese and the Caucasian population and subsequently used for the prediction of time- and dose-dependent interethnic differences in kinetics and biomarker formation as well as for reverse dosimetry to



translate CPO concentration-dependent data on inhibition of RBC AChE to in vivo dose-response curves for CPF-induced inhibition of RBC AChE.

The results obtained revealed a marked interethnic difference in toxicokinetics of CPF, with CYP450-mediated bioactivation to CPO being lower in Chinese, but PON1-mediated detoxification of CPO being higher in Chinese, resulting in higher predicted blood C_{max} values for the toxic metabolite CPO in the Caucasian than in the Chinese population at similar dose levels (Figure 8A). This interethnic difference in toxicokinetics of CPF may be related to differences between the ethnic groups in the frequency of different alleles of the relevant CYP2B6, CYP2C19, CYP3A4, and PON1 enzymes. For example, lower frequencies for 2 CYP2B6 single-nucleotide polymorphisms (SNPs) have been observed in the Chinese population (Guan et al., 2006), SNPs that were shown to result in a relatively higher catalytic efficiency for 7-ethoxy-4-trifluoromethylcoumarin O-deethylation (substrate of CYP2B6) compared with wild type (Guan et al., 2006; Jinno et al., 2003), suggesting that the Chinese population might be less efficient in CYP2B6-catalyzed CPO formation than the Caucasian. Besides, it has been documented that the catalytic efficiency for hydroxylation of the CYP2B6 substrate bupropion by Chinese microsomes was 1.8-fold lower than that for Caucasian microsomes (Yang et al., 2012). Moreover, Barter et al. (2013) reported that the hepatic abundance of CYP2C19 is only 8 pmol/mg in Chinese but 14 pmol/mg in Caucasian, and the frequency of CYP2C19 poor metabolizers is 13% in Chinese but only 2.4% in Caucasian. In addition, it has been reported that PON1R192 hydrolyses CPO faster than PON1Q192 (Ali and Chia, 2008; Eyer et al., 2009; Mutch et al., 2007), so that a higher efficiency of CPO hydrolysis in the Chinese population could be due to a relatively higher frequency of the RR genotype in the Chinese. To our knowledge, no comparison of genotype frequency of hepatic PON1 among these 2 races has been reported, but a study by Ali and Chia (2008) showed that Chinese have a higher RR genotype frequency (33%) of plasma PON1 than Caucasians (8.7%). Because plasma PON1 activity may result from release of the enzyme from the liver (Ali and Chia, 2008), similar differences might be expected in liver PON1 activity.

Evaluation of the developed PBK model against literature data available on cumulative urinary elimination of TCPy and blood C_{max} of TCPy (Bouchard et al., 2005; Nolan et al., 1984; Timchalk et al., 2002), indicated that the model was highly sensitive to the f_a . However, when taking the f_a reported in the respective studies into account revealed that the defined PBK model was able to adequately predict the kinetics of CPF in the human body. In subsequent

steps the PBK models were used to evaluate interethnic variation in biomarker formation and toxicity of CPF.

The prediction of cumulative urinary TCPy elimination, which often used as a biomarker for CPF exposure, revealed an around 2-fold lower cumulative TCPy elimination in the Chinese than the Caucasian when they were exposed to the same CPF dose level (Figure 8D). In other words, to reach a similar urinary TCPy elimination as the Caucasian, the corresponding dose level of CPF exposure should be 1.3- to 5-fold higher in the Chinese (Figure 8D). These results imply that when using urinary TCPy elimination as a biomarker for the CPF exposure of the Chinese population, dose levels will be relatively underestimated for the Chinese population if these interethnic differences are not taken into account.

The consequences of interethnic differences in CPF kinetics for its potential toxicity for Chinese and Caucasians were also investigated using PBK modeling-facilitated reverse dosimetry. To that end, the CPO concentration-dependent curve for RBC AChE inhibition (Eyer et al., 2009) was translated to in vivo dose-response curves for CPF-mediated RBC AChE inhibition for both ethnic groups. The data thus obtained for the Caucasian matched with the available in vivo human data available for this ethnic group (Figure 9). This further validates the developed-CPF PBK models and also provides support for the in vitro-PBK model-facilitated reverse dosimetry approach to obtain in vivo dose-response curves suitable for defining PODs for risk assessment. In line with the differences between the ethnic groups in formation and detoxification of the toxic CPO metabolite, the obtained in vivo dose-response curves predicted CPF to be 4- to 7-fold more toxic for the Caucasian than for the Chinese population. This was also reflected by the ED_{10/20} and ED_{10/20/3} values derived from the predicted dose-response curves, being 5- to 6-fold higher for the Chinese than the Caucasian population. Important to note as well is that the predicted-PODs obtained from the present study matches relatively well with the PODs defined previously by both EFSA and EPA in their risk assessment of CPF (BfR, 2012; EFSA, 2014; Fan, 2014; Koshlukova and Reed, 2014).

Although the outcomes of our predictions are considered adequate, the limitations of the approach presented should be considered as well. Thus, it is of importance to mention that the CPO concentration-response curve for RBC AChE inhibition used in the current study was based on data reported by Eyer et al. (2009), obtained with blood samples from Sri Lankan patients with acute CPF poisoning (Eyer et al., 2009). In the present study, we assumed that a

2

similar CPO concentration-dependent RBC AChE inhibition would occur in the Chinese and Caucasian individuals, which implies that interethnic differences in AChE sensitivity (if existing) are not (yet) taken into account. However, given the similar primary and tertiary structure of the AChE, it seems likely that interethnic differences in toxicodynamics may be limited, so that the differences in toxicokinetics, as defined in the present study, may have the largest influence on interethnic differences in toxicity. Besides, because the values of kinetic parameters (V_{max4c} and K_{m4} in vitro) for PON1-mediated CPO hydrolysis in blood for the Chinese are not available and Chinese plasma samples were not commercially available, this V_{max4c} in $\mu\text{mol/h}$ for the Chinese population was defined by multiplying the value reported by Mosquin et al. (2009) in $\mu\text{mol/h/kg bw}^{0.75}$ with the Chinese average body weight $^{0.75}$, whereas K_{m4} was kept unchanged. It is important to mention that based on the sensitivity analysis, the impact of V_{max4c} and K_{m4} on the predicted maximum blood concentration of CPO appeared to be quite low (the SCs amount to a value of <0.01 data not shown), which indicates that the impact of PON1-mediated CPO hydrolysis in blood on the predicted maximum blood concentration of CPO appears to be limited if not negligible. This is supported by the fact that a 10-fold change in either V_{max4c} or K_{m4} in the Chinese model did not affect the predicted maximum blood concentration of CPO (Supplementary Data IV).

In conclusion, our developed-CPF PBK models together with reverse dosimetry are capable of predicting the in vivo kinetics and biomarker characteristics of CPF as well as CPF exposure related RBC AChE inhibition in human in a quantitative way. By developing the model for both the Chinese and Caucasian population, insight was obtained in the ethnic-related variation in these parameters. The observed interethnic variation in the derived PODs for the 2 populations may be caused by the racial variation in hepatic patterns of the enzymes preferably involved in CPF bioactivation and detoxification, in particular CYP2B6 and PON1, respectively. This variation in enzymes involved may be related to variation in the frequency of relevant SNPs between the Chinese and Caucasian population (Ali and Chia, 2008; Guan et al., 2006; Lamba et al., 2003;). Altogether, it is concluded that the interethnic variation in kinetics of CFP may affect both its biomarker-based exposure assessment and its toxicity and risk assessment, and the developed-CPF PBK models are able to facilitate characterization and quantification of these interethnic differences.

Acknowledgements

This work was funded by a Grant from the China Scholarship Council (No. 201707720063 to ZHAOSHENSHENG).

Conflict of interests

The authors declared no potential conflicts of interest with respect to the research, authorship, and/or publication of this article.

2

References

- Al-Subeihi A. A., Spenkeliink B., Punt A., Boersma M. G., van Bladeren P. J., Rietjens I. M. C. M. (2012). Physiologically based kinetic modeling of bioactivation and detoxification of the alkenylbenzene methyleugenol in human as compared with rat. *Toxicol. Appl. Pharmacol.* 260, 271–284.
- Al-Malahmeh A. J., Al-Ajlouni A., Wesseling S., Soffers A. E. M. F., Al-Subeihi A., Kiwamoto R., Vervoort J., Rietjens I. M. C. M. (2017). Physiologically based kinetic modeling of the bioactivation of myristicin. *Arch. Toxicol.* 91, 713–734.
- Ali S. M., Chia S. E. (2008). Interethnic variability of plasma paraoxonase (PON1) activity towards organophosphates and PON1 polymorphisms among Asian populations—A short review. *Ind. Health* 46, 309–317.
- Barter Z. E., Tucker G. T., Rowland-Yeo K. (2013). Differences in cytochrome p450-mediated pharmacokinetics between chinese and caucasian populations predicted by mechanistic physiologically based pharmacokinetic modelling. *Clin. Pharmacokinet.* 52, 1085–1100.
- Barter Z., Bayliss M., Beaune P., Boobis A., Carlile D., Edwards R., Brian Houston J., Lake B., Lipscomb J., Pelkonen O., et al. (2007). Scaling factors for the extrapolation of in vivo metabolic drug clearance from in vitro data: Reaching a consensus on values of human microsomal protein and hepatocellularity per gram of liver. *Curr. Drug Metab.* 8, 33–45.
- BfR. (2012). Reconsideration of the human toxicological reference values (ARfD, ADI) for chlorpyrifos—BfR opinion No 026/2012, 1 June. Available at: <https://www.bfr.bund.de/cm/349/reconsideration-of-the-human-toxicological-reference-values-arfd-adi-for-chlorpyrifos.pdf>. Accessed January 23, 2019.
- Bouchard M., Carrier G., Brunet R. C., Bonvalot Y., Gosselin N. H. (2005). Determination of biological reference values for chlorpyrifos metabolites in human urine using a toxicokinetic approach. *J. Occup. Environ. Hygiene* 2, 155–168.
- Bouchard M. F., Chevrier J., Harley K. G., Kogut K., Vedar M., Calderon N., Norma C., Trujillo C., Johnson C., Bradman A., et al. (2011). Prenatal exposure to organophosphate pesticides and IQ in 7-year-old children. *Environ. Health Perspect.* 119, 1189.
- Brock A., Brock V. (1990). Plasma cholinesterase activity in a healthy population group with no occupational exposure to known cholinesterase inhibitors: Relative influence of some factors related to normal inter- and intra-individual variations. *Scand. J. Clin. Lab. Investig.* 50, 401–408.
- Brown R. P., Delp M. D., Lindstedt S. L., Rhomberg L. R., Beliles R. P. (1997). Physiological parameter values for physiologically based pharmacokinetic models. *Toxicol. Ind. Health* 13, 407–484.
- Brzak K. A. (2000). A rising dose toxicology study to determine the no-observable-effect-levels (NOEL) for erythrocyte acetylcholinesterase (AChE) inhibition and cholinergic signs and symptoms of chlorpyrifos at three dose levels α Part B (Report No 981176). Toxicology & Environmental Research and Consulting.
- Carr R. L., Dail M. B., Chambers H. W., Chambers J. E. (2015). Species differences in paraoxonase mediated hydrolysis of several organophosphorus insecticide metabolites. *J. Toxicol.* 2015, 1.
- DeJongh J., Verhaar H. J., Hermens J. L. (1997). A quantitative property-property relationship (QPPR) approach to estimate in vitro tissue-blood partition coefficients of organic chemicals in rats and humans. *Arch. Toxicol.* 72, 17–25.
- Di L., Keefer C., Scott D. O., Strelevitz T. J., Chang G., Bi Y. A., Lai Y., Duckworth J., Fenner K., Troutman M. D., et al. (2012). Mechanistic insights from comparing intrinsic clearance values between human liver microsomes and hepatocytes to guide drug design. *Eur. J. Med. Chem.* 57, 441–448.
- Drevenkar V., Stengl B., Fröbe Z. (1994). Microanalysis of dialkylphosphorus metabolites of organophosphorus pesticides in human blood by capillary gas chromatography and by phosphorus-selective and ion trap detection. *Anal. Chim. Acta* 290, 277–286.
- Eaton D. L., Daroff R. B., Autrup H., Bridges J., Buffler P., Costa L. G., Coyle J., McKhann G., Mobley W. C., Nadel L., et al. (2008). Review of the toxicology of chlorpyrifos with an emphasis on human exposure and neurodevelopment. *Crit. Rev. Toxicol.* 38, 1–125.

- European Food Safety Authority. (2014). Conclusion on the peer review of the pesticide human health risk assessment of the active substance chlorpyrifos. *EFSA J.* 12, 3640.
- EPA. (1999). Data Evaluation Record Study Type: Special Non-Guideline Assessment for RBC Cholinesterase in Humans. Available at: <https://archive.epa.gov/scipoly/sap/meetings/web/pdf/kisickider.pdf>. Accessed January 23, 2019.
- EPA. (2011). Chlorpyrifos Physiologically Based Pharmacokinetic and Pharmacodynamic (PBPK/PD) Modeling Linked to Cumulative and Aggregate Risk Evaluation System (CARES). Available at: <https://archive.epa.gov/scipoly/sap/meetings/web/pdf/021511minutes.pdf>. Accessed November 1, 2018.
- EPA. (2016). Chlorpyrifos: Revised Human Health Risk Assessment for Registration Review. Available at: <https://www.regulations.gov/document/EPA-HQ-OPP-2015-0653-0454>. file ID: EPA-HQ-OPP-2015-0653-0454. Accessed January 23, 2019.
- Evans M. V., Andersen M. E. (2000). Sensitivity analysis of a physiological model for 2,3,7,8-tetrachlorodibenzo-p-dioxin (TCDD): Assessing the impact of specific model parameters on sequestration in liver and fat in the rat. *Toxicol. Sci.* 54, 71–80.
- Eyer F., Roberts D. M., Buckley N. A., Eddleston M., Thiermann H., Worek F., Eyer P. (2009). Extreme variability in the formation of chlorpyrifos oxon (CPO) in patients poisoned by chlorpyrifos (CPF). *Biochem. Pharmacol.* 78, 531–537.
- Fan A. M. (2014). Biomarkers in toxicology, risk assessment, and environmental chemical regulations. In *Biomarkers in Toxicology* (pp. 1057–1080). <https://doi.org/10.1016/B978-0-12-404630-6.00064-6>.
- Foxenberg R. J., Ellison C. A., Knaak J. B., Ma C., Olson J. R. (2011). Cytochrome P450-specific human PBPK/PD models for the organophosphorus pesticides: Chlorpyrifos and parathion. *Toxicology* 285, 57–66.
- Foxenberg R. J., McGarrigle B. P., Knaak J. B., Kostyniak P. J., Olson J. R. (2007). Human hepatic cytochrome p450-specific metabolism of parathion and chlorpyrifos. *Drug Metab. Dispos.* 35, 189–193.
- Flaskos J. (2014). The neuronal cytoskeleton as a potential target in the developmental neurotoxicity of organophosphorothionate insecticides. *Basic Clin. Pharmacol. Toxicol.* 115, 201–208.
- Furlong C. E., Richter R. J., Seidel S. L., Costa L. G., Motulsky A. G. (1989). Spectrophotometric assays for the enzymatic hydrolysis of the active metabolites of chlorpyrifos and parathion by plasma paraoxonase/arylesterase. *Anal. Biochem.* 180, 242–247.
- González-Alzaga B., Lacasaña M., Aguilar-Garduño C., Rodríguez-Barranco M., Ballester F., Rebagliato M., Hernández A. F. (2014). A systematic review of neurodevelopmental effects of prenatal and postnatal organophosphate pesticide exposure. *Toxicol. Lett.* 230, 104–121.
- Griffin P., Mason H., Heywood K., Cocker J. (1999). Oral and dermal absorption of chlorpyrifos: A human volunteer study. *Occup. Environ. Med.* 56, 10–13.
- Guan S., Huang M., Li X., Chen X., Chan E., Zhou S. F. (2006). Intra- and inter-ethnic differences in the allele frequencies of cytochrome P450 2B6 gene in Chinese. *Pharm. Res.* 23, 1983–1990.
- Hardt J., Angerer J. (2000). Determination of dialkyl phosphates in human urine using gas chromatography-mass spectrometry. *J. Anal. Toxicol.* 24, 678–684.
- Heilmair R., Eyer F., Eyer P. (2008). Enzyme-based assay for quantification of chlorpyrifos oxon in human plasma. *Toxicol. Lett.* 181, 19–24.
- Hung D. Z., Yang H. J., Li Y. F., Lin C. L., Chang S. Y., Sung F. C., Tai S. C. (2015). The long-term effects of organophosphates poisoning as a risk factor of CVDs: A nationwide population-based cohort study. *PLoS One* 10, e0137632.
- Jinno H., Tanaka-Kagawa T., Ohno A., Makino Y., Matsushima E., Hanioka N., Ando M. (2003). Functional characterization of cytochrome P450 2B6 allelic variants. *Drug Metab. Dispos.* 31, 398–403.
- Koshlukova S. E., Reed N. R. (2014). Chlorpyrifos. <https://doi.org/10.1016/B978-0-12-386454-3.00115-9>.
- Lamba V., Lamba J., Yasuda K., Strom S., Davila J., Hancock M. L., Fackenthal J. D., Rogan P. K., Ring B., Wrighton S. A., et al. (2003). Hepatic CYP2B6 expression: Gender and ethnic differences and relationship to CYP2B6 genotype and CAR (constitutive androstane receptor)

- expression. *J. Pharmacol. Exp. Ther.* 307, 906–922.
- Lefkowitz L. J., Kupina J. M., Hirth N. L., Henry R. M., Noland G. Y., Barbee J. Y., Zhou J. Y., Weese C. B. (2007). Intraindividual stability of human erythrocyte cholinesterase activity. *Clin. Chem.* 53, 1358–1363.
- Leoni C., Balduzzi M., Buratti F. M., Testai E. (2012). The contribution of human small intestine to chlorpyrifos biotransformation. *Toxicol. Lett.* 215, 42–48.
- Liu P., Wu C. H., Chang X. L., Qi X. J., Zheng M. L., Zhou Z. J. (2014). Assessment of chlorpyrifos exposure and absorbed daily doses among infants living in an agricultural area of the Province of Jiangsu, China. *Int. Arch. Occup. Environ. Health* 87, 753–762.
- Lu C., Holbrook C. M., Andres L. M. (2009). The implications of using a physiologically based pharmacokinetic (PBPK) model for pesticide risk assessment. *Environ. Health Perspect.* 118, 125–130.
- Mosquin P. L., Licata A. C., Liu B., Sumner S. C., Okino M. S. (2009). Reconstructing exposures from small samples using physiologically based pharmacokinetic models and multiple biomarkers. *J. Exposure Sci. Environ. Epidemiol.* 19, 284.
- Mutch E., Daly A. K., Williams F. M. (2007). The relationship between PON1 phenotype and PON1-192 genotype in detoxification of three oxons by human liver. *Drug Metab. Dispos.* 35, 315–320.
- Naksen W., Prapamontol T., Mangklabruks A., Chantara S., Thavornnyutikarn P., Robson M. G., Ryan P. B., Barr D. B., Panuwet P. (2016). A single method for detecting 11 organophosphate pesticides in human plasma and breastmilk using GC-FPD. *J. Chromatogr. B* 1025, 92–104.
- NHFPC. (2007a). Reference individuals for use in radiation protection—Part 1: Physique parameters. vol GBZ/T 200.1, Pub. L. No. GBZ/T 200.1. China: National Health and Family Planning Commission of the People's Republic of China. Available at: <http://www.nirp.cn/userfiles/file/GBZT200.1-2007.pdf>. Accessed January 23, 2019.
- NHFPC. (2007b). Reference individuals for use in radiation protection—Part 2: Masses of main organs and tissues. vol GBZ/T 200.2, Pub. L. No. GBZ/T 200.2. China: National Health and Family Planning Commission of the People's Republic of China. Available at: <http://www.nirp.cn/userfiles/file/GBZT200.2-2007.pdf>. Accessed January 23, 2019.
- NHFPC. (2014). Reference individuals for use in radiation protection—Part 3: Main physiological parameters. vol GBZ/T 200.3, Pub. L. No. GBZ/T 200.3. China: National Health and Family Planning Commission of the People's Republic of China. Available at: <http://www.nirp.cn/userfiles/file/GBZT200.3-2014.pdf>. Accessed January 23, 2019.
- Ning J., Lousse J., Spenkelink B., Wesseling S., Rietjens I. M. C. M. (2017). Study on inter-ethnic human differences in bioactivation and detoxification of estragole using physiologically based kinetic modeling. *Arch. Toxicol.* 91, 3093–3108.
- Nolan R. J., Rick D. L., Freshour N. L., Saunders J. H. (1984). Chlorpyrifos: Pharmacokinetics in human volunteers. *Toxicol. Appl. Pharmacol.* 73, 8–15.
- Poet T. S., Kousba A. A., Dennison S. L., Timchalk C. (2004). Physiologically based pharmacokinetic/pharmacodynamic model for the organophosphorus pesticide diazinon. *Neurotoxicology* 25, 1013–1030.
- Punt A., Paini A., Boersma M. G., Freidig A. P., Delatour T., Scholz G., Schilter B., Bladeren P., Rietjens I. M. C. M. (2009). Use of physiologically based biokinetic (PBBK) modeling to study estragole bioactivation and detoxification in humans as compared with male rats. *Toxicol. Sci.* 110, 255–269.
- Punt A., Freidig A. P., Delatour T., Scholz G., Boersma M. G., Schilter B., van Bladeren P. J., Rietjens I. M. C. M. (2008). A physiologically based biokinetic (PBBK) model for estragole bioactivation and detoxification in rat. *Toxicol. Appl. Pharmacol.* 231, 248–259.
- Smith J. N., Timchalk C., Bartels M. J., Poet T. S. (2011). In vitro age-dependent enzymatic metabolism of chlorpyrifos and chlorpyrifos-oxon in human hepatic microsomes as well as chlorpyrifos-oxon in plasma. *Drug Metab. Dispos.*, Dmd-111 39, 1353.
- Stauber J. L., Chariton A., Apte S. (2016). Global change. In *Marine Ecotoxicology* (pp. 273–313). Academic Press. <https://doi.org/http://dx.doi.org/10.1016/B978-0-12-803371-5.00010-2>.
- Tang J., Cao Y., Rose R. L., Brimfield A. A., Dai D., Goldstein J. A., Hodgson E. (2001). Metabolism of chlorpyrifos by human cytochrome P450 isoforms and human, mouse, and rat liver

- microsomes. *Drug Metab. Dispos.* 29, 1201–1204.
- Timchalk C., Nolan R. J., Mendrala A. L., Dittenber D. A., Brzak K. A., Mattsson J. L. (2002). A physiologically based pharmacokinetic and pharmacodynamic (PBPK/PD) model for the organophosphate insecticide chlorpyrifos in rats and humans. *Toxicol. Sci.* 66, 34–53.
- Wagner D. (1999). Pesticide residues in food. Available at: <http://www.bvsde.ops-oms.org/bvsacg/e/cd-cagua/guias/b.parametos/4.BasTox/IPCS/029.ChlorpyrifosIPCS.pdf>. Accessed January 23, 2019.
- Wang P., Tian Y., Wang X. J., Gao Y., Shi R., Wang G. Q., Hu G. H., Shen X. M. (2012). Organophosphate pesticide exposure and perinatal outcomes in Shanghai, China. *Environ. Int.* 42, 100–104.
- Yang J., He M. M., Niu W., Wrighton S. A., Li L., Liu Y., Li C. (2012). Metabolic capabilities of cytochrome P450 enzymes in Chinese liver microsomes compared with those in Caucasian liver microsomes. *Br. J. Clin. Pharmacol.* 73, 268–284.
- Zhang Y., Han S., Liang D., Shi X., Wang F., Liu W., Zhang L., Chen L., Gu Y., Tian Y. (2014). Prenatal exposure to organophosphate pesticides and neurobehavioral development of neonates: A birth cohort study in Shenyang, China. *PLoS One* 9, e88491.
- Zhang Y., Reviriego J., Lou Y. Q., Sjöqvist F., Bertilsson L. (1990). Diazepam metabolism in native Chinese poor and extensive hydroxylators of S-mephenytoin: Interethnic differences in comparison with white subjects. *Clin. Pharmacol. Ther.* 48, 496–502.

Supplementary materials

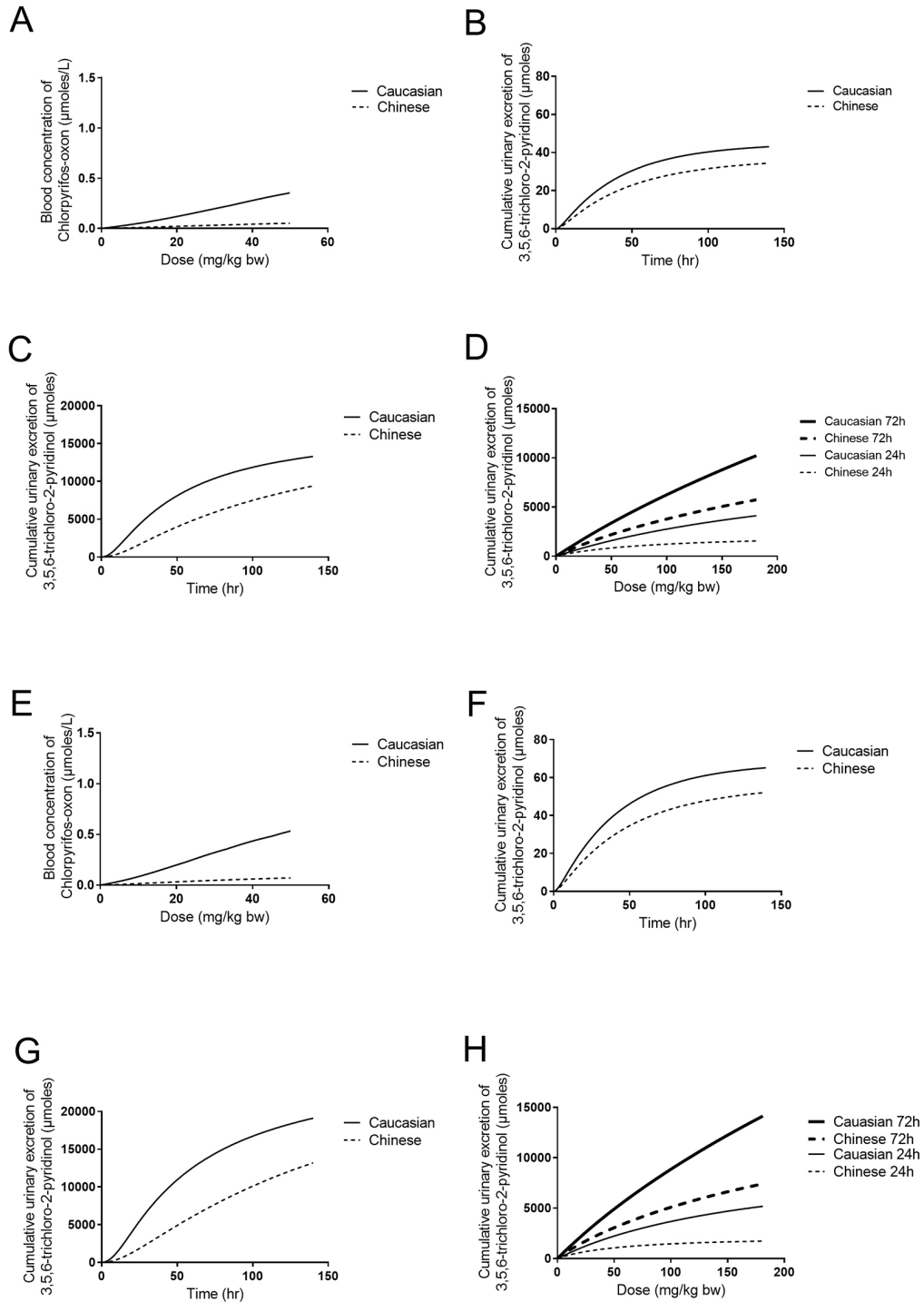
For convenience, **Supplementary material I** can be found at the following link:

<https://academic.oup.com/toxsci/article/171/1/69/5520467?login=true>.



2

Supplementary material II



(A) and (E) Overview of prediction of the dose-dependent C_{max} of CPO, (B) (C) and (F) (G) Prediction of the time-dependent cumulative urinary excretion of TCPy, at dose of 0.5 mg/kg and 180 mg/kg, respectively, as well as (D) and (H) prediction of the dose-dependent cumulative urinary excretion of TCPy, in the Caucasian (solid line) and Chinese (dash line) population, with $f_a=0.462$ (A), (B), (C), (D) and 0.7 (E), (F), (G), (H) (Nolan et al., 1984) at 24h (thin solid/dashed line) and 72h (thick solid/dashed line), respectively.



Supplementary material III

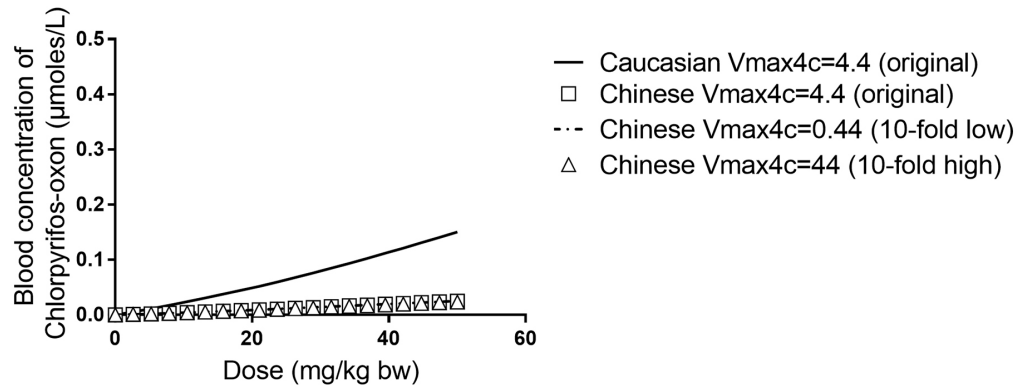
Comparison of the predicted point of departure (POD) of both the Caucasian and Chinese population with the reported POD for CPF risk assessment. (fa=0.224 (Nolan et al., 1984), fa=0.462 (calculated here from the present study) and fa=0.7 (Timchalk et al., 2002))

Group PODs	Caucasian			Chinese		
	fa=0.224	fa=0.462	fa=0.7	fa=0.224	fa=0.462	fa=0.7
ED ₁₀ ^a	0.80	0.38	0.25	4.40	2.20	1.42
ED ₁₀ / 3 ^b	0.27	0.13	0.08	1.47	0.73	0.47
ED ₂₀ ^c	2.60	1.26	0.83	13.51	6.61	4.32
ED ₂₀ / 3 ^d	0.87	0.42	0.28	4.50	2.20	1.44

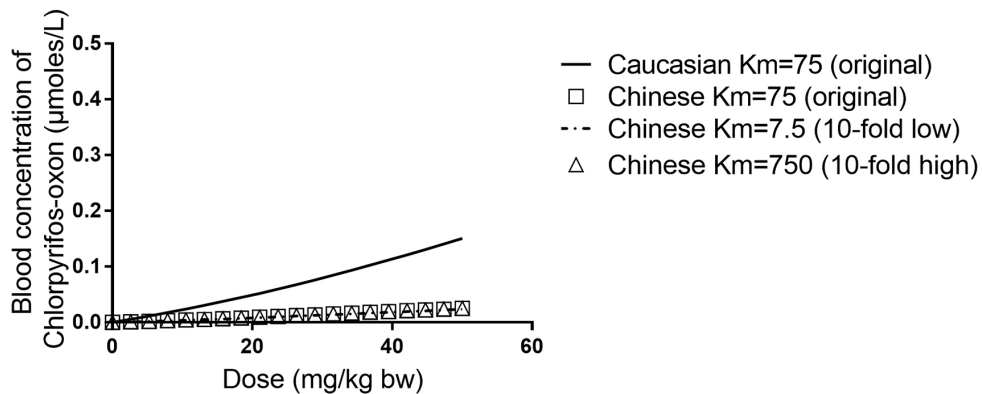
^{a b c d} in mg/kg bw per day

Supplementary data IV

A



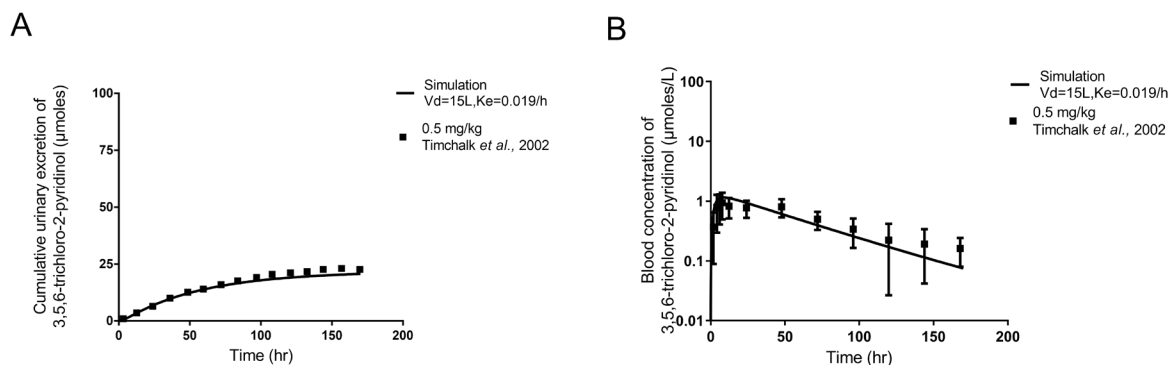
B



Comparison between predicted dose-dependent C_{max} of CPO for the Caucasian and the Chinese population using the original V_{max4c} and K_m values (solid line represent prediction for Caucasian and unfilled square represent prediction for Chinese) and (A) different V_{max4c} values for the Chinese population (dash line represent prediction using 10-fold lower V_{max4c}, and triangle represent prediction using 10-fold higher V_{max4c}) and (B) different K_m values for the Chinese population (dash line represent prediction using 10-fold lower K_m, and triangle represent prediction using 10-fold higher K_m). All predictions conducted at f_a=0.224



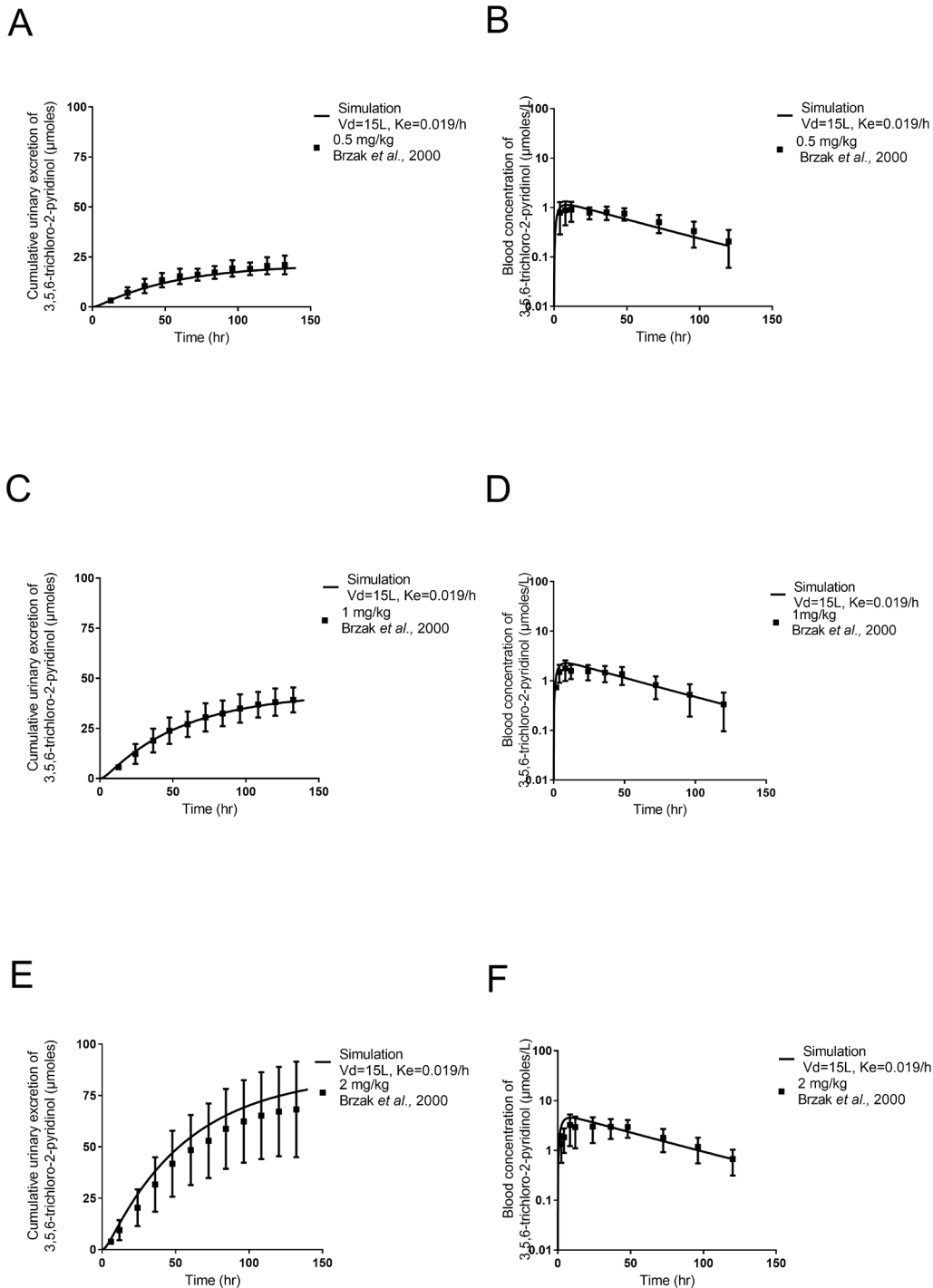
Supplementary data V



2

Comparison of PBK model-predicted and experimentally determined time-dependent (A) cumulative urinary excretion of TCPy (Timchalk *et al.*, 2002; Lu *et al.*, 2009) and (B) blood concentrations of TCPy in Caucasian volunteers upon oral administration of 0.5 mg CPF/kg bw (Timchalk *et al.*, 2002). The simulations were performed using a $f_a=0.224$, $V_d=15\text{L}$ and $K_e=0.019/\text{h}$ and are presented as solid lines, while the squares represent the values from the human volunteer study (Timchalk *et al.*, 2002; Lu *et al.*, 2009).

Supplementary data VI



Comparison of PBK model-predicted (solid lines) and experimentally determined (solid squares) time-dependent cumulative urinary excretion of TCPy at an oral dose of (A) 0.5 mg CPF/kg bw, (C) 1.0 mg CPF/kg bw, and (E) 2 mg CPF/kg bw, and of PBK model predicted (solid lines) and experimentally determined (solid squares) blood concentration of TCPy at an oral dose of (B) 0.5 mg CPF/kg bw, (D) 1 mg CPF/kg bw, and (F) 2 mg CPF/kg bw. Experimental data were taken from Bouchard et al. (2005), which originally were from Brzak et al., (2000). The simulations were performed using a $fa=0.22$, $Vd=15L$ and $Ke=0.019/h$.

Chapter 3

Prediction of dose-dependent in vivo
acetylcholinesterase inhibition by profenofos in
rats and humans using physiologically based
kinetic (PBK) modeling-facilitated reverse
dosimetry

Isaac Omwenga, Shensheng Zhao, Laetitia Kanja, Hans Mol, Ivonne M. C. M. Rietjens and
Jochem Louisse

Published in Archives of Toxicology (2021) 95:1287–1301

Abstract

Organophosphate pesticides (OPs) are known to inhibit acetylcholinesterase (AChE), a critical effect used to establish health-based guidance values. This study developed a combined in vitro–in silico approach to predict AChE inhibition by the OP profenofos in rats and humans. A physiologically based kinetic (PBK) model was developed for both species. Parameter values for profenofos conversion to 4-bromo-2-chlorophenol (BCP) were derived from in vitro incubations with liver microsomes, liver cytosol, and plasma from rats (catalytic efficiencies of 1.1, 2.8, and 0.19 ml/min/mg protein, respectively) and humans (catalytic efficiencies of 0.17, 0.79, and 0.063 ml/min/mg protein, respectively), whereas other chemical-related parameter values were derived using in silico calculations. The rat PBK model was evaluated against literature data on urinary excretion of conjugated BCP. Concentration-dependent inhibition of rat and human AChE was determined in vitro, and these data were translated with the PBK models to predicted dose-dependent AChE inhibition in rats and humans in vivo. Comparing predicted dose-dependent AChE inhibition in rats to literature data on profenofos-induced AChE inhibition revealed an accurate prediction of in vivo effect levels. Comparison of rat predictions (BMDL₁₀ of predicted dose–response data of 0.45 mg/kg bw) and human predictions (BMDL₁₀ of predicted dose–response data of 0.01 mg/kg bw) suggests that humans are more sensitive than rats, being mainly due to differences in kinetics. Altogether, the results demonstrate that in vivo AChE inhibition upon acute exposure to profenofos was closely predicted in rats, indicating the potential of this novel approach method in chemical hazard assessment.

1. Introduction

Organophosphorus or organophosphate pesticides (OPs) have been extensively used for the control of agricultural and household pests globally (Kumari and John 2019). Exposure to these pesticides has been reported for various segments of the population, including agriculture workers and their families, house hold members during home application of pesticides, people that live in proximity to farms, or the general public via residues on food (Bradman et al. 2003; Lu et al. 2000; Quandt et al. 2004). Consequently, OPs and their metabolites have been found in human blood, serum, urine, and breast milk (Liu et al. 2014; Hardt and Angerer 2000; Zhang et al. 2014; Naksen et al. 2016). Since various OPs have shown to cause adverse effects to the environment and to human health, many OPs are currently not registered for use as pesticides, and some OPs have even been banned (Hertz-Picciotto et al. 2018).

Epidemiological studies have linked chronic OP exposure to reproductive disorders, developmental toxicity, birth defects, cancer, Parkinson's disease, Alzheimer's disease, diabetes, chronic respiratory disease, cardiovascular diseases, chronic nephropathies and amyotrophic lateral sclerosis (ALS) (Mostafalou and Abdollahi 2013). The critical effects of OPs in animal studies are related to neurotoxicity, which has been reported to be related to, amongst others, inhibition of acetylcholinesterase (AChE), neuropathy target esterase (NTE) (Costa 2018), acylpeptide hydrolase (APH) (Richards et al. 2000), fatty acid amide hydrolase (FAAH) (Quistad et al. 2001; Buntyn et al. 2017), muscarinic M2 receptors (Costa 2006), and a variety of lipases (Quistad et al. 2006).

Inhibition of AChE is one of the mechanisms by which OPs cause acute neurotoxicity (Jamal et al. 2002; Farahat et al. 2003), characterized by decreased hydrolysis of acetylcholine in both central and peripheral cholinergic synapses, resulting initially in overstimulation of nicotinic and muscarinic receptors, followed by receptor down-regulation on post-synaptic membranes (Costa 2006). Acute or repeated exposure to OPs can lead to organophosphate ester induced delayed polyneuropathy (OPIDP), a neurodegenerative disorder caused by inhibition and aging of at least 70% of the activity of the neuropathy target esterase (NTE) present in nerve tissues as well as other tissues (e.g., lymphocytes, testis) (Johnson and Glynn 1995, 2001; Costa 2018). In the hazard and risk assessment of OPs, *in vivo* animal studies on OP-induced inhibition of AChE have been used to derive a point of departure (POD) to set safe exposure levels, such as an Acute Reference Dose (ARfD). ARfDs for chlorpyrifos, acephate, methamidofos, omethoate and profenofos as reported by organizations as the European Food Safety Authority

(EFSA), United States Environmental Protection Agency (US EPA), and the Joint FAO/WHO Meeting on Pesticide Residues (JMPR) have been derived from data on OP-induced AChE inhibition from animal studies (JMPR 2007; EPA 2006, 2011, 2016; EFSA 2019). Although these *in vivo* studies do not measure complex neurotoxicity endpoints, the information on OP-induced inhibition of AChE *in vivo* is considered an important piece of information in the hazard characterization. In these *in vivo* studies, AChE activity is usually measured in blood and sometimes also brain tissue after OP exposure. In the present study, we aimed to assess whether *in vivo* dose-dependent OP-induced AChE inhibition can be predicted by an animal-free approach.

To inhibit AChE in the *in vivo* situation, the OP needs to reach its target (AChE) at sufficiently high concentrations. The *in vivo* potency of an OP to inhibit AChE is, thus, dependent on its intrinsic ability (potency) to inhibit AChE and the amount of OP that reaches that target. The potency of an OP to inhibit AChE can be determined using *in vitro* approaches. To estimate the amount of OP that reaches the target, so called physiologically based kinetic (PBK) models can be used. A PBK model permits the simulation of the chemical's *in vivo* kinetics (ADME) and can relate external exposure to internal exposure at the target sites. When having PBK models for different exposure routes and/or different species, these models can be used for exposure route and/or species extrapolations. These models can also be used as a tool to estimate exposure applying reverse dosimetry of biomonitoring data (e.g., chemical levels in blood or urine), as has been shown, for example, for chlorpyrifos in rats and humans (Timchalk et al. 2002), and chlorpyrifos in children (Rigas et al. 2001). Furthermore, these models can be used for reverse dosimetry of *in vitro* toxicity data, thereby translating *in vitro* effect concentrations to *in vivo* doses, enabling prediction of *in vivo* dose-dependent toxicity, as has been shown for the OP chlorpyrifos (Zhao et al. 2019). Such PBK modeling-facilitated reverse dosimetry of *in vitro* toxicity data is considered crucial in the transition to non-animal based novel approach methods (NAMs) for the safety assessment of chemicals (Louisse et al. 2017).

PBK models have been developed for various OPs including chlorpyrifos (Timchalk et al. 2002; Bouchard et al. 2005; Mosquin et al. 2009; Lu et al. 2010; Zhao et al. 2019), malathion (Bouchard et al. 2003, 2017; Bogen and Singhal 2017), parathion (Sultatos 1990) and diazinon (Poet et al. 2004). To date, no PBK model has been built for the OP profenofos, despite its widespread use in developing countries and reported cases of human accidental poisoning (Gotoh et al. 2001; Eddleston et al. 2009).

Profenofos [O-(4-bromo-2-chlorophenyl) O-ethyl S-propyl phosphorothioate] (Figure 1) is a thiophosphate OP pesticide (O=P-S-C) that was developed for pest strains resistant to chlorpyrifos and other OPs (Gotoh et al. 2001). Profenofos has been classified as a moderately hazardous (Toxicity Class II) pesticide by the World Health Organization (WHO) with moderate level of acute toxicity (LD50 of 358–1178 mg/kg in rat) following oral administration (Reported in JMPR (2007)). Dietary intake of profenofos is the primary exposure route for humans (Greish et al. 2011) and residue levels exceeding EU MRLs have been found in various vegetables in Kenya (Karanja et al. 2012). Our recent study reported profenofos as one of the most frequently encountered pesticide residues in vegetables sampled in peri-urban Nairobi, Kenya (Omwenga et al. 2021).

The present study aims to develop a PBK model for profenofos in rats and humans and apply the models to predict dose-dependent in vivo AChE inhibition using PBK modeling-facilitated reverse dosimetry of in vitro data on profenofos-induced AChE inhibition, allowing interspecies comparisons and providing a proof-of-principle that OP-induced AChE inhibition can be predicted for both rats and humans without the need for in vivo studies. To that end, profenofos PBK models were developed based on in silico and in vitro-derived input parameter values. The rat PBK model was evaluated by comparing PBK model predictions with available in vivo kinetic data in rats. Subsequently, in vitro data on profenofos-induced AChE inhibition were translated to predicted in vivo dose-dependent AChE inhibition in rats and humans, and predictions on dose-dependent AChE inhibition in rats were evaluated by comparison with available in vivo data.

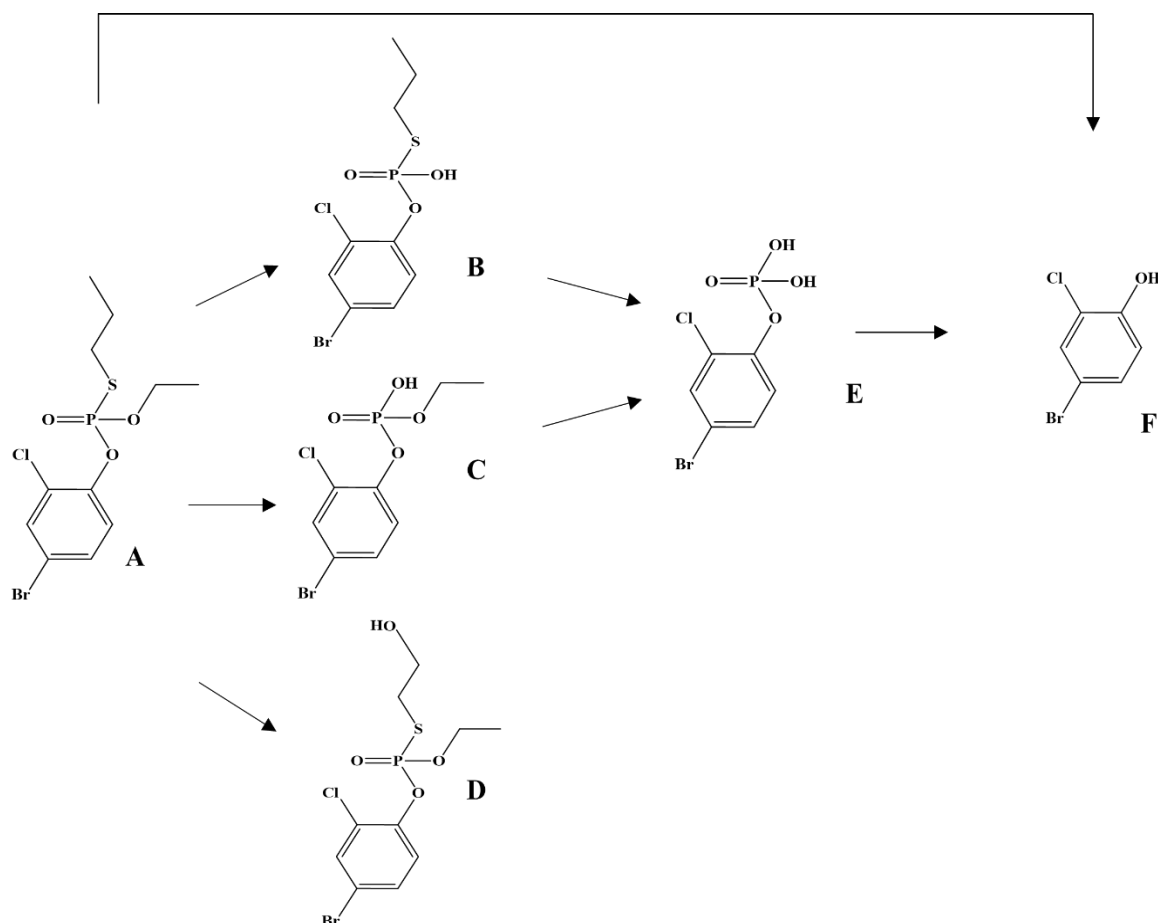


Fig 1. Metabolic pathways for metabolism of profenofos (A) based on data reported in previous studies (Gotoh et al., 2001; Dadson et al., 2013). Metabolites include desethylated profenofos (B), desthiopropylprofenofos / des-S-propylated profenofos (C), hydroxypropyl profenofos (D), 4-bromo-2-chlorophenyl dihydrogen phosphate (E), and 4-bromo-2-chlorophenyl (BCP) (F).

2. Materials and methods

2.1 Materials

Profenofos, 4-bromo-2-chlorophenol (BCP), bovine serum albumin (BSA), reduced nicotinamide adenine dinucleotide phosphate (NADPH), 5,5-dithiobis (2-nitrobenzoic acid) (DTNB) and acetylthiocholine iodide (ATC) were purchased from Sigma-Aldrich (Zwijndrecht, The Netherlands). Magnesium chloride hexahydrate ($\text{MgCl}_2 \cdot 6\text{H}_2\text{O}$), trifluoroacetic acid (TFA), dimethylsulfoxide (DMSO), and calcium chloride dihydrate ($\text{CaCl}_2 \cdot 2\text{H}_2\text{O}$) were purchased from VWR International (Amsterdam, The Netherlands). Acetonitrile (ACN, UPLC/MS grade) was purchased from Biosolve (Valkenswaard, The Netherlands). Human liver microsomes and cytosol (pooled from 150 human donors, mixed

gender), rat liver microsomes and rat liver cytosol (pooled from 20 male Sprague–Dawley rats) were purchased from Corning (Amsterdam, The Netherlands). Recombinant human acetylcholinesterase was purchased from Sigma-Aldrich (Zwijndrecht, The Netherlands). Rat blood was purchased from BioIVT (Westbury, USA), human and rat plasma were purchased from Innovate (New York, USA).

2.2 PBK model development

2.2.1 Model structure and software

The PBK model structure applied (Figure 2) is based on a generic PBK model that has been developed for humans (Jones and Rowland-Yeo 2013). Physiological parameter values (tissue volumes and blood flows) for rats and humans were taken from Jones and Rowland-Yeo (2013) and Brown et al. (1997) (Supplementary Table 1) as collected previously by Punt et al. (2020). The generic model contains separate compartments for liver, the gastrointestinal tract (GI-tract), fat, muscle, skin, bone, brain, heart, kidney, lung, spleen, venous blood, arterial blood, and a rest-of-body compartment. The uptake of profenofos from the GI-tract was described as a first-order process with an absorption rate constant of 1 h^{-1} . All absorbed profenofos was assumed to be transferred directly to the liver compartment via the portal vein. Tissue:plasma partition coefficients were estimated based on the method of Berezhkovskiy (2004) using $\log K_{ow}$, pKa and fraction unbound plasma (fup) as input parameters. $\log K_{ow}$ and pKa values were estimated using chemicalize (www.chemicalize.com) and fup was estimated (based on LogP and pKa) using the online simcyp tool (<https://www.certara.com/software/pbpbk-modeling-and-simulation/>).

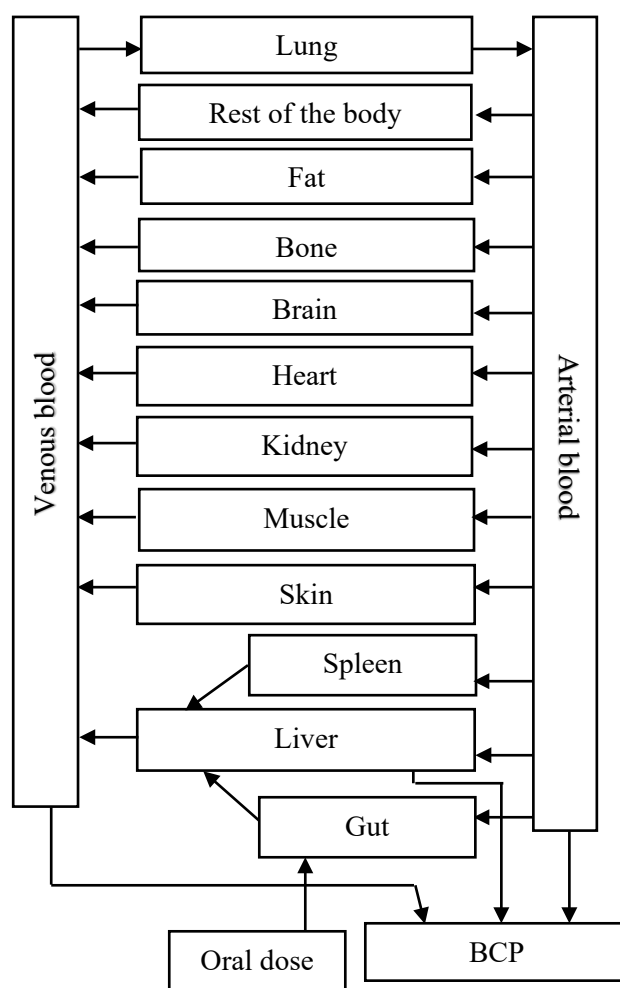


Fig 2. Schematic diagram of the PBK model for profenofos for rats and humans.

The main metabolite of profenofos reported *in vivo* is 4-bromo-2-chlorophenol (BCP), which has been reported to be formed upon paraoxonase 1 (PON1)-mediated hydrolysis of profenofos (JMPR 2007; EPA 2016; Dadson et al. 2013) (Figure 1). Profenofos hydrolysis (BCP formation) was quantified in the present study using rat and human liver microsomes, liver cytosol and plasma (In vitro incubations to derive kinetic parameter values for description of metabolic clearance in the PBK model). Profenofos clearance was included in the blood and liver compartments of the PBK model. In *in vitro* studies, also CYP-mediated formation of other metabolites has been reported (in the presence of inhibitors of hydrolysis enzymes) (Dadson et al. 2013), but these are considered less relevant, since the hydrolysis reaction is more efficient than the CYP-mediated oxidations, as indicated in our *in vitro* metabolism studies with liver microsomes or cytosol in which practically all profenofos was converted into BCP. Since BCP was shown to not inhibit AChE (see "Results"), only profenofos kinetics were

considered relevant for the reverse dosimetry and included in the PBK model (Figure 2). The only in vivo data publicly available on profenofos kinetics in rats or humans, required for model evaluation, relate to the urinary excretion of conjugated BCP in rats. Therefore, to allow model evaluation, the rat PBK model was extended to include a sub-model on BCP and BCP-glucuronide formation (Supplementary Figure 1). Estimated tissue:plasma partition coefficients of BCP and BCP-glucuronide and fraction unbound plasma (fup) values used for these sub-models are presented in Supplementary Table 1.

Renal excretion is also included in the model which is described by a passive renal clearance (via glomerular filtration) of the unbound fraction in blood at the rate of 6.7 L h^{-1} in humans and 0.078 L h^{-1} in rats. The model equations were coded and numerically integrated in Berkeley Madonna 9.1.18 (UC Berkeley, CA, USA), using the Rosenbrock's algorithm for stiff systems. The PBK models' differential equations are provided in the Supplementary Materials.

2.2.2 In vitro incubations to derive kinetic parameter values for description of metabolic clearance in the PBK model

Incubations of profenofos with rat and human liver microsomes, liver cytosol and plasma were performed to quantify in vitro rates of BCP formation. Conditions were optimized to be linear for metabolite formation with regard to incubation time and microsomal, cytosolic and plasma protein concentration (data not shown). The final incubations were carried out in 100 mM Tris HCl (pH 7.4, 37 °C) containing (final concentrations) 5 mM MgCl₂, 2 mM CaCl₂ [to stimulate PON1 activity (Carr et al. 2015)], 2 mM NADPH (cofactor to also include CYP-mediated metabolism), enzyme preparation (final concentration 2 mg/ml for human liver microsomes and cytosol and 4.4 mg/ml for human plasma; 0.5 mg/ml for rat microsomes and cytosol and 1.65 mg/ml for rat plasma) and profenofos (at final concentrations ranging from 1 to 100 µM, added from 100 times concentrated stock solutions in DMSO). Control incubations were performed in the absence of microsomes, cytosol or plasma. After 2 min pre-incubation, the reaction was initiated by adding the substrate and mixtures were incubated for 2 min in a 37 °C water bath. The total volume of the incubation mixtures was 200 µl. The reaction was terminated by the addition of 50 µl ice cold ACN and samples were kept on ice. The mixture was centrifuged at 14,000g for 20 min at 4 °C and the supernatant was analyzed using UPLC-UV.

2.2.3 UPLC-UV analysis

All samples from incubations were analyzed using a Waters Acquity UPLC H class system that consisted of a quaternary solvent manager, a sample manager, and a photodiode array (PDA) detector, equipped with a Water Acquity UPLC® BEH C18 column (1.7 μm, 2.1 × 50 mm) and Waters Xbridge UPLC® BEH C18 pre-column (1.7 μm, 2.1 × 5 mm). The temperature of the column was kept at 40 °C and the auto sampler at 10 °C during the UPLC analysis. The mobile phases used for the analysis consisted of (A) 0.1% TFA in nanopure water and (B) 100% ACN. A gradient elution at a flow rate of 0.6 ml/min was applied for the analysis with the initial condition of 100% A:0% B (v/v), changing in a linear way to 0% A:100% B from 0 to 6 min, which was maintained for 30 s, and then changed back to the initial conditions in 30 s, which were maintained for 1 min. The injection volume for each sample was 3.5 μl.

Under these conditions, the retention times of profenofos and BCP were 4.76 and 3.37 min, respectively. The amounts of profenofos and BCP were quantified by integrating the peak areas at 237 nm using calibration curves that were prepared using commercially available standards.

3

2.2.4 In vitro metabolism data analysis and scaling in the PBK model

Kinetic parameters including the apparent maximum velocity (V_{max}) and the apparent Michaelis–Menten constant (K_m) for BCP formation were obtained by fitting the data for the substrate concentration-dependent rate of conversion (expressed in nmol/min/mg protein) using GraphPad Prism 5, version 5.04 (San Diego, California, USA) to the standard Michaelis–Menten equation:

$$V = V_{max} * [S] / (K_m + [S])$$

in which the S represents the concentration of substrate, expressed in μM, V and V_{max} the velocity and the maximum velocity of the reaction, respectively, expressed in nmol/ min/mg protein, and K_m the apparent Michaelis–Menten constant, expressed in μM. The kinetic parameter values for conversion of profenofos to BCP in the liver microsomes, liver cytosol and plasma were determined. To determine the catalytic efficiency, V_{max} was divided by the K_m .

The in vitro V_{max} values were scaled in the PBK model code (Supplementary Materials) using the following scaling factors for rats and humans: 35 mg microsomal protein/g liver, 80.7 mg

cytosolic protein/g liver and 550 mg plasma/g blood (Medinsky et al. 1994; Cubitt et al. 2011). The apparent V_{max} values obtained from enzymatic incubations expressed in nmol/min/mg protein were converted into $\mu\text{mol/h/kg}$ liver and plasma in the PBK model code. The in vivo K_m values were assumed to be equal to those obtained in vitro (taking into account the differences in free fraction in vitro vs in vivo).

2.2.5 Model evaluation

Since the only in vivo data available on profenofos kinetics for model evaluation were on the urinary excretion of conjugated BCP in rats, the rat PBK model was extended to include a sub-model on BCP and BCP-glucuronide (Supplementary Figure 1). Estimated partition coefficients and f_{up} values of BCP and BCP-glucuronide used for these sub-models are presented in Supplementary Table 1 and conversion of BCP to BCP-glucuronide was assumed to take place only in the liver having the same apparent K_m and V_{max} values as reported before by Strikwold et al. (2013) for phenol glucuronidation. The PBK model-predicted cumulative urinary excretion of BCP-glucuronide were compared with reported in vivo data on conjugated BCP excretion in profenofos-exposed rats (Cho et al. 2002).

Furthermore, a sensitivity analysis was performed to estimate the impact of the chemical-specific parameters on the model output [maximum free (unbound) blood concentrations of profenofos in this study]. Normalized sensitivity coefficients (SCs) were calculated using the following equation:

$$SC = (C' - C) / (P' - P) \times (P / C)$$

in which P represents the parameter value in the PBK model and P' the parameter value with a 5% increase (Evans and Andersen 2000). Likewise, C' represents the model output obtained with the 5% increase in P, while C is the model output using the initial model parameter value. The sensitivity analysis was conducted for oral exposure to predicted effect doses obtained with the reverse dosimetry analysis (BMDL₁₀ values). BMDL₁₀ values were selected since a BMDL₁₀ value from a rat study on profenofos-induced AChE inhibition was recently used to derive the POD to obtain an acute reference dose (ARfD) for profenofos by the US EPA (EPA 2016).

2.3 Determination of in vitro AChE inhibition by profenofos and quantitative in vitro to in vivo extrapolation (QIVIVE) using reverse dosimetry

To perform reverse dosimetry of in vitro AChE inhibition by profenofos, first the in vitro AChE activity in the absence or presence of increasing concentrations of profenofos was determined. For humans, commercially available recombinant AChE was used. For rats, no commercially available recombinant AChE was available, so rat AChE was obtained from rat blood as described below.

2.3.1 Derivation of a concentration–response curve for human recombinant AChE inhibition

3

AChE inhibition was determined following the protocol of Ellman et al. (1961) as modified by Chambers and Chambers (1989). The concentration of acetylthiocholine and recombinant AChE were optimized to be linear for metabolite formation (data not shown). Human recombinant AChE was dissolved in 0.1 M sodium phosphate (pH 7.4) containing 1 mg/ml BSA (which was present to stabilize human recombinant AChE (Rosenfeld and Sultatos 2006)) to reach an enzyme concentration of 200 U/ml. Subsequently, the AChE enzyme solution was further diluted with 0.1 M sodium phosphate (pH 7.4) containing 1 mg/ml BSA to a working concentration of 1 U/ml. A range of concentrated stock solutions of profenofos were prepared in ethanol and 50 times diluted by adding 5 μ l of stock solution to 245 μ l of 0.1 M sodium phosphate (pH 7.4) (containing 0.1 mg/ml BSA). For the negative control, 5 μ l of ethanol without profenofos was added to 245 μ l of 0.1 M sodium phosphate (pH 7.4) (containing 0.1 mg/ml BSA). Subsequently, 5 μ l of these working solutions was added into wells of a 96-well plate already containing 44- μ l sodium phosphate (pH 7.4) (containing 0.1 mg/ml BSA). To start the reaction (in absence or presence of a range of profenofos concentrations), 1- μ l enzyme solution was added, giving a total volume of 50 μ l per reaction with an AChE concentration of 0.02 U/ml and an ethanol concentration of 0.2%, a level that had no effect on the activity of the enzyme. After 15-min incubation at 37 °C, the reactions were stopped by adding 150 μ l of a mixture of 5,5-dithiobis (2-nitrobenzoic acid) (DTNB) and acetylthiocholine (ATC) (final DTNB and ATC concentrations were 0.075 and 0.15 mM, respectively). Subsequently, the time-dependent increase in absorbance due to formation of chromophore

(DTNB+thiocholine) was measured at 37 °C using a wavelength of 412 nm during a period of 10 min, using a spectrophotometer (SpectraMax, Molecular Devices, UK).

AChE activity was expressed as enzyme activity (percent of control). The concentration of profenofos that produced a 50% decrease in AChE activity (IC₅₀) was determined from best-fit plots of the mean (±SD) percentages of inhibition vs. the 10log logarithm of profenofos concentrations using GraphPad Prism 5, version 5.04 (San Diego, California, USA) equation:

$$Y = 100 / (1 + 10^{(X - \text{LogIC}_{50})})$$

2.3.2 Derivation of a concentration–response curve for rat erythrocyte AChE inhibition

2.3.2.1 Blood sample processing and enzyme extraction

Rat blood samples were processed according to a method reported by Larsen et al. (2019) with a few modifications to isolate the extrinsic membrane bound AChE. Briefly, the blood sample (2 ml) was centrifuged at 3000g for 15 min to separate plasma and cells. Aliquots of 500 µl of the cells were resuspended in 4.5 ml lysis buffer (20 mM sodium phosphate; pH 7.4) and frozen at – 80 °C for 24 h. After that, the cell samples were thawed and centrifuged (4000g) for 15 min at 4 °C. The supernatant was poured off and the precipitate was suspended in 4.5-ml lysis buffer. This treatment was repeated another two times. The residue containing what is called erythrocyte ‘ghost’ membranes, was resuspended in 500-µl analysis buffer (100 mM sodium phosphate; pH 7.4), and stored at – 80 °C until analysis. Aliquots of erythrocyte ‘ghost’ membrane preparations were used for protein measurement using the Pierce™ BCA Protein Assay Kit (Thermo Fisher) with BSA as standard for quantification (Lowry et al. 1951), and for AChE activity assessment.

2.3.2.2 Rat red blood cell (RBC) AChE activity

The effect of profenofos on rat AChE activity was assessed as described above for human recombinant AChE, with a few modifications. Briefly, a typical reaction mixture (200 µl) for AChE activity contained 0.005 mg/ml erythrocyte ‘ghost’ membrane protein. The rest of the steps were as described above for measurement of human recombinant AChE activity.

2.3.3 QIVIVE of AChE inhibition data with PBK modeling-facilitated reverse dosimetry

In the present study, it was assumed that in vivo dose-dependent AChE inhibition (in blood) depends on the maximum concentration (C_{max}) of profenofos reached in the blood. For adequate PBK modeling-facilitated reverse dosimetry, the active (unbound) concentration of a test chemical in the in vitro test system should be linked to the in vivo freely available chemical at the target site. This is important since it is assumed that it is the fraction unbound that causes the effect (AChE inhibition). In the in vitro incubations, a very low concentration of BSA (0.1 mg/mL) is present. Heilmair et al. (2008) reported that with such low BSA concentrations, the free concentration of chlorpyrifos oxon is not affected. Furthermore, Rosenfeld and Sultatos (2006) found no evidence of binding of paraoxon by BSA even at a higher concentration (1 mg/ml) during incubations. Based on these observations, no significant effect on the free fraction of profenofos in the in vitro AChE inhibition studies is expected, which corroborated with estimations on profenofos binding in the in vitro incubations with help of the online simcyp tool (<https://www.certara.com/software/pbpbk-modeling-and-simulation/>). A description of the fraction unbound in blood is incorporated in the PBK model, hence, the predicted in vivo unbound C_{max} values in blood were related to the profenofos concentrations we applied in vitro.

By calculating with the PBK model, the external dose required to reach (as unbound C_{max}) the concentrations applied in the in vitro test, each in vitro concentration was translated into an in vivo dose. In this way, the concentration–response curves for rat and human AChE inhibition were converted into in vivo dose–response curves for profenofos-induced AChE inhibition in rats and humans, respectively.

2.4 Evaluation of predicted dose–response curves for rat and human AChE inhibition

To evaluate the performance of the PBK modeling-facilitated reverse dosimetry approach to predict in vivo AChE inhibition, the predicted dose–response curve for rat AChE inhibition upon exposure to profenofos was compared with available in vivo data on AChE inhibition in rats (JMPR 2007). Furthermore, the predicted dose–response data were used for BMD modeling, using EFSA PROAST version 69.0 (<https://shiny-efsa.openanalytics.eu/app/bmd>) using the model averaging approach to allow evaluation of the prediction by comparison of

BMDL₁₀ values obtained from the predicted dose–response data to points of departure derived by regulatory bodies (EPA 2016; JMPR 2007, EFSA 2019). To that end, the obtained BMDL₁₀ values were compared with a reported BMDL₁₀ value from a rat study on profenofos-induced RBC AChE inhibition, which was recently used to obtain an ARfD by the US EPA (EPA 2016), and a reported NOAEL value on profenofos-induced rat brain acetylcholinesterase inhibition, which has been used to obtain an ARfD by JMPR (2007).

3. Results

3.1 In vitro conversion of profenofos to BCP

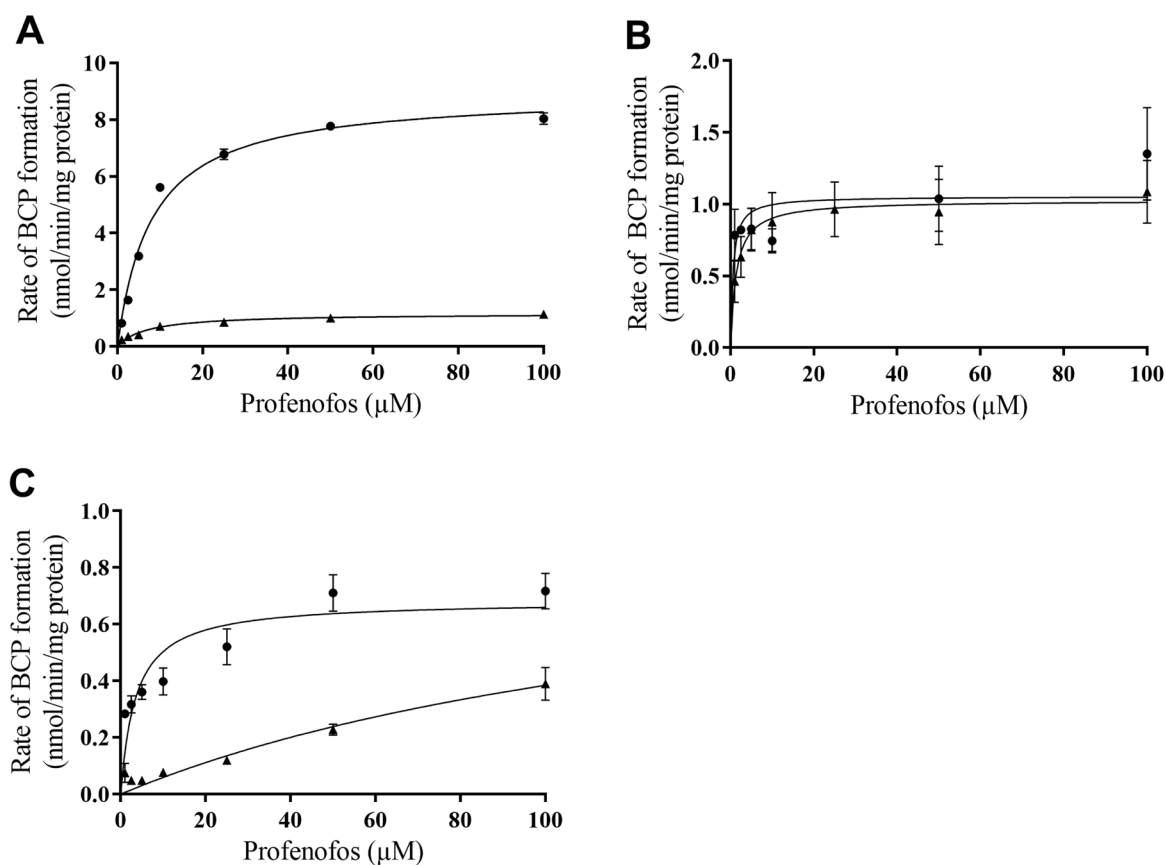


Fig 3. Concentration-dependent rate of profenofos conversion to BCP in incubations with human (triangles) and rat (dots) (A) liver microsomal proteins, (B) liver cytosolic proteins, and (C) plasma proteins. Results represent data from 3 independent experiments and are presented as mean \pm SEM.

The conversion of profenofos to BCP was measured in incubations with both rat and human liver microsomes, cytosol and plasma. UPLC analysis revealed that only one peak (BCP)



appeared when analyzing the samples obtained from these incubations. In control incubations, small amounts (max 0.04% of the amount of profenofos added) of BCP were detected, indicating some spontaneous hydrolysis of profenofos in the aqueous environment, which has also been observed in previous studies (Aly and Badawy 1982). The BCP formation data for microsomes, cytosol and plasma were, therefore, corrected for BCP levels detected in control incubations.

The concentration-dependent velocity of BCP formation following incubation of profenofos with both human and rat liver microsomes, liver cytosol and plasma is depicted in Figure 3A–C. The kinetic parameters derived from these data (K_m and V_{max}) as well as the catalytic efficiencies, calculated as V_{max}/K_m , are presented in Table 1.

The results indicate differences in the catalytic efficiencies for conversion of profenofos to BCP by rats and humans (Table 1). The catalytic efficiency for microsomal biotransformation of profenofos to BCP was 6.5-fold lower in incubations with human liver microsomes than with rat liver microsomes, due to a 7.7-fold lower V_{max} and a 1.2-fold lower K_m (Table 1). Likewise, the catalytic efficiency for cytosolic biotransformation of profenofos to BCP was 3.8-fold lower for human liver cytosol, with a 1.1-fold higher V_{max} , and a 4.1-fold higher K_m for human liver cytosol as compared to rat liver cytosol. Largest differences were observed for plasma, indicated by the 32-fold lower catalytic efficiency of biotransformation of profenofos to BCP for human plasma than for rat plasma, due to a 1.5-fold higher V_{max} and 44-fold higher K_m for human plasma as compared to rat plasma.

Inter-species differences in red blood cell acetylcholinesterase inhibition of profenofos

Table 1. Kinetic parameter values (K_m , V_{max}) and catalytic efficiencies (V_{max}/K_m) for in vitro conversion of profenofos to BCP.

	Human	Rat
Liver microsomes		
K_m (μM)	6.9	8.1
V_{max} (nmol/min/mg microsomal protein)	1.2	8.9
Catalytic efficiency (ml/min/mg protein)	0.17	1.1
Liver cytosol		
K_m (μM)	1.4	0.34
V_{max} (nmol/min/mg cytosolic protein)	1.1	0.95
Catalytic efficiency (ml/min/mg protein)	0.79	2.8
Plasma		
K_m (μM)	158	3.6
V_{max} (nmol/min/mg plasma protein)	0.99	0.68
Catalytic efficiency (ml/min/mg protein)	0.0063	0.19

3

3.2 PBK model development and evaluation

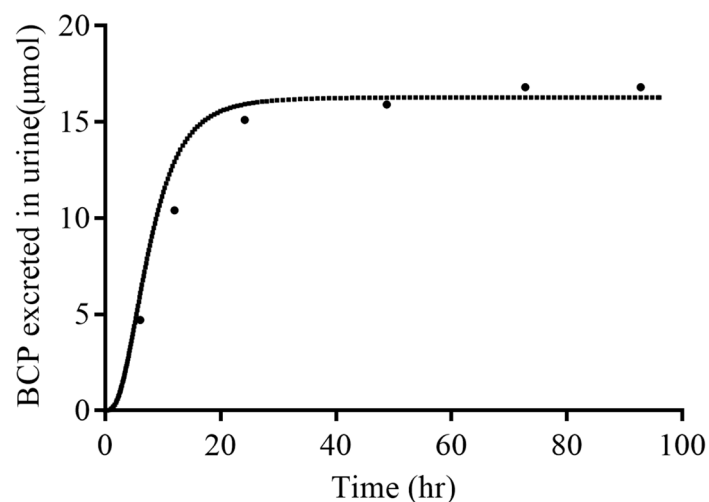


Fig 4. Comparison of PBK model-predicted (continuous line) and experimentally determined (symbols, Cho et al., 2002) time-dependent cumulative urinary excretion of BCP-glucuronide in rats upon oral administration of 35.8 mg profenofos/kg bw.

3

Using the kinetic parameters defined *in vitro* and the input parameters obtained with *in silico* methods summarized in Supplementary Table 1, PBK models for profenofos in rat and human were made. Figure 4 presents the rat PBK model-based prediction of the urinary BCP excretion. In a subsequent step, first, the developed rat profenofos PBK model was evaluated against *in vivo* data on urinary excretion of conjugated BCP in rats from a study by Cho et al. (2002). These results indicate that the predictions made by the newly developed PBK model for rat match the reported *in vivo* data well. Due to a lack of *in vivo* kinetic data for humans, evaluation of the performance of the PBK model for profenofos in humans could not be performed. However, the human model was considered to be adequate, since it is based on the same conceptual model and *in vitro*- and *in silico*-derived input parameters were defined in the same way as those for the rat model.

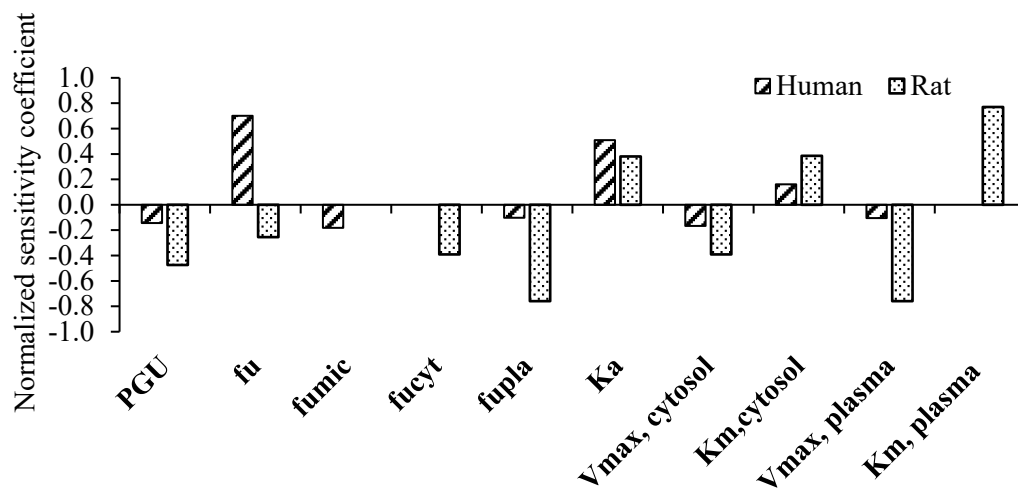


Fig 5. Sensitivity analysis representing the influence of model parameters on the predicted blood C_{max} of profenofos in humans and rats at predicted $BMDL_{10}$ values of 0.01 and 0.45 mg/kg bw, respectively. PGU gut:plasma partition coefficient, fu fraction unbound in plasma, fumic fraction unbound in microsomal incubation, fucyt fraction unbound in cytosolic incubation, fupla fraction unbound in incubation with plasma, ka absorption constant, V_{max} , cytosol=maximum rate of conversion of profenofos to BCP by liver cytosol, K_m cytosol Michaelis–Menten constant for conversion of profenofos to BCP by liver cytosol, V_{max} plasma=maximum rate of conversion of profenofos to BCP by plasma, K_m plasma=Michaelis–Menten constant for conversion of profenofos to BCP by plasma.

Further evaluation of the PBK models included a local sensitivity analysis in which the impact of each chemical-specific parameter on the predicted free (unbound) C_{max} of profenofos in the rat and human PBK model was determined upon exposure to predicted effect doses ($BMDL_{10}$ values derived from predicted dose–response data). Figure 5 presents the parameters for which the SCs are higher than 0.1 (absolute value). For both rat and human models, the prediction of the C_{max} of profenofos appeared to be mainly affected by the kinetic parameters for conversion of profenofos to BCP by enzymes from especially plasma and liver cytosol, in addition to the absorption rate constant (ka) and the gut to plasma partition coefficient.

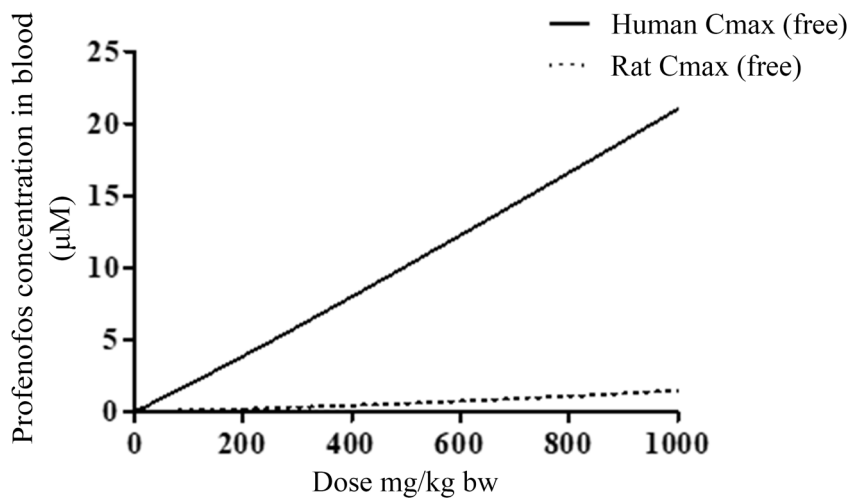


Fig 6. PBK model-predicted dose-dependent C_{max} (free) in blood upon oral profenofos exposure in rats (dotted line) and humans (continuous line).

The obtained PBK models reveal differences in kinetics in rats and humans (Figure 6). Figure 6 shows the PBK model-predicted dose-dependent C_{max} values (free concentration) in rats and humans, indicating that humans are expected to reach around 20-fold higher blood concentrations than rats at equal oral exposure levels, mainly due to the lower catalytic efficiency for metabolic clearance of profenofos in humans.

3.3 Prediction of in vivo dose-dependent AChE inhibition by PBK modeling-facilitated reverse dosimetry of in vitro data and comparison with reported in vivo effect data

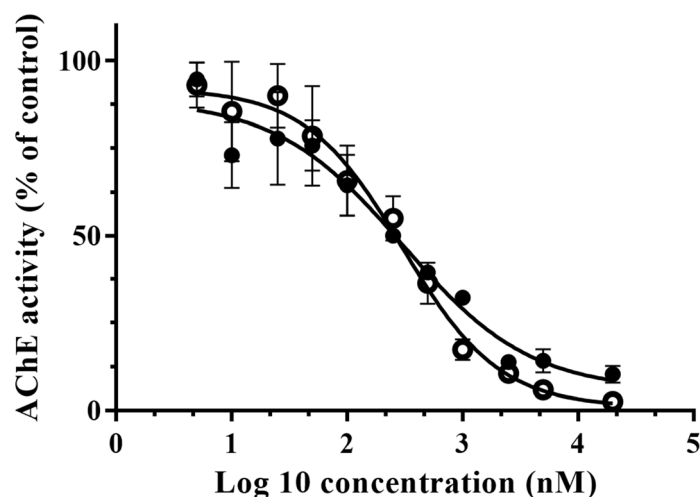


Fig 7. Acetylcholinesterase (AChE) activity in RBCs of Sprague–Dawley rats (closed symbols) and of human recombinant AChE (open symbols) with increasing concentrations of profenofos. AChE activity in the solvent control is set at 100%. Results represent data from 3 independent experiments and are presented as mean \pm SEM.

Concentration-dependent inhibition of rat RBC AChE (obtained from rat blood) and human (recombinant) AChE by profenofos were obtained in vitro (Figure 7). Profenofos inhibited human AChE with an IC₅₀ value of 302 nM, which is very close to the IC₅₀ value of 350 nM reported by Das and Jamil (2006) using freshly obtained human erythrocytes. Profenofos inhibited rat AChE with an IC₅₀ of 312 nM, suggesting no species difference in profenofos-induced AChE inhibition, based on effect concentrations related to 50% AChE inhibition.



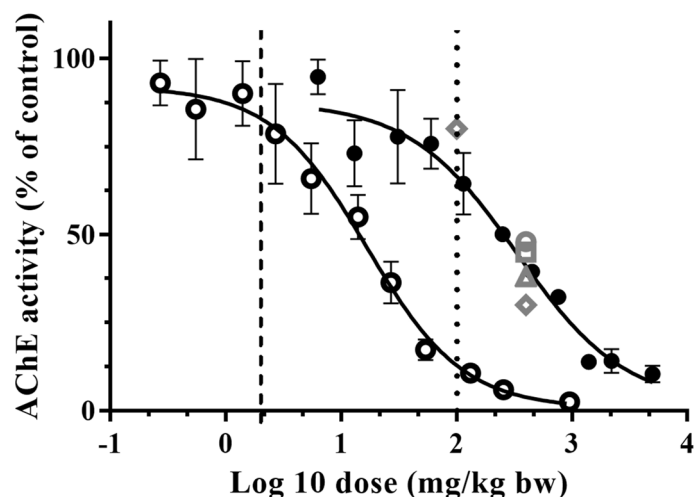


Fig 8. Predicted dose–response curves for profenofos-induced decrease of AChE activity in rats (closed black circles) and humans (open black circles). In vivo data on profenofos-induced AChE inhibition in rats as reported in Jmpr (2007) are included: open grey diamond—male rat RBC inhibition, open grey triangle—male rat brain inhibition, open grey square—female rat brain inhibition, open grey circle—female rat RBC inhibition. EPA BMDL10 and Jmpr NOAEL are indicated by the vertical lines (EPA 2016: dashed line; Jmpr 2007: dotted line).

3

The concentration-dependent AChE inhibition curves obtained in this study were converted into in vivo dose-dependent AChE inhibition curves in rats and humans (Figure 8) using the PBK modeling-facilitated reverse dosimetry approach as described in the materials and methods section. Figure 8 also presents in vivo data for male and female rat profenofos-induced AChE inhibition in RBCs and in the brain available from literature (Jmpr 2007). The results reveal that predicted in vivo dose–response curves for rat AChE inhibition are close to the reported in vivo data for male and female rat AChE inhibition in RBCs and in the brain (Jmpr 2007), indicating that with this combined in vitro–in silico approach, good predictions for rats were obtained. Predictions for humans indicate that humans are expected to be more sensitive than rats regarding profenofos-induced AChE inhibition (Figure 8), which is mainly due to the slower metabolic clearance of profenofos, resulting in higher C_{max} values at the same dose levels (Figure 6). Toxicity data for humans for further evaluation of the predicted dose–response curves are not available.

BMD analysis was performed on predicted dose–response data for rats and human. Results of these analyses are presented in Supplementary Tables 2 and 3 and Supplementary Figures 2 and 3. BMDL₁₀ values obtained for rats and humans upon model averaging were 0.45 and 0.01 mg/kg bw, respectively, predicting humans to be more sensitive than rats. In theory, BMD

values obtained from predicted dose–response data may serve as PODs for setting safe exposure levels, i.e., an ARfD, and these BMD values were, therefore, compared with PODs that have been used by the US EPA, JMPR and EFSA in their assessments.

The US EPA considered erythrocyte (RBC) AChE inhibition to be more suitable to derive a POD for human safety assessments, since it is more sensitive than brain AChE inhibition in case of profenofos exposure (EPA 1999, 2016). A 10% RBC inhibition of AChE has been adopted by the US EPA to obtain a POD to define the ARfD for profenofos (EPA 2016). The US EPA reported a BMDL₁₀ of 1.99 mg/kg bw for profenofos-induced RBC AChE inhibition in adult rats upon a single exposure to profenofos, being 4 times higher than the BMDL₁₀ obtained from the predicted dose–response data for rats in our study (0.45 mg/kg bw).

JMPR used a NOAEL value of 100 mg/kg bw to derive an ARfD, based on a dataset on profenofos-induced inhibition of brain AChE in rats (upon a single exposure to profenofos). This NOAEL value is 50-fold higher than the BMDL₁₀ value reported by the US EPA and 200-fold higher than the BMDL₁₀ value obtained from our predicted dose–response data in rats (0.45 mg/kg bw), suggesting the NOAEL to result in a POD that may be too high.

In a recent report from EFSA (EFSA 2019), an ARfD for profenofos of 0.005 mg/kg bw was reported, based on a German evaluation in 2001 that defined an ARfD based on a NOAEL in a dog study using inhibition of brain cholinesterase activity as critical effect. Unfortunately, no further information (e.g., NOAEL) on that particular dog study is publicly available. If a safety factor of 100 was used to derive this ARfD, the NOAEL derived from the dog study would be close to the BMDL₁₀ value obtained from our predicted dose–response data in rats (0.45 mg/kg bw (~100-fold higher than the ARfD)).

4. Discussion

The aim of the current study was to develop a physiologically based kinetic (PBK) model in rats and humans solely based on in vitro and in silico input parameters to be applied for the prediction of in vivo AChE inhibition by the OP pesticide profenofos by reverse dosimetry of in vitro AChE inhibition data. To this end, profenofos PBK models were developed for rats and humans and used to predict dose-dependent internal profenofos concentrations, which were applied for reverse dosimetry to translate in vitro concentration-dependent data on profenofos-induced inhibition of AChE to in vivo dose–response curves for profenofos-induced inhibition

of AChE in blood. The results indicate that profenofos-induced AChE inhibition in rats was closely predicted and that humans are predicted to be more sensitive to profenofos-induced AChE inhibition than rats upon acute exposure.

This study has shown marked interspecies differences in toxicokinetics of profenofos with predicted blood C_{max} values for profenofos in humans being around 20-fold higher than in rats at equal levels of exposure (Figure 6). This is mainly due to higher catalytic efficiencies for microsomal, cytosolic and plasma biotransformation of profenofos to BCP in rats as compared to humans as observed in this study (Table 1). Profenofos, being an oxon, is mainly detoxified through hydrolysis by hepatic and plasma PON1 and CYP450-mediated detoxification, resulting in the production of BCP (JMPR 2007; EPA 2016; Dadson et al. 2013). Interspecies differences in activities between human and rat PON1 have been reported, with human PON1 having lower catalytic activity as compared to rat PON1 (KalisteKorhonen et al. 1996). Another possible reason for the differences in profenofos detoxification may be related to quantitative differences in B-esterases in rats and humans, which may affect the metabolism and disposition of ester compounds including OPs (Ecobichon and Comeau 1973; Maxwell et al. 1987). B-esterases, such as carboxylesterase (CaE), butyrylcholinesterase (BuChE) and acetylcholinesterase (AChE), detoxify oxons, but these enzymes are inhibited by the oxons as a consequence (Chanda et al. 1997). It has been reported that rat plasma contains almost all types of esterases including CaE, PON1, BChE, and AChE (Bahar et al. 2012; Satoh and Hosokawa 2006), whereas humans are deficient of plasma CaE (Williams et al. 2011; Berry et al. 2009; Li et al. 2005) and plasma AChE (Ecobichon and Comeau 1973). The relevance of CaE in OP detoxification is indicated by a study that demonstrated that *in vivo* inhibition of CaEs by cresylbenzodioxaphosphorin oxide (CBDP) caused an increase in the toxicity of many OPs in rats, mice, rabbits and guinea pigs (Ecobichon and Comeau 1973; Maxwell et al. 1987). In the same study, the interspecies differences observed in the toxicity of OPs were lost in the group treated with the *in vivo* CaE inhibitor (CBDP) (Maxwell et al. 1987). The absence of CaE in human plasma in addition to low PON1 activity may, therefore, be responsible for lower profenofos clearance resulting in higher sensitivity of humans to profenofos as compared to rodents (KalisteKorhonen et al. 1996). In this way, B-esterases may play a protective role in rats but not humans.

Data on RBC AChE inhibition can be considered as an appropriate surrogate measure of potential organophosphate effects on the peripheral and central nervous systems in absence of brain AChE inhibition data (Chen et al. 1999; Das and Jamil 2006). To predict profenofos dose

levels that result in AChE inhibition in rats and humans, profenofos in vitro concentration–response curves for RBC AChE inhibition (Figure 7) were translated to in vivo dose–response curves for RBC AChE inhibition for both rats and humans (Figure 8). The predicted data thus obtained for the rat matched with the available in vivo rat data as reported by JMPR (2007) (Figure 8), and the BMDL₁₀ obtained from the predicted dose–response data differed only fourfold from the BMDL₁₀ obtained from data from an in vivo rat study on profenofos-induced blood AChE inhibition used by the US EPA for determination of an ARfD for profenofos. This indicates that in vivo dose-dependent AChE inhibition was closely predicted based on our approach, giving confidence in the human predictions, which could not be further evaluated because of the lack of human in vivo data on this endpoint. Our predictions suggest that humans are more sensitive than rats towards profenofos-induced AChE inhibition. The interspecies differences (45-fold difference in BMDL₁₀) were predicted to be mainly due to interspecies differences in toxicokinetics, as discussed above, and these would not be covered by the standard uncertainty factor of 10 to account for interspecies differences. Currently, we work on the assessment of human interindividual differences in profenofos metabolic clearance (using plasma and liver fractions of different donors) to be incorporated in PBK models, providing insight into whether a combined uncertainty factor of 100 (10 for interspecies differences and 10 for intraspecies differences) applied to the rat AChE inhibition data is expected to be sufficiently protective for sensitive human individuals.

In the present study, the BMDL₁₀ calculated based on predicted rat data was 4 times lower than the BMDL₁₀ value used by EPA and 200-fold lower than the NOAEL used by JMPR to obtain an ARfD, implying that our prediction is more conservative as compared to the rat data used by the two agencies. In a possible future risk assessment paradigm that would be independent of animal data, BMDL₁₀ values obtained from the predicted human dose–response data may be applied. In the present study, we determined a BMDL₁₀ value for ‘an average human’ (0.01 mg/kg bw), not quantifying possible interindividual differences. To take interindividual differences into account, an uncertainty factor may be applied, but it would be scientifically more sound to quantify interindividual differences in the human population in profenofos detoxification. This is especially of interest given the reported genetic polymorphisms of human PON1 (and BuChE) with related phenotypes of low and high activities (Schwarz et al. 1995; Geldmacher et al. 1989), which may play a role in the interindividual differences in PON1 activity (Darney et al. 2020), suggesting possible large human interindividual differences in profenofos detoxification. As indicated above, we currently work on the

determination of such interindividual differences in profenofos detoxification in humans and integrate these data in the human PBK modeling-based predictions of profenofos toxicity.

Although the current models quantitatively predicted profenofos tissue dosimetry and the resulting AChE inhibition, possible limitations of the approach should be considered. In the current PBK model, gut absorption of profenofos was estimated to be 100% using a first-order process with an absorption rate constant of 1 h^{-1} . Although this resulted in the adequate prediction of time-dependent BCP-glucuronide in rat urine, it must be noted that specific model output is not so sensitive to the k_a (data not shown), whereas the (unbound) C_{max} is (Figure 5). It is noteworthy that the extent of absorption varies depending on the dosing method, dose formulation (solution) and variations in species, strain and gender (Kararli 1995). Furthermore, profenofos absorption as present in the food matrix may be different.

3

We used a static approach to determine the AChE inhibitory effect concentrations, using a single pre-incubation time point (15 min). When including more time points, information on the time-dependent inhibition kinetics can be obtained. However, a previous study with chlorpyrifos oxon showed that human recombinant AChE active sites were 100% inhibited after a pre-incubation period of 11 min (Kaushik et al. 2007). One would expect that effect concentrations would decrease with longer incubation times until 100% of the binding sites is inhibited, as shown before by Aurbek et al. (2006) and Krstić et al. (2008). With a relatively long pre-incubation time of 15 min as we have used in the present study, similar to incubation times previously applied by other research groups (e.g., Aurbek et al. 2006; Kasteel et al. 2020), we aimed to obtain a relevant and conservative estimation of the effect concentrations, as also indicated by the small difference between the BMDL_{10} value obtained with our predicted rat dose–response data and the BMDL_{10} value from a reported in vivo study in rats.

It must also be noted that the approach used in this study may be suitable to estimate AChE inhibition upon a single exposure, while not predicting effects upon repeated exposure, since upon longer exposures, one must take the time-dependent de novo AChE production into account to adequately estimate the AChE activity upon a second and further exposure. In that regard, a phenomenon referred to as steady state AChE inhibition is of interest, which is the situation when the degree of AChE inhibition reaches equilibrium with the production of new enzyme at which AChE inhibition remains constant at a specified dose over the exposure period (EPA 2016). Adequate prediction of these processes based on only in vitro data, as applied in the present study, seems at this stage not possible. Furthermore, one must consider that OPs

inhibit detoxifying enzymes, such as CaE and BuChe, which may result in a decrease in metabolic clearance, and related higher internal concentrations and increased sensitivity upon repeated dosing.

Another limitation of the approach is that the prediction of OP toxicity was only based on AChE inhibition as the endpoint. It should, however, be noted that OPs may affect a number of additional targets (such as Neuropathy target esterase (NTE) (Costa 2018), muscarinic M2 receptors (Costa 2006), acylpeptide hydrolase (APH) (Richards et al. 2000), fatty acid amide hydrolase (FAAH) (Quistad et al. 2001; Buntyn et al. 2017) and a variety of lipases (Quistad et al. 2006)) that lead to OP toxicity, including neuroinflammation, autoimmunity and axonal transport deficits (Naughton and Terry 2018). On the other hand, AChE inhibition has been used as an endpoint to set a POD for the risk assessment (EPA 2016; EFSA 2019), indicating its relevance. The QIVIVE approach could be extended in the future to also predict dose-dependent effects related to other OP targets, allowing a more extensive hazard assessment based on NAMs.

In conclusion, the predicted dose-dependent profenofos-induced AChE inhibition in rats are close to reported data on dose-dependent *in vivo* AChE inhibition in rats upon single dosing, providing also confidence in the predictions obtained for humans. Results from this study suggest that humans may be more sensitive to AChE inhibition upon profenofos exposure than rats, which is mainly due to differences in profenofos detoxification. Altogether, the results demonstrate the ability to predict *in vivo* AChE inhibition by profenofos, providing another proof-of-principle that with NAMs *in vivo* effects of chemicals can be predicted without the use of *in vivo* studies.

Acknowledgements

This work is supported by the Netherlands Universities Foundation for International Cooperation (Nufc) [scholarship granted to Isaac Omwenga (PhD.17/0019)], the China Scholarship Council [scholarship (No. 201707720063) Granted to ZHAOSHENG], and the Dutch Ministry of Agriculture, Nature and Food Quality (project KB-23-002-021).

Conflict of interests

The authors declare that they have no conflicts of interest.

References

- Aly OA, Badawy MI (1982) Hydrolysis of organophosphate insecticides in aqueous media. *Environ Int* 7:373–377
- Aurbek N, Thiermann H, Szinicz L, Eyer P, Worek F (2006) Analysis of inhibition, reactivation and aging kinetics of highly toxic organophosphorus compounds with human and pig acetylcholinesterase. *Toxicology* 224:91–99
- Bahar FG, Ohura K, Ogihara T, Imai T (2012) Species difference of esterase expression and hydrolase activity in plasma. *J Pharm Sci* 101:3979–3988
- Berezhkovskiy LM (2004) Volume of distribution at steady state for a linear pharmacokinetic system with peripheral elimination. *J Pharm Sci* 93:1628–1640
- Berry LM, Wollenberg L, Zhao Z (2009) Esterase activities in the blood, liver and intestine of several preclinical species and humans. *Drug Metab Lett* 3:70–77
- Bogen KT, Singhal A (2017) Malathion dermal permeability in relation to dermal load: Assessment by physiologically based pharmacokinetic modeling of in vivo human data. *J Environ Sci Health B* 52:138–146
- Bouchard M, Gosselin NH, Brunet RC, Samuel O, Dumoulin MJ, Carrier G (2003) A toxicokinetic model of malathion and its metabolites as a tool to assess human exposure and risk through measurements of urinary biomarkers. *Toxicol Sci* 73:182–194
- Bouchard M, Carrier G, Brunet RC, Bonvalot Y, Gosselin NH (2005) Determination of biological reference values for chlorpyrifos metabolites in human urine using a toxicokinetic approach. *J Occup Environ Hyg* 2:155–168
- Bouchard M, Gosselin NH, Brunet RC, Samuel O, Dumoulin M, Carrier G (2017) A toxicokinetic model of malathion and its metabolites as a tool to assess human exposure and risk through measurements of urinary biomarkers. *Toxicol Sci* 73:182–194
- Bradman A, Barr DB, Claus-Henn BG, Drumheller T, Curry C, Eskenazi B (2003) Measurement of pesticides and other toxicants in amniotic fluid as a potential biomarker of prenatal exposure: a validation study. *Environ Health Perspect* 111:1779–1182
- Buntyn RW, Alugubelly N, Hybart RL, Mohammed AN, Nail CA, Parker GC, Ross MK, Carr RL (2017) Inhibition of endocannabinoid-metabolizing enzymes in peripheral tissues following developmental chlorpyrifos exposure in rats. *Int J Toxicol* 36:395–402
- Carr RL, Dail MB, Chambers HW, Chambers JE (2015) Species differences in paraoxonase mediated hydrolysis of several organophosphorus insecticide metabolites. *J Toxicol* 47:189
- Chambers JE, Chambers JW (1989) Oxidative desulfuration of chlorpyrifos, chlorpyrifos-methyl and leptophos by rat brain and liver. *J Biochem Toxicol* 4:201–203
- Chanda SM, Mortensen SR, Moser VC, Padilla S (1997) Tissue-specific effects of chlorpyrifos on carboxylesterase and cholinesterase activity in adult rats: an in vitro and in vivo comparison. *Fundam Appl Toxicol* 38:148–157
- Chen WL, Sheets JJ, Nolan RJ, Mattsson JL (1999) Human red blood cell acetylcholinesterase inhibition as the appropriate and conservative surrogate endpoint for establishing chlorpyrifos reference dose. *Regul Toxicol Pharmacol* 29:15–22
- Cho Y, Min K, Lee I, Cha C (2002) Determination of urinary metabolite of profenofos after oral administration and dermal application to rats. *J Food Hyg Saf* 17:20–25
- Costa LG (2006) Current issues in organophosphate toxicology. *Clin Chim Acta* 366:1–13
- Costa LG (2018) Organophosphorus compounds at 80: some old and new issues. *Toxicol Sci* 162:24–35
- Cubitt HE, Houston JB, Galetin A (2011) Prediction of human drug clearance by multiple metabolic pathways: integration of hepatic and intestinal microsomal and cytosolic data. *Drug Metab Dispos* 39:864–873
- Dadson OA, Ellison CA, Singleton ST, Chi L, McGarrigle BP, Pamela J, Lein JP, Farahat FM, Farahat T, Olson JR (2013) Metabolism of profenofos to 4-bromo-2-chlorophenol, a specific and sensitive exposure biomarker. *Toxicology* 306:35–39
- Darney K, Kasteel EEJ, Buratti FM, Turco L, Vichi S, Béchaux C, Roudot AC, Kramer NI, Testai E, Dorne JLCM, Di Consiglio

- Das GP, Jamil K (2006) Effect of four organophosphorus compounds on human blood acetylcholinesterase. *Vitro Stud Toxicol Mech Methods* 16:455–459
- Ecobichon DJ, Comeau AM (1973) Pseudocholinesterases of mammalian plasma: Physicochemical properties and organophosphate inhibition in eleven species. *Toxicol Appl Pharmacol* 24:92–100
- Eddleston M, Worek F, Eyer P, Thiermann H, Von Meyer L, Jeganathan K, Sherif MHR, Dawson AH, Buckley NA (2009) Poisoning with the S-Alkyl organophosphorus insecticides profenofos and prothiofos. *QJM Int J Med* 102:785–792
- Ellman GL, Courtney KD, Andres V, Featherstone RM (1961) A new rapid colorimetric determination of acetylcholinesterase activity. *Biochem Pharmacol* 7:88–95
- EFSA (European Food Safety Authority) (2019) Scientific report on scientific support for preparing an EU position in the 51st Session of the Codex Committee on Pesticide Residues (CCPR). *EFSAJ* 17:5797
- EPA (1999) Data evaluation record study type: special non-guideline assessment for RBC Cholinesterase in humans. <https://archive.epa.gov/scipoly/sap/meetings/web/pdf/kisickider.pdf> Accessed Jan 2019
- EPA (2006) Reregistration eligibility decision for dimethoate. https://archive.epa.gov/pesticides/reregistration/web/pdf/dimethoate_red.pdf. Accessed Dec 2020
- EPA (2011) Chlorpyrifos preliminary human health risk assessment DP No. D388070. <https://www.regulations.gov/contentStreamer?documentId=EPA-HQ-OPP-2008-0850-0025&contentType=pdf> Accessed Dec 2020
- EPA (2016) Profenofos: Human health draft risk assessment (DRA) for registration review. https://www3.epa.gov/pesticides/chem_search/cleared_reviews/csr_PC-111401_19-Oct-16.pdf Accessed Mar 2020
- Evans MV, Andersen ME (2000) Sensitivity analysis of a physiological model for 2, 3, 7, 8-tetrachlorodibenzo-p-dioxin (TCDD): assessing the impact of specific model parameters on sequestration in liver and fat in the rat. *Toxicol Sci* 54:71–80
- Farahat TM, Abdelrasoul GM, Amr MM, Shebl MM, Farahat FM, Anger WK (2003) Neurobehavioral effects among workers occupationally exposed to organophosphorus pesticides. *Occup Environ Med* 60:279–286
- Geldmacher-v M, Diepgen TL (1989) Human serum paraoxonase polymorphism, specificity, classification. In: Reiner E, Aldridge WN, Hoskin FCG (eds) *Enzymes hydrolyzing organophosphorus compounds* Ellis Horwood Limited. West Sussex, England, pp 15–29
- Gotoh M, Sakata M, Endo T, Hayashi H, Seno H, Suzuki O (2001) Profenofos metabolites in human poisoning. *Forensic Sci Int* 116:221–226
- Greish S, Ismail SM, Mosleh Y, Loutfy N, Dessouki AA, Ahmed MT (2011) Human risk assessment of profenofos: a case study in Ismailia. *Egypt Polycycl Aromat Compd* 31:28–47
- Hardt J, Angerer J (2000) Determination of dialkyl phosphates in human urine using gas chromatography–mass spectrometry. *J Anal Toxicol* 24:678–684
- Heilmair R, Eyer F, Eyer P (2008) Enzyme-based assay for quantification of chlorpyrifos oxon in human plasma. *Toxicol Lett* 181:19–24
- Hertz-Picciotto I, Sass JB, Engel S, Bennett DH, Bradman A, Eskenazi B, Lanphear B, Whyatt B (2018) Organophosphate exposures during pregnancy and child neurodevelopment: recommendations for essential policy reforms. *PLoS Med* 15(10):e1002671
- Jamal GA, Hansen S, Julu POO (2002) Low level exposures to organophosphorus esters may cause neurotoxicity. *Toxicology* 181–182:23–33
- Johnson MK, Glynn P (1995) Neuropathy target esterase (NTE) and 675 organophosphorus induced delayed polyneuropathy (OPIDP): recent 676 advances. *Toxicol Lett* 82–83:459–463
- Johnson MK, Glynn P (2001) Neuropathy target esterase. In: Krieger R (ed) *Handbook of pesticide toxicology*. Academic Press, San Diego, pp 953–965
- Joint FAO/WHO Meeting on Pesticide Residues (JMPR) (2007) Pesticide residues in food 2007. <http://www.inchem.org/documents/jmpr/jmpmono/v2007pr01.pdf>. Accessed Aug 2020
- Jones HM, Rowland-Yeo K (2013) Basic concepts in physiologically based pharmacokinetic modeling in drug discovery and development. *CPT Pharmacometr Syst Pharmacol* 2:e63

- Kaliste-Korhonen E, Tuovinen K, Hänninen O (1996) In vitro interspecies differences in enzymes reacting with organophosphates and their inhibition by paraoxon. *Hum Exp Toxicol* 15:972
- Karanja NK, Njenga M, Mutua GK, Lagerkvist CJ, Kutto E, Okello JJ (2012) Concentrations of heavy metals and pesticide residues in leafy vegetables and implications for peri-urban farming in Nairobi, Kenya. *J Agric Food Syst Commun Dev* 3:255–267
- Kararli TT (1995) Comparison of the gastrointestinal anatomy, physiology and biochemistry of humans and commonly used laboratory animals. *Biopharm Drug Dispos* 16:351–380
- Kasteel EEJ, Nijmeijer SM, Darney K, Lautz LS, Dorne JLCM, Kramer NI, Westerink RHS (2020) Acetylcholinesterase inhibition in electric eel and human donor blood: an in vitro approach to investigate interspecies differences and human variability in toxicodynamics. *Arch Toxicol* 94:4055–4065
- Kaushik R, Rosenfeld CA, Sultatos LG (2007) Concentration-dependent interactions of the organophosphates chlorpyrifos oxon and methyl paraoxon with human recombinant acetylcholinesterase. *Toxicol Appl Pharmacol* 221:243–250
- Krstić DZ, Colović M, Kralj MB, Franko M, Krinulović K, Trebse P, Vasić V (2008) Inhibition of AChE by malathion and some structurally similar compounds. *J Enzyme Inhib Med Chem* 23:562–573
- Kumari D, John S (2019) Health risk assessment of pesticide residues in fruits and vegetables from farms and markets of Western Indian Himalayan Region. *Chemosphere* 224:162–167
- Larsen KE, Lifschitz AL, Lanusse CE, Virkel GL (2019) In vitro and in vivo effects of chlorpyrifos and cypermethrin on blood cholinesterases in sheep. *J Vet Pharmacol Therap* 42:548–555
- Li B, Sedlacek M, Manoharan I, Boopathy R, Duysen EG, Masson P, Lockridge O (2005) Butyrylcholinesterase, paraoxonase, and albumin esterase, but not carboxylesterase, are present in human plasma. *Biochem Pharmacol* 70:1673–1684
- Liu P, Wu CH, Chang XL, Qi XJ, Zheng ML, Zhou ZJ (2014) Assessment of chlorpyrifos exposure and absorbed daily doses among infants living in an agricultural area of the Province of Jiangsu, China. *Int Arch Occup Environ Health* 87:753–762
- Louisse J, Beekmann K, Rietjens IMCM (2017) Use of physiologically based kinetic modeling-based reverse dosimetry to predict in vivo toxicity from in vitro data. *Chem Res Toxicol* 30:114–125
- Lowry O, Rosebrough N, Farr A, Randall R (1951) Protein measurement with the folin phenol reagent. *J Biol Chem* 193:265–275
- Lu C, Fenske RA, Simcox NJ, Kalman D (2000) Pesticide exposure of children in agricultural community: evidence of household proximity to farmland and take home exposure pathways. *Environ Res Sect A* 84:290–302
- Lu C, Holbrook CM, Andres LM (2010) The implications of using a physiologically based pharmacokinetic (PBPK) model for pesticide risk assessment. *Environ Health Perspect* 118:125–130
- Maxwell DM, Lenz DE, Grof WA, Kaminskis A, Froehlich HL (1987) The effects of blood flow and detoxification on in vivo cholinesterase inhibition by soman in rats. *Toxicol Appl Pharmacol* 88:66–76
- Medinsky MA, Leavens TL, Csanady GA, Gargas ML, Bond JA (1994) In vivo metabolism of butadiene by mice and rats: a comparison of physiological model predictions and experimental data. *Carcinogenesis* 15:1329–1340
- Mosquin PL, Licata AC, Liu B, Sumner SC, Okino MS (2009) Reconstructing exposures from small samples using physiologically based pharmacokinetic models and multiple biomarkers. *J Expo Sci Environ Epidemiol* 19:284–297
- Mostafalou S, Abdollahi M (2013) Pesticides and human chronic diseases: evidences, mechanisms, and perspectives. *Toxicol Appl Pharmacol* 268:157–177
- Naksen W, Prapamontol T, Mangklabruks A, Chantara S, Thavornnyutikarn P, Robson MG, Panuwet P (2016) A single method for detecting 11 organophosphate pesticides in human plasma and breastmilk using GC-FPD. *J Chromatogr B Analyt Technol Biomed Life Sci* 1025:92–104
- Naughton SX, Terry AV Jr (2018) Neurotoxicity in acute and repeated organophosphate exposure. *Toxicology* 408:101–112
- Omwenga I, Kanja L, Zomer P, Louisse J, Rietjens IMCM, Mol H (2021) Organophosphate and carbamate pesticide residues and accompanying risks in commonly consumed vegetables in

- Kenya. *Food Addit Contam Part B* 14:48–58
- Poet TS, Kousba AA, Dennison SL, Timchalk C (2004) Physiologically based pharmacokinetic/pharmacodynamic model for the organophosphorus pesticide diazinon. *Neurotoxicology* 25:1013–1030
- Punt A, Pinckaers N, Peijnenburg A, Louisse J (2021) Development of a web-based toolbox to support quantitative in vitro-to-in vivo extrapolations (QIVIVE) within non-animal testing strategies. *Chem Res Toxicol* 34:460–472
- Quandt SA, Arcury TA, Rao P, Snively BM, Camann DE, Doran AM, Yau AY, Hoppin JA, Jackson DS (2004) Agricultural and residential pesticides in wipe samples from farmworker family residences in North Carolina and Virginia. *Environ Health Perspect* 112:382–387
- Quistad GB, Sparks SE, Casida JE (2001) Fatty acid amide hydrolase inhibition by neurotoxic organophosphorus pesticides. *Toxicol Appl Pharmacol* 173:48–55
- Quistad GB, Liang SN, Fisher KJ, Nomura DK, Casida JE (2006) Each lipase has a unique sensitivity profile for organophosphorus inhibitors. *Toxicol Sci* 91:166–172
- Richards PG, Johnson MK, Ray DE (2000) Identification of acylpeptide hydrolase as a sensitive site for reaction with organophosphorus compounds and a potential target for cognitive enhancing drugs. *Mol Pharmacol* 58:577–583
- Rigas ML, Okino MS, Quackenboss JJ (2001) Use of a pharmacokinetic model to assess chlorpyrifos exposure and dose in children, based on urinary biomarker measurements. *Toxicol Sci* 61:374–381
- Rosenfeld CA, Sultatos LG (2006) Concentration-dependent kinetics of acetylcholinesterase inhibition by the organophosphate paraoxon. *Toxicol Sci* 90:460–469
- Satoh T, Hosokawa M (2006) Structure, function and regulation of carboxylesterases. *Chem Biol Interact* 162:195–211
- Schwarz M, Loewenstein-Lichtenstein Y, Glick D, Liao J, NorgaardPedersen B, Soreq H (1995) Successive organophosphate inhibition and oxime reactivation reveals distinct responses of recombinant human cholinesterase variants. *Brain Res Mol Brain Res* 31:101–110
- Strikwold M, Spenkelink B, Woutersen R, Rietjens IMCM, Punt A (2013) Combining in vitro embryotoxicity data with physiologically based kinetic (PBK) modelling to define in vivo dose response curves for developmental toxicity of phenol in rat and human. *Arch Toxicol* 87:1709–1723
- Sultatos LG (1990) A physiologically based pharmacokinetic model of parathion based on chemical-specific parameters determined in vitro. *J Am Coll Toxicol* 9:611–619
- Timchalk C, Nolan RJ, Mendrala AL, Dittenber DA, Brzak KA, Mattsson JL (2002) A physiologically based pharmacokinetic and pharmacodynamic (PBPK/PD) model for the organophosphate insecticide chlorpyrifos in rats and humans. *Toxicol Sci* 66:34–53
- Williams ET, Bacon JA, Bender DM, Lowinger JJ, Guo WK, Ehsani ME, Wang X, Wang H, Qian YW, Ruterbories KJ, Wrighton SA, Perkins EJ (2011) Characterization of the expression and activity of carboxylesterases 1 and 2 from the beagle dog, cynomolgus monkey, and human. *Drug Metab Dispos* 39:2305–2313
- Zhang Y, Han S, Liang D, Shi X, Wang F, Liu W, Zhang L, Chen L, Gu Y, Tian Y (2014) Prenatal exposure to organophosphate pesticides and neurobehavioral development of neonates: a birth cohort study in Shenyang. *China PloS one* 9:88491
- Zhao S, Kamelia L, Boonpawa R, Wesseling S, Spenkelink B, Rietjens IMCM (2019) Physiologically based kinetic modelling-facilitated reverse dosimetry to predict in vivo red blood cell acetylcholinesterase inhibition following exposure to chlorpyrifos in the Caucasian and Chinese population. *Toxicol Sci* 171:69–83

Supplementary materials

For convenience, **Supplementary materials** can be found at the following link:

<https://link.springer.com/article/10.1007%2Fs00204-021-03004-4>

Chapter 4

Physiologically based kinetic modelling based
prediction of in vivo rat and human
acetylcholinesterase (AChE) inhibition upon
exposure to diazinon

Shensheng Zhao, Sebastiaan Wesseling, Bert Spenkeliink, and Ivonne. M.C.M Rietjens

Published in Archives of Toxicology (2021) 95:1573–1593

Abstract

The present study predicts in vivo human and rat red blood cell (RBC) acetylcholinesterase (AChE) inhibition upon diazinon (DZN) exposure using physiological based kinetic (PBK) modelling-facilitated reverse dosimetry. Due to the fact that both DZN and its oxon metabolite diazoxon (DZO) can inhibit AChE, a toxic equivalency factor (TEF) was included in the PBK model to combine the effect of DZN and DZO when predicting in vivo AChE inhibition. The PBK models were defined based on kinetic constants derived from in vitro incubations with liver fractions or plasma of rat and human, and were used to translate in vitro concentration–response curves for AChE inhibition obtained in the current study to predicted in vivo dose–response curves. The predicted dose–response curves for rat matched available in vivo data on AChE inhibition, and the benchmark dose lower confidence limits for 10% inhibition (BMDL₁₀ values) were in line with the reported BMDL₁₀ values. Humans were predicted to be 6-fold more sensitive than rats in terms of AChE inhibition, mainly because of interspecies differences in toxicokinetics. It is concluded that the TEF-coded DZN PBK model combined with quantitative in vitro to in vivo extrapolation (QIVIVE) provides an adequate approach to predict RBC AChE inhibition upon acute oral DZN exposure, and can provide an alternative testing strategy for derivation of a point of departure (POD) in risk assessment.

1. Introduction

Diazinon (DZN) is the common name for *O,O*-diethyl *O*-2-isopropyl-6-methylpyrimidin-4-yl phosphorothioate (Figure 1), which is used as a pesticide in agriculture or veterinary medicine (JMPR 2016). DZN belongs to the class of thiophosphate insecticides for which acute toxicity is associated with irreversible inhibition of acetylcholinesterase (AChE) resulting in accumulation of acetylcholine at the synaptic cleft (Čolović et al. 2013). Different physiological symptoms such as headache, abdominal cramps, difficulty in breathing, and even death can result from acute DZN exposure (Burgess et al. 2008). Beside AChE, other B-esterases such as butyrylcholinesterase (BuChE) and carboxylesterase (CaE) can also be inhibited by DZN exposure (Poet et al. 2004). Although little is known about the profile of BuChE and CaE in human, it is known that inhibition of BuChE does not induce toxic effects (Jokanović 2009; Jokanović et al. 2020).

Upon oral administration, DZN undergoes multiple metabolic pathways (Fig 1) in different tissues, particularly in the liver, due to the high abundance of cytochromes P450 (CYP450) in this organ (Ellison et al. 2012; Sams et al. 2004). Previous studies reported that CYP450 are capable of bioactivating DZN to its active oxon metabolite diazoxon (DZO) (Fig 1) which is a stronger AChE inhibitor than DZN, and of detoxifying DZN to 2-isopropyl-4-methyl-6-hydroxypyrimidine (IMHP) and diethylthiophosphate (DETP) (Fig 1) (Ellison et al. 2012; Mutch and Williams 2006; Sams et al. 2004). In human, the bioactivation of DZN is mediated by especially CYP2B6, CYP2C19 and CYP3A4, while the detoxification is catalysed by CYP1A1, CYP1A2, CYP2B6, CYP2C19 and CYP3A4 (Ellison et al. 2012; Kappers et al. 2001; Mutch and Williams 2006; Sams et al. 2004). Paraoxonase 1 (PON1) is another enzyme involved in biotransformation of DZN, catalysing detoxification of DZO to IMHP and diethylphosphate (DEP) (Fig 1). Different from CYP450-mediated conversions, PON1-mediated detoxification occurs not mainly in the liver but also in blood due to the excretion of PON1 from liver to blood (Pyati et al. 2015).

To date, the point of departure (POD) to define an acute reference dose (ARfD) for risk assessment of acute exposure to DZN is based on the no-observed-adverse-effect level (NOAEL) of acute AChE inhibition and neurotoxicity in rats (EFSA 2006; JMPR 2016), or on the BMDL₁₀, the lower confidence limit of the benchmark dose (BMD) causing 10% inhibition of red blood cell (RBC) AChE activity in in vivo animal experiments (USEPA 2016), because of the absence of adequate human data. However, the use of animal data to define health based

guidance values may not (fully) reflect the human situation (Martignoni et al. 2006). To overcome this issue, alternative testing strategies can be considered, including physiologically based kinetic (PBK) modelling facilitated reverse dosimetry (Louisse et al. 2017) that enables quantitative in vitro to in vivo extrapolation (QIVIVE), as a potential novel approach in risk assessment. The PBK modelling-based alternative approach has been successfully used to predict chlorpyrifos-related AChE inhibition (Timchalk et al. 2002; Zhao et al. 2019) and also a variety of other chemical-induced adverse effects including for example cardiotoxicity induced by methadone, liver toxicity induced by pyrrolizidine alkaloids and developmental toxicity of retinoids, glycoethers and phenols (Boonpawa et al. 2017; Louisse et al. 2010; Ning et al. 2019; Shi et al. 2020; Strikwold et al. 2017; Strikwold et al. 2013). In case of DZN, previously a physiologically-based pharmacokinetic and pharmacodynamic model was developed for both human and rat (Poet et al. 2004). However, in this previous study, the predicted AChE inhibition was assumed to be caused by the metabolite DZO only, not taking the contribution of the parent compound DZN on AChE inhibition into account. Furthermore, the kinetic parameters were solely determined using rat liver microsomes and scaled for further use in rat and human PBK models, while the kinetic parameters for DZO detoxification in blood were assumed to be equal to those in liver. Apart from that, the model was not used to define an in vivo dose-response curve for AChE inhibition from which a POD for human risk assessment could be derived.

4

Therefore, the aim of the present study was to assess the possibility of using mainly in vitro and in silico data as input for PBK modelling-facilitated QIVIVE to derive a POD for acute toxicity of DZN. The kinetic parameters of DZN biotransformation for rat and human PBK models were determined in a species-specific way by incubating a range of concentrations of DZN or DZO with rat or human liver microsomes and plasma. Considering that both DZN and DZO are able to inhibit AChE, a toxic equivalency factor (TEF) approach was employed and incorporated into the PBK model to describe the internal combined effective concentration of DZN and DZO in DZO equivalents. The TEF coded-PBK model was subsequently used to translate in vitro concentration-response curves for DZO concentration dependent inhibition of rat AChE or recombinant human AChE (rhAChE) to predicted-in vivo dose-response curves for DZN exposure mediated RBC AChE inhibition enabling definition of a BMDL₁₀ as POD for risk assessment and quantification of potential interspecies differences between rat and human.

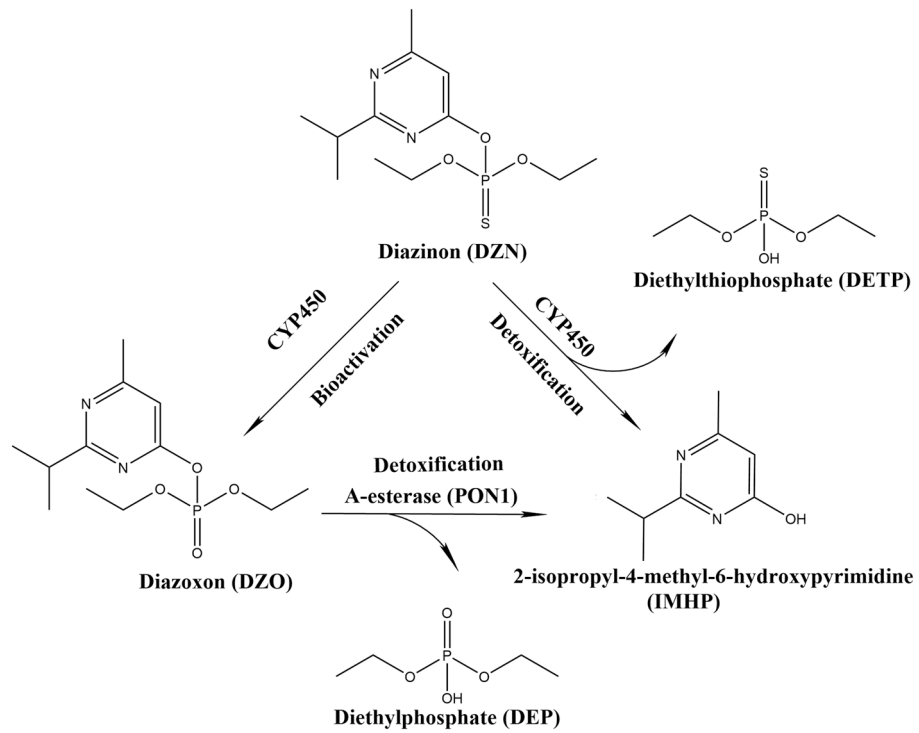


Fig 1. Biotransformation pathways of DZN. PON1, Paraoxonase 1; CYP450, cytochrome P450



2. Materials and Methods

2.1 Materials

2.1.1 Chemicals

Diazinon (DZN), 2-isopropyl-4-methyl-6-hydroxypyrimidine (IMHP), acetylthiocholine iodide (ATC), 5,5'-dithiobis (2-nitrobenzoic acid) (DTNB), bovine serum albumin (BSA), tetraisopropyl pyrophosphoramidate (iso-OMPA), reduced nicotinamide adenine dinucleotide phosphate (NADPH) and Trizma®base were purchased from Sigma-Aldrich (Zwijndrecht, The Netherlands). Diazoxon (DZO) was purchased from TRC-Canada (Toronto, Ontario, Canada). Magnesium chloride hexahydrate ($\text{MgCl}_2 \cdot 6\text{H}_2\text{O}$), hydrochloric acid (HCl), sodium hydroxide (NaOH), ethylenediaminetetraacetic acid disodium salt dihydrate (EDTA) and calcium chloride dihydrate ($\text{CaCl}_2 \cdot 2\text{H}_2\text{O}$) were purchased from VWR International (Amsterdam, The Netherlands). Acetonitrile (ACN, UPLC/MS grade) and methanol (UPLC/MS grade) were purchased from Biosolve (Valkenswaard, The Netherlands). Rapid equilibrium dialysis (RED) materials (RED inserts, RED based plate and sealing tape), and Pierce™ BCA protein assay kit were purchased from Thermo Fisher Scientific (Rockford, IL, USA). Phosphate-buffered saline (PBS pH 7.4 (1X)) was purchased from GIBCO (Paisley, UK)

4

2.1.2 Biological material

Human liver microsomes (pooled from 20 donors, mixed gender) and rat liver microsomes (Sprague-Dawley, male) were purchased from Corning (Amsterdam, The Netherlands). Human plasma (pooled from 6 donors, mixed gender) were purchased from Zen-Bio, Inc (NC, USA). Rat plasma (Sprague-Dawley) was purchased from Innovative Research Inc. (MI, USA). For the rat samples further information on number of animals used to create the samples (liver microsomes and plasma) or on gender (plasma) was not provided by the provider. Rat blood was purchased from BioIVT (West Sussex, UK). rhAChE was purchased from Sigma-Aldrich Co. (St. Louis, MO, USA), and the enzyme was stabilized with 1 mg/ml BSA.

2.2 Methods

2.2.1 Protein determination

The total protein concentration of human and rat plasma was measured by using a Pierce™ BCA protein assay kit (Thermo Fisher Scientific 2020). The experiment was conducted using the manufacturer's protocol. In detail, 25 µl sample or protein standard solution were incubated with 200 µl working reagents in a 96-well plate at 37°C for 30 minutes. Next, the plate was cooled to room temperature, followed by measuring the absorbance at 562 nm for each sample or protein standard. The protein concentration of the unknown sample was quantified based on the calibration curve (protein concentration versus 562nm absorbance value) generated with the protein standards.

2.2.2 In vitro metabolic incubations for deriving kinetic parameters

The in vitro incubations for investigating CYP450-mediated biotransformation of DZN were performed using rat and human liver microsomes based on the method described by Sams et al. (2004) and Smith et al. (2011) with some modifications. Preliminary studies were carried out to optimize both incubation time and microsomal protein concentration, to define conditions at which metabolism was linear with respect to time and the amount of microsomal protein (data not shown) to be used for further kinetic studies. The final incubations contained 50 mM Tris-HCl (pH 7.4), 5 mM MgCl₂, 1 mM EDTA (as an A-esterase PON1 inhibitor) (Bizoń and Milnerowicz 2018), 50 µM iso-OMPA (as a B-esterases inhibitor) (Lane et al. 2006), 1 mM NADPH, and DZN at final concentrations of 1, 2.5, 5, 10, 25, 50, 100 and 250 µM (added from 100 times concentrated stock solutions in methanol). In these incubations, the formed DZO might also be further hydrolyzed to IMHP by esterases present in the liver microsomes, hampering accurate quantification of the formation of DZO or IMHP by the CYP450-mediated reactions. Therefore, in order to adequately define the CYP450-mediated conversion from DZN to DZO and from DZN to IMHP, esterase inhibitors (EDTA and iso-OMPA) were added to prevent this 'untargeted' conversion of DZO to IMHP in these microsomal incubations. Addition of esterase inhibitors EDTA and iso-OMPA has been commonly applied when studying CYP450-mediated conversion of organophosphate (OP) pesticides in liver microsomal incubations for determining kinetic parameters for their CYP450-mediated pathways (Buratti et al. 2005; Dadson et al. 2013; Ellison et al. 2012;

Foxenberg et al. 2007; Poet et al. 2003; Smith et al. 2011). Based on previous studies, CYP450-mediated activities are not adversely affected by the addition of these inhibitors (1 mM EDTA and 50 μ M iso-OMPA) to the microsomal incubations (Buratti et al. 2003; Rasmussen 2012). After 1 minute preincubation in a 37°C water bath, 2.5 μ l of human or rat liver microsomes (final concentration 0.25 mg microsomal protein/ml) were added to initiate the reaction. The total incubation mixture was 200 μ l. Control incubations were carried out by replacing NADPH with buffer. The reaction was terminated after 2.5 minutes by adding 200 μ l ice-cold ACN. After the incubation, samples were centrifuged at 16000g (4°C) for 5 minutes, and supernatants of rat samples were further diluted 2x in a mixture of ACN and 50 mM Tris-HCl (pH 7.4) (ratio 1:1, v/v). At the end, both diluted rat sample supernatants and undiluted human sample supernatants were analysed by LC-MS/MS for quantification of metabolite formation.

The *in vitro* incubations for quantification of kinetic parameters for PON1-mediated detoxification of DZO were conducted by using both liver microsomes and plasma from either human or rat based on the method from Poet et al. (2003) with some modifications. It should be noted that the enzyme activity detected in these DZO detoxification incubations with tissue fractions could in theory be due to various enzymes, but based on literature data (Costa et al. 1999; Jokanović et al. 2020; Poet et al. 2004), the activity can be mainly ascribed to the activity of PON1. Preliminary studies were carried to optimize and select the incubation conditions with respect to linearity for both incubation time and microsomal/plasma protein concentration (data not shown). The final incubations contained 2 mM CaCl₂ in 50 mM Tris-HCl (pH 7.4) and DZO at final concentrations of 0.5, 1, 2.5, 5, 10, 25, 50, 100, 250, 500 and 1000 μ M (added from 100 times concentrated stock solutions in methanol). After 1 minute preincubation in a 37°C water bath, 1 μ l of human or rat liver microsomes (final concentration 0.1 mg microsomal protein/ml), or 1 μ l of human or rat plasma (final concentration 0.385 mg plasma protein/ml for human plasma and 0.300 mg plasma protein/ml for rat plasma) was added to initiate the reaction. The total incubation mixture was 200 μ l. Control incubations were carried out by replacing liver microsomes or plasma with buffer. The reaction was terminated after 1 minute incubation (human samples) or 2 minutes incubation (rat samples) by adding 200 μ l ice-cold ACN. Subsequently, samples were centrifuged at 16000g (4°C) for 5 minutes, and supernatants were further diluted (30x for liver sample and 40x for plasma sample) in a mixture of ACN and 50 mM Tris-HCl (pH 7.4) (ratio 1:1, v/v) before analysis by LC-MS/MS for quantification of metabolite formation.

2.2.3 Quantification of DZN and DZO metabolites by LC-MS/MS

The amounts of parent compound DZN and formed DZO and IMHP in samples from the microsomal and plasma incubations were identified and quantified using a Shimadzu Nexera XR LC-20AD-xr UHPLC system coupled to a Shimadzu LCMS-8045 mass spectrometer (Kyoto, Japan) equipped with an electrospray ionization (ESI) interface. The chromatographic separations were conducted on a Kinetex[®] 1.7 μm Phenyl-Hexyl 100 \AA LC column (100 x 2.1 mm). The injection volume was 1 μl at a flow rate of 0.3 ml/min. The temperature of the column was kept at 40°C. The mobile phase A consisted of ultrapure water with 0.1% (v/v) formic acid, and mobile phase B consisted of acetonitrile (ACN) with 0.1% (v/v) formic acid. The gradient started with 0% B and was linearly increased to 100% B in 12 minutes, kept at 100% B for 1 minute and then changed to the initial condition (0% B) at 13.5 minutes and kept for 5.5 minutes to re-equilibrate the column before the next injection. The instrument was used in positive mode with multiple reaction monitoring (MRM). The optimized acquisition parameters for DZN, DZO and the metabolite IMHP are listed in Supplementary material I.

2.2.4 Calculation of kinetic parameters

The Michaelis-Menten parameters for conversion of DZN to DZO and of DZN to IMHP in incubations with liver microsomes, and of DZO to IMHP in incubations with liver or plasma samples were determined by fitting the data to equation 1 (Eq1):

$$v = \frac{V_{\text{max}} * [S]}{(K_{\text{m}} + [S])} \quad (\text{Eq1})$$

Where v represents the rate of reaction in nmol/min/mg microsomal protein or in nmol/min/mg plasma protein, S represents the substrate concentration (in μM), K_{m} the apparent Michaelis-Menten constant in μM , and V_{max} the apparent maximum rate in nmol/min/mg microsomal protein or in nmol/min/mg plasma protein. The calculation was done using GraphPad Prism 5 for Windows, version 5.04 (GraphPad software, San Diego California USA).

2.2.5 In vitro AChE inhibition assay to derive concentration-response curves

2.2.5.1 Preparation of rat RBC AChE

Rat RBC AChE was prepared according to the protocol previously described (Dodge et al. 1963; Patel et al. 2000) with some modifications. In the current study, 7 ml rat whole blood was first centrifuged at 2000 g for 10 mins (4°C) to separate plasma and RBCs (pellet). Subsequently, the RBCs were suspended in 5 ml 0.9% saline (sodium chloride) and centrifuged at 2000 g for 10 mins (4°C) to wash away plasma residue. After three of these washing steps, the washed RBCs were resuspended in 2 ml PBS and lysed by addition of 18 ml lysis buffer (20 mM sodium phosphate, pH=7.4) and freezing at -80°C for 24 h. The lysed RBCs were defrozed and the membrane fraction (containing AChE) was sedimented by centrifugation at 20,000 g for 40 mins, and the supernatant was carefully removed. The pellet was washed for another two times by resuspending in lysis buffer and sedimenting as described above. Afterwards the pellet was resuspended in 1 ml 100 mM sodium phosphate (pH=7.4) and was successively centrifuged for 2 mins at 2000 g using a Microcentrifuge (VWR, Mini start silverline) to obtain the AChE (supernatant). The enzyme concentration of the isolated rat AChE, expressed in mU/ml, was quantified based on the calibration curve generated using the commercially available rhAChE.

4

2.2.5.2 AChE activity assay

In the present study, AChE activity of rhAChE and of the extracted rat RBC AChE were used to characterize the inhibitory potency of DZO or DZN on human and rat RBC AChE, based on the protocol from Ellman et al. (1961). Recombinant human AChE was used since it is easy to use (no lysing and washing steps are required compared to use of AChE extracted from native red blood cell), the obtained results will not be affected by hemoglobin (George and Abernethy 1983), and its characteristics are comparable with those of human natural RBC AChE in term of sensitivity towards OP (Amitai et al. 1998; Velan et al. 1991). However, since recombinant rat AChE was not commercially available, extracted rat RBC AChE was used. Preliminary studies were carried out to select the rhAChE enzyme concentration and substrate ATC concentration that would be within the linear range with respect to formation of the yellow-colored product 5-thio-2-nitrobenzoic acid (data not shown) and thus optimal to quantify the AChE activity upon inhibition by DZO or DZN. The concentration of DTNB was calculated

based on the concentration ratio (ATC/DTNB) of 2 (Stern et al. 2014). To this end, series of increasing concentrations of DZO or DZN in ethanol, 5000 μM chlorpyrifos-oxon in ethanol (CPO, positive control) and 100% ethanol (solvent control) were all diluted 50x in 100 mM sodium phosphate (pH=7.4) containing 0.1 mg/ml BSA. Incubation was conducted in 96 well-plates with 44 μl 100 mM sodium phosphate (pH=7.4) containing 0.1 mg/ml BSA, and 5 μl DZO solution (final concentrations 0.0005, 0.001, 0.005, 0.01, 0.025, 0.05 0.1, 0.25 0.5 and 1 μM), or DZN solution (final concentrations 1, 2.5, 5, 10, 25, 50, 100, 500 and 1000 μM) or 5 μl positive control (CPO at a final concentration of 10 μM) or 5 μl solvent control (ethanol at a final concentration 0.2%). To initiate the inhibition reaction, 1 μl rhAChE or rat AChE was added to the incubation. The total incubation volume was 50 μl . After 15 minutes incubation at 37°C, 150 μl reaction reagents (mixture of ATC at a final concentration of 150 μM and DTNB at a final concentration of 75 μM) were added into each well. The final total volume of each well was 200 μl (final enzyme concentration is 0.6 mU/ml). Subsequently, the 96-well plate was measured continuously for 10 minutes at absorbance 412 nm at 37°C to quantify the remaining AChE activity.

2.2.5.3 AChE activity data analysis

The rhAChE and rat AChE activity were expressed as the remaining AChE activity relative to solvent control (100% activity) and positive control (0% activity) based on equation 2 (Eq2):

$$\text{AChE activity}\% = \frac{A_{412}(t_{10} - t_0)\text{Test Compound} - A_{412}(t_{10} - t_0)\text{Positive Control}}{A_{412}(t_{10} - t_0)\text{Solvent Control} - A_{412}(t_{10} - t_0)\text{Positive Control}} * 100\% \text{ (Eq2)}$$

where the $A_{412}(t_{10} - t_0)\text{Test Compound}$ is the change in the absorbance at 412 nm between 0 min and 10 min for the test compound, the $A_{412}(t_{10} - t_0)\text{Positive Control}$ is the change in the absorbance at 412 nm between 0 min and 10 min for the CPO sample, and the $A_{412}(t_{10} - t_0)\text{Solvent Control}$ is the change in the absorbance at 412nm between 0 min and 10 min for the 0.2% ethanol sample.

The concentration-dependent human and rat AChE inhibition curves were analysed to define the half maximal inhibitory concentrations (IC₅₀) for both DZO and DZN using non-linear regression, Dose Response-Inhibition-Variable, log(inhibitor) vs. response-variable slope (four

parameters) in GraphPad Prism 5, version 5.04 (GraphPad software, San Diego California USA), with 95% confidential interval. To further define whether the concentration-dependent DZN and DZO AChE inhibition curves in both rat and human were parallel or not, the hillslope values of these curves were statistically compared using non-linear regression, Dose Response-Inhibition-Variable, log(inhibitor) vs. response-variable slope (four parameters), compare tab “Do the best fit values of selected parameters differ between data sets” in GraphPad Prism 5, version 5.04 (GraphPad software, San Diego California USA) based on instruction from GraphPad (GraphPad 2009).

2.2.6 Determination of unbound fraction of DZO and DZN in the *in vitro* medium and *in vivo*

A previous study from Heilmair et al. (2008) showed that the presence of a low level of BSA (0.1 mg/ml) will not significantly affect the free concentration of OP chlorpyrifos-oxon in solution. Based on this observation, the *in vitro* unbound fraction of both DZN ($f_{u}DZN_{in\ vitro}$) and DZO ($f_{u}DZO_{in\ vitro}$) in the *in vitro* medium are set at 1. To assess whether this assumption is reasonable, the $f_{u}DZO_{in\ vitro}$ was determined. This was done by using rapid equilibrium dialysis (RED) performed in line with the manufacturer’s protocol (Thermo Fisher Scientific 2012). To this end, 200 μ l *in vitro* medium containing 0.05 μ M DZO were added to the sample chamber and 350 μ l PBS buffer consisting of 100 mM sodium phosphate and 150 mM sodium chloride to the buffer chamber, separated by a semipermeable membrane in the RED insert device. The whole device was then incubated for 5 hours at 37°C on a shaker at 250 rpm in order to reach equilibrium. Then 50 μ l of post-incubation sample were separately collected from the sample and buffer chambers into the corresponding Eppendorf tubes. After this 50 μ l of PBS buffer was added to the sample taken from the sample chamber and 50 μ l of *in vitro* medium was added to the sample taken from buffer chamber and subsequently 300 μ l ice-cold 90% acetonitrile (ACN/water, v/v) were added to both samples to precipitate the protein. All samples were put on ice for 30 minutes, followed by centrifugation for 30 minutes at 15000 g. The supernatants were collected for LC-MS/MS analysis of the amount of DZO. The $f_{u}DZO_{in\ vitro}$ was calculated by dividing the concentration of DZO in the buffer chamber by the concentration DZO in the sample chamber.

Given that only the free concentration of DZN and DZO can inhibit AChE in vivo, the fraction of unbound DZN in vivo ($fuDZN_{in\ vivo}$) and of unbound DZO in vivo ($fuDZO_{in\ vivo}$) were estimated based on SMILES string of compound using the pkCSM prediction tool (Pires et al. 2015; pkCSM n.d.).

2.2.7 PBK model for DZN

The PBK model for DZN was developed based on the model from Poet et al. (2004) with some modifications for both rat and human. The model structure is presented in Figure 2. The model contains a sub-model for the metabolite DZO and was defined to include compartments for rapidly perfused tissue, slowly perfused tissue, liver, fat and blood for both the parent compound DZN and its metabolite DZO. The model also contains a compartment to describe the urinary elimination of the metabolites IMHP and DAP (sum of DEP and DETP). In the currently developed model, oral exposure was included since we aimed at defining a POD for risk assessment of exposure via food and drinking water, and intravenous (IV) exposure was included for model evaluation. The fractional absorption (fa) was set equal to literature reported values, being 0.8 in rat (Poet et al. 2004) and 0.66 in human (Garfitt et al. 2002) and applied to the overall dose. The absorption of DZN from the stomach into the liver was described using a two-compartment gastrointestinal tract model as reported by Poet et al. (2004), with a first-order rate constant for absorption of DZN from the stomach into the liver (KaS) of 0.1 /h for rat and 0.32/h for human (Poet et al. 2004), a first order rate constant for transfer of DZN from the stomach into the intestine (KsI) of 0.48/h for both rat and human, a first order rate constant for absorption DZN from the intestine into the liver (KaI) of 0.59/h for both rat and human, (Poet et al. 2004), and Ke values for the elimination of IMHP or DAP (sum of DEP and DETP) into the urine amounting to $Ke\ IMHP = 0.29/h$, $Ke\ DEP = 0.29 /h$ and $Ke\ DETP = 0.29/h$ for rat (Poet et al. 2004), and $Ke\ IMHP = 12/h$, $Ke\ DEP = 12 /h$ and $Ke\ DETP=12/h$ for human (Garfitt et al. 2002; Poet et al. 2004).

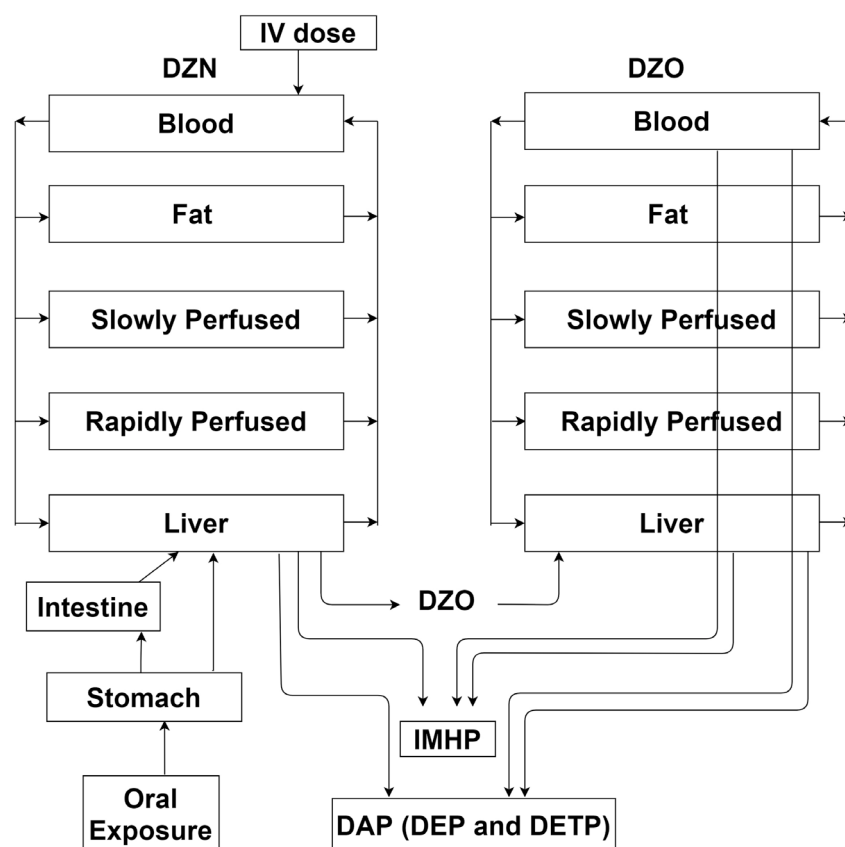


Fig 2. Structure of the PBK model for DZN in rat and human with a submodel for DZO.

4

The physiological parameters for rat and human were obtained from Brown et al. (1997) as well as Gearhart et al. (1990), and are summarised in Table 1. The partition coefficients for both DZN and DZO were obtained using the approach described by DeJongh et al. (1997), based on the value $\text{Log}K_{ow}$ which was derived from $\text{clog}P$ estimated using ChemDraw professional 16.0 (Cambrigesoft) (Table 1). The kinetic parameters for biotransformation of DZN in rat and human were obtained by conducting *in vitro* liver microsomal/plasma incubations as described in the section “*In vitro* metabolic incubations for deriving kinetic parameters”. The bioactivation and detoxification of DZN by CYP450 were assumed to occur only in the liver (Poet et al. 2004), and the resulting DZO was transferred to the DZO sub-model. In the current model, only unbound DZN and DZO are assumed to be metabolised. The first-pass metabolism of DZN by the intestine was not taken into account in the current model because the metabolic conversion in the intestine derived from the conversion in incubations with intestinal microsomes upon scaling to the whole organ, appeared less than 5% of that obtained in a similar way for the liver (data not shown). Since PON1 can be expected to be present in both liver and blood, the PON1-mediated detoxification of DZO was modeled to

occur in these two compartments (Pyati et al. 2015). To scale the in vitro V_{max} values to the in vivo situation, the following scaling factors were used; 35 mg microsomal protein/g liver for rat hepatic metabolism (Medinsky et al. 1994), 32 mg microsomal protein/g liver for human hepatic metabolism (Barter et al. 2007), 77mg plasma protein/ml plasma (total plasma protein concentration) for human plasma metabolism, and 60 mg plasma protein/ml plasma (total plasma protein concentration) for rat plasma metabolism. Plasma volume in rat and human were assumed as 55% of their corresponding blood volume (O'Neil 1999). The K_m values determined in vitro were assumed to be equal to in vivo K_m values. When lacking experimental values the blood plasma ratio (B/P) is often assumed to be 1 for basic compounds or 0.55 (1-haematocrit) for acidic compounds (Cubitt et al. 2009). In the current study, because experimental data were not available, and both DZN and DZO are basic compounds, the B/P ratio of DZN and DZO were assumed to be 1. Therefore, no correction was required between blood and plasma concentration.

Table 1. Summary of physiological and physicochemical parameters for the PBK models for DZN and its metabolite DZO in rat and human (Brown et al. 1997; DeJongh et al. 1997; Gearhart et al. 1990).

Model parameters	Rat	Human
Physiological parameters		
Body weight (BW; kg)	0.25	70.0
Percentage of body weight		
Liver	3.4	2.6
Fat	7.0	21.4
Rapidly perfused	4.8	5.4
Slowly perfused	66.7	58.0
Blood	7.4	7.9
Flow (l/hr/kg BW^{0.74})		
Cardiac output	15.0	15.0
Percentage of cardiac output		
Liver	25.0	22.7
Fat	9.0	5.2
Rapidly perfused	51.6	43.0
Slowly perfused	14.4	29.1
Tissue: blood partition coefficients for DZN		
Liver	13.7	7.1
Fat	211.0	137.7
Rapidly perfused	13.7	7.1
Slowly perfused	8.7	4.5
Tissue: blood partition coefficients for DZO		
Liver	3.9	2.6
Fat	89.6	72.4
Rapidly perfused	3.9	2.6
Slowly perfused	2.4	1.9

Because previously it was shown that not only DZO but also its parent compound DZN are able to inhibit AChE (Li et al. 2019), in the present study both DZN and DZO were considered to be able to act as AChE inhibitor. To determine the combined effect of DZN and DZO at the

target site, the free effective blood maximum concentration of DZN and DZO was expressed in DZO equivalents using a toxic equivalency factor (TEF) (see equation 3 (Eq3))

$$\begin{aligned} &\text{Total free in vivo DZN and DZO concentration expressed in DZO equivalents} \\ &= [\text{DZN}] * \text{fuDZN in vivo} * \text{TEFDZN} + [\text{DZO}] * \text{fuDZO in vivo} * \text{TEFDZO} \quad (\text{Eq3}) \end{aligned}$$

In which the Total free in vivo DZN and DZO concentration expressed in DZO equivalents represents the free blood maximum concentration of DZO plus DZN expressed in DZO equivalents using the TEF values for DZO and DZN, [DZN] and [DZO] represent the total blood maximum concentrations of DZN and DZO, which were corrected to their corresponding free internal maximum concentrations using their unbound fraction in vivo $\text{fuDZN}_{\text{in vivo}}$ and $\text{fuDZO}_{\text{in vivo}}$, and the TEFDZN and TEFDZO are the toxic equivalency factors of DZN and DZO. The TEF for DZO was set at 1.0 and the TEF for DZN was defined using equation 4 (Eq4) based on its IC50 and the IC50 of DZO for inhibition of rat AChE or human hrAChE for the rat and human model, respectively.

$$\text{TEF DZN} = \frac{\text{IC50 DZO}}{\text{IC50 DZN}} \quad (\text{Eq4})$$

The free internal maximum concentration of DZN plus DZO expressed in DZO equivalents was subsequently used to extrapolate the in vitro AChE concentration-response curve of DZO to its corresponding in vivo DZN-dose response curve using reverse dosimetry (see below).

All differential equations and the mass balance were coded in Berkeley Madonna software version 8.3.18 ((Macey and Oster, UC Berkeley, California) using Rosenbrock's algorithm for stiff systems. The full model code is presented in Supplementary material II.

2.2.8 Sensitivity analysis

The key parameters that have the largest influence on the prediction of the model parameter of interest, being the maximum combined DZN and DZO free blood concentration expressed in DZO equivalents was identified by performing a sensitivity analysis at low non-toxic dose levels of DZN of 3 mg/kg bw (rat) and 0.011 mg/kg bw (human), and at high DZN dose levels of 300 mg/kg bw (rat) and 293 mg/kg bw (human), the latter two dose levels representing toxic

dose levels reported for rat and human respectively (JMPR 2016; Poklis et al. 1980). The normalized sensitivity coefficients (SC) were calculated based on equation 5 (Eq5):

$$SC = \frac{(C' - C)}{(P' - P)} * \left(\frac{P}{C}\right) \quad (\text{Eq5})$$

In which P represents the original parameter value in the PBK model and P' is the parameter value with a 5% increase, while C is the model output with the original parameter values and C' is the model output with a parameter value with an increase of 5%. Each parameter was analyzed individually while other parameters were kept at their initial value.

2.2.9 Model evaluation

The developed rat DZN model was evaluated by comparing predicted time-dependent plasma concentrations of DZN (both upon oral and IV administration) with their corresponding available in vivo data (Lu et al. 2003; Poet et al. 2004; Wu et al. 1996). The performance of the human DZN model was assessed by comparing the predicted urinary DAP excretion against available in vivo data (Garfitt et al. 2002).

4

2.2.10 Translation of the in vitro concentration response curve to an in vivo dose response curve

In this step, the species-specific in vitro DZO AChE inhibition concentration-response curves were converted to the corresponding DZN dose-response curves via reverse dosimetry using the rat or human TEF-coded PBK models. To this end, the in vitro DZO concentrations were assumed to be equal to the nominal concentrations given that the $f_{u\text{DZO in vitro}}$ was considered equal to 1. Subsequently, the DZO concentration in vitro was set equal to the free maximum DZN and DZO concentration expressed in DZO equivalents by multiplying with TEF_{DZO}, to determine the DZN dose that would result in this concentration, leading to the corresponding inhibition, ultimately generating the predicted DZN dose-response curve for in vivo RBC AChE inhibition in rat and human by DZN exposure. This was done using equation 6 (Eq6)

$$\begin{aligned} &\text{Total free in vivo DZN and DZO concentration expressed in DZO equivalents} \\ &= [\text{DZO}]_{\text{in vitro}} * f_{u\text{DZO in vitro}} * \text{TEFDZO} \quad (\text{Eq6}) \end{aligned}$$

The correction for protein binding in vivo was done as described above (See Eq3).

2.2.11 Determination of a point of departure (POD) based on the predicted in vivo dose-response curve

The predicted in vivo RBC AChE inhibition dose-response curves obtained for rat were validated against available in vivo data (JMPR 2016; USEPA 2016), and subsequently used to derive a POD for evaluation of the acute toxicity upon oral exposure using a BMD analysis. In the present study, the BMDL₁₀ was used as POD since also the USEPA used the BMDL₁₀ as POD to define the acute reference dose (ARfD) (USEPA 2016). To obtain the BMDL₁₀, the Benchmark Dose Software version 3.1.2 (USEPA) was used. Of all available models (Exponential, Hill, Power, Linear and Polynomial) for fitting of continuous data, only the Exponential and Hill models provided adequate fits to the data, and were employed for derivation of predicted BMDL₁₀ values for rat or human with BMR type of Std. Dev, confidential level of 0.95, distribution type of normal and variance type of constant. The BMDL₁₀ value with the lowest AIC was chosen as POD. Finally, the obtained POD values were evaluated against reported BMDL₁₀ values or POD values from EFSA (2006), JMPR (2016) and USEPA (2016).

3. Results

3.1 Kinetic data and total protein concentration

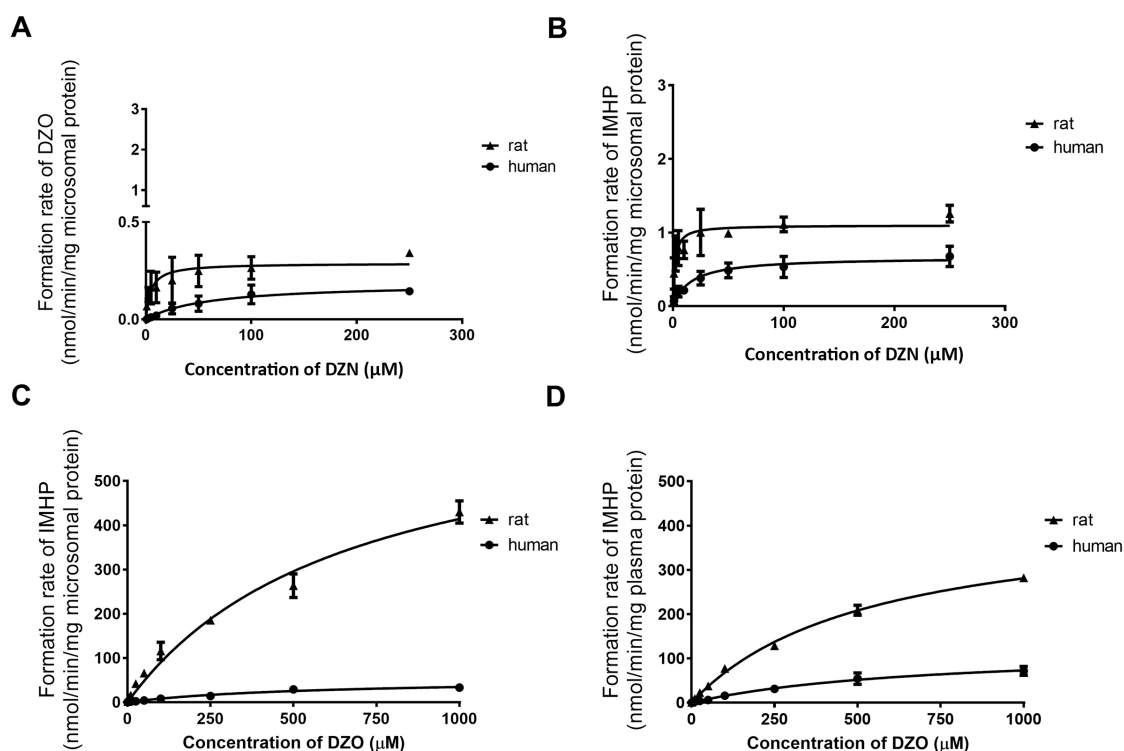


Fig 3. CYP450-mediated DZN concentration-dependent formation of (A) DZO and (B) IMHP in incubations with pooled rat (filled triangle) or human (filled circle) liver microsomes, and PON1-mediated DZO concentration-dependent formation of IMHP in incubations with (C) pooled rat (filled triangle) or human (filled circle) liver microsomes, or (D) pooled rat (filled triangle) or human (filled circle) plasma. Data points represent mean \pm SD of two experiments for each conversion.

The kinetic parameters for biotransformation of DZN and DZO by the different pathways were determined by incubating increasing concentrations of DZN with pooled human or rat liver microsomes, and DZO with pooled human or rat liver microsomes or plasma (Fig 3). The apparent V_{max} , K_m and the catalytic efficiency (calculated as V_{max}/K_m) derived from these data, as well as the determined total protein concentration of plasma are shown in Table 2. In general, for both rat and human, the CYP450-mediated detoxification of DZN to IMHP is faster than its CYP450-mediated bioactivation to DZO. The PON1-mediated detoxification of DZO in liver and plasma was even faster and more efficient. Together these data indicate that detoxification is preferred over bioactivation in both rat and human. Comparison of the data

for rat and human, reveals that the unscaled catalytic efficiency of CYP450-mediated bioactivation is 20-fold higher in rat than human while detoxification is 15-fold more efficient in rat compared to human. These differences originate from a 12.6-fold lower K_m for the CYP450-mediated bioactivation reaction, and a 9.3-fold lower K_m for CYP450-mediated detoxification in rat than in human. PON1-mediated conversion of DZO in rat liver and plasma was 10.7-fold and 4.5-fold faster than that in human liver and plasma, respectively, due to a 12.9-fold higher V_{max} in rat liver and 3.5-fold higher V_{max} in rat plasma as compared to human plasma. Besides, the results also show that rat plasma and human plasma have comparable total protein concentrations, being 60 mg/ml in rat plasma and 77 mg/ml in human plasma (Table 2).

Table 2. Kinetic parameters for biotransformation of DZN and DZO in liver and plasma

Pathway	Rat	Human
Liver		
DZN to DZO		
V _{max} (nmol/min/mg microsomal protein)	0.288	0.187
K _m (μM)	4.745	59.600
CE (ml/min/mg microsome protein) ^a	0.060	0.003
DZN to IMHP		
V _{max} (nmol/min/mg microsomal protein)	1.098	0.665
K _m (μM)	1.764	16.340
CE (ml/min/mg microsome protein) ^a	0.620	0.041
DZO to IMHP		
V _{max} (nmol/min/mg microsomal protein)	691.100	53.490
K _m (μM)	668.000	557.400
CE (ml/min/mg microsome protein) ^a	1.030	0.096
Plasma		
DZO to IMHP		
V _{max} (nmol/min/mg plasma protein)	431.400	124.000
K _m (μM)	535.600	701.000
CE (ml/min/mg plasma protein) ^a	0.810	0.180
Total protein concentration (mg/ml)	60.000	77.000

^a CE = catalytic efficiency (ml/min/mg microsome protein or ml/min/mg plasma protein) calculated as V_{max}/K_m



3.2 AChE inhibition concentration-response curve and TEF calculation

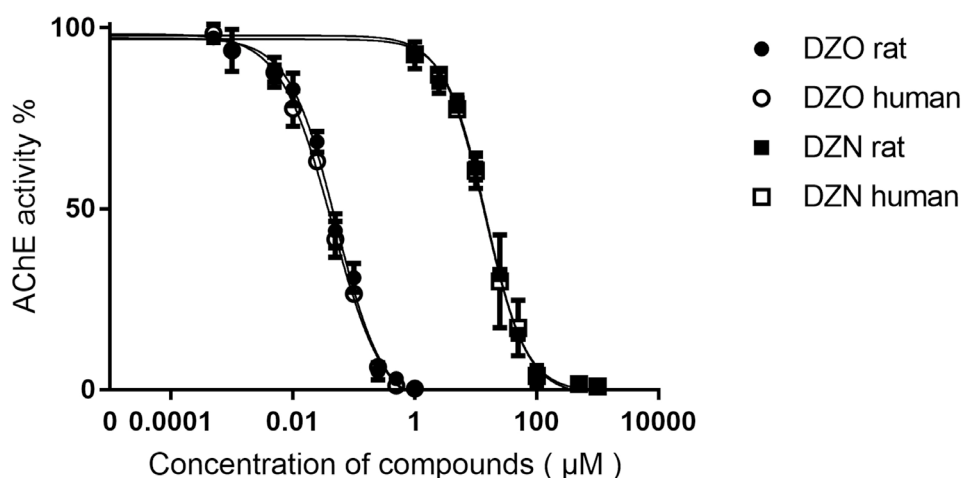


Fig 4. Effect of increasing concentration of DZO (circle) and DZN (square) on AChE activity of rat (filled circle or square) and human (unfilled circle or square) at 37°C. Each value represents the mean \pm SD of three independent experiments.

4

Figure 4 shows the DZO concentration-dependent inhibition of rat and human AChE activity, with 50% inhibition (IC_{50}) being observed at a concentration of 0.0515 μ M (with the 95% confidence interval ranging from 0.0443 μ M to 0.0610 μ M) for rat and 0.0440 μ M (with the 95% confidence interval ranging from 0.0380 μ M to 0.0521 μ M) for human. The IC_{50} values observed for DZN were substantially higher amounting to 14.66 μ M (with the 95% confidence interval ranging from 12.91 μ M to 16.63 μ M) for rat and 14.26 μ M (with the 95% confidence interval ranging from 11.64 μ M to 17.59 μ M) for human (Figure 4). These IC_{50} values indicate that rat and human AChE appear to show comparable sensitivity towards *in vitro* inhibition following DZO and DZN exposure. Besides, the comparison of hillslope values of the curves indicated that the DZN and DZO curves are parallel for both human and rat (the hillslope value of AChE inhibition induced by DZN and DZO in human is -1.2700, and -1.0200, with p value of 0.0797, and that in rat is -1.3220 and -1.1240, with p value of 0.1504). To incorporate the TEF method into the PBK model developed for predicting the combined free blood concentration of DZN and DZO at the target site (RBC AChE) in DZO equivalents, the TEF value for DZN was calculated based on the IC_{50} values derived from the *in vitro* concentration-AChE inhibition curves, setting the TEF of DZO at 1.0. The TEF values thus obtained for DZN and DZO are 0.00351 and 1.0 in rat, and 0.00310 and 1.0 in human.

3.3 PBK model validation

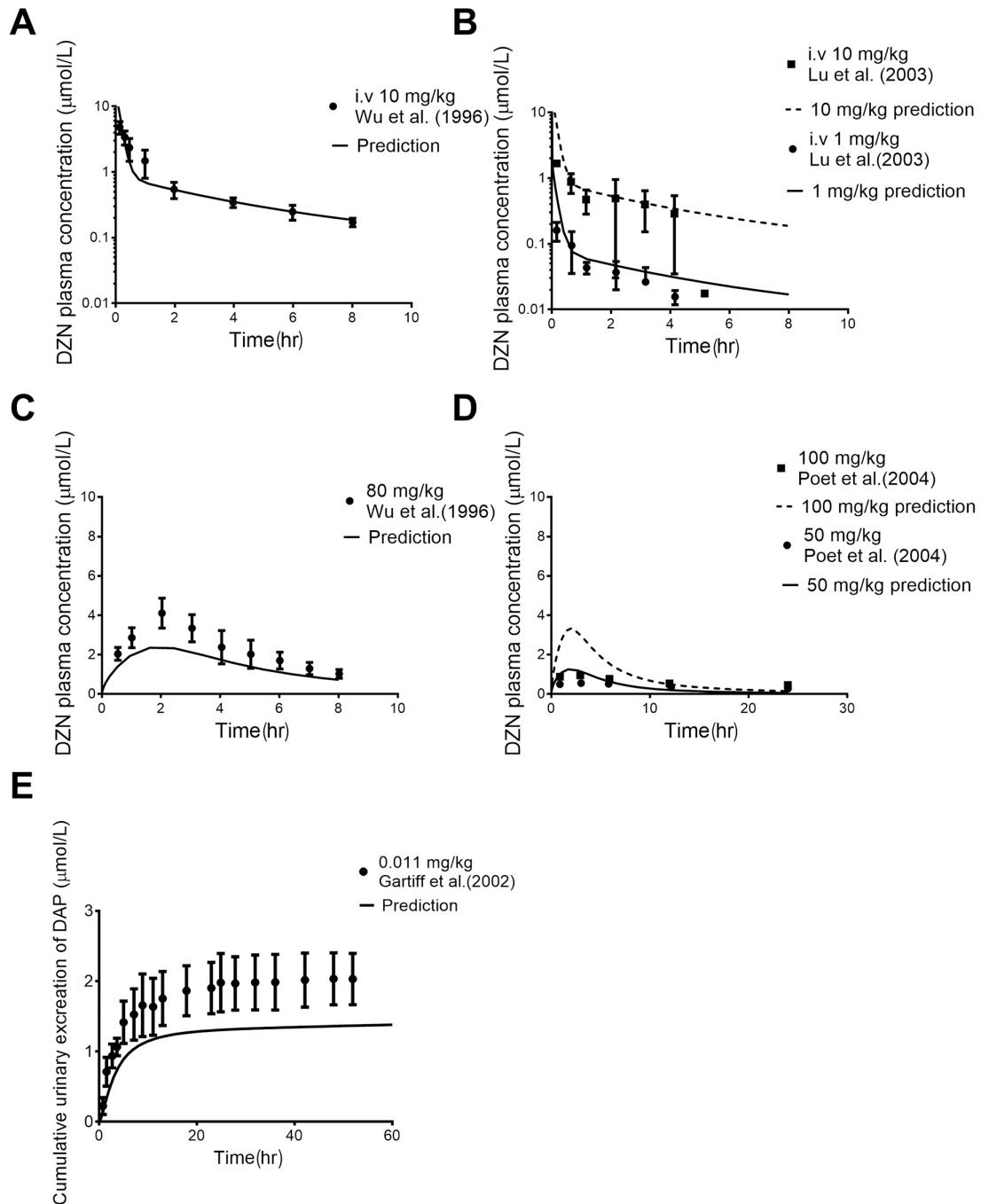


Fig 5. Comparison between reported in vivo data and PBK model predictions for (A) the time-dependent DZN plasma concentration in rats upon IV administration of DZN at 10 mg/kg bw (Wu et al. 1996); (B) the time-dependent DZN plasma concentration in rats upon IV administration of DZN at 1 mg/kg bw and 10 mg/kg bw (Lu et al. 2003); (C) the time-dependent DZN plasma concentration in rats upon oral administration of DZN at 80 mg/kg bw (Wu et al. 1996); (D) the time-dependent DZN plasma concentration in rats upon an oral DZN dose of 50, and 100 mg/kg bw (Poet et al. 2004); (E) the urinary excretion of DAP in humans upon an oral dose of 0.011 mg/kg bw (Garfitt et al. 2002).



The PBK models developed for DZN were evaluated against *in vivo* data. For the rat model, the evaluation was based on comparison of the model predictions with four sets of available *in vivo* data. These included: 1) the time-dependent DZN plasma concentration upon IV administration of DZN at 10 mg/kg bw (Fig 5A) (Wu et al. 1996); 2) the time-dependent DZN plasma concentration upon IV administration of DZN at 1 and 10 mg/kg bw (Fig 5B) (Lu et al. 2003); 3) the time-dependent DZN plasma concentration upon oral administration of DZN at 80 mg/kg bw (Fig 5C) (Wu et al. 1996); and 4) the time-dependent DZN plasma concentration upon an oral DZN dose of 50, and 100 mg/kg bw (Fig 5D) (Poet et al. 2004). The data reveal that the model adequately predicts the DZN plasma concentration upon IV administration (Fig 5A and 5B). Upon oral dosing, the predictions vary, but this seems to be also related to differences in the experimental data. The DZN plasma levels reported by Poet et al. (2004) for example are around 7-fold and 4-fold lower at a dose level of 50 and 100 mg/kg bw than what is reported by Wu et al. (1996) at a dose level of 80 mg/kg bw, pointing at a discrepancy in between these *in vivo* data. In the present study, the PBK model predictions matched the reported plasma DZN levels from Wu et al. (1996) well based on the acceptance criteria from the WHO (WHO 2010) (predictions are between 0.8- to 2-fold different from *in vivo* data) (Fig 5C), while the predictions are 2- to 3-fold different from the values reported by Poet et al. (2004) (Fig 5D). Given that the PBK model accurately predicted the data from the Wu et al. (1996) (Fig 5C), and the fact that the maximum plasma concentration levels reported by Poet et al. (2004) at dose levels of 50 and 100 mg/kg bw are 7.4- and 4.4-fold lower than the concentration level reported by Wu et al. (1996) at 80 mg/kg bw (instead of only 1.6-fold lower and 1.25-fold higher in line with the dose differences), it is concluded that these lower values reported by Poet et al. (2004) might be related to an experimental factor resulting from for example lower oral bioavailability of the administered dose. Based on these considerations it was concluded that the PBK model was acceptable for further reverse dosimetry. This is further supported by the data presented in Figure 5E show that the related human PBK model well predicted urinary excretion of DAP (within 1.5-fold difference compared with DAP urinary excretion data in human) upon an oral dose of 0.011 mg/kg bw given to human subjects (four men and one woman, age range 30–50 years, weight range 76–90 kg) by Garfitt et al. (2002).

3.4 Sensitivity analysis

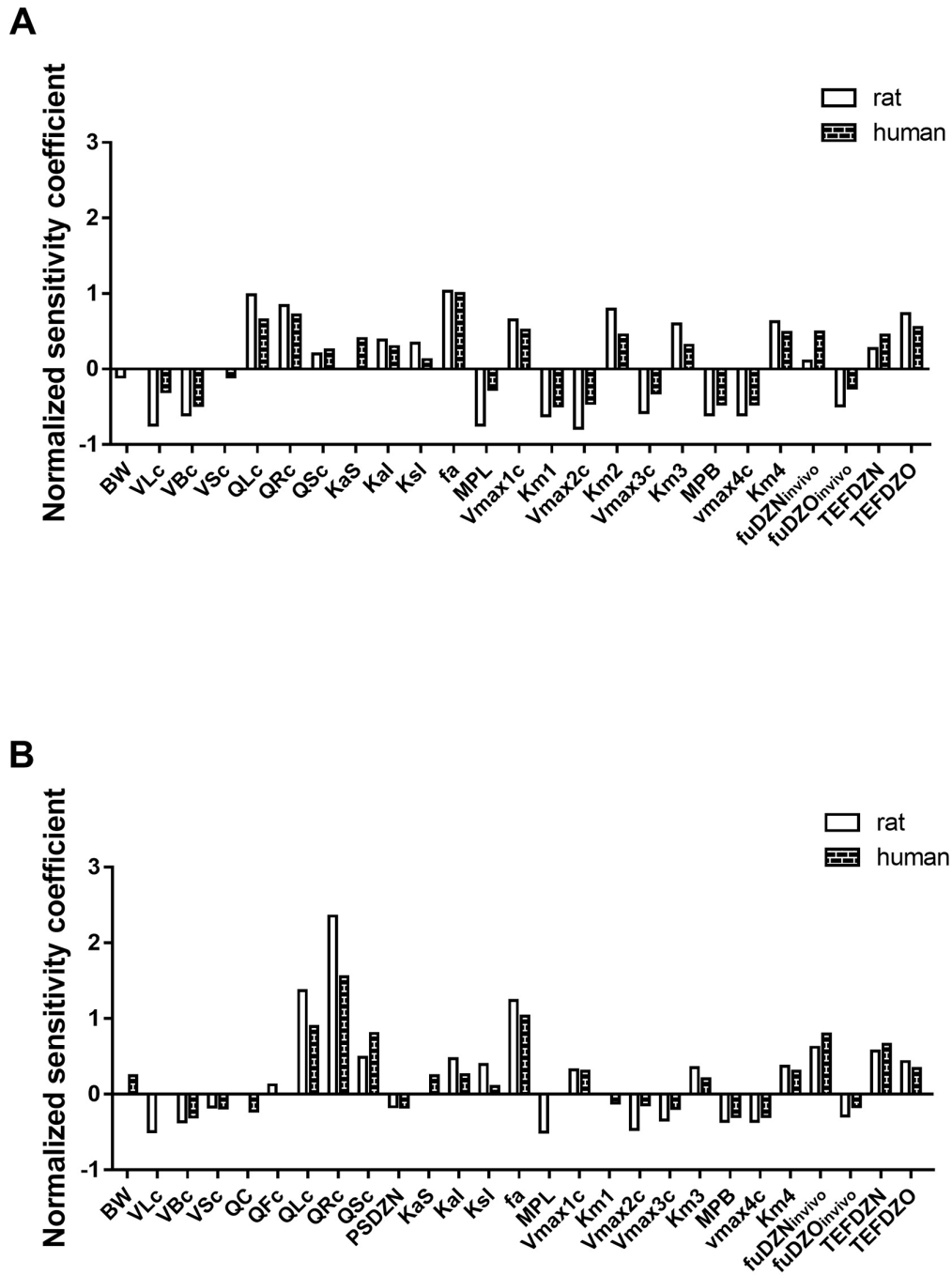


Fig 6. Sensitivity analysis for the predicted free blood concentration of DZN plus DZO expressed in DZO equivalents at (A) low dose levels of DZN of 3 mg/kg (rat) and 0.011 mg/kg bw (human), and (B) high dose levels of DZN of 300 mg/kg (rat) and 293 mg/kg bw (human). The parameters represent: BW= body weight, VLc = fraction of liver tissue, VBc = fraction of blood, VSc = fraction of slowly perfused tissue (bone, muscle and skin), QC = cardiac output, QFc = fraction of blood flow to fat, QLc = fraction of blood flow to liver, QRc = fraction of blood flow to richly perfused tissue, QSc = fraction of blood flow to slowly perfused tissue (muscle, skin, bone),



PSDZN = slowly perfused tissue/blood partition coefficient of DZN, K_{aS} = first order rate constant for absorption DZN from stomach into liver, K_{aI} = first order rate constant for absorption DZN from intestine into the liver, K_{sI} = first order rate constant for transfer of DZN from stomach to intestine, f_a = fractional absorption, MPL = liver microsomal protein yield, V_{max1c} = maximum rate for conversion of DZN to DZO, K_{m1} = Michaelis Menten constant for conversion of DZN to DZO, V_{max2c} = maximum rate for conversion of DZN to IMHP, K_{m2} = Michaelis Menten constant for conversion of DZN to IMHP, V_{max3c} = maximum rate for conversion of DZO to IMHP in liver, K_{m3} = Michaelis Menten constant for conversion of DZO to IMHP in liver, V_{max4c} = maximum rate for conversion of DZO to IMHP in plasma, K_{m4} = Michaelis Menten constant for conversion of DZO to IMHP in plasma, MPB = plasma protein scaling factor, $f_{uDZN_{in vivo}}$ = free fraction of DZN in vivo, $f_{uDZO_{in vivo}}$ = free fraction of DZO in vivo, TEFDZN = toxic equivalency factor of DZN, TEFDZO = toxic equivalency factor of DZO.

In the present study, the impact of each parameter on the model output (the maximum free blood concentration of DZO plus DZN expressed in DZO equivalents) was determined by performing a sensitivity analysis. Only the parameters with normalized sensitivity coefficient higher than 0.1 (absolute value) are shown in Figure 6.

4

For both rat and human, the predicted maximum blood free concentration of DZN plus DZO expressed in DZO equivalents is substantially influenced by body weight, kinetic parameters for all pathways of DZN, volume of liver, volume of blood, blood flow to rapidly and slowly perfused tissue as well as to liver tissue. In addition, all three absorption rate constants, fraction of dose absorbed, liver microsomal protein yield scaling factor, plasma protein scaling factor, the $f_{uDZN_{in vivo}}$, $f_{uDZO_{in vivo}}$ as well as the TEFDZN and TEFDZO appear to have a substantial influence on the prediction at low dose of DZN. At high dose level, similar results were obtained except for the influence of the kinetic parameters and plasma total protein concentration that became less influential, while slowly perfused tissue/blood partition coefficient of DZN and cardiac output started to play a role.

3.5 Unbound fraction of DZO and DZN in the in vitro medium and in vivo

The $f_{uDZN_{in vivo}}$ and $f_{uDZO_{in vivo}}$ were predicted to be 0.329 and 0.302, respectively. An $f_{uDZO_{in vitro}}$ value of 0.96 was obtained (with the recovery rate of post-dialysis of DZO in the in vitro medium being 74%), indicating that the presence of a low level (0.1mg/ml) of BSA in the in vitro medium does not substantially affect the free fraction of DZO. This observation is

in line with the data reported by Heilmair et al. (2008) as mentioned above. A similar result is expected for DZN since DZN and DZO have comparable unbound fractions in plasma. Therefore, the unbound fraction of both DZN and DZO in vitro was set at 1.

3.6 Relative contribution of DZN and DZO to plasma DZO equivalents

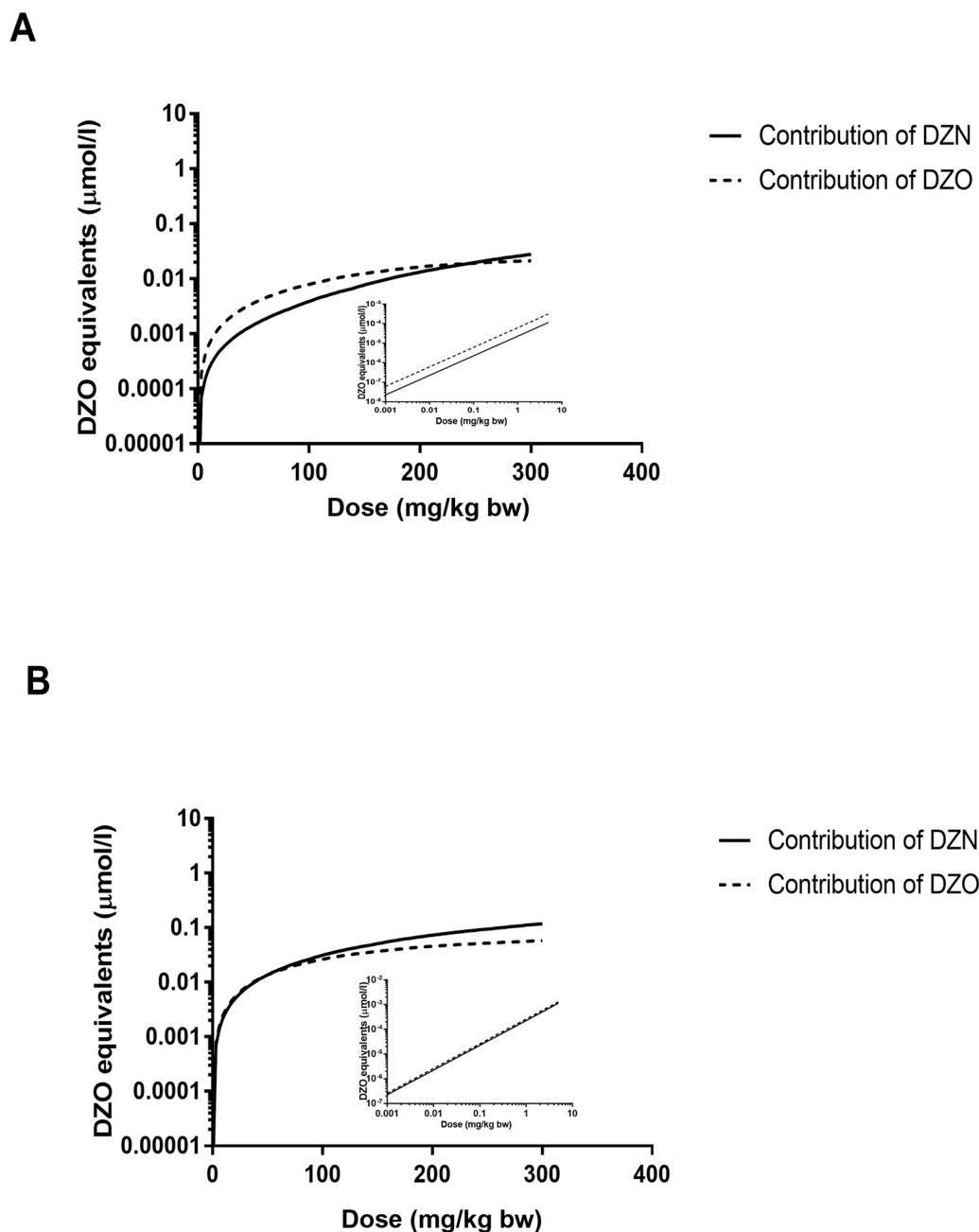


Fig 7. The PBK model based predicted dose-dependent relative contribution of DZN and DZO to the free blood concentration expressed in DZO equivalents in (A) rat and (B) human. The insert presents the data at the lower dose levels (up to 10 mg/kg bw) in some more detail.

Figure 7 shows the predicted dose-dependent relative contribution of DZN and DZO to the total free blood concentration expressed in DZO equivalents in rat and human. These results indicate that, apart from DZO, DZN is predicted to be another major contributor to the blood

DZO equivalents, in spite of its relatively low TEF values of 0.00351 in rat and 0.00310 in human. This is especially apparent at high dose levels (at dose levels higher than 240 mg/kg in rat and 50 mg/kg in human), the role of DZN even outweighs that of its active metabolite DZO because of its high concentration and the almost saturation of its conversion to DZO. Similarly, the predicted free blood maximum concentration of DZO for a DZN dose range from 0 up to 300 mg/kg bw (supplementary material III) in humans is around 2- to 4-fold higher than that in rats, while this inter-species difference increases to around 4- to 10-fold when comparing the predicted dose-dependent maximum blood concentrations expressed in DZO equivalents in human and rat, with the values in human being higher (supplementary material III). Overall, Figure 7 and supplementary material III together reflect the relatively higher contribution of DZN to the toxicity in human than in rats, and also that it is essential to take the contribution of both DZN and DZO into account.

3.7 Predicted in vivo dose-response curves for AChE inhibition and their evaluation

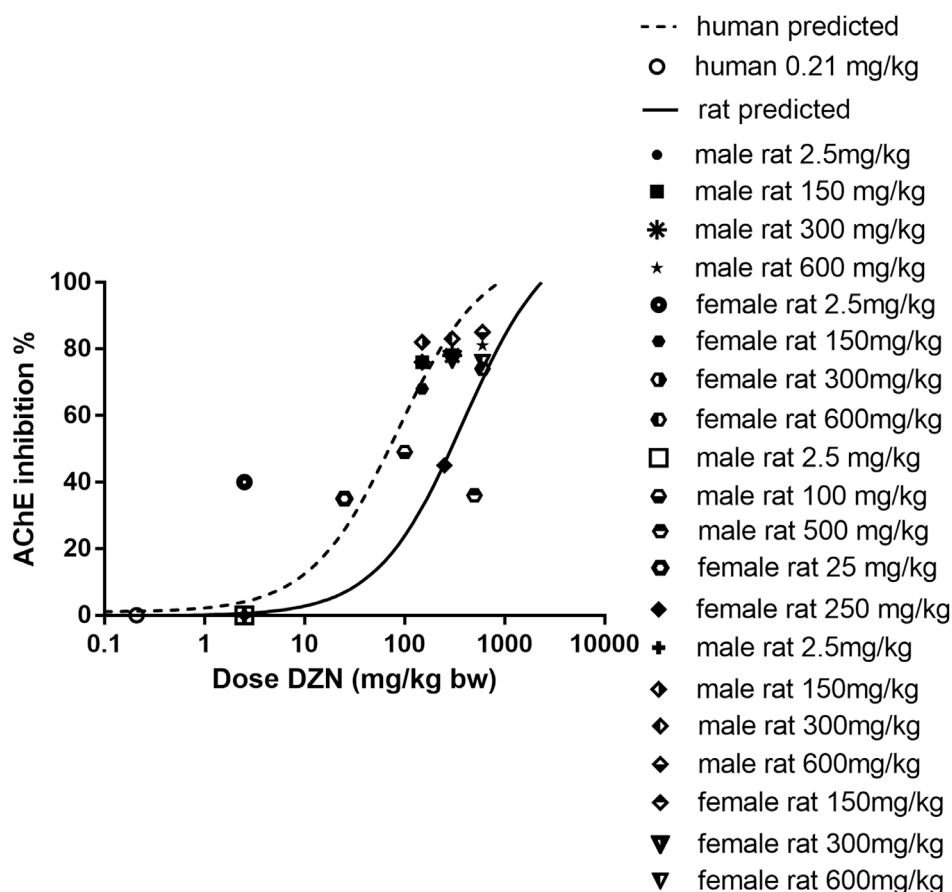


Fig 8. The predicted in vivo dose-response curves for AChE inhibition upon DZN exposure in rat (solid line) and human (dashed line) using PBK-model-based reverse dosimetry. The individual data points represent available in vivo data for RBC AChE inhibition in rat and human upon oral exposure to DZN at different dose levels as reported by JMPR (2016) and USEPA (2016).

Figure 8 presents the predicted in vivo dose-response curves for AChE inhibition upon DZN exposure in rat and human. Based on the predicted dose-response curves obtained, human seems more sensitive than rat in terms of AChE inhibition caused by DZN exposure, although a similar intrinsic potency was found from the in vitro concentration-response curves for human and rat AChE inhibition from which these in vivo predicted curves were derived (Figure 4).

This indicates that differences in kinetics influence the interspecies differences in in vivo sensitivity.

For comparison, Figure 8 also presents the individual data points for AChE inhibition as reported by JMPR and USEPA (JMPR 2016; USEPA 2016). Comparison of these data to the predicted curves reveals that the predictions are in line with the reported in vivo data.

3.8 Predicted BMDL₁₀ values and their evaluation

The dose-response curves obtained were used to derive BMDL₁₀ values for both rat and human allowing comparison to PODs available from previous evaluations (EFSA 2006; JMPR 2016; USEPA 2016). The predicted BMDL₁₀ values amounted to 2.1 and 12.6 mg/kg bw for human and rat respectively (Table 3). The BMDL₁₀ value for human was 6-fold lower than that for rat, a difference that is lower than the default uncertainty factor of 10 for interspecies differences, providing support for a chemical-specific adjustment factor. The BMDL₁₀ of 12.6 mg/kg bw for rat, compares well to the BMDL₁₀ for inhibition of brain and RBC AChE in male adult rats upon oral DZN administration, amounting to 12.175 mg/kg bw/day for inhibition of brain AChE and 4.804 mg/kg bw/day for inhibition of RBC AChE, respectively (USEPA 2016). The predicted BMDL₁₀ of the present study for rat RBC AChE inhibition appears the same as the BMDL₁₀ reported for inhibition of brain AChE and 2.6-fold higher than that for inhibition of RBC AChE. However, EPA used a BMDL₁₀ value of 3 mg/kg bw derived from RBC AChE inhibition in female rat pups (PND11) (USEPA 2016) as the POD for deriving an ARfD. A previous study indicated that the inhibition of brain AChE in pups at postnatal day 17 was 2-fold higher than in adult rats (75% instead of 38%) at a similar oral dose of 75 mg/kg bw (Padilla et al. 2004), suggesting that the early life stage of rat (pups) show a greater sensitivity than adult rats. Therefore the predicted BMDL₁₀ in the current study for adult rats can be further corrected by this factor 2, resulting in a POD of 6.3 mg/kg bw which is 2.1-fold higher than the POD of 3 mg/kg bw used by the EPA (USEPA 2016).

Different from the EPA, JMPR used a no-observed-adverse-effect level (NOAEL) of 2.5 mg/kg bw from an acute (neuro)toxicity study of DZN in rats (JMPR 2016) based on inhibition of brain and RBC AChE activity in female rat at a lowest observed adverse effect level (LOAEL) of 25 mg/kg bw. Similarly, EFSA used an overall NOAEL of 2.5 mg/kg bw from three rat studies (EFSA 2006) based on AChE inhibition alone or AChE inhibition together with

reversible neurotoxic effects occurring at a LOAEL of 25 mg/kg or 150 mg/kg. Because of the wide dose range used in these studies resulting in a large dose range between the NOAEL and LOAEL values, the NOAEL of 2.5 mg/kg bw derived from these studies may provide a relatively low POD. Taking this consideration into account, the predicted BMDL₁₀ values in the present study also seem to be in line with these reported NOAEL values.

Table 3. Comparison of predicted BMDL₁₀ values to reported BMDL₁₀ values and to the NOAEL values established by USEPA (2016), EFSA (2006) and JMPR (2016) for DZN

PODs	Reported NOAEL from EFSA and JMPR (adult rat) (mg/kg bw)	Reported BMDL ₁₀ from EPA (adult rat) (mg/kg bw)	Reported BMDL ₁₀ from EPA (pups) (mg/kg bw)	Predicted BMDL ₁₀ for adult rat (mg/kg bw)	Predicted BMDL ₁₀ for rat pups (mg/kg bw)	Predicted BMDL ₁₀ for human (mg/kg bw)
Diazinon	2.5	4.8	3.0	12.6	6.3 *	2.1

* Value derived from the BMDL₁₀ for adult rats taking into account the results from an in vivo study (Padilla et al. 2004), showing that pups are expected to be 2-fold more sensitive than adults

4. Discussion

The present study aimed to assess the feasibility of using a TEF-coded PBK model for DZN, containing a submodel for its active metabolite DZO, together with reverse dosimetry as an alternative approach to predict rat and human *in vivo* RBC AChE inhibition dose-response curves for DZN. The models were based on mainly *in silico* and *in vitro* data. The rat DZN model was built and evaluated first and used as the basis for developing the human DZN model since less human *in vivo* data are available for model evaluation (EFSA 2006; JMPR 2016; USEPA 2016). The results obtained reveal that the developed rat model adequately predicted the toxicokinetic profile of DZN in rat, and could also adequately convert the *in vitro* concentration-response curve to an *in vivo* dose response curve for DZN mediated-AChE inhibition, resulting in a BMDL₁₀ value comparable to the BMDL₁₀ reported for inhibition of rat brain AChE and 2.6-fold different from the reported BMDL₁₀ for inhibition of rat RBC AChE, respectively (EFSA 2006; JMPR 2016; USEPA 2016). Furthermore, the obtained results also show the predicted BMDL₁₀ of human to be 6-fold lower than that of rat, in spite of similar *in vitro* concentration response curves for DZN or DZO mediated AChE inhibition. This result indicates that interspecies differences in toxicokinetics of DZN between rat and human play an important role in the ultimate species differences in *in vivo* toxicity. This 6-fold difference in the BMDL₁₀ values as derived for adult populations is smaller than the default uncertainty factor for interspecies differences of 10. However, the actual uncertainty value for interspecies differences may be affected when considering potential species differences in sensitivity at different life stages, with rats showing 2-fold higher sensitivity at younger life stages. On the other hand, when using a QIVIVE based POD derived using human data, use of an interspecies uncertainty factor would no longer be required. In that case an extra uncertainty factor may be considered to account for the fact that the *in vitro-in silico* QIVIVE approach brings other uncertainties. Altogether, establishment of the actual size of the overall uncertainty factor has to await further studies also including data for potentially vulnerable groups within the human population, like children and pregnant women. Besides, the obtained results also revealed that, in spite of an around 300-fold lower AChE inhibitory potency of DZN than of its active metabolite DZO, DZN still plays a substantial role in the induced AChE inhibition, indicating AChE inhibition induced by DZN should be taken into account in DZN risk assessment. At dose levels higher than 240 mg/kg bw in rat and 50 mg/kg in human, the role of DZN even outweighs that of its active metabolite DZO, mainly due to its substantially higher plasma levels caused by the high dose levels and metabolic capacities for both its bioactivation

and detoxification approaching saturation. Overall, our findings show that the reverse dosimetry approach combining *in vitro* data and the TEF-coded PBK models provides a promising tool to predict *in vivo* dose-response curves for OP-induced AChE inhibition.

The obtained kinetic data revealed that, for both rat and human, CYP450-catalysed conversion of DZN results primarily in detoxification to IMHP rather than giving rise to bioactivation to DZO, which is in line with the conclusion from other studies (Mutch and Williams 2006; Poet et al. 2003; Sams et al. 2004). The K_m values for these CYP450-mediated conversions appeared to be substantially lower than what was reported before (Poet et al. 2003), a discrepancy most likely due to the concentration ranges used to define the kinetic parameters. In the present study, K_m values were determined using a range of DZN concentration (1 μM to 250 μM) that allowed to fully capture both initial kinetics at low concentrations as well as the saturation phase, while in the literature (Poet et al. 2003), the K_m was defined based on the activity measured only at concentrations (80 μM to 800 μM) exceeding the actual K_m , thus resulting in inaccurate K_m values. For PON1-mediated detoxification, there were no differences in kinetic parameters for liver and plasma samples of rat or human, indicating that the PON1 activities in these two tissues display similar kinetics, an observation in line with the fact that PON1 in blood originates from synthesis in and release from the liver (Pyati et al. 2015).

Detailed comparison of the species differences between rat and human reveal that rat display a faster metabolic rate for CYP450-mediated bioactivation and detoxification of DZN than human, indicating that at the same exposure level, and assuming similar bioavailability, levels of DZN will be lower in rat than human. This is one of the reasons why differences in kinetics cause a species difference in *in vivo* toxicity. In addition, PON1-mediated detoxification of DZO to IMHP is faster in rat than human in both liver and blood, counteracting the faster DZO formation from DZN in rat than human. Clearly the PBK models provide a way to evaluate the combined influence of all these differences in kinetics on the ultimate *in vivo* toxicity. The interspecies kinetic differences in CYP450-mediated conversions may be explained by different CYP450 involved in DZN metabolism in rat and human liver. For rat, metabolism of DZN to DZO and IMHP are mainly catalysed by CYP1A2, CYP2C11, CYP3A2, and CYP2B1/2 (Fabrizi et al. 1999; Ueyama et al. 2007), while in human, the metabolism is mainly mediated by CYP1A1, CYP1A2, CYP2B6, CYP2C19 and CYP3A4 (Ellison et al. 2012; Kappers et al. 2001; Mutch and Williams 2006; Sams et al. 2004). Although the detoxification of DZO in rat and human are both mediated by PON1, in the present study, the rat appeared to

be a faster DZO metaboliser than human, which could be explained, at least partly, by higher PON1 activity in rat than human (Berry et al. 2009; Kaliste-Korhonen et al. 1996; Makhaeva et al. 2009). This observation is in line with data reported by Makhaeva et al. (2009) for another OP, indicating an approximately 4-fold faster PON1 mediated-hydrolysis of paraoxon by rat than human plasma samples.

To assess the inhibitory capability of DZO on human RBC AChE, the *in vitro* human AChE inhibition assay was conducted using rhAChE. rhAChE has been widely used to assess AChE inhibition (Amitai et al. 1998; Kaushik et al. 2007; Li et al. 2019; Sultatos 2007), and the IC₅₀ value of DZN obtained using rhAChE in the present study of 14.26 μ M is comparable to the value reported previously for natural human RBC AChE (IC₅₀=24.45 μ M) (Fakhri-Bafghi et al. 2016). Therefore, the use of rhAChE is expected to be adequate to describe the inhibitory profile of DZN and DZO on human RBC AChE. It is also of interest to note that there was no interspecies difference in the *in vitro* DZO-induced AChE inhibition between rat and human in the present study, and a similar conclusion has been previously reported for dichlorvos, another OP (MacGregor et al. 2005).

In the present study, a TEF-coded PBK model was used to describe free blood concentrations of DZO plus DZN expressed in DZO equivalents at the target site RBC AChE. The results reveal that the free blood concentration of DZN contributes substantially to the DZO equivalents, indicating it is of critical importance to take internal free DZN concentrations into account when conducting DZN risk assessment. The use of the TEF approach is based on the assumptions that i) DZN and DZO initiate toxicity via the same mode of toxic action (AChE inhibition); ii) their concentration-response curves are parallel; iii) their toxicity is additive (Starr et al. 1999; Watt et al. 2016). The first assumption is supported by the fact that both DZN and DZO induce inhibition of AChE activity. The second assumption was supported by statistical comparison of the hillslope values describing the steepness of the concentration-response curves of DZN and DZO in both human and rat. The comparison showed that the hillslope values of DZN and DZO are similar in both human and rat, with *p* values of 0.0797 and 0.1504, respectively, indicating the DZN and DZO curves are parallel in both species. In terms of assumption three, the combined effect of DZN and DZO was assessed by incubating rhAChE with DZO only or an equipotent mixture of DZO+DZN in which the concentration of DZN and DZO were selected in such a way that each compound would contribute 50% to the AChE inhibition based on the TEF values of DZN and DZO derived in the present paper. The results (Supplementary material IV) obtained showed that the curves coincided indicating the

combined effect of DZN and DZO to be additive. This additive combined effect between DZN and DZO was also observed in the study of Čolović et al. (2011). Different from the conventional TEF approach that defines TEF values based on dose-response curves from in vivo models (USEPA 2016), the TEF values derived in the present study were based on IC50 values derived from in vitro concentration-response curves. This implies that the TEF values do not include the contribution of in vivo toxicokinetics, including absorption, distribution, metabolism, and excretion. These aspects are accounted for by the PBK model itself when performing reverse dosimetry. Using TEF in a toxicokinetic-toxicodynamic (TK-TD) model has been successfully applied in a previous study to predict internal concentrations of a metal mixture and its resulting toxicity (Gao et al. 2016; Gao et al. 2018).

To evaluate whether the currently developed TEF-coded PBK model-facilitated reverse dosimetry approach can be used to determine POD values for DZN risk assessment, BMDL₁₀ values obtained from the predicted dose-response curves were compared with EPA reported BMDL₁₀ values for both pups and adult rat, showing that the approach provided a reasonable estimation of the BMDL₁₀.

4

Although the currently developed method is promising to be used in future risk assessment, it is of importance to also mention its limitations. The first is that interindividual variations have not (yet) been taken into account. Previously reported studies indicated potentially large interindividual variations in the expression of enzymes involved in DZN metabolism. For the biotransformation of DZN to DZO, this includes an up to 20-fold variation in CYP2C19 human hepatic expression levels, an up to 100-fold variation in CYP2B6 human hepatic expression levels, and an up to 40-fold variation for CYP3A4 expression in liver and small intestine donor tissues (Ellison et al. 2012; Koukouritaki et al. 2004; Lamba et al. 2002; Lang et al. 2001; Tracy et al. 2016; Westlind et al. 1999). Such interindividual variability in CYP450 was reflected by data on DZO formation from DZN showing a 6- to 59-fold difference between 15 human liver samples (Kappers et al. 2001). Similarly, a substantial about 40-fold interindividual human variation in the activity of PON1, the key enzyme for detoxification of DZO, has been observed (Costa et al. 2006). Given that the present study focussed on the average adult population using kinetic data defined with pooled human samples, a further study of the consequences of these interindividual differences for the predicted AChE inhibition remains an interesting topic for future research. The second limitation relates to the reverse dosimetry approach. This PBK based approach does not account for dynamic changes in AChE activity due to for example AChE regeneration, aging, degradation, and inhibition. This implies that it can predict acute

toxicity but may be less appropriate for prediction of toxicity upon repeated exposure, resulting in inhibition of RBC AChE activity and neurotoxicity of DZN (Hernández et al. 2005). This is further illustrated by the fact the BMDL₁₀ values for this subchronic exposure related AChE inhibition are generally lower than the ones reported for inhibition of RBC AChE upon single dose exposure (USEPA 2016). In addition, the potential protective effects of other B-esterases enzymes such as BuChE and CaE were not included in the current study. As reported in previous studies, B-esterases like BuChE and CaE might influence the OP induced AChE inhibition, by binding the OP so that less oxon-metabolites are available in the circulation to inhibit AChE in vital tissues (Chanda et al. 2002; Chanda et al. 1997; Costa 2001; Costa 2006; Jokanović 2009). Such a potential protective role of BuChE and CaE has been investigated especially in animals. Raveh et al. (1997) reported that pretreatment of monkeys with human plasma derived BuChE can protect against toxicity induced by a lethal dose of the OP ethyl-S-(2-diisopropylaminoethyl) methyl-phosphonothiolate. Similarly, a study from Duysen et al. (2011) showed that exposure to 3 mg/kg bw of the OP soman coumarin can be lethal to mice deficient in plasma CaE but not to the wild type mice, indicating a possible potential protective role of CaE. However the role of BuChE and CaE in OP toxicity in human is still not well known (Chanda et al. 2002; Jokanović et al. 2020). The potential protective effect of BuChE and CaE might depend on: 1) the affinity between the enzymes and the respective OP (Chanda et al. 2002); 2) the endogenous level and activity of the enzymes (Chanda et al. 2002; Jokanović et al. 2020); 3) the genotype of the enzymes (Eaton et al. 2008). In the present study this potential protective role of the B-esterases was not specifically considered. This may in theory result in an over-estimation of the predicted dose-dependent AChE inhibition. However, the QIVIVE values in the present study do not seem to overpredict the toxicity as reflected by the good match between the predicted dose-response curves for AChE inhibition in rat and the actual in vivo data available from literature (Figure 8), suggesting the influence of the B-esterases to be limited if any.

In spite of these limitations the results of the present study show that the DZN TEF coded-PBK model together with QIVIVE appeared a suitable method to predict RBC AChE inhibition upon acute oral exposure to DZN in human and rat. The obtained results indicate an interspecies difference in toxicokinetics of DZN, resulting in the predicted BMDL₁₀ of human to be around 6-fold lower than that of rat, indicating that the default uncertainty factor of 10 for interspecies extrapolation might be overprotective. Given the fact that this method is based on mainly an *in silico* and *in vitro* approach, it provides an alternative method reducing animal testing for

setting PODs in human risk assessment. Furthermore, by replacing relevant parameters (e.g. the absorption and excretion constants) with the data derived based on *in silico* and *in vitro* assays, a PBK model for human can be defined and used to derive a POD for human risk assessment without the need for *in vivo* studies.

Acknowledgements

This work was funded by a Grant from the China Scholarship Council (No. 201707720063 to ZHAOSHENSHENG).

Conflict of interests

The authors declared no potential conflicts of interest with respect to the research, authorship, and/or publication of this article.

References

- Amitai G, Moorad D, Adani R, Doctor B (1998) Inhibition of acetylcholinesterase and butyrylcholinesterase by chlorpyrifos-oxon *Biochemical pharmacology* 56:293-299
- Barter ZE et al. (2007) Scaling factors for the extrapolation of in vivo metabolic drug clearance from in vitro data: reaching a consensus on values of human micro-somal protein and hepatocellularity per gram of liver *Current drug metabolism* 8:33-45
- Berry LM, Wollenberg L, Zhao Z (2009) Esterase activities in the blood, liver and intestine of several preclinical species and humans *Drug metabolism letters* 3:70-77
- Bizoń A, Milnerowicz H (2018) The effect of divalent metal chelators and cadmium on serum phosphotriesterase, lactonase and arylesterase activities of paraoxonase 1 *Environmental Toxicology and Pharmacology* 58:77-83
- Boonpawa R, Spenkelink A, Punt A, Rietjens IMCM (2017) Physiologically based kinetic modeling of hesperidin metabolism and its use to predict in vivo effective doses in humans *Molecular nutrition & food research* 61:1600894
- Brown RP, Delp MD, Lindstedt SL, Rhomberg LR, Beliles RP (1997) Physiological parameter values for physiologically based pharmacokinetic models *Toxicology and industrial health* 13:407-484
- Buratti FM, D'aniello A, Volpe MT, Meneguz A, Testai E (2005) Malathion bioactivation in the human liver: the contribution of different cytochrome P450 isoforms *Drug metabolism and disposition* 33:295-302
- Buratti FM, Volpe MT, Meneguz A, Vittozzi L, Testai E (2003) CYP-specific bioactivation of four organophosphorothioate pesticides by human liver microsomes *Toxicology and applied pharmacology* 186:143-154
- Burgess P, Harper C, Todd GD, Wohlers D (2008) Toxicological profile for diazinon. <https://www.atsdr.cdc.gov/toxprofiles/tp86.pdf>. Accessed 3 March 2021
- Chanda S, Lassiter T, Moser V, Barone S, Padilla S (2002) Tissue carboxylesterases and chlorpyrifos toxicity in the developing rat *Human and Ecological Risk Assessment* 8:75-90
- Chanda S, Mortensen S, Moser V, Padilla S (1997) Tissue-specific effects of chlorpyrifos on carboxylesterase and cholinesterase activity in adult rats: an in vitro and in vivo comparison *Toxicological Sciences* 38:148-157
- Čolović MB, Krstić DZ, Lazarevic-Pasti TD, Bondzic AM, Vasić VM (2013) Acetylcholinesterase inhibitors: pharmacology and toxicology *Current neuropharmacology* 11:315-335
- Čolović MB, Krstić DZ, Ušćumlić GS, Vasić VM (2011) Single and simultaneous exposure of acetylcholinesterase to diazinon, chlorpyrifos and their photodegradation products *Pesticide biochemistry and physiology* 100:16-22
- Costa L (2001) Pesticide exposure: differential risk for neurotoxic outcomes due to enzyme polymorphisms *Clin Occup Environ Med* 1:511-523
- Costa L, Li W, Richter R, Shih D, Lusi A, Furlong C (1999) The role of paraoxonase (PON1) in the detoxication of organophosphates and its human polymorphism *Chemico-biological interactions* 119:429-438
- Costa LG (2006) Current issues in organophosphate toxicology *Clinica chimica acta* 366:1-13
- Costa LG, Cole TB, Vitalone A, Furlong CE (2006) Paraoxonase polymorphisms and toxicity of organophosphates. In: *Toxicology of Organophosphate & Carbamate Compounds*. Elsevier, pp 247-255. doi:<https://doi.org/10.1016/B978-012088523-7/50019-3>
- Cubitt HE, Houston JB, Galetin A (2009) Relative importance of intestinal and hepatic glucuronidation—impact on the prediction of drug clearance *Pharmaceutical research* 26:1073
- Dadson OA et al. (2013) Metabolism of profenofos to 4-bromo-2-chlorophenol, a specific and sensitive exposure biomarker *Toxicology* 306:35-39
- DeJongh J, Verhaar HJ, Hermens JL (1997) A quantitative property-property relationship (QPPR) approach to estimate in vitro tissue-blood partition coefficients of organic chemicals in rats and humans *Archives of Toxicology* 72:17-25
- Dodge JT, Mitchell C, Hanahan DJ (1963) The preparation and chemical characteristics of hemoglobin-free ghosts of human erythrocytes *Archives of biochemistry and biophysics* 100:119-130

- Duysen EG, Koentgen F, Williams GR, Timperley CM, Schopfer LM, Cerasoli DM, Lockridge O (2011) Production of ES1 plasma carboxylesterase knockout mice for toxicity studies *Chemical research in toxicology* 24:1891-1898
- Eaton DL et al. (2008) Review of the toxicology of chlorpyrifos with an emphasis on human exposure and neurodevelopment *Critical reviews in toxicology* 38:1-125
- EFSA (2006) Conclusion regarding the peer review of the pesticide risk assessment of the active substance diazinon. <https://efsa.onlinelibrary.wiley.com/doi/epdf/10.2903/j.efsa.2006.85r>.
- Ellison CA, Tian Y, Knaak JB, Kostyniak PJ, Olson JR (2012) Human hepatic cytochrome P450-specific metabolism of the organophosphorus pesticides methyl parathion and diazinon *Drug Metabolism and Disposition* 40:1-5
- Ellman GL, Courtney KD, Andres Jr V, Featherstone RM (1961) A new and rapid colorimetric determination of acetylcholinesterase activity *Biochemical pharmacology* 7:88-95
- Fabrizi L, Gemma S, Testai E, Vittozzi L (1999) Identification of the cytochrome P450 isoenzymes involved in the metabolism of diazinon in the rat liver *Journal of biochemical and molecular toxicology* 13:53-61
- Fakhri-Bafghi MS, Ghasemi-Niri SF, Mostafalou S, Navaei-Nigjeh M, Baeri M, Mohammadirad A, Abdollahi M (2016) Protective effect of selenium-based medicines on toxicity of three common organophosphorus compounds in human erythrocytes in vitro *Cell Journal (Yakhteh)* 17:740
- Foxenberg RJ, McGarrigle BP, Knaak JB, Kostyniak PJ, Olson JR (2007) Human hepatic cytochrome p450-specific metabolism of parathion and chlorpyrifos *Drug metabolism and disposition* 35:189-193
- Gao Y, Feng J, Han F, Zhu L (2016) Application of biotic ligand and toxicokinetic-toxicodynamic modeling to predict the accumulation and toxicity of metal mixtures to zebrafish larvae *Environmental Pollution* 213:16-29
- Gao Y, Feng J, Kang L, Xu X, Zhu L (2018) Concentration addition and independent action model: Which is better in predicting the toxicity for metal mixtures on zebrafish larvae *Science of the Total Environment* 610:442-450
- Garfitt S, Jones K, Mason H, Cocker J (2002) Exposure to the organophosphate diazinon: data from a human volunteer study with oral and dermal doses *Toxicology letters* 134:105-113
- Gearhart JM, Jepson GW, Clewell III HJ, Andersen ME, Conolly RB (1990) Physiologically based pharmacokinetic and pharmacodynamic model for the inhibition of acetylcholinesterase by diisopropylfluorophosphate *Toxicology and applied pharmacology* 106:295-310
- George P, Abernethy M (1983) Improved Ellman procedure for erythrocyte cholinesterase *Clinical chemistry* 29:365-368
- GraphPad (2009) How do I determine whether two dose-response curves are parallel? <https://www.graphpad.com/support/faq/how-do-i-determine-whether-two-dose-response-curves-are-parallel/>. Accessed 22 December 2020
- Heilmair R, Eyer F, Eyer P (2008) Enzyme-based assay for quantification of chlorpyrifos oxon in human plasma *Toxicology letters* 181:19-24
- Hernández AF et al. (2005) Changes in erythrocyte enzymes in humans long-term exposed to pesticides: influence of several markers of individual susceptibility *Toxicology letters* 159:13-21
- JMPR (2016) Pesticide residues in food 2016. <http://www.fao.org/3/a-i5693e.pdf>. Accessed 18 September 2020
- Jokanović M (2009) Current understanding of the mechanisms involved in metabolic detoxification of warfare nerve agents *Toxicology letters* 188:1-10
- Jokanović M, Ristić D, Kovač B, Stojiljković MP (2020) Biotransformation of warfare nerve agents. In: *Handbook of Toxicology of Chemical Warfare Agents*. Elsevier, pp 953-966. doi:<https://doi.org/10.1016/B978-0-12-819090-6.00055-6>
- Kaliste-Korhonen E, Tuovinen K, Hänninen O (1996) Interspecies differences in enzymes reacting with organophosphates and their inhibition by paraoxon in vitro *Human & experimental toxicology* 15:972-978
- Kappers WA, Edwards RJ, Murray S, Boobis AR (2001) Diazinon is activated by CYP2C19 in human liver *Toxicology and applied pharmacology* 177:68-76

- Kaushik R, Rosenfeld CA, Sultatos L (2007) Concentration-dependent interactions of the organophosphates chlorpyrifos oxon and methyl paraoxon with human recombinant acetylcholinesterase *Toxicology and applied pharmacology* 221:243-250
- Koukouritaki SB, Manro JR, Marsh SA, Stevens JC, Rettie AE, McCarver DG, Hines RN (2004) Developmental expression of human hepatic CYP2C9 and CYP2C19 *Journal of Pharmacology and Experimental Therapeutics* 308:965-974
- Lamba JK, Lin YS, Schuetz EG, Thummel KE (2002) Genetic contribution to variable human CYP3A-mediated metabolism *Advanced drug delivery reviews* 54:1271-1294
- Lane RM, Potkin SG, Enz A (2006) Targeting acetylcholinesterase and butyrylcholinesterase in dementia *International Journal of Neuropsychopharmacology* 9:101-124
- Lang T et al. (2001) Extensive genetic polymorphism in the human CYP2B6 gene with impact on expression and function in human liver *Pharmacogenetics and Genomics* 11:399-415
- Li S, Zhao J, Huang R, Santillo MF, Houck KA, Xia M (2019) Use of high-throughput enzyme-based assay with xenobiotic metabolic capability to evaluate the inhibition of acetylcholinesterase activity by organophosphorous pesticides *Toxicology in Vitro* 56:93-100
- Louisse J, Beekmann K, Rietjens IMCM (2017) Use of physiologically based kinetic modeling-based reverse dosimetry to predict in vivo toxicity from in vitro data *Chemical research in toxicology* 30:114-125
- Louisse J, de Jong E, van de Sandt JJM, Blaauboer BJ, Woutersen RA, Piersma AH, Rietjens IMCM, Verwei M (2010) The use of in vitro toxicity data and physiologically based kinetic modeling to predict dose-response curves for in vivo developmental toxicity of glycol ethers in rat and man *Toxicological Sciences* 118:470-484
- Lu C, Irish R, Fenske R (2003) Biological monitoring of diazinon exposure using saliva in an animal model *Journal of Toxicology and Environmental Health Part A* 66:2315-2325
- MacGregor JA, Plunkett LM, Youngren SH, Manley A, Plunkett JB, Starr TB (2005) Humans appear no more sensitive than laboratory animals to the inhibition of red blood cell cholinesterase by dichlorvos *Regulatory Toxicology and Pharmacology* 43:150-167
- Makhaeva G, Rudakova E, Boltneva N, Sigolaeva L, Eremenko A, Kurochkin I, Richardson R (2009) Blood esterases as a complex biomarker for exposure to organophosphorus compounds. In: *Counteraction to Chemical and Biological Terrorism in East European Countries*. Springer, pp 177-194
- Martignoni M, Groothuis GM, de Kanter R (2006) Species differences between mouse, rat, dog, monkey and human CYP-mediated drug metabolism, inhibition and induction *Expert opinion on drug metabolism & toxicology* 2:875-894
- Medinsky MA, Leavens TL, Csanády GA, Gargas ML, Bond JA (1994) In vivo metabolism of butadiene by mice and rats: a comparison of physiological model predictions and experimental data *Carcinogenesis* 15:1329-1340
- Mutch E, Williams FM (2006) Diazinon, chlorpyrifos and parathion are metabolised by multiple cytochromes P450 in human liver *Toxicology* 224:22-32
- Ning J, Chen L, Strikwold M, Louisse J, Wesseling S, Rietjens IMCM (2019) Use of an in vitro–in silico testing strategy to predict inter-species and inter-ethnic human differences in liver toxicity of the pyrrolizidine alkaloids lasiocarpine and riddelliine *Archives of toxicology* 93:801-818
- O'Neil D (1999) Blood Components. https://web.archive.org/web/20130605052544/http://anthro.palomar.edu/blood/blood_components.htm. Accessed 12 October 2020
- Padilla S, Sung H-J, Moser V (2004) Further assessment of an in vitro screen that may help identify organophosphorus pesticides that are more acutely toxic to the young *Journal of Toxicology and Environmental Health, Part A* 67:1477-1489
- Patel HG, Aras RV, Katyare SS (2000) Kinetic attributes of Na⁺, K⁺ ATPase and lipid/phospholipid profiles of rat and human erythrocyte membrane *Zeitschrift für Naturforschung C* 55:770-777
- Pires DE, Blundell TL, Ascher DB (2015) pkCSM: predicting small-molecule pharmacokinetic and toxicity properties using graph-based signatures *Journal of medicinal chemistry* 58:4066-4072
- pkCSM (n.d.) prediction tools-distribution-Fraction unbound. <http://biosig.unimelb.edu.au/pkcsml/>. Accessed 18 September 2020

- Poet TS, Kousba AA, Dennison SL, Timchalk C (2004) Physiologically based pharmacokinetic/pharmacodynamic model for the organophosphorus pesticide diazinon *Neurotoxicology* 25:1013-1030
- Poet TS, Wu H, Kousba AA, Timchalk C (2003) In vitro rat hepatic and intestinal metabolism of the organophosphate pesticides chlorpyrifos and diazinon *Toxicological Sciences* 72:193-200
- Poklis A, Kutz FW, Sperling JF, Morgan DP (1980) A fatal diazinon poisoning *Forensic science international* 15:135-140
- Pyati AK, Halappa CK, Pyati SA (2015) Serum basal paraoxonase 1 activity as an additional liver function test for the evaluation of patients with chronic hepatitis *Journal of clinical and diagnostic research: JCDR* 9:BC12
- Rasmussen MK (2012) Regulation of Porcine Hepatic Cytochrome P450 by Chicory Root-Implication of Boar Taint. Aarhus University
- Raveh L, Grauer E, Grunwald J, Cohen E, Ashani Y (1997) The stoichiometry of protection against soman and VX toxicity in monkeys pretreated with human butyrylcholinesterase *Toxicology and applied pharmacology* 145:43-53
- Sams C, Cocker J, Lennard M (2004) Biotransformation of chlorpyrifos and diazinon by human liver microsomes and recombinant human cytochrome P450s (CYP) *Xenobiotica* 34:861-873
- Shi M, Bouwmeester H, Rietjens IMCM, Strikwold M (2020) Integrating in vitro data and physiologically based kinetic modeling-facilitated reverse dosimetry to predict human cardiotoxicity of methadone *Archives of toxicology* 94:2809-2827
- Smith JN, Timchalk C, Bartels MJ, Poet TS (2011) In vitro age-dependent enzymatic metabolism of chlorpyrifos and chlorpyrifos-oxon in human hepatic microsomes and chlorpyrifos-oxon in plasma *Drug metabolism and disposition* 39:1353-1362
- Starr TB, Greenlee WF, Neal RA, Poland A, Sutter TR (1999) The trouble with TEFs *Environmental health perspectives* 107:A492-A493
- Stern A, Guidotti M, Shaubi E, Popov M, Linder C, Heldman E, Grinberg S (2014) Steric environment around acetylcholine head groups of bolaamphiphilic nanovesicles influences the release rate of encapsulated compounds *International Journal of Nanomedicine* 9:561
- Strikwold M, Spenkelink B, de Haan LH, Woutersen RA, Punt A, Rietjens IMCM (2017) Integrating in vitro data and physiologically based kinetic (PBK) modelling to assess the in vivo potential developmental toxicity of a series of phenols *Archives of toxicology* 91:2119-2133
- Strikwold M, Spenkelink B, Woutersen RA, Rietjens IMCM, Punt A (2013) Combining in vitro embryotoxicity data with physiologically based kinetic (PBK) modelling to define in vivo dose-response curves for developmental toxicity of phenol in rat and human *Archives of toxicology* 87:1709-1723
- Sultatos LG (2007) Concentration-dependent binding of chlorpyrifos oxon to acetylcholinesterase *Toxicological sciences* 100:128-135
- Thermo Fisher Scientific (2012) INSTRUCTIONS-RED Device Inserts. https://assets.thermofisher.com/TFS-Assets/LSG/manuals/MAN0011571_RED_Device_Insert_UG.pdf. Accessed 20 December 2020
- Thermo Fisher Scientific (2020) Pierce BCA Protein Assay Kit User Guide. https://www.thermofisher.com/document-connect/document-connect.html?url=https%3A%2F%2Fassets.thermofisher.com%2FTFS-Assets%2FLSG%2Fmanuals%2FMAN0011430_Pierce_BCA_Protein_Asy_UG.pdf&title=VXNlciBHdWlkZTogUGllcmNlIEJDQSBQcm90ZWluIEFzc2F5IEtpdA==. Accessed 10 January 2021
- Timchalk C, Nolan R, Mendrala A, Dittenber D, Brzak K, Mattsson J (2002) A physiologically based pharmacokinetic and pharmacodynamic (PBPK/PD) model for the organophosphate insecticide chlorpyrifos in rats and humans *Toxicological Sciences* 66:34-53
- Tracy TS et al. (2016) Interindividual variability in cytochrome P450-mediated drug metabolism *Drug Metabolism and Disposition* 44:343-351
- Ueyama J et al. (2007) Toxicity of diazinon and its metabolites increases in diabetic rats *Toxicology letters* 170:229-237

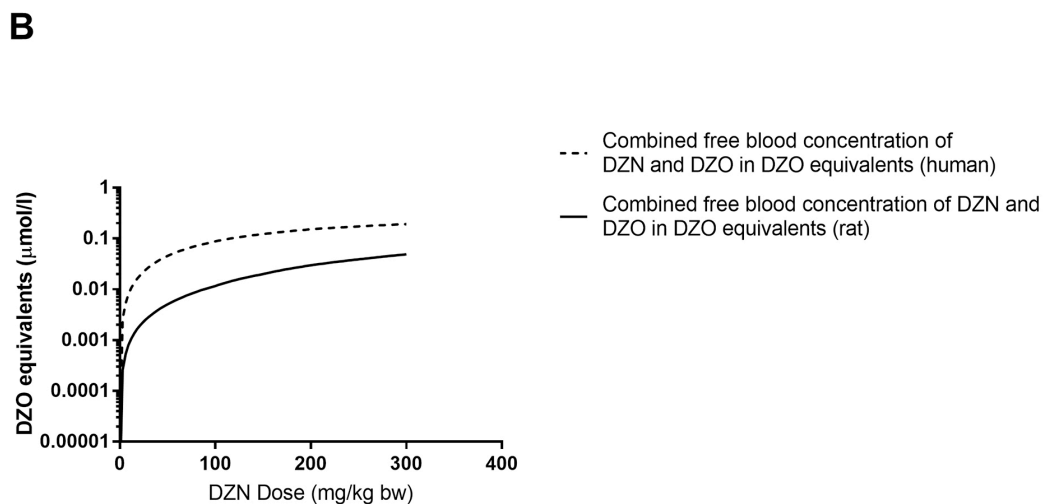
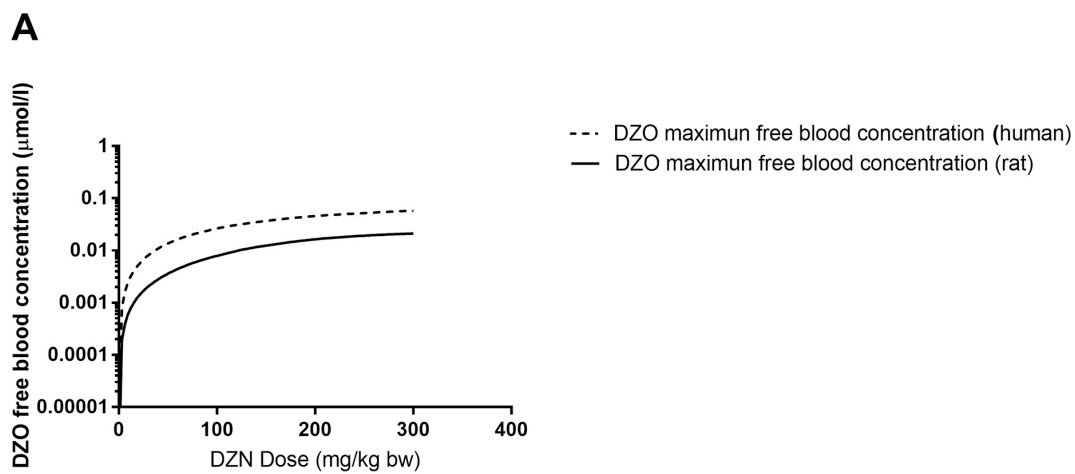
- USEPA benchmark Dose Software (BMDS) Version 3 Release History. <https://www.epa.gov/bmds/benchmark-dose-software-bmds-version-3-release-history#312>. Accessed 27 December 2020
- USEPA (2016) Diazinon Draft Human Health Risk Assessment for Registration Review file:///C:/Users/zhaos/Downloads/EPA-HQ-OPP-2008-0351-0093_content.pdf.
- Velan B et al. (1991) Recombinant human acetylcholinesterase is secreted from transiently transfected 293 cells as a soluble globular enzyme Cellular and molecular neurobiology 11:143-156
- Watt J, Webster TF, Schlezinger JJ (2016) Generalized concentration addition modeling predicts mixture effects of environmental PPAR γ agonists Toxicological Sciences 153:18-27
- Westlind A, Löfberg L, Tindberg N, Andersson TB, Ingelman-Sundberg M (1999) Interindividual differences in hepatic expression of CYP3A4: relationship to genetic polymorphism in the 5'-upstream regulatory region Biochemical and biophysical research communications 259:201-205
- WHO (2010) Characterization and application of physiologically based pharmacokinetic models in risk assessment World Health Organization, International Programme on Chemical Safety, Geneva, Switzerland
- Wu H, Evreux-Gros C, Descotes J (1996) Diazinon toxicokinetics, tissue distribution and anticholinesterase activity in the rat Biomedical and Environmental Sciences: BES 9:359-369
- Zhao S, Kamelia L, Boonpawa R, Wesseling S, Spenkeliink B, Rietjens IMCM (2019) Physiologically based kinetic modeling-facilitated reverse dosimetry to predict in vivo red blood cell acetylcholinesterase inhibition following exposure to chlorpyrifos in the Caucasian and Chinese population Toxicological Sciences 171:69-83

Supplementary materials

For convenience, **Supplementary materials I** and **II** can be found at the following link:

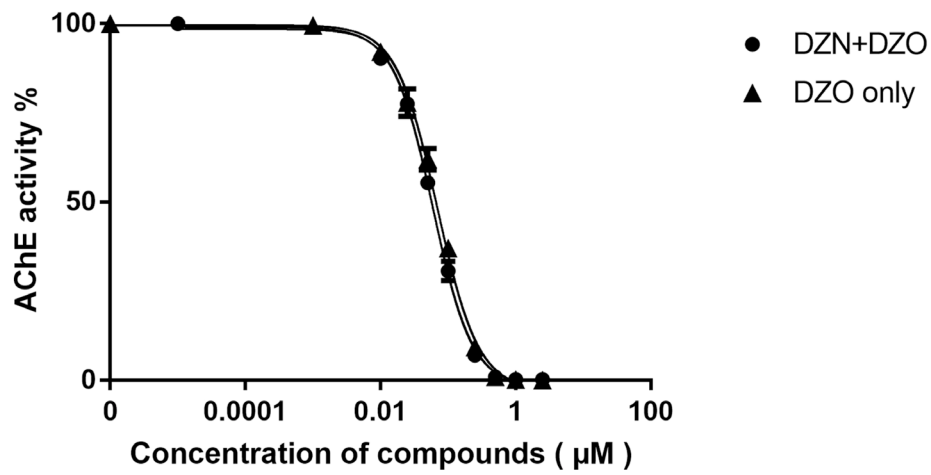
<https://link.springer.com/article/10.1007%2Fs00204-021-03015-1#Sec31>

Supplementary material III



The PBK model based predicted (A) DZN dose-dependent maximum free blood concentration of DZO and (B) DZN dose-dependent combined free blood concentration of DZN plus DZO expressed in DZO equivalents in rat (solid line) and human (dash line)

Supplementary material IV



Effect of increasing concentration of DZO only (triangles) and an equipotent mixture of DZO+DZN (circles) on acetylcholinesterase (AChE) activity of human at 37°C. Each value represents the mean \pm SD of two independent experiments.

Chapter 5

Inter-individual variation in chlorpyrifos
toxicokinetics characterized by physiologically
based kinetic (PBK) and Monte Carlo simulation
comparing human liver microsome and
SupersomeTM cytochromes P450 (CYP)-specific
kinetic data as model input

Shensheng Zhao, Sebastiaan Wesseling, Ivonne. M.C.M. Rietjens and Marije Strikwold

In preparation

Abstract

The present study compares two approaches to evaluate the effects of inter-individual differences in the biotransformation of chlorpyrifos (CPF) on the sensitivity towards in vivo red blood cell (RBC) acetylcholinesterase (AChE) inhibition and to calculate a chemical specific adjustment factor (CSAF) to account for inter-individual differences in kinetics (HK_{AF}). These approaches included use of a Supersome™ cytochrome P450 (CYP)-based and a human liver microsome (HLM)-based physiologically based kinetic (PBK) model, both combined with Monte Carlo simulations. The results revealed that bioactivation of CPF exhibits biphasic kinetics caused by distinct differences in the K_m of CYPs involved, which was elucidated by Supersome™ CYP rather than by HLM. Use of Supersome™ CYP-derived kinetic data was influenced by the accuracy of the intersystem extrapolation factors (ISEFs) required to scale CYP isoform activity of Supersome™ to HLMs. The predicted dose-response curves for average, 99th percentile and 1st percentile sensitive individuals were found to be similar between the two approaches when biphasic kinetics was also included in the HLM-based approach, resulting in similar benchmark dose lower confidence limits for 10% inhibition ($BMDL_{10}$) and HK_{AF} values. The HK_{AF} values at the 99th percentile were around 1.4-fold higher than those at the 95th percentile, and were even slightly higher than the default uncertainty factor of 3.16, reflecting possible inadequate protection by the default factor for the extremely sensitive individuals. Given that the HLM-based approach may miss the biphasic kinetics, it is concluded that the Supersome™ CYP-based approach appeared more adequate for identifying inter-individual variation in biotransformation of CPF and its resulting RBC AChE inhibition.

1. Introduction

Chlorpyrifos (CPF) is the organophosphate most studied in the past decades due to its intensive use as an insecticide in nearly 100 countries (The Dow Chemical Company). Inhibition of acetylcholinesterase (AChE) following irreversible binding of the potent metabolite of CPF chlorpyrifos-oxon (CPO), has been characterized as the main cause of acute CPF exposure-related (neuro)toxicity (Sato and Gupta 2011). On 10 January 2020, The European Commission formally adopted regulations that revoke the renewal of approval for CPF (European Commission 2020) because: i) the potential genotoxicity of CPF remained unclear, leading the European Food Safety Authority (EFSA) to conclude that no toxicological reference dose could be derived, hampering the risk assessment for consumers, operators, workers, bystanders and residents; ii) developmental neurotoxicity has been observed in epidemiological studies; and iii) CPF is classified as reproduction category 1B (regarding developmental toxicity) (EFSA 2019). Recently, although more and more countries ban the use of CPF or allow its use only under certain restrictions, CPF residues are still frequently and widely found in food, and in some samples residue levels have been reported to exceed the European Union Maximum Residue Levels (EUMRL) or to result in exposures above the acute reference dose (ARfD) (EFSA 2020; HEAL and PAN Europe 2019; Hongsibsong et al. 2020). Given that measuring the AChE inhibition in the nervous system is not straightforward, measurement of red blood cell (RBC) AChE inhibition has been widely used as a surrogate endpoint to derive points of departure (PODs) in human risk assessment for organophosphate pesticides (OPs) including CPF (EFSA 2014; USEPA 2014). Also in the present study, RBC AChE inhibition was used as critical adverse effect for the assessment.

The metabolic pathways of CPF (Figure 1) have been well characterized and include: i) bioactivation of CPF to the potent AChE inhibitor CPO by cytochrome P450 (CYP) (pathway 1) (Foxenberg et al. 2007; Sams et al. 2004); ii) detoxification of CPF to 3,5,6-trichloro-2-pyridinol (TCPy) and diethyl thiophosphate (DETP) by CYP (pathway 2) (Foxenberg et al. 2007; Sams et al. 2004); iii) detoxification of the bioactive metabolite CPO to TCPy and diethyl phosphate (DEP) by paraoxonase1 (PON1) present in liver (pathway 3) and in plasma (pathway 4) (Furlong et al. 1989; Timchalk et al. 2002). Available data (Foxenberg et al. 2007) indicate that the bioactivation reaction is mainly mediated by the isoforms CYP2B6, CYP1A2 and to a lesser extent by CYP2C19, CYP3A4, CYP3A5 and CYP3A7, while the detoxification reaction is mainly catalyzed by CYP2C19 and CYP1A2, and to a lesser extent by CYP2B6, CYP3A4

as well as CYP3A5. Additionally, Foxenberg et al. (2007) also pointed out that the Michaelis-Menten constant (K_m) of CYP1A2, CYP2B6, CYP2C19 towards CPF is one to two orders of magnitude lower than that of CYP3A4, indicating the possible primary roles of CYP1A2, CYP2B6, CYP2C19 in CPF biotransformation at low level exposure.

Previous studies have shown that the expression and activity of enzymes involved in CPF biotransformation are highly variable among the general human population (Lang et al. 2001; Tracy et al. 2016; Westlind-Johnsson et al. 2003). For example, a 100-fold difference in protein levels of CYP2B6 between human individuals (Lang et al. 2001), a 40-fold inter-individual variation in protein levels of CYP3A4 (Westlind-Johnsson et al. 2003) and up to 20-fold variation in CYP2C19 expression within different individuals (Ellison et al. 2012; Koukouritaki et al. 2004) have been shown. Moreover, PON1 shows a 40-fold inter-individual variation in activity (Coasta et al. 2006). Such inter-individual variability in the expression of CPF biotransformation-related enzymes may ultimately lead to inter-individual differences in sensitivity toward CPF poisoning, because the susceptibility of human individuals towards CPF poisoning is determined by the balance between bioactivation of CPF and detoxification of CPF and CPO in the human body (Poet et al. 2003; Timchalk et al. 2002).

To address inter-individual human variation in metabolism upon exposure to different compounds, so called physiologically based kinetic (PBK) model has been used. A PBK model enables translation of external exposure into internal concentrations of a chemical based on physico-chemical, physiological, and kinetic parameters (Boonpawa et al. 2015; Ning et al. 2019; Poet et al. 2017; Smith et al. 2014; Strikwold et al. 2017). A PBK model can describe the absorption, distribution, metabolism and excretion (ADME) of a compound in an organism, and by integrating Monte Carlo simulations into the PBK model, it provides the opportunity to investigate the effect of inter-individual differences in toxicokinetics. To apply this approach for CPF, the related biotransformation parameters and their inter-individual variability must be quantified. This can be done using either Supersome™ CYP (from now on written as Supersome™, genetically engineered enzyme systems with a relatively high catalytic activity of an individual CYP) or human liver microsome (HLM). In the present study, both methods were applied to allow a comparison. The kinetic parameters derived by either Supersome™ or HLM *in vitro* were used as input for the PBK model to further assess the inter-individual variation in metabolism of CPF and the resulting susceptibility towards CPF exposure-induced RBC AChE inhibition. Theoretically, the HLM-based PBK model approach can capture and represent variation in hepatic CYP-mediated metabolism in different human individuals well

since variation of HLM is described based on kinetic data obtained from individual HLMs. However, this approach normally requires large number of individual HLMs to capture the variation representative for the population as a whole, and the obtained kinetic data cannot be used as a basis for extrapolation when deriving the distribution of other age, gender and ethnicity groups (Foxenberg et al. 2007; Knaak et al. 2004). To circumvent these limitations, the SupersomeTM-based PBK approach can be used, as it is based on the combination of the intrinsic activity of CYP isoforms for the compound of interest and intersystem extrapolation factors (ISEFs), to scale CYP isoforms activity in the SupersomeTM toward HLMs, and subsequent multiplication with the hepatic abundance of CYPs representative for the target individuals of interest (i.e. with regard to age, gender, ethnicity, etc) (Proctor et al. 2004). Such an approach thus provides the possibility to extrapolate in vitro-derived metabolic kinetic constants from a set of relevant CYP SupersomeTM toward in vivo values for various target groups.

The aim of the present study was to compare the applicability and outcome of the SupersomeTM-based PBK model approach and the HLM-based PBK model approach to characterize inter-individual variability in metabolism of CPF and its resulting RBC AChE inhibition, and calculate a chemical specific adjustment factor (CSAF) for the inter-individual variation in kinetics (HK_{AF}) for CPF. To this end, experiment-derived and literature-obtained kinetic parameters of SupersomeTM, HLM and human plasma (HP) were collected and used as input for the SupersomeTM-based PBK model and HLM-based PBK model, which were both developed based on the previously developed CPF PBK model (Zhao et al. 2019). Furthermore, the two models were extended to include Monte Carlo simulations and coefficients of variation (CVs) for each kinetic parameter, to predict inter-individual kinetic variation. Finally, PBK model-based reverse dosimetry was applied to predict in vivo dose-response curves for RBC AChE inhibition by translating in vitro recombinant human AChE (rhAChE) inhibition data for the average and sensitive subgroups within the adult population.

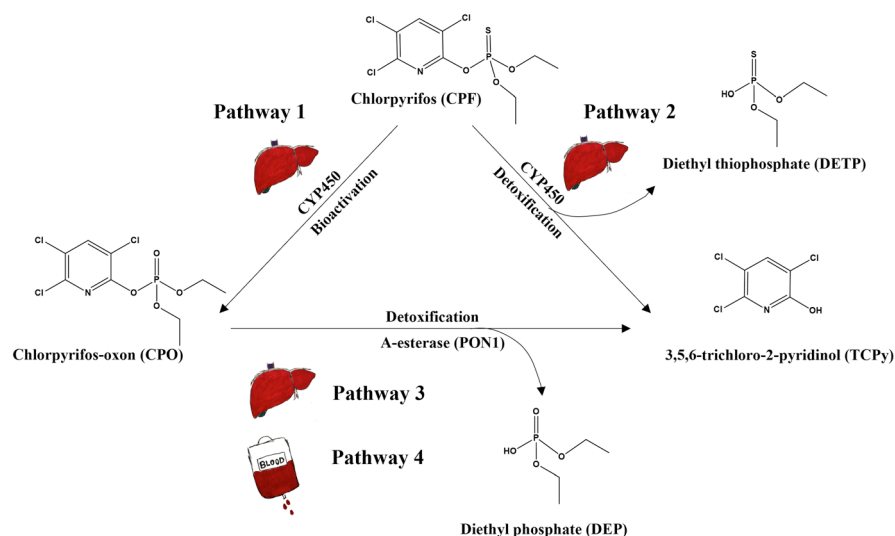


Fig 1. Proposed metabolic pathways of chlorpyrifos in human

2. Materials and methods

2.1 Chemicals and biological materials

5

CPF, TCPy, acetylthiocholine iodide (ATC), 5,5'-dithiobis (2-nitrobenzoic acid) (DTNB), bovine serum albumin (BSA), tetraisopropyl pyrophosphoramidate (iso-OMPA), reduced nicotinamide adenine dinucleotide phosphate (NADPH), sodium phosphate dibasic dihydrate ($\text{Na}_2\text{HPO}_4 \cdot 2\text{H}_2\text{O}$), sodium phosphate monobasic dihydrate ($\text{NaH}_2\text{PO}_4 \cdot 2\text{H}_2\text{O}$), phenacetin, acetaminophen, bupropion, (\pm)-hydroxybupropion solution, 4-hydroxymephenytoin, testosterone, 6β -hydroxytestosterone solution, and trizma[®]base were purchased from Sigma-Aldrich (Zwijndrecht, The Netherlands). (S)-mephenytoin was purchased from Santa Cruz Biotechnology, Inc. (Dallas, TX, USA). CPO was purchased from TRC-Canada (Toronto, Ontario, Canada). Magnesium chloride hexahydrate ($\text{MgCl}_2 \cdot 6\text{H}_2\text{O}$), hydrochloric acid (HCl), sodium hydroxide (NaOH), ethylenediaminetetraacetic acid disodium salt dihydrate (EDTA), trifluoroacetic acid (TFA), formic acid and calcium chloride dihydrate ($\text{CaCl}_2 \cdot 2\text{H}_2\text{O}$) were purchased from VWR International (Amsterdam, The Netherlands). Acetonitrile (ACN, UPLC/MS grade) and methanol (UPLC/MS grade) were purchased from Biosolve

(Valkenswaard, The Netherlands). Pierce™ BCA protein assay kit was purchased from Thermo Fisher Scientific (Rockford, IL, USA).

HLM (pooled from 150 donors, mixed gender), human Supersome™ (human CYP1A2+reductase, human CYP2B6+reductase+cytochrome b5, human CYP2C19+reductase+cytochrome b5, human CYP3A4+reductase+cytochrome b5) were purchased from Corning (Amsterdam, The Netherlands). 25 Individual HP samples of Caucasian origin (13 males and 12 females within the age range from 25 to 75 years old) were purchased from BioIVT (West Sussex, UK). rhAChE was purchased from Sigma-Aldrich Co. (St. Louis, MO, USA), and in solutions the enzyme was stabilized with 1 mg/ml BSA (Kaushik et al. 2007).

2.2 Outline of PBK-based reverse dosimetry approaches with Monte Carlo simulation

PBK-based reverse dosimetry linked with Monte Carlo simulations was applied to predict the effect of inter-individual human kinetic variation in CPF metabolism for the inter-individual differences in RBC AChE inhibition following CPF exposure. Two approaches were used to define the metabolic variation in the PBK model, namely a Supersome™-based PBK model approach and an HLM-based PBK model approach. The whole procedure consisted of the following steps: 1) Establishment of an in vitro concentration-response curve for CPO in the AChE inhibition assay using rhAChE, 2) Collection of kinetic parameters (the maximum velocity (V_{max}) and K_m) for each metabolic pathway for the two approaches either from literature or from experiments, 3) Development of PBK models, and performance of Monte Carlo simulations by including kinetic data obtained in step 2, and CVs for each variable input parameter (V_{max} , K_m for HLM and abundance of each CYP isoform for Supersome™) obtained from either the literature or the experiments of the present study, and calculation of an HK_{AF} , 4) PBK model-based reverse dosimetry to extrapolate the in vitro concentration-response curve to in vivo dose-response curves, 5) BMD analysis of the predicted in vivo dose-response curves and evaluation. In step 3, inter-individual variation was introduced by including the CVs of the CYP abundances from the Simcyp Simulator (V18 Release1 Certara, Sheffield, UK), the CVs on HLM-related kinetic data ($n=30$) from Smith et al. (2011), and the CVs on plasma-related kinetic data ($n=25$) from the present study. The outline of the whole procedure is schematically presented in Figure 2.

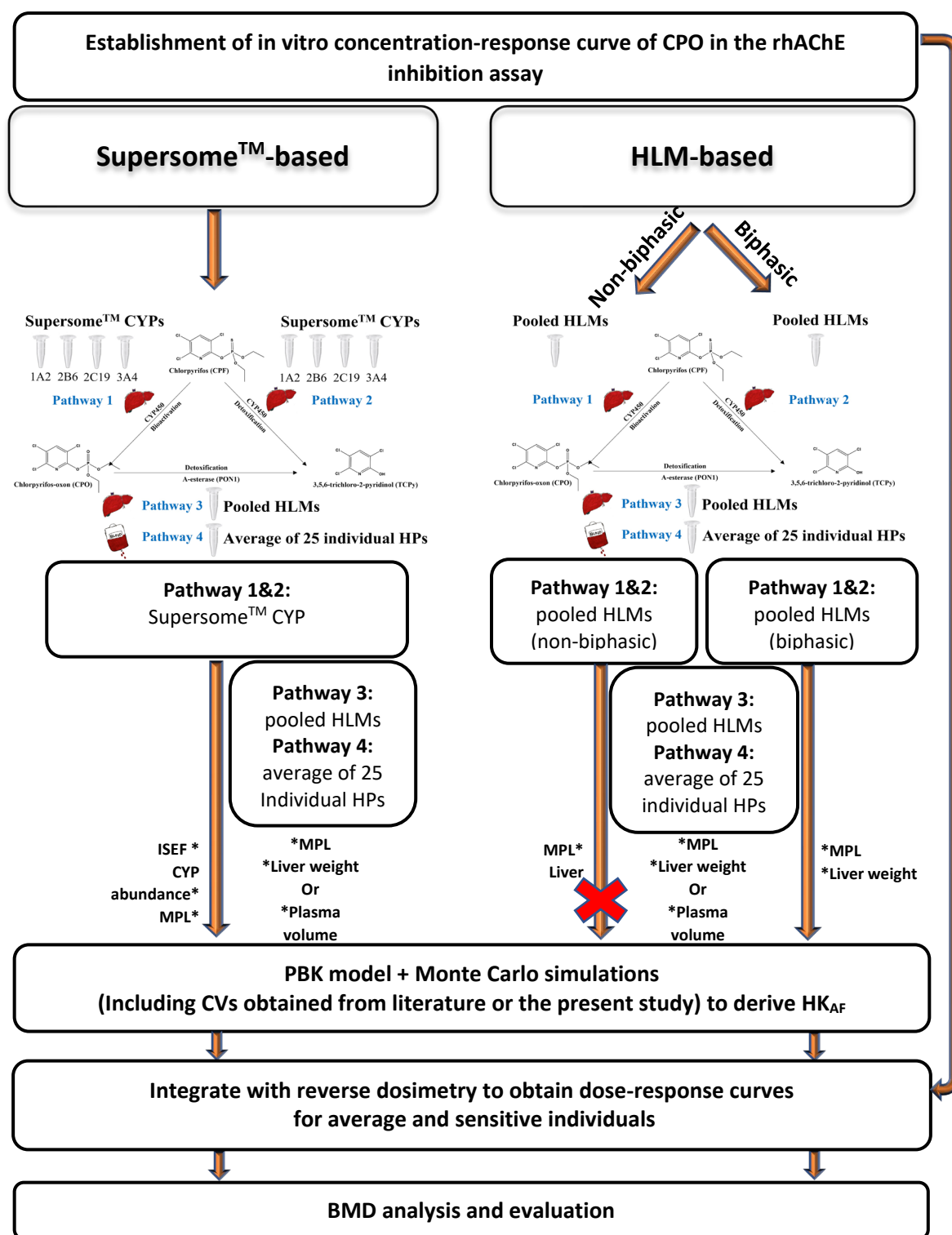


Fig 2. Schematic presentation of the two approaches that were applied in the present study to assess inter-individual variation in the biotransformation of CPF and its resulting HK_{AF} values as well as dose-response curves for CPF-mediated RBC AChE inhibition. CYP is Cytochrome P450, CPF is chlorpyrifos, HLM is human liver microsomes, HP is human plasma, CVs is coefficients of variation, HK_{AF} is the chemical-specific adjustment factor (CSAF) for human variability in toxicokinetics of chlorpyrifos, MPL is liver microsomal protein scaling factor, ISEF is the inter-system extrapolation factor for each CYP derived based on differences in activity between Supersome™ and HLM by incubating them with each relevant CYP specific probe substrate, BMD is benchmark dose, “X” means the approach was terminated.

2.3 In vitro AChE inhibition assay to derive CPO concentration-response curves

In the present study, the inhibitory effect of the active CPF metabolite CPO on RBC AChE was measured using rhAChE, as a proxy for RBC AChE, using the method previously published (Zhao et al. 2021), based on the method from Ellman et al. (1961). The working solutions were prepared by diluting a series of increasing concentrations of CPO (in ethanol) 50-fold in 100 mM sodium phosphate (pH=7.4) containing 0.1 mg/ml BSA. In a similar fashion, a 5000 μ M CPO solution in ethanol (positive control) and a 100% ethanol solution (solvent control) was diluted. The rhAChE activity experiment was conducted in 96 well-plates. In each well, 44 μ l 100 mM sodium phosphate (pH=7.4) containing 0.1 mg/ml BSA, with 5 μ l of CPO working solution (final concentrations 0.05, 0.1, 0.5, 1, 2.5, 5, 10, 25 and 50 nM), or 5 μ l positive control (CPO at a final concentration of 10000 nM) or 5 μ l solvent control (resulting in a final ethanol concentration of 0.2%) was added. The inhibition reaction was initiated by adding 1 μ l rhAChE, resulting in a total incubation volume of 50 μ l. The whole plate was incubated at 37°C for 15 minutes. Subsequently, the inhibition reaction was terminated by adding 150 μ l reaction reagents (mixture of ATC at a final concentration of 150 μ M and DTNB at a final concentration of 75 μ M) into each well to yield a final volume of 200 μ l in each well (final enzyme concentration is 0.6 mU/ml). Finally, the solutions in the 96-well plate were measured continuously for 10 minutes at an absorbance of 412 nm at 37°C to quantify the rhAChE activity.

The rhAChE activity was expressed as the remaining rhAChE activity relative to the solvent control (100% activity) and the positive control (0% activity) based on equation 1 (Eq1):

$$\text{rhAChE activity\%} = \frac{A_{412}(t_{10} - t_0)\text{Test Compound} - A_{412}(t_{10} - t_0)\text{Positive Control}}{A_{412}(t_{10} - t_0)\text{Solvent Control} - A_{412}(t_{10} - t_0)\text{Positive Control}} * 100\% \text{ (Eq1)}$$

where the $A_{412}(t_{10} - t_0)\text{Test Compound}$ is the change in the absorbance at 412 nm between 0 min and 10 min for the test compound, the $A_{412}(t_{10} - t_0)\text{Positive Control}$ is the change in the absorbance at 412 nm between 0 min and 10 min for the CPO sample at the final concentration of 10000 nM, and the $A_{412}(t_{10} - t_0)\text{Solvent Control}$ is the change in the absorbance at 412 nm between 0 min and 10 min for the 0.2% ethanol sample.

Concentration-response curves were constructed and the half maximal inhibitory concentrations (IC₅₀) for CPO were derived, applying a non-linear regression model for Dose

Response-Inhibition-Variable, with the equation $\log(\text{inhibitor})$ vs. response-variable slope (four parameters) in GraphPad Prism 5, version 5.04 (GraphPad software, San Diego California USA), with 95% confidential interval.

2.4 Collection of in vitro kinetic parameters for the PBK models

2.4.1 SupersomeTM-based PBK model

2.4.1.1 Pathway 1 and Pathway 2

Metabolic kinetic constants (V_{\max} and K_m) of the hepatic CYP-catalyzed biotransformation of CPF (pathway 1 and pathway 2) (Figure 1) were generated using the four CYP isoform SupersomeTM (CYP1A2, CYP2B6, CYP2C19 and CYP3A4) known to be the most dominant CYPs in the metabolism of CPF on the basis of the results from Foxenberg et al. (2007). CYP3A5 and CYP3A7 that were included in Foxenberg et al. (2007) were not included in the present study due to their limited contribution to the conversion of CPF. The in vitro kinetic incubations were conducted based on the method reported by Foxenberg et al. (2007) with some modifications. In detail, preliminary experiments were performed first to optimize the formation of metabolites to be linear with time and amount of SupersomeTM protein (data not shown) for each CYP separately.

5

The final incubations were carried out in 50 mM Tris-HCl (pH 7.4) containing 5 mM $MgCl_2$, 1 mM EDTA (as an A-esterase PON1 inhibitor) (Bizoń and Milnerowicz 2018), 50 μM isomPA (as a B-esterases inhibitor) (Lane et al. 2006), SupersomeTM isoform (at final concentration of 0.005 nmol CYP/ml for 1A2, 0.001 nmol CYP/ml for 2B6, 0.01 nmol CYP/ml for 2C19, and 0.01 nmol CYP/ml for 3A4) and CPF at different final concentrations (0.05, 0.1, 0.25, 0.5, 1, 5 and 10 μM for 1A2, 0.05, 0.1, 0.25, 0.5, 1, 5 10 and 25 μM for 2B6, 1, 2.5, 5, 10, 25 and 50 μM for 2C19, and 0.5, 1, 2.5, 5, 10, 25 and 50 μM for 3A4), which were added from 100 times concentrated stock solutions in ACN. After 1 minute preincubation in a 37°C water bath, 5 μl NADPH (final concentration 1 mM) was added to the incubation system. Control incubations were performed by replacing NADPH with the same amount of Tris-HCl buffer (pH 7.4). The total volume of the incubation mixtures was 200 μl . The incubations lasted for 2 min at 37°C and were terminated by addition of 50 μl ice cold ACN and subsequently put on ice. After that, samples were centrifuged at 16000 g (4°C) for 5 minutes and supernatants of samples were separated into two equal portions for Ultra-Performance Liquid Chromatography- Photodiode Array (UPLC-PDA) and Liquid Chromatography Mass

Spectrometry (LC-MS/MS) analysis, respectively. For the samples that were measured by UPLC-PDA for quantification of TCPy formation, no further dilution was required, but for samples that were analyzed by LC-MS/MS to quantify CPO formation (limit of detection (LOD) = 3.1 nM), the one that originally contained 2.5, 5, 10, 25, 50 μ M of CPF were diluted 2.5x, 5x, 10x, 25x and 50x, respectively in a mixture of ACN and 50 mM Tris-HCl (pH 7.4) (ratio 1:4, v/v).

2.4.1.2 ISEF (intersystem extrapolation factors)

To normalize for differences in intrinsic CYP activity between SupersomeTM and pooled HLMs and enable scaling of the activities to the in vivo situation, CYP specific ISEF values need to be established. The ISEF determination for each CYP was performed using SupersomeTM and pooled HLMs-derived Vmax values for metabolite formation of probe substrates (specifically metabolized by a single CYP), being phenacetin (CYP1A2), bupropion (CYP2B6), (S)-mephenytoin (2C19) and testosterone (3A4) (Chen et al. 2011; Faucette et al. 2000). The incubation conditions used for these studies are summarized in Table 1. These incubation conditions were optimized and selected with respect to linearity for the formation of the metabolite of the CYP-specific probe substrate using both SupersomeTM and pooled HLMs (data not shown). The incubation method was similar as used for the CPF kinetic incubation assay described above, except that certain incubation conditions were replaced by the conditions listed in Table 1. The samples obtained were analyzed by UPLC-PDA for acetaminophen, 4-hydroxymephenytoin, and 6 β -hydroxytestosterone formation catalyzed by 1A2, 2C19 and 3A4, or LC-MS/MS for (\pm)-hydroxybupropion formation catalyzed by 2B6. For the samples that were analyzed by LC-MS/MS for quantification of (\pm)-hydroxybupropion formation, the ones that contained 100, 250, 500, 1000, 1500 and 2000 μ M bupropion were further diluted 2x, 5x, 10x, 20x, 40x and 40x, respectively in a mixture of ACN and 50 mM Tris-HCl (pH 7.4) (ratio 1:4, v/v). LC-MS/MS was used for quantification of (\pm)-hydroxybupropion formation because it is allowing low levels of (\pm)-hydroxybupropion (LOD= 15.5 nM) to be detected.

Table 1. Selected probe substrate for each CYP and their corresponding incubation conditions used to derive ISEF

Pooled HLMs					
CYP isoform	Probe substrate	Specific metabolite	Pooled HLMs concentration (mg/ml)	Substrate concentration range (μ M)	Incubation time (min)
1A2	phenacetin	acetaminophen	0.5	10, 25, 50, 100, 250, 500	40
2B6	bupropion	(\pm)-hydroxybupropion	0.05	5, 10, 25, 50, 100, 250, 500, 1000, 1500, 2000	20
2C19	(S)-mephenytoin	4-hydroxymephenytoin	0.5	5, 10, 25, 50, 100, 300, 500	40
3A4	testosterone	6 β -hydroxytestosterone	0.2	10, 25, 50, 100, 250, 500	5
Supersome TM					
CYP isoform	Probe substrate	Specific metabolite	Supersome TM concentration (pmol CYP/ml)	Substrate concentration range (μ M)	Incubation time (min)
1A2	phenacetin	acetaminophen	0.01	10, 25, 50, 100, 250, 500	20
2B6	bupropion	(\pm)-hydroxybupropion	0.01	5, 25, 50, 100, 250, 500, 1000, 2000	10
2C19	(S)-mephenytoin	4-hydroxymephenytoin	0.01	5, 10, 25, 50, 100, 300, 500	20
3A4	testosterone	6 β -hydroxytestosterone	0.005	10, 25, 50, 100, 250, 500	2

5

2.4.1.3 Pathway 3

For the hepatic PON1-mediated detoxification of CPO (pathway 3), the previously established kinetic parameters (V_{max} and K_m) by Zhao et al. (2019) using pooled HLMs were used.

2.4.1.4 Pathway 4

The metabolic parameters of the PON1-catalyzed detoxification of CPO in plasma (pathway 4) were obtained by incubating different concentrations of CPO with 25 individual HP samples. Pilot studies were conducted to optimize the metabolite formation to be linear with the in vitro plasma concentration and time of incubation (data not shown). Briefly, the incubations were carried out in 50 mM Tris-HCl (pH 7.4) containing 2 mM CaCl₂ and CPO at final concentrations of 10, 50, 100, 250, 500 and 1000 μ M (added from 100 times concentrated stock solutions in ACN). After 1 minute preincubation in a shaking 37°C water bath, 1 μ l of individual HP was added into the incubation system. Control incubations were performed by

replacing plasma with the same amount of 50 mM Tris-HCl (pH 7.4). The total volume of the incubation mixtures was 200 μ l. The incubation lasted for 1.5 min at 37°C and was terminated by addition of 200 μ l ice cold ACN and subsequently put on ice. Samples were subsequently centrifuged at 16000 g (4°C) for 5 minutes and analyzed by UPLC-PDA.

2.4.2 HLM-based PBK model

2.4.2.1 Pathway 1 (contains two scenarios)

The previously published kinetic parameters (Sams et al. 2004) for bioactivation of CPF obtained using incubations with pooled HLMs were employed in the present study (scenario 1, non-biphasic) (Figure 2). In this study (Sams et al. 2004), the CPF concentration range used (3 μ M to 100 μ M) covered the K_m of CYP3A4, as reflected by consistency in the apparent K_m obtained in pooled HLMs from Sams et al. (2004) (29.8 μ M) and that in SupersomeTM CYP3A4 reported by Foxenberg et al. (2007) (27.3 μ M) and obtained in the present study (29.8 μ M) (Table 3). On the other hand, this CPF concentration range far exceeds the K_m of CYP1A2, CYP2B6, CYP2C19 reported to amount to 0.38 μ M, 0.81 μ M, 1.23 μ M (Foxenberg et al. 2007), or 0.61 μ M, 0.14 μ M, 1.89 μ M (the present study, Table 3), respectively. Use of CPF concentrations far exceeding the K_m may inadequately describe the high affinity kinetic phase mediated by these high affinity (low K_m) CYPs at low concentrations (<3 μ M). Therefore, to identify the importance of including such high affinity kinetics in PBK model descriptions of the bioactivation of CPF to CPO, a second kinetic scenario (biphasic) was defined for the HLM approach (Figure 2). This biphasic scenario includes a high affinity kinetic phase in addition to the low affinity (high K_m) kinetic phase. To describe the high affinity kinetics of the HLM, the apparent K_m and V_{max} defined at the low concentration range of 0.02 μ M to 10 μ M in pooled HLMs as reported by Buratti et al. (2003) were used. In this way, the biphasic kinetics of the bioactivation of CPF at both low and high concentration ranges could be fully captured. Application of biphasic kinetics is further supported by the scaled SupersomeTM kinetic data presented below in the Result section. Also, Ma and Chambers (1995) reported biphasic kinetics for bioactivation of CPF by rat liver microsomes, reflected by a high affinity and a low affinity metabolic phase, with the K_m value for the high affinity phase being 50-fold lower than that for the low affinity phase.

2.4.2.2 Pathway 2

To describe the detoxification of CPF by pooled HLMs (Pathways 2 in Figure 1), the previously published monophasic kinetic parameters of Sams et al. (2004) were used. Applying monophasic kinetics, and not biphasic kinetics as applied for Pathway 1, is based on the data from the present study (see Result section), showing that for this reaction the conversion at low concentrations was not dominated by a high affinity CYP.

2.4.2.3 Pathway 3 and Pathway 4

In the HLM-based PBK model, for the PON1-mediated detoxification of CPO in liver and plasma, respectively, the same kinetic parameters as described in the section “Supersome™-based PBK model, Pathway 3” and section “Supersome™-based PBK model, Pathway 4” were used.

2.4.3 Determination of total protein concentration in individual human plasma samples

The total protein concentration of the 25 individual HP samples was measured using a Pierce™ BCA protein assay kit (ThermoFisher Scientific 2020), enabling scaling of the kinetic parameters measured for pathway 4 from per mg protein to per ml plasma. The experiment was performed based on the manufacturer’s protocol. In detail, 25 µl sample or protein standard solution at concentrations of 0.025, 0.125, 0.25, 0.5, 0.75, 1 and 2 mg/ml were added and incubated with 200 µl working reagents at 37°C for 30 minutes in a 96-well plate. After that, the plate was cooled to room temperature, and each sample and each protein standard was measured at 562 nm (absorbance). The total protein concentration of each unknown sample was calculated based on the calibration curve (protein concentration versus 562 nm absorbance value) generated with the protein standards.

2.4.4 Calculation of kinetic parameters

As mentioned before, the in vitro apparent kinetic parameters (V_{max} and K_m) for pathway 1 and pathway 2 in the HLM-based approach, and pathway 3 in both approaches were all

obtained directly from reported studies using pooled HLMs (Buratti et al. 2003; Sams et al. 2004; Zhao et al. 2019). Therefore, no extra calculations were required to define these parameters. The kinetic parameters for the ISEF calculation, pathway 1 and 2 in the SupersomeTM-based approach, and pathway 4 in both approaches (25 individuals) were all obtained by fitting the experimental data to the Michaelis-Menten model using GraphPad (GraphPad Prism 5.0 software, San Diego, CA, USA). It should be noted that the kinetic parameters for pathway 4 used in the two approaches were calculated as mean of the kinetic parameters (V_{max} and K_m) obtained using 25 individual HP samples (with correction for total protein concentration of each plasma sample).

2.4.5 Quantification of metabolites of CPF, CPO and probe substrates by UPLC-PDA and LC-MS/MS

The analysis method, gradient elution and retention time for each compound by UPLC-PDA or LC-MS/MS are described in Supplementary material I.

2.5 Development of the PBK model, Monte Carlo simulations and establishment of chemical-specific adjustment factors (CSAFs)

2.5.1 Model development

In the present study, our previously developed PBK model for CPF (predicting total blood concentrations of CPO) in Caucasian (Zhao et al. 2019) was used as a starting point for the PBK model, which is used for evaluation of inter-individual variation in metabolism of CPF and the consequences of this variation for the induced RBC AChE inhibition. Compared to the PBK model of Zhao et al. (2019), only the fractional absorption (f_a) was changed to 0.462, which is the mean value of reported f_a values from Timchalk et al. (2002) ($f_a=0.224$) and Nolan et al. (1984) ($f_a=0.7$), while for the other model parameters (non-kinetic), the mean values as reported in Zhao et al. (2019) were used.

2.5.1.1 SupersomeTM-based PBK model

Compared to the model of Zhao et al. (2019), in the SupersomeTM-based PBK model approach, the kinetic parameters of pathway 1 and pathway 2 were replaced from HLM-derived values to SupersomeTM-derived values, while the kinetic parameters of pathway 3 were kept the same. For pathway 4, instead of using the reported kinetic parameters from Mosquin et al. (2009), the calculated mean values of kinetic parameters obtained based on 25 individual HP samples derived by the present study were used. The kinetic equation that was applied for each metabolic pathway in the PBK model is indicated below:

2.5.1.1.1 Pathway 1 and Pathway 2

The overall kinetic parameters of four CYP isoforms (CYP1A2, CYP2B6, CYP2C19 and CYP3A4) in liver were described by equation 2 (Eq 2) (Foxenberg et al. 2007):

$$V_{\text{overall supersome}}^{\text{TM}} = \sum \left(\frac{V_{\text{max}_i} * [S]}{(K_{\text{m}_i} + [S])} \right) \text{ (Eq2)}$$

where $V_{\text{overall supersome}}^{\text{TM}}$ is the overall (summed) in vivo metabolic rate for all four CYP isoforms (umol/hr); i represent different CYPs isoform (CYP1A2, CYP2B6, CYP2C19 and CYP3A4), $[S]$ is the blood concentration of CPF (μM), V_{max_i} and K_{m_i} are in vivo maximum velocity (umol/hr) and the Michaelis-Menten constant (μM) for each respective CYP isoform in either pathway 1 or pathway 2. The in vivo K_{m_i} values were assumed to be equal to the apparent $K_{\text{m}_i(\text{app})}$ values (μM) obtained in the in vitro incubations, while the in vivo V_{max_i} for each CYP isoform was derived from their corresponding apparent CYP isoform $V_{\text{max}_i(\text{app})}$ (pmol/min/pmolCYP) using equation 3 (Eq 3):

$$V_{\text{max}_i} = \frac{V_{\text{max}_i(\text{app})} * \text{CYP}_i \text{ abundance} * \text{ISEF} * 60 * \text{MPL} * 1000 * \text{VL}}{1000000} \text{ (Eq3)}$$

In the equation CYP_i abundance is the average endogenous abundance (pmolCYP/mg microsomal protein, represent the amount of the respective CYP per mg of microsomal protein) of CYP isoform i (CYP1A2=52, CYP2B6=16, CYP2C19=5.4 and CYP3A4=137) in HLM obtained from Simcyp (Simcyp Simulator V18 Release 1, Certara, Sheffield, UK), 60 is to account for the unit change from min to hr, MPL is the microsomal protein yield of 32 mg/g liver (Barter et al. 2007), 1000 is to account for the unit change from g to kg, VL is the weight of the liver tissue (kg), 1000000 is to account for the unit change from pmol to μmol , and ISEF $_i$

is the intersystem extrapolation factor for the CYP isoform i , which were determined based on the ratio between the apparent V_{max} of metabolite formation for each CYP-specific probe substrate in pooled HLMs and the respective SupersomeTM (with correction for the average CYP abundance in HLM), according to equation 4 (Eq4):

$$ISEF_i = \frac{V_{max\ probe\ z(pooled\ HLMs)} * 1000}{V_{max\ probe\ z(Supersome^{TM})} * CYP_i\ abundance} \quad (Eq4)$$

In which z represent the probe substrate (phenacetin, bupropion, (S)-mephenytoin and testosterone), $V_{max\ probe\ z(pooled\ HLM)}$ is the apparent maximum rate (nmol/min/mg microsomal protein) for the kinetic conversion of probe substrate z obtained using pooled HLMs, and $V_{max\ probe\ z(Supersome^{TM})}$ is the apparent maximum rate (pmol/min/pmol CYP) for the kinetic conversion of probe substrate z obtained using SupersomeTM, 1000 is to account for the unit change from pmol/min/pmolCYP to nmol/min/pmolCYP, and the CYP_i abundance (pmol CYP/mg microsomal protein) is defined as above.

2.5.1.1.2 Pathway 3 & Pathway 4

The metabolic reactions for pathway 3 and pathway 4 were described by equation 5 (Eq5):

$$v_{HLM} = \frac{V_{max\ HLM} * [S]}{(K_{m\ HLM} + [S])} \quad \text{or} \quad v_{HP} = \frac{V_{max\ HP} * [S]}{(K_{m\ HP} + [S])} \quad (Eq5)$$

Where v_{HLM} and v_{HP} represent the in vivo rate of the metabolic reaction ($\mu\text{mol/hr}$) of pathway 3 or pathway 4, S represents the blood concentration of CPO (μM), $V_{max\ HLM}$ and $K_{m\ HLM}$ are the in vivo maximum velocity ($\mu\text{mol/hr}$) and the Michaelis–Menten constant (μM) of pathway 3, and $V_{max\ HP}$ and $K_{m\ HP}$ are the in vivo maximum velocity ($\mu\text{mol/hr}$) and the Michaelis–Menten constant (μM) of pathway 4.

In pathway 3, the in vivo $V_{max\ HLM}$ ($\mu\text{mol/hr}$) was extrapolated from its corresponding apparent $V_{max\ HLM(app)}$ (in nmol/min/mg microsomal protein) using equation 6 (Eq6):

$$V_{max\ HLM} = \frac{V_{max\ HLM(app)} * 60 * MPL * 1000 * VL}{1000} \quad (Eq6)$$

In this equation, 60 is to account for the unit change from min to hr, MPL is the microsomal protein yield of 32 mg/g liver (Barter et al. 2007), 1000 is to account for the unit change from g to kg or nmol to μmol , and VL is the weight of the liver tissue (kg).



In pathway 4, the in vivo $V_{\max_{HP}}$ ($\mu\text{mol/hr}$) was extrapolated from its corresponding mean of the apparent $V_{\max_{HP(\text{app})}}$ ($\text{nmol/min/ml plasma}$) of 25 individuals HPs using equation 7 (Eq7):

$$V_{\max_{HP}} = \frac{V_{\max_{HP(\text{app})}} * 60 * 1000 * VB * 0.55}{1000} \quad (\text{Eq7})$$

In this equation 60 is to account for the unit change from min to hr, 1000 is to account for the unit change from mL to L, VB is the volume of the blood (L), 0.55 represents the plasma to blood volume ratio used to scale the unit of V_{\max} of PON1-mediated conversion (Pathway 4) from per ml plasma to the whole plasma of blood compartment, based on the fact that the PON1 is present in plasma and the human plasma volume amounts to 55% of the blood volume (Li et al. 2005; O'Neil 1999).

The in vivo K_m values for both pathway 3 and pathway 4 were assumed to be equal to their corresponding apparent K_m values obtained in the in vitro incubations.

2.5.1.2 HLM-based PBK model

For the development of the HLM-based PBK model, scenario 1 (non-biphasic) was excluded due to the inadequate kinetic description of CPO formation at low dose levels (see Results section “Bioactivation and detoxification of CPF in SupersomeTM enzymes”). For scenario 2 (biphasic), the kinetic parameters of pathway 1 used in the original model described by pooled HLM (Zhao et al. 2019) were replaced by reported kinetic parameters for the high affinity phase (Buratti et al. 2003) and the low affinity phase (Sams et al. 2004), while those for pathway 2 were replaced by data from Sams et al. (2004). The kinetic parameters of pathway 3 and pathway 4 used for the HLM-based PBK model were the same as the ones used for the SupersomeTM-based PBK model. The kinetic equation for each pathway in the human model was described as presented below:

2.5.1.2.1 Pathway 1

The total velocity for hepatic bioactivation of CPF was described by biphasic kinetics using equation 8 (Eq8) (Venkatakrisnan et al. 2001):

$$V_{\text{overall HLM}} = \frac{V_{\max_{\text{high affinity}}} * [S]}{(K_{m_{\text{high affinity}}} + [S])} + \frac{V_{\max_{\text{low affinity}}} * [S]}{(K_{m_{\text{low affinity}}} + [S])} \quad (\text{Eq8})$$

where $V_{\text{overall HLM}}$ ($\mu\text{mol/hr}$) is the overall in vivo metabolic rate of pathway 1 (including both the high and low affinity phase); $[S]$ is the blood concentration of CPF (μM), $V_{\text{max high affinity}}$ and $K_{\text{m high affinity}}$ are the in vivo maximum velocity ($\mu\text{mol/hr}$) and the Michaelis–Menten constant (μM) of the high affinity phase, while $V_{\text{max low affinity}}$ and $K_{\text{m low affinity}}$ are those of the low affinity phase. The in vivo K_{m} values were assumed to be equal to the apparent K_{m} values obtained from the in vitro experiments, and the in vivo V_{max} for both the high and low affinity phase were extrapolated from their corresponding apparent V_{max} values obtained in the in vitro experiments using Eq6

2.5.1.2.2 Pathway 2

The hepatic reaction of pathway 2 was described using Eq5 and Eq6.

2.5.1.2.3 Pathway 3 & Pathway 4

The metabolic reactions of pathway 3 and pathway 4 were described in the same way as done for the SupersomeTM-based PBK model approach (see section “Model development, SupersomeTM-based PBK model, pathway3 & pathway4”).

2.5.2 Model evaluation

The performance of the SupersomeTM-based PBK model and HLM-based PBK model (biphasic) were evaluated by comparing their predicted time-dependent TCPy and CPF blood concentrations including the maximum total (bound and unbound) blood concentration (C_{max}) or time-dependent blood concentration, and the cumulative time-dependent urinary TCPy excretion with corresponding available in vivo data (Drevenkar et al. 1993; Nolan et al. 1984; Timchalk et al. 2002) upon similar dosing regimens or estimated dose level. The time-dependent CPF concentration data from Drevenkar et al. (1993) relate to concentrations in plasma. To allow comparison to PBK model-based predicted blood concentrations, these plasma concentrations of CPF were converted to a blood concentration by multiplying with the blood to plasma ratio for CPF of 1.3 (the ratio of the CPF concentration in blood to the CPF concentration in plasma), which was estimated using Simcyp (2016a) based on CPF LogP of 4.784 (ChemAxon) and a fraction unbound of 0.021 for plasma (Simcyp 2016b)). Drevenkar

et al. (1993) reported these time-dependent CPF concentration for a poisoning victim who drunk 30-60 ml of pesticide product Chromorel D[®]. Given that the concentration of CPF in Chromorel D[®] is 500 g/l (see <https://www.agroklub.ba/poljoprivredni-oglasnik/oglas/chromorel-d/16769/>), the CPF intake for this victim was assumed to be 30-60 ml of 500 g CPF/l corresponding to 15,000 to 30,000 mg CPF. The corresponding estimated dose was calculated on the basis of a body weight of 70 kg, to amount to 214 - 429 mg/kg bw.

2.5.3 Sensitivity analysis

The sensitivity analysis was performed as described by Zhao et al. (2019) to identify model parameters that influence the predicted free blood C_{max} of CPO at single oral dose levels of CPF (0.5 mg/kg bw and 180 mg/kg bw).

2.5.4 Monte Carlo simulations

To include the inter-individual variation in the biotransformation reactions of CPF in human in the model-based predictions, a Monte Carlo simulation using the CV of the kinetic parameters for each metabolic pathway in the Supersome[™]-based PBK model and the HLM-based PBK model (biphasic) was incorporated into the PBK models. More specifically, in the Supersome[™]-based PBK model, kinetic variation in pathway 1 and 2 was described based on kinetic data (V_{max} and K_m) from Supersome[™] together with reported CV in CYP abundance, while in the HLM-based PBK model (biphasic), the variation in these two pathways was described based on pooled HLM kinetic data (V_{max} and K_m) together with reported CV for these pathways obtained from HLM kinetic data from 30 individuals (Smith et al. 2011). Both in the Supersome[™]-based and the HLM-based PBK model, variation in pathway 3 was based on pooled HLM kinetic data (V_{max} and K_m) together with reported CV for this pathway observed in 30 individuals (Smith et al. 2011), while variation in pathway 4 was based on the mean values of kinetic data of CPO detoxification in plasma measured for 25 individual HP samples together with their corresponding CV values derived in the present study.

Since it is the goal of the present study to compare two approaches for assessing the inter-individual variation in the metabolism of CPF and the consequences of this variability for the inter-individual differences in the sensitivity toward CPF exposure-induced RBC AChE

inhibition, no other parameters than variation in CYP abundance and the kinetic parameters (Vmax and Km) were taken into account in the Monte Carlo analysis.

The input parameters (CYP abundance, Vmax and Km) were assumed to follow a lognormal distribution. Given that Berkeley Madonna only offers the 'NORMAL' distribution function for sampling random numbers and not a lognormal function, the mean (μ_x) and standard deviations (σ_x) from these lognormally distributed parameters (Vmax or Km or abundance of relative CYP) were first transformed to parameters following a normal distribution using equation 9 (Eq9) (Zhang et al. 2007):

$$\mu_w = \ln\left(\frac{\mu_x}{\sqrt{1 + CV_x^2}}\right) \quad \text{and} \quad \sigma_w^2 = \ln(1 + CV_x^2) \quad (\text{Eq9})$$

where μ_x is the mean of Vmax or Km or abundance of the respective CYP, and CV_x is the coefficient of variation for each of the values, after which the exponential function (equation 10 (Eq10)) on the normally distributed μ_w and σ_w was applied to obtain the lognormally distributed input parameters in the model (Li et al. 2017):

$$\mathbf{lognormal}(\mu_x, \sigma_x) = \mathbf{exp(Normal}(\mu_w, \sigma_w)) \quad (\text{Eq10})$$

A summary of the mean and the CV values that define the distributions for the input parameters Vmax, Km and CYP abundance used for the Monte Carlo simulation in the two models is shown in Table 2. It should be noted that the parameters obtained using pooled HLMs were considered to represent a mean value (Table 2). Different than CYP1A2 and CYP3A4 for which only one phenotype is known, more than one phenotype is known for CYP2B6 and CYP2C19. Therefore, in the SupersomeTM-based PBK model, the variation in the activity of CYP2B6 and CYP2C19 was characterized by considering different phenotype abundances and relative frequencies in the general population obtained from Simcyp (Simcyp Simulator V18 Release 1, Certara, Sheffield, UK) in the Monte Carlo analysis.

Table 2. A summary of the mean values and coefficient of variation (CV) for Vmax, Km, CYP abundance of each CYP phenotype and their relative frequency in the general population.

SupersomeTM-based PBK model				
Pathway 1 & Pathway2 (CYP abundance)				
Parameter	Mean ^a	CV	Frequency	Reference
1A2 (EM ^b)	52.0	0.67	1.000	Simcyp ¹
2B6 (EM ^b)	17.0	1.22	0.890	Simcyp ¹
2B6 (PM ^c)	6.0	2.00	0.110	Simcyp ¹
2C19 (EM ^b)	4.4	0.71	0.590	Simcyp ¹
2C19 (PM ^c)	0.0	0.00	0.092	Simcyp ¹
2C19 (UM ^d)	8.7	0.71	0.318	Simcyp ¹
3A4 (EM ^b)	137	0.41	1.000	Simcyp ¹
Pathway 3 (Vmax, Km)				
Parameter	Mean	Reference	CV ^k	Reference
Vmax	37.980 ^e	Zhao et al. (2019)	0.57	Smith et al. (2011)
Km	627.900 ^f	Zhao et al. (2019)	0.39	Smith et al. (2011)
Pathway 4 (Vmax, Km)				
Parameter	Mean	Reference	CV	Reference
Vmax	1844.000 ⁱ	Calculated ^j	0.29	Calculated ^j
Km	290.000 ^f	Calculated ^j	0.33	Calculated ^j

HLM-based PBK model (biphasic)

Pathway 1 (Vmax, Km)

Parameter	Mean ^k	Reference	CV ^k	Reference
Vmax (high affinity) ^g	0.275	Buratti et al. (2003)	0.59	Smith et al. (2011)
Km (high affinity) ^h	0.270	Buratti et al. (2003)	0.61	Smith et al. (2011)
Vmax (low affinity) ^e	0.353	Sams et al. (2004)	0.59	Smith et al. (2011)
Km (low affinity) ^f	29.800	Sams et al. (2004)	0.61	Smith et al. (2011)

Pathway 2 (Vmax, Km)

Parameter	Mean ^k	Reference	CV ^k	Reference
Vmax ^e	0.653	Sams et al. (2004)	0.53	Smith et al. (2011)
Km ^f	12.000	Sams et al. (2004)	0.89	Smith et al. (2011)

Pathway 3 & Pathway 4 (Vmax, Km)

Same as the values reported in SupersomeTM-based PBK model for Pathway 3, Pathway 4

^a pmol CYP/ mg microsomal protein

^b EM = extensive metabolizer

^c PM = poor metabolizer

^d UM = ultra-rapid metabolizer

^e Vmax obtained using a high concentration range (3 μ M to 100 μ M) of CPF, in nmol/min/mg microsomal protein

^f Km obtained using a high concentration range (3 μ M to 100 μ M) of CPF, in μ M

^g V_{max} obtained using low concentration range (0.02 μM to 10 μM) of CPF, in nmol/min/mg microsomal protein

^h K_m obtained using low concentration range (0.02 μM to 10 μM) of CPF, in μM

ⁱ nmol/min/ml plasma

^j the value is calculated using the kinetic data from 25 individual HP samples characterized in the present study, the detailed results are presented in the section “Supplementary IV”

^k data obtained from Smith et al. (2011) for CV calculation, based on the fact that the metabolic reactions of CPF bioactivation, CPF and CPO detoxification are not age-dependent in HLM when expressed on the basis of per mg microsomal protein

^l Simcyp (Simcyp Simulator V18 Release 1, Certara, Sheffield, UK)

In total 10000 simulations were performed for the Monte Carlo analysis. In each simulation, the parameter values were randomly taken from the distributions of the input parameters. To avoid sampling unrealistic values, a minimum and maximum value for each parameter distribution was established by applying a cut-off value corresponding to $\pm 3 \sigma_w$ of the mean μ_w (Strikwold et al. 2017). It is of important to mention that no correlation was assumed between different metabolic pathways of CPF in the present study. As mentioned above, some CYP isoforms contained different sub-phenotypes, therefore the Monte Carlo analysis for the SupersomeTM-based PBK model took different phenotypes and their corresponding frequencies (include in Table 2) in the general population into account. In total, there were six possible combinations of different CYP phenotypes (1A2EM, 2B6EM, 2C19EM, 3A4EM; 1A2EM, 2B6EM, 2C19PM, 3A4EM; 1A2EM, 2B6EM, 2C19UM, 3A4EM; 1A2EM, 2B6PM, 2C19EM, 3A4EM; 1A2EM, 2B6PM, 2C19PM, 3A4EM; 1A2EM, 2B6PM, 2C19UM, 3A4EM). To obtain the overall frequency distributions for the entire population, the six possible combinations were run independently for 10000 runs, and their resulting distributions were corrected with the corresponding frequency of the phenotype of the respective CYPs in the general population (Table 2), and summed together at the end.

The HK_{AF} of CPF at a dose of 0.47 mg/kg bw was calculated as the ratio between the 95th or 99th percentile of CPO formation and the geometric mean (GM) for the whole population (IPCS 2005). Use of a dose level of 0.47 mg/kg bw for this calculation was based on the fact that it represents the benchmark dose lower confidence limits for 10% inhibition (BMDL₁₀), which is used as the POD for setting a health based guidance value (USEPA 2014).

2.5.5 Reverse dosimetry to extrapolate in vitro AChE inhibition data to in vivo dose-response curves

In the present study, PBK model-based reverse dosimetry was applied to translate the in vitro rhAChE inhibition concentration-response curve into in vivo RBC AChE inhibition dose-response curves first for the average adult population. To this end, in vitro effective concentrations of CPO were set equal to the in vivo free blood C_{\max} values of CPO in the PBK model according to the following equation 11 (Eq11) (Shi et al. 2020):

$$C_{\text{total in vitro}} * fuCPO_{\text{in vitro}} = C_{\text{total in vivo}} * fuCPO_{\text{in vivo(blood)}} \quad (\text{Eq11})$$

Herein the $C_{\text{total in vitro}}$ represents the total concentration of CPO in the in vitro assay and $fuCPO_{\text{in vitro}}$ is the unbound fraction of CPO in the vitro assay. In the present study, the $fuCPO_{\text{in vitro}}$ was assumed to be 1, which is based on the observation from Heilmair et al. (2008) that the presence of only a low level (0.1 mg/ml) of albumin in the in vitro medium as routinely used to stabilize the enzyme does not substantially affect the free fraction of CPO. $C_{\text{total in vivo}}$ represents the total concentration of CPO in human blood. To obtain the corresponding unbound blood concentrations, the $C_{\text{total in vivo}}$ was multiplied with the unbound fraction of CPO in blood ($fuCPO_{\text{in vivo(blood)}}$), which was obtained by dividing the unbound fraction of CPO in plasma ($fuCPO_{\text{in vivo(plasma)}}$) by the ratio of the CPO concentration in blood to the CPO concentration in plasma, the CPO blood to plasma ratio (BPCPO), as below (Eq12) (Shi et al. 2020):

$$fuCPO_{\text{in vivo(blood)}} = \frac{fuCPO_{\text{in vivo(plasma)}}}{BPCPO} \quad (\text{Eq12})$$

The BPCPO value of 2.7 was estimated by Simcyp (Simcyp 2016a) based on the logP value (3.89) of CPO from ChemAxon (ChemAxon) and the unbound fraction of CPO in plasma ($fuCPO_{\text{in vivo(plasma)}}=0.15$) from Heilmair et al. (2008).

The external dose values thus obtained together with corresponding inhibitory effects were used to construct RBC AChE inhibition dose-response curves for the average population. The dose-response curves for the most sensitive individuals (99th percentile) and least sensitive individuals (1st percentile) were derived by applying the obtained HK_{AF} (99th percentile) or the ratio between the 1st percentile and the GM of CPO formation distribution of the whole population to the dose-response curve of the average population.

2.5.6 BMD analysis and evaluation of the PBK model-based reverse dosimetry predictions

A BMD analysis was performed to derive a POD from the predicted *in vivo* dose–response curves obtained for the average population. In the present study, the BMDL₁₀ values were used as POD based on the fact that the United States Environmental Protection Agency (USEPA) also used a 10% effect level to define a health based guidance value (2011; 2014). BMD analysis was carried out using the Benchmark Dose Software version 3.1.2 (USEPA 2019), with exponential or hill models because of their adequacy in predicting continuous data. The BMDL₁₀ value with the lowest AIC was chosen and further evaluated by comparing the obtained values with reported BMDL₁₀ by USEPA (2011; 2014).

3. Results

3.1 *In vitro* AChE inhibition concentration-response curve

The CPO concentration-dependent inhibition of rhAChE activity is shown in Figure 3. The 50% inhibition of enzyme activity occurred at a CPO concentration of 1.89 nM, with the 95% confidence interval ranging from 1.65 nM to 2.16 nM.

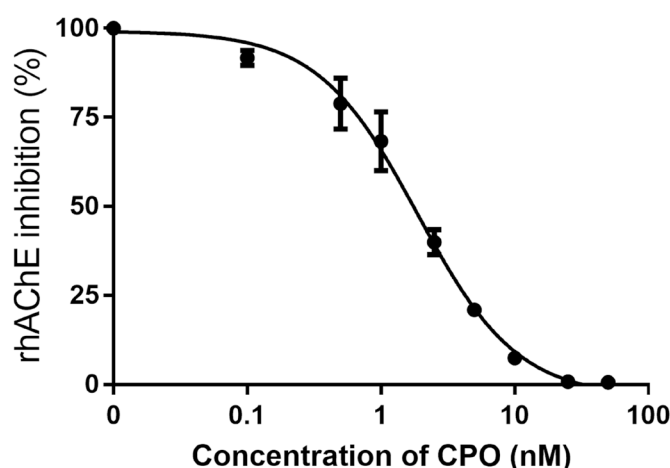


Fig 3. Effect of increasing concentration of CPO on recombinant human acetylcholinesterase (rhAChE) activity at 37 °C. Each value represents the mean \pm SD of five independent experiments.

3.2 Kinetic data, ISEF and total protein concentration

3.2.1 Bioactivation and detoxification of CPF in Supersome™ enzymes

The CPF concentration-dependent increase in the rate of bioactivation of CPF to CPO and detoxification of CPF to TCPy obtained with different Supersome™ is presented in Supplementary material II. The apparent V_{max} , K_m and the CE (calculated as V_{max}/K_m) derived from these in vitro data are shown in Table 3. Overall, the Supersome™ data reveal that the four CYPs known to be active in CPF to CPO conversion vary in their velocity and affinity, with CYP2B6 showing the highest CE for bioactivation of CPF, and CYP2C19 showing the highest CE in terms of detoxification. CYP3A4 has the lowest CE for both pathways.

In the next step, the CYP-specific ISEFs were defined. The ISEFs were calculated based on the measured apparent V_{max} in incubations with Supersome™ and pooled HLMs and are presented in Table 3. The highest ISEF value was found for CYP2B6 (0.48) and the lowest one for CYP1A2 (0.07).

Table 3. Kinetic parameters for biotransformation of CPF in incubations with Supersome™, and ISEFs for hepatic CYP-mediated biotransformation of probe substrates as determined based on incubations with pooled HLM or Supersome™. Data represent mean of two experiments for each parameter.

Biotransformation of CPF				
	CYP1A2	CYP2B6	CYP2C19	CYP3A4
Pathway 1				
Km(app) ^a	0.61	0.14	1.89	29.77
Vmax(app) ^b	3.96	7.76	2.74	17.78
CE ^c	6.49	55.43	1.45	0.60
Scaled Vmax(app) ^d	51.81	203.94	10.81	910.77
Scaled CE ^e	84.93	1456.70	5.71	30.59
Pathway 2				
Km(app) ^a	1.25	1.28	1.37	18.13
Vmax(app) ^b	2.96	5.49	17.51	23.86
CE ^c	2.37	4.29	12.78	1.32
Scaled Vmax(app) ^d	38.73	144.28	69.06	1222.21
Scaled CE ^e	30.98	112.72	50.41	67.41
ISEF determination				
	CYP1A2	CYP2B6	CYP2C19	CYP3A4
Probe substrate	phenacetin	bupropion	(S)-mephenytoin	testosterone
CYP abundance ^f	52.00	15.80	5.40	137.00
Vmax (pooled HLMs) ^g	0.15	0.31	0.02	17.29
Vmax (Supersome™) ^h	39.06	40.77	20.59	1179
ISEF ⁱ	0.07	0.48	0.21	0.11

^a μM

^b pmol/min/pmolCYP

^c CE = in vitro catalytic efficiency (μl/min/ pmol CYP) calculated as $V_{max (app)}/K_m (app)$

^d scaled Vmax (umol/hr), calculated based on Eq 3,

^e scaled catalytic efficiency (l/hr), calculated as scaled $V_{max (app)}/K_m (app)$

^f CYP abundance (pmol CYP/mg microsomal protein) is the average endogenous abundance of each CYP isoform in HLM, which is obtained from Simcyp (Simcyp Simulator V18 Release 1, Certara, Sheffield, UK)

^g nmol/min/mg microsomal protein

^h pmol/min/pmol CYP

ⁱ ISEF calculated on the basis of Eq4



To gain a better insight in the contribution of each CYP to the metabolism of CPF in vivo at different concentrations of CPF, the apparent Supersome™ kinetic data were scaled toward the whole liver according to Eq3. The corresponding Michaelis-Menten plot for each CYP upon extrapolation is presented in Figure 4.

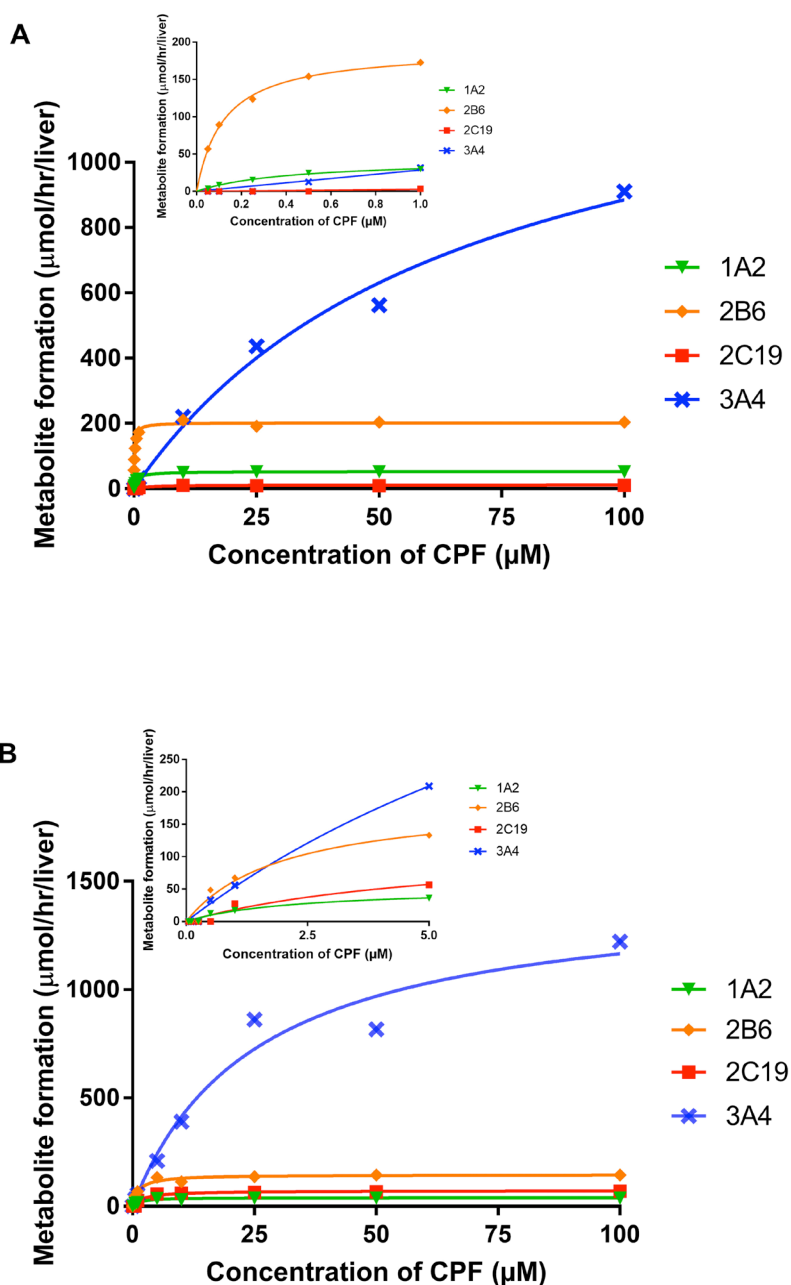


Fig 4. Concentration-dependent metabolic velocity of each CYP in whole liver for (A) bioactivation of CPF to CPO and (B) detoxification of CPF to TCPy. Since different concentration ranges were used in the different CYP incubations, the velocity of concentrations exceeding the incubation concentration range of each CYP were set

equal to its corresponding V_{max} value, to facilitate the graphical comparison. The insert presents the data at the lower concentration range (up to $1\mu\text{M}$ in A, and $5\mu\text{M}$ in B) in some more detail.

Figure 4A shows that at a low concentration ($<1\mu\text{M}$), CYP1A2 and especially CYP 2B6 play the primary role in bioactivation of CPF to CPO. However, with increasing concentration, CYP1A2 and CYP2B6 approach saturation while the 3A4-mediated conversion starts to become an important contributor to CPO formation from concentration levels higher than $10\mu\text{M}$ onwards. CYP2C19 appears to have only a minor contribution at both low and high concentrations. These findings indicate that there are high affinity components (low K_m for CYP1A2, 2B6 and 2C19) and a low affinity component (high K_m for CYP 3A4) to be taken into account to adequately describe the bioactivation of CPF, resulting in biphasic kinetics. The one to two orders of magnitude lower K_m for CYP1A2, 2B6 and 2C19 compared to the K_m for CYP3A4 (Table 3) reflect this biphasic behavior. Differently, in detoxification of CPF (Figure 4B), CYP3A4 plays a main role in the formation of TCPy at low concentrations, and it is becoming even more pronounced at CPF concentrations higher than $1\mu\text{M}$, with CYP 1A2, CYP2B6 and CYP2C19 being involved in the detoxification pathway to a more limited extent.

Thus, the SupersomeTM data depicted in Figure 4 indicate biphasic kinetics to occur in the CYP-mediated bioactivation pathway, which is supported by the Eadie–Hofstee plot (Supplementary material III) for the summed enzyme velocities of the individual CYPs for pathway 1. However, the CYP-mediated detoxification pathway of CPF does not show such distinctive biphasic behavior, in line with the fact that Figure 4b reveals that for this reaction the conversion at low concentrations was not dominated by a high affinity CYP, resulting in a comparable (1.4-fold difference) sum of the scaled catalytic efficiency (CE) of the four individuals SupersomeTM in pathway 2 at low and high concentration ranges, allowing the kinetics for this reaction to be described in a monophasic way.

To evaluate the performance of the SupersomeTM together with the ISEF to predict the bioactivation of CPF, the sum of the scaled CE of the four individual SupersomeTM was compared to the CE obtained for the pooled HLMs (for both non-biphasic and biphasic scenarios). The comparison reveals that the summed scaled CE of SupersomeTM (CE= 1578 l/hr) is in line with that of pooled HLMs when biphasic kinetics was taken into account (CE=3600 l/hr), but is not comparable when the high affinity phase was excluded (CE=41 l/hr), indicating it is of critical importance to include the high affinity phase when characterizing a metabolic conversion that is catalyzed by two or more CYP isoforms with distinct affinities.

Given these results, the non-biphasic HLM-based approach was excluded in later steps presented below because of its incomplete characterization of CPF bioactivation.

3.2.2 In vitro metabolic conversion of CPO to TCPy in plasma

The apparent and scaled V_{max} , K_m , and CE for detoxification of CPO in plasma as well as the determined total protein concentration of plasma samples of 25 individuals are presented in Supplementary material IV. In general, the difference between the highest and the lowest CE is around 2.6-fold. This difference is mainly caused by individuals 15 and 16, due to a 1.5-fold lower apparent K_m in individual 15 and a 2-fold lower apparent V_{max} in individual 16 compared to the mean K_m (290 μM) and V_{max} (1844 nmol/min/ml plasma or 320937 $\mu\text{mol/hr}$), respectively (Table 2). The calculated CV of the V_{max} amounted to 0.29, and the CV for the K_m was 0.33 (Table 2). The results also show that the 25 individuals have relatively comparable total protein concentrations in plasma, showing an only 1.3-fold difference between the highest and the lowest value (Supplementary material IV).

3.3 PBK model evaluation

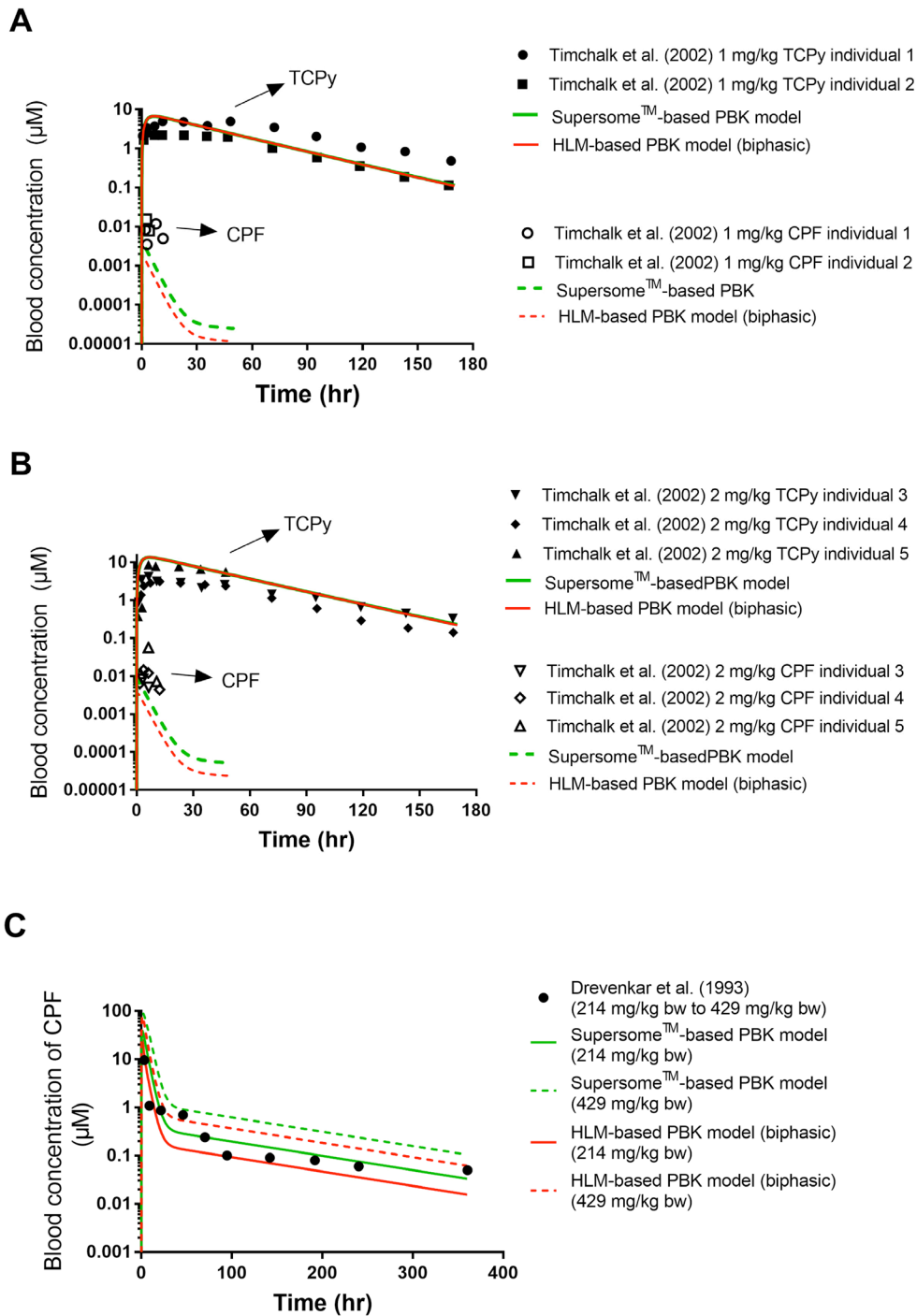


Fig 5. Comparison between reported in vivo data and PBK model predictions for time-dependent blood concentrations of CPF and time-dependent blood concentrations of TCPy at 1 mg/kg bw (A), and 2 mg/kg bw (B) (Timchalk et al. 2002), and 214 mg/kg bw (solid line) to 429 mg/kg bw (dash line) (C) the latter equal to the estimated dose range, for the estimated intake dose of poisoning victim A (Drevenkar et al. 1993).

The performances of the SupersomeTM and HLM-based PBK models were evaluated against available *in vivo* data obtained from the literature (Figure 5 and Supplementary material V). The data in the Supplementary material V reveal that the two models adequately predict the TCPy blood concentration, the predicted C_{max} value was 2.2-fold different from the mean value of C_{max} in *in vivo* data (Nolan et al. 1984) and the urinary TCPy excretion upon oral administration of 0.5 mg/kg bw is predicted to result in a concentration at 120 hr that is 0.8-fold different from the *in vivo* value (Nolan et al. 1984). Similar results were observed when comparing the predicted C_{max} of TCPy from the two models with *in vivo* data from 5 individuals (Timchalk et al. 2002) (Figure 5 A, and B), with the predictions being 1.3-fold to 4.0-fold different from the *in vivo* values. Apart from that, the two models were further evaluated by comparison of the predicted CPF blood concentration with the corresponding *in vivo* data from the 5 individuals. As illustrated in Figure 5, an either 0.04- to 0.99-fold difference or 0.02- to 0.44-fold difference was found when comparing the predicted blood concentration of CPF by the SupersomeTM-based PBK model or the HLM-based PBK model, respectively to the reported blood concentration data. To better evaluate the time-dependent CPF concentration in blood, the predictions were also compared with CPF blood concentration data from Drevenkar et al. (1993) for poisoning victim. The results show that, at the estimated dose range of 214 to 429 mg/kg bw which reflects the estimated intake range of poisoning victim, the CPF blood concentrations predicted by the SupersomeTM and HLM-based PBK models are in line with the reported CPF blood concentration of poisoning victim (Drevenkar et al. 1993).

5

3.4 Sensitivity analysis

In the present study, the impact of each parameter of the SupersomeTM-based model and the HLM-based PBK model (biphasic) on the model output (free blood C_{max} of CPO) was determined by performing a sensitivity analysis. Only the parameters with normalized sensitivity coefficient higher than 0.1 (absolute value) are shown in Supplementary material VI. In general, no large difference was found in the sensitivity analysis of the two approaches. At low dose levels (0.5 mg/kg bw), the model output was mainly influenced by body weight, volume of liver, volume of blood, cardiac output, blood flow to liver and rapidly perfused tissue, absorption rate constants, fraction of dose absorbed, liver microsomal protein yield scaling factor, the unbound fraction of CPO *in vivo* as well as blood to plasma ratio of CPO. In addition to that, the free blood C_{max} of CPO appears also to be significantly affected by the kinetic

parameters of CPO detoxification in both approaches, and to a lesser extent by CYP2B6-derived kinetic parameters of CPO bioactivation in the SupersomeTM-based model. At the exposure dose of 180 mg/kg bw, similar results were obtained, except that the parameters such as volume of liver, absorption rate constants, fraction of dose absorbed, and liver microsomal protein yield scaling factor had less influence on the model output. In contrast, CYP-derived kinetic parameters of CPO bioactivation (especially CYP3A4) and its related parameters (ISEF and CYP abundance) in the SupersomeTM-based model, and HLM-derived kinetic parameters of CPO bioactivation in HLM-based PBK model (biphasic) became influential on the model output.

3.5 Monte Carlo simulation and CSAF (HK_{AF})

The frequency distributions of the predicted C_{max} of CPO obtained using the SupersomeTM-based PBK model approach and the HLM-based PBK model approach including biphasic kinetics are presented in Supplementary material VII, and the corresponding GM, 95th and 99th percentile values of the distributions are shown in Table 4. Supplementary material VII and Table 4 together reveal that there are no substantial differences in the frequency distributions of the predicted C_{max} of CPO obtained by the two approaches, resulting in more or less similar GM, 95th and 99th percentile values between the two approaches (maximum 1.2-fold different). These values were used to calculate the HK_{AF} values, which were obtained by dividing the 95th or 99th percentile of the general population by the GM of the general population. As presented in Table 4, a slight difference was observed between both approaches when using the 95th percentile providing a HK_{AF} of 2.6 and 2.5 for the SupersomeTM-based PBK model and the HLM-based PBK model, respectively. When using the 99th percentile, the calculated HK_{AF} values were consistent, amounting to 3.6 for both approaches.

Table 4. Geometric mean values, the 95th and the 99th percentile values of the distribution for the predicted free blood maximum concentration (C_{max}) of CPO after a single oral CPF dose of 0.47 mg/kg bw in Monte Carlo simulations, and its resulting CSAFs in the SupersomeTM-based PBK model and the HLM-based PBK model approach.

	Supersome TM -based PBK model	HLM-based PBK model
CSAF(HK_{AF})^a		
P95/GM	2.6	2.5
P99/GM	3.6	3.6
Total runs	58792	9712

^a Chemical specific adjustment factor (CSAF) for human variability in toxicokinetics (HK_{AF})

3.6 Reverse dosimetry to extrapolate in vitro AChE inhibition data to in vivo dose-response curves

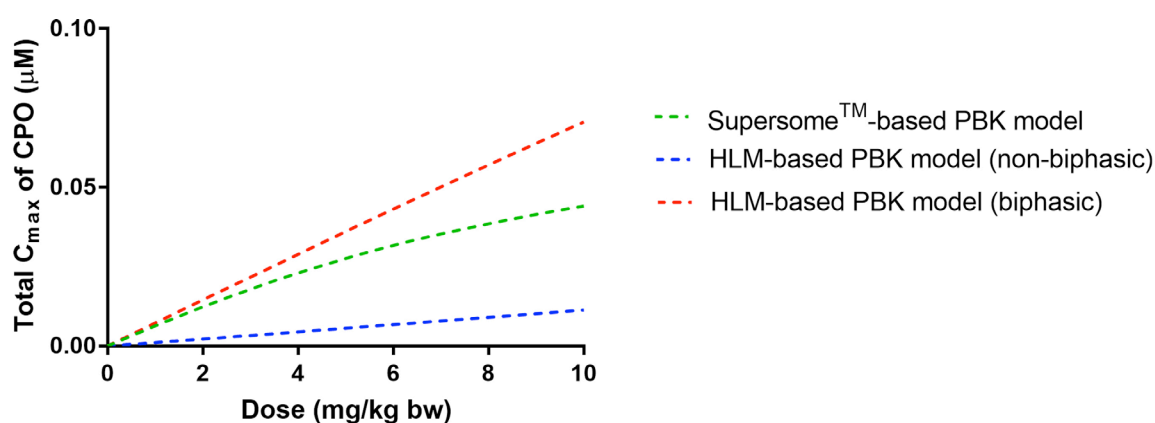


Fig 6. Comparison of the prediction for the CPF dose-dependent total C_{max} of CPO by the different approaches

For further evaluation of the newly defined PBK models, Figure 6 shows a comparison of the CPF dose-dependent predicted total blood C_{max} of CPO using the PBK models developed in the present study. The comparison reveals that the predictions by especially the non-biphasic HLM-based model deviates from the predictions by the other models, while the data provided by SupersomeTM-based PBK model and those obtained with HLM-based PBK model (biphasic) were found to be similar, with a difference of 1.1-fold to 1.6-fold, increasing with the dose.

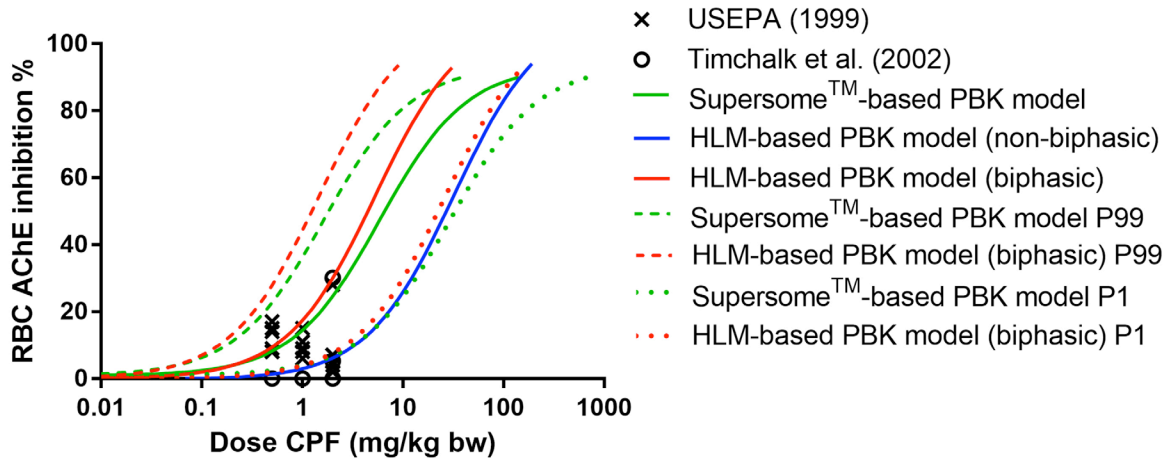


Fig 7. The predicted in vivo dose–response curves for AChE inhibition upon CPF exposure in human using the Supersome™-based PBK model (green solid line for average population, green dash line for 99th percentile sensitive individuals, and green dot line for 1st percentile sensitive individuals), the HLM-based PBK model (non-biphasic, blue solid line) and the HLM-based PBK model (biphasic, red solid line for average population, red dash line for 99th percentile sensitive individuals, and red dot line for 1st percentile sensitive individuals) for the reverse dosimetry. The individual data points represent available in vivo data for RBC AChE inhibition in human upon oral exposure to CPF at different dose levels as reported by USEPA (1999) and Timchalk et al. (2002).

Finally Figure 7 illustrates that when using the different PBK models to translate the in vitro concentration-response curve for CPO-mediated inhibition of rhAChE inhibition to in vivo dose-response curves using reverse dosimetry, the predicted dose-response curves for the average population by the Supersome™-based PBK model and HLM-based PBK model (biphasic) were in line with in vivo data points, while the curve obtained with the HLM-based PBK model (non-biphasic) appeared to inadequately describe the actual inhibition reported at low dose levels for some individuals. Additionally, Figure 7 presents the dose-response curves predicted for the 99th percentile and 1st percentile of the population, reflecting the possible inter-individual variation in the RBC AChE response predicted by the Supersome™-based PBK model approach and the HLM-based PBK model approach (biphasic). The curves obtained for 99th percentile and 1st percentile individuals by the Supersome™-based PBK model are similar to those predicted by the HLM-based PBK model (biphasic), except for the fact that the curves obtained with the HLM-based biphasic approach are somewhat steeper than those obtained with the Supersome™-based approach.



3.7 BMD analysis and evaluation of the PBK model-based reverse dosimetry predictions

Figure 8 and Supplementary material VIII, present the BMDL₁₀ values derived as PODs from the dose-response curves for the average population presented in Figure 7. From these results it can be derived that the POD values obtained with the PBK model defined in the present study by the SupersomeTM-based PBK model and the HLM-based biphasic PBK model for the average population were comparable to the reported human model-derived BMDL₁₀ values (1.9-fold and 1.8-fold lower, respectively) (USEPA 2014). However, when the high affinity component was excluded in the non-biphasic HLM-based PBK model, the predicted BMDL₁₀ values was found to be 3.3-fold higher than the reported human model-derived BMDL₁₀ values (USEPA 2014).

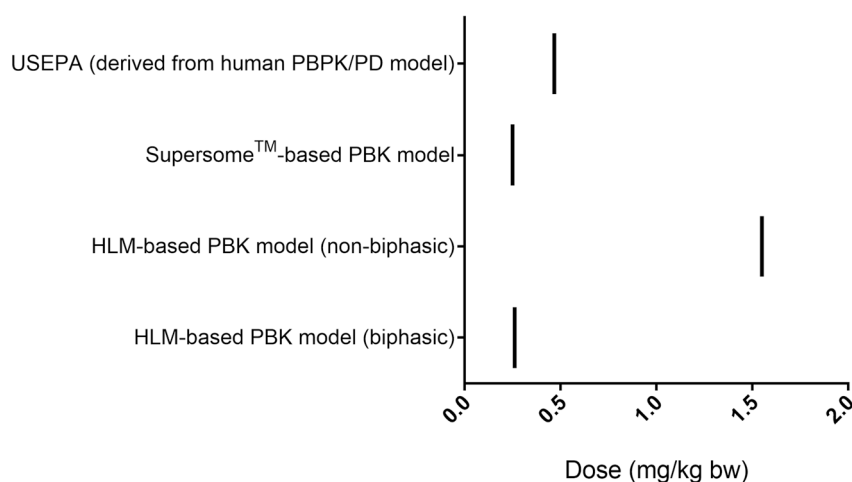


Fig 8. Comparison of predicted BMDL₁₀ values by the present study to reported BMDL₁₀ values established by USEPA (2014).

4. Discussion

The present study compared the performance of two different approaches on characterization of the inter-individual variation in metabolism of CPF and its resulting RBC AChE inhibition using PBK-based reverse dosimetry linked with Monte Carlo simulations. In one approach, variation in metabolism was calculated using SupersomeTM together with reported variation in CYP abundance, while in the other approach, variation was quantified using individual HLM data from Smith et al. (2011). The obtained results revealed that both approaches adequately

predicted the time-dependent blood concentration profile of CPF and its metabolite TCPy, and could be used to successfully translate the *in vitro* concentration-response curves for RBC AChE inhibition by the active metabolite CPO to corresponding *in vivo* dose-response curves for CPF induced inhibition of RBC AChE activity, resulting in a derived BMDL₁₀ value that was comparable to the reported BMDL₁₀ value from the USEPA (2014). Additionally, the similar results obtained from the SupersomeTM-based approach and the HLM-based approach (biphasic) imply that there is a good match between the two approaches, thus also resulting in comparable HK_{AF} values. When comparing the obtained HK_{AF} values with the default uncertainty factor of 3.16, the HK_{AF} value derived using the 95th percentile is found to be well covered by the default value of 3.16, while the HK_{AF} defined using the 99th percentile, was slightly higher than 3.16, reflecting a possible inadequate protection by the default safety factor for a small part of the population. It also needs to be considered that the HK_{AF} values obtained account for only the variation in metabolism-related parameters, while the variability in other kinetic parameters including absorption-, distribution- related processes are not yet taken into account.

In the present study, the IC₅₀ value obtained from the CPO-induced concentration-response curve in rhAChE was found to be comparable to the IC₅₀ value of 3.1 nM (taking into account a correction for the unbound fraction of CPF in plasma amounting to 0.15 (Heilmair et al. 2008)) reported in the study of Eyer et al. (2009). In this study the plasma samples from the patients poisoned with CPF were incubated with uninhibited RBCs from a healthy donor. This similar IC₅₀ value indicates that rhAChE and native human RBC have a comparable sensitivity towards *in vitro* inhibition following CPO exposure.

The kinetic parameters obtained by SupersomeTM incubations revealed that the bioactivation of CPF exhibits biphasic kinetics, based on the fact that the Km of CYP1A2, CYP2B6 and CYP2C19 were one to two orders of magnitude lower than that of CYP3A4 (Foxenberg et al. 2007). As a result, the combined kinetic data from these four main CYPs generated a characteristic pattern of biphasic kinetic in the Eadie-Hofstee plot (Supplementary material III). However, in incubations with HLM, only the low affinity component was identified when using CPF at a concentration range of 3 to 100 µM (Sams et al. 2004; Zhao et al. 2019), while the high affinity component was not. These differences indicate that identifying such multiple CYP isoform-mediated biotransformation reactions of CPF using HLM might be problematic. Different from the SupersomeTM-derived kinetic data that reflect each CYP-specific intrinsic kinetic profile and parameters (Km and Vmax) towards the chemical of interest, the HLM-

derived kinetic data represent the overall metabolic conversion by all relevant CYPs. Therefore, using substrate concentration ranges that far exceed the K_m of some of the CYPs involved could lead to an incomplete capture of the kinetic phase, resulting in an under-estimation of the metabolic rate especially at low concentrations and dose levels. In theory, this issue can be overcome by extending the substrate incubation concentration range. In practice, however, the quantification of formation of CPO in incubations with HLM at low substrate concentrations (in this case CPF $< 1 \mu\text{M}$) may be challenging, because of the detection limits for the metabolite of interest. Buratti et al. (2003) employed a highly sensitive detection method for CPO (based on AChE inhibition) for the metabolic reaction of CPF using HLM. However, the assay was only able to identify the high affinity CYP kinetic components due to the complete inhibition of the AChE at high substrate concentrations and high formed CPO metabolite concentrations (Buratti et al. 2003). These observed incomplete captures of HLM kinetic data will occur less often with SupersomeTM, since they have a higher catalytic activity compared with the native CYPs present in HLM, allowing identification of both low and high affinity components using normal enzyme incubation assay conditions and established LC-MS/MS or ULPC-PDA detection methods.

Although SupersomeTM seems a promising system for studying the metabolic turnover of chemicals, the activities of CYP enzymes from SupersomeTM are different from native sources, as SupersomeTM is a recombinant enzyme system made using baculovirus-transfected insect cells and exhibiting very high levels of catalytic activities. Therefore use of SupersomeTM requires an ISEF to correct for differences in activity compared to the HLM, before scaling the activities to the *in vivo* situation. Applying such an ISEF may lead to an over- or under-estimation of metabolism, due to the possible variations in determination of ISEF values such as variability in the commercially supplied SupersomeTM and HLM systems used, the probe substrate used, and the laboratory conditions applied (Chen et al. 2011; Proctor et al. 2004). In the present study the variabilities and inconsistencies related to ISEF values were minimized by using a probe substrate for the relevant CYPs in both enzyme systems to derive the ISEFs (instead of using default ISEF values), and using the same batch of SupersomeTM and HLM for all ISEF determinations in the same laboratory. The overall extrapolated V_{max} values using ISEF values established in the present study from SupersomeTM kinetic data were found to be 1.9- and 0.9- fold different from the V_{max} values derived from the HLM data for the high and low affinity component, respectively (Buratti et al. 2003; Sams et al. 2004; Smith et al. 2011; Zhao et al. 2019), indicating the adequacy of the ISEF values established in the present study.

Different from the bioactivation of CPF to CPO (pathway 1), the detoxification of CPF (pathway 2) was shown in the present study to be adequately described by only one set of V_{max} and K_m . However, it is true that both bioactivation and detoxification of CPF were mainly catalyzed by similar type of CYPs, therefore biphasic kinetics may in theory also be expected to occur in the detoxification. Based on the results obtained, however, it appeared that the detoxification reaction kinetics were dominated by the contribution of only CYP3A4 at both low and high concentrations. Therefore, it eliminates the need for description of biphasic kinetics in the pathway 2. A similar kinetic behavior for the conversion of CPF to TCPy was also observed in a previous study in rat liver microsomes (Ma and Chambers 1995).

The consequences of using different in vitro kinetic data as input of model-based reverse dosimetry were described by the $BMDL_{10}$ values obtained in the present study. The $BMDL_{10}$ value (for the average population) obtained using the HLM-based approach taking biphasic kinetics into account was found to be comparable to the $BMDL_{10}$ values reported by the USEPA (2014), but was 6-fold lower than that obtained from the HLM-based approach in which the high affinity component was not included. Such a difference is obviously due to the fact that without including the high affinity component, the contribution of CYP1A2, CYP2B6 and CYP 2C19 at low concentrations to the bioactivation of CPF to CPO was neglected. Therefore, it is of importance to take biphasic kinetics into account, as an incomplete kinetic profile of bioactivation of CPF to CPO apparently results in an under-estimation of the POD leading to an inadequate protection of human health at especially realistic low dose exposure levels. When comparing the $BMDL_{10}$ value obtained using the HLM-based PBK model that takes biphasic kinetics into account with the $BMDL_{10}$ obtained with the SupersomeTM-based PBK model for the average population, no substantial difference was observed (1.04-fold), consistent with the comparable in vitro kinetic data predicted by the two approaches.

In the present study, for the Monte Carlo simulations, no covariation was assumed between different pathways. This was dependent on the following considerations. Based on the previous reported CE data for each pathway from Smith et al. (2011), the Pearson r was calculated (The correlation analysis, GraphPad Prism 5, version 5.04), which showed only low to mediate correlations between pathway 1 with either pathway 2 or 3 (Pearson r of Pathway 1 versus Pathway 2 = 0.63, and Pearson r of Pathway 1 versus Pathway 3 = 0.35), and mediate correlations between pathway 2 with pathway 3 (Pearson r = 0.51). Based on the fact that a low to moderate correlation will not substantially affect the model outcome (Bukowski et al. 1995; Poet et al. 2017), no correlations between these three pathways were included in the present

study. Regarding Pathway 3 and 4 (PON1-mediated detoxification of CPO in liver and plasma, respectively), one may expect they will correlate with each other since plasma PON1 is known to be released from the liver (Ali and Chia 2008). However, there are no data that describe such a correlation between these two pathways. Moreover, by assuming that pathway 3 and pathway 4 completely correlate with each other, some possible combinations of kinetic data of the two pathways might be excluded in the Monte Carlo analysis. Therefore, to be conservative, these two pathways were treated as independent. Altogether, including no covariation between the different pathways maximizes the variability of the predicted CPO C_{max} (model output). As a result, the derived HK_{AF} values can be regarded to represent a conservative scenario.

Altogether, both the SupersomeTM-based model and the HLM-based model with biphasic kinetics appeared suitable to predict inter-individual variation in the metabolism of CPF, and this approach can be further advanced by considering the following improvement. In the present study, the HK_{AF} obtained relates to the general adult population, but did not yet relate to specific sub-population groups (e.g. pregnant women, infants and children). Some data suggest that there is a different capacity for CPO detoxification between specific sub-groups and general adults. Ferré et al. (2006) for example reported that the metabolic capacity can be altered during pregnancy, and that pregnancy can lead to an approximately 30% reduction in PON1 activity, which may result in a decreased capacity for CPO detoxification. In addition, an age-dependent increase of PON1 levels and activity have been reported (Huen et al. 2010), suggesting that human fetuses, infants, and young children may have lower capacity to detoxify CPO than adults. This observation has been corroborated by the human plasma kinetic data from Smith et al. (2011) reporting that V_{max} values (on a per ml plasma basis) of CPO detoxification positively correlated with age. Therefore, the HK_{AF} derived in the present study may not provide full protection for these sensitive sub-group. In further research, the SupersomeTM-based approach could be extended to also include sub-populations, allowing definition of a more comprehensive HK_{AF} .

In conclusion, the present study demonstrates that using the SupersomeTM-based model and HLM-based model (biphasic), together with Monte Carlo simulations and reverse dosimetry can adequately predict the inter-individual variation in metabolism of CPF and its resulting RBC AChE response, providing comparable $BMDL_{10}$ and HK_{AF} values in both approaches. Using SupersomeTM-derived kinetic parameters together with corresponding CYP abundances to describe inter-individual variability of CPF toxicokinetics enables to capture different kinetic affinity components, which may have been problematic when using HLMs alone. On the other

hand, using the SupersomeTM-based approach might be hindered by the accuracy of ISEF values used. Overall, taking these advantages and disadvantages of the two approach into account, the SupersomeTM-based approach seems more appropriate than the HLM-based approach for identifying inter-individual variation in biotransformation of CPF and its resulting RBC AChE inhibition.

Acknowledgements

This work was funded by a Grant from the China Scholarship Council (No. 201707720063 to ZHAOSHENSHENG).

Conflict of interests

The authors declared no potential conflicts of interest with respect to the research, authorship, and/or publication of this article.

References

- Ali SM, Chia SE (2008) Interethnic variability of plasma Paraoxonase (PON1) activity towards organophosphates and PON1 polymorphisms among Asian populations— a short review *Industrial health* 46:309-317
- Barter ZE, Bayliss MK, Beaune PH, Boobis AR, Carlile DJ, Edwards RJ, . . . Pelkonen OR (2007) Scaling factors for the extrapolation of in vivo metabolic drug clearance from in vitro data: reaching a consensus on values of human micro-somal protein and hepatocellularity per gram of liver *Current drug metabolism* 8:33-45
- Bizoń A, Milnerowicz H (2018) The effect of divalent metal chelators and cadmium on serum phosphotriesterase, lactonase and arylesterase activities of paraoxonase 1 *Environmental Toxicology and Pharmacology* 58:77-83
- Boonpawa R, Moradi N, Spenkelink A, Rietjens IMCM, Punt A (2015) Use of physiologically based kinetic (PBK) modeling to study interindividual human variation and species differences in plasma concentrations of quercetin and its metabolites *Biochemical pharmacology* 98:690-702
- Bukowski J, Korn L, Wartenberg D (1995) Correlated inputs in quantitative risk assessment: the effects of distributional shape *Risk Analysis* 15:215-219
- Buratti FM, Volpe MT, Meneguz A, Vittozzi L, Testai E (2003) CYP-specific bioactivation of four organophosphorothioate pesticides by human liver microsomes *Toxicology and applied pharmacology* 186:143-154
- ChemAxon Chemicalize. <https://chemaxon.com/products/chemicalize>. Accessed 21 February 2021
- Chen Y, Liu L, Nguyen K, Fretland AJ (2011) Utility of intersystem extrapolation factors in early reaction phenotyping and the quantitative extrapolation of human liver microsomal intrinsic clearance using recombinant cytochromes P450 *Drug metabolism and disposition* 39:373-382
- Coasta LG, Cole TB, Vitalone A, Furlong C (2006) Paraoxonase polymorphisms and toxicity of organophosphates. In: *Toxicology of Organophosphate & Carbamate Compounds*. Elsevier, pp 247-255
- Drevenkar V, Vasilic Ž, Štengl B, Fröbe Z, Rumenjak V (1993) Chlorpyrifos metabolites in serum and urine of poisoned persons *Chemico-biological interactions* 87:315-322
- EFSA (2014) Conclusion on the peer review of the pesticide human health risk assessment of the active substance chlorpyrifos *EFSA Journal* 12:3640
- EFSA (2019) Statement on the available outcomes of the human health assessment in the context of the pesticides peer review of the active substance chlorpyrifos *EFSA Journal* 17:e05809
- EFSA (2020) The 2018 European Union report on pesticide residues in food *EFSA Journal* 18
- Ellison CA, Tian Y, Knaak JB, Kostyniak PJ, Olson JR (2012) Human hepatic cytochrome P450-specific metabolism of the organophosphorus pesticides methyl parathion and diazinon *Drug Metabolism and Disposition* 40:1-5
- Ellman GL, Courtney KD, Andres Jr V, Featherstone RM (1961) A new and rapid colorimetric determination of acetylcholinesterase activity *Biochemical pharmacology* 7:88-95
- European Commission (2020) Chlorpyrifos & Chlorpyrifos-methyl. https://ec.europa.eu/food/plant/pesticides/approval_active_substances/chlorpyrifos_chlorpyrifos-methyl_en.
- Eyer F, Roberts DM, Buckley NA, Eddleston M, Thiermann H, Worek F, Eyer P (2009) Extreme variability in the formation of chlorpyrifos oxon (CPO) in patients poisoned by chlorpyrifos (CPF) *Biochemical pharmacology* 78:531-537
- Faucette SR, Hawke RL, Lecluyse EL, Shord SS, Yan B, Laethem RM, Lindley CM (2000) Validation of bupropion hydroxylation as a selective marker of human cytochrome P450 2B6 catalytic activity *Drug metabolism and disposition* 28:1222-1230
- Ferré N, Camps J, Fernández-Ballart J, Arija V, Murphy MM, Marsillach J, Joven J (2006) Longitudinal changes in serum paraoxonase-1 activity throughout normal pregnancy *Clinical Chemistry and Laboratory Medicine (CCLM)* 44:880-882
- Foxenberg RJ, McGarrigle BP, Knaak JB, Kostyniak PJ, Olson JR (2007) Human hepatic cytochrome p450-specific metabolism of parathion and chlorpyrifos *Drug metabolism and disposition* 35:189-193

- Furlong CE, Richter RJ, Seidel SL, Costa LG, Motulsky AG (1989) Spectrophotometric assays for the enzymatic hydrolysis of the active metabolites of chlorpyrifos and parathion by plasma paraoxonase/arylesterase *Analytical biochemistry* 180:242-247
- HEAL and PAN Europe (2019) Chlorpyrifos residues in fruits The case for a Europe-wide ban to protect consumers. https://www.pan-europe.info/sites/pan-europe.info/files/June%202019%20-%20PAN%20HEAL%20Briefing%20chlorpyrifos_web.pdf. Accessed 13, December 2020
- Heilmair R, Eyer F, Eyer P (2008) Enzyme-based assay for quantification of chlorpyrifos oxon in human plasma *Toxicology letters* 181:19-24
- Hongsibsong S, Prapamontol T, Xu T, Hammock BD, Wang H, Chen Z-J, Xu Z-L (2020) Monitoring of the organophosphate pesticide chlorpyrifos in vegetable samples from local markets in Northern Thailand by developed Immunoassay *International Journal of Environmental Research and Public Health* 17:4723
- Huen K, Harley K, Bradman A, Eskenazi B, Holland N (2010) Longitudinal changes in PON1 enzymatic activities in Mexican–American mothers and children with different genotypes and haplotypes *Toxicology and applied pharmacology* 244:181-189
- IPCS (2005) Chemical-specific adjustment factors for interspecies differences and human variability: guidance document for use of data in dose/concentration-response assessment. In: Chemical-specific adjustment factors for interspecies differences and human variability: guidance document for use of data in dose/concentration-response assessment. pp 96-96
- Kaushik R, Rosenfeld CA, Sultatos L (2007) Concentration-dependent interactions of the organophosphates chlorpyrifos oxon and methyl paraoxon with human recombinant acetylcholinesterase *Toxicology and applied pharmacology* 221:243-250
- Knaak JB, Dary CC, Power F, Thompson CB, Blancato JN (2004) Physicochemical and biological data for the development of predictive organophosphorus pesticide QSARs and PBPK/PD models for human risk assessment *Critical reviews in toxicology* 34:143-207
- Koukouritaki SB, Manro JR, Marsh SA, Stevens JC, Rettie AE, McCarver DG, Hines RN (2004) Developmental expression of human hepatic CYP2C9 and CYP2C19 *Journal of Pharmacology and Experimental Therapeutics* 308:965-974
- Lane RM, Potkin SG, Enz A (2006) Targeting acetylcholinesterase and butyrylcholinesterase in dementia *International Journal of Neuropsychopharmacology* 9:101-124
- Lang T, Klein K, Fischer J, Nüssler AK, Neuhaus P, Hofmann U, . . . Zanger UM (2001) Extensive genetic polymorphism in the human CYP2B6 gene with impact on expression and function in human liver *Pharmacogenetics and Genomics* 11:399-415
- Li B, Sedlacek M, Manoharan I, Boopathy R, Duysen EG, Masson P, Lockridge O (2005) Butyrylcholinesterase, paraoxonase, and albumin esterase, but not carboxylesterase, are present in human plasma *Biochemical pharmacology* 70:1673-1684
- Li M, Gehring R, Riviere JE, Lin Z (2017) Development and application of a population physiologically based pharmacokinetic model for penicillin G in swine and cattle for food safety assessment *Food and Chemical Toxicology* 107:74-87
- Ma T, Chambers JE (1995) A kinetic analysis of hepatic microsomal activation of parathion and chlorpyrifos in control and phenobarbital-treated rats *Journal of biochemical toxicology* 10:63-68
- Mosquin PL, Licata AC, Liu B, Sumner SC, Okino MS (2009) Reconstructing exposures from small samples using physiologically based pharmacokinetic models and multiple biomarkers *Journal of exposure science & environmental epidemiology* 19:284-297
- Ning J, Rietjens IMCM, Strikwold M (2019) Integrating physiologically based kinetic (PBK) and Monte Carlo modelling to predict inter-individual and inter-ethnic variation in bioactivation and liver toxicity of lasiocarpine *Archives of toxicology* 93:2943-2960
- Nolan R, Rick D, Freshour N, Saunders J (1984) Chlorpyrifos: pharmacokinetics in human volunteers *Toxicology and applied pharmacology* 73:8-15
- O'Neil D (1999) Blood components. https://web.archive.org/web/20130605052544/http://anthro.palomar.edu/blood/blood_components.htm. Accessed 15 March 2021

- Poet TS, Timchalk C, Bartels MJ, Smith JN, McDougal R, Juberg DR, Price PS (2017) Use of a probabilistic PBPK/PD model to calculate Data Derived Extrapolation Factors for chlorpyrifos Regulatory Toxicology and Pharmacology 86:59-73
- Poet TS, Wu H, Kousba AA, Timchalk C (2003) In vitro rat hepatic and intestinal metabolism of the organophosphate pesticides chlorpyrifos and diazinon Toxicological Sciences 72:193-200
- Proctor N, Tucker G, Rostami-Hodjegan A (2004) Predicting drug clearance from recombinantly expressed CYPs: intersystem extrapolation factors Xenobiotica 34:151-178
- Sams C, Cocker J, Lennard M (2004) Biotransformation of chlorpyrifos and diazinon by human liver microsomes and recombinant human cytochrome P450s (CYP) Xenobiotica 34:861-873
- Satoh T, Gupta RC (2011) Anticholinesterase pesticides: metabolism, neurotoxicity, and epidemiology. John Wiley & Sons,
- Shi M, Bouwmeester H, Rietjen IMCM, Strikwold M (2020) Integrating in vitro data and physiologically based kinetic modeling-facilitated reverse dosimetry to predict human cardiotoxicity of methadone Archives of toxicology 94:2809-2827
- Simcyp (2016a) Blood to Plasma Partition Ratio (B/P). <https://members.simcyp.com/account/tools/BP/>. Accessed 27 March 2021
- Simcyp (2016b) Simcyp prediction tools-fu. <https://members.simcyp.com/account/tools/fuc/>. Accessed 27 March 2021
- Smith JN, Hinderliter PM, Timchalk C, Bartels MJ, Poet TS (2014) A human life-stage physiologically based pharmacokinetic and pharmacodynamic model for chlorpyrifos: development and validation Regulatory Toxicology and Pharmacology 69:580-597
- Smith JN, Timchalk C, Bartels MJ, Poet TS (2011) In vitro age-dependent enzymatic metabolism of chlorpyrifos and chlorpyrifos-oxon in human hepatic microsomes and chlorpyrifos-oxon in plasma Drug metabolism and disposition 39:1353-1362
- Strikwold M, Spengelink B, Woutersen RA, Rietjens IMCM, Punt A (2017) Development of a combined in vitro physiologically based kinetic (PBK) and Monte Carlo modelling approach to predict interindividual human variation in phenol-induced developmental toxicity Toxicological sciences 157:365-376
- The Dow Chemical Company Dow ap Chlorpyrifos. <https://corporate.dow.com/en-us/news/press-releases/dow-ap-chlorpyrifos.html>. Accessed 13, December 2020
- ThermoFisher Scientific (2020) Pierce™ BCA Protein Assay Kit. https://www.thermofisher.com/document-connect/document-connect.html?url=https%3A%2F%2Fassets.thermofisher.com%2FTFS-Assets%2FSLSG%2Fmanuals%2FMAN0011430_Pierce_BCA_Protein_Asy_UG.pdf&title=VXNlciBHdWlkZTogUGlcmNlIEJDQSBQcm90ZWluIEFzc2F5IEtpdA. Accessed 21 June 2021
- Timchalk C, Nolan R, Mendrala A, Dittenber D, Brzak K, Mattsson J (2002) A physiologically based pharmacokinetic and pharmacodynamic (PBPK/PD) model for the organophosphate insecticide chlorpyrifos in rats and humans Toxicological Sciences 66:34-53
- Tracy TS, Chaudhry AS, Prasad B, Thummel KE, Schuetz EG, Zhong X-b, . . . Shireman LM (2016) Interindividual variability in cytochrome P450-mediated drug metabolism Drug Metabolism and Disposition 44:343-351
- USEPA (1999) Data Evaluation Record Study Type: Special Non-Guideline Assessment for RBC Cholinesterase in Humans. <https://archive.epa.gov/scipoly/sap/meetings/web/pdf/kisickider.pdf>. Accessed 27 March 2021
- USEPA (2011) Preliminary Human Health Risk Assessment. <https://www.regulations.gov/document?D=EPA-HQ-OPP-2008-0850-0025>. Accessed 27 March 2021
- USEPA (2014) Chlorpyrifos: Revised Human Health Risk Assessment for Registration Review. Chlorpyrifos: Revised Human Health Risk Assessment for Registration Review. Accessed 27 March 2021
- USEPA (2019) Benchmark Dose Software (BMDS) Version 3 Release History. <https://www.epa.gov/bmbs/benchmark-dose-software-bmbs-version-3-release-history>. Accessed 10 April 2021

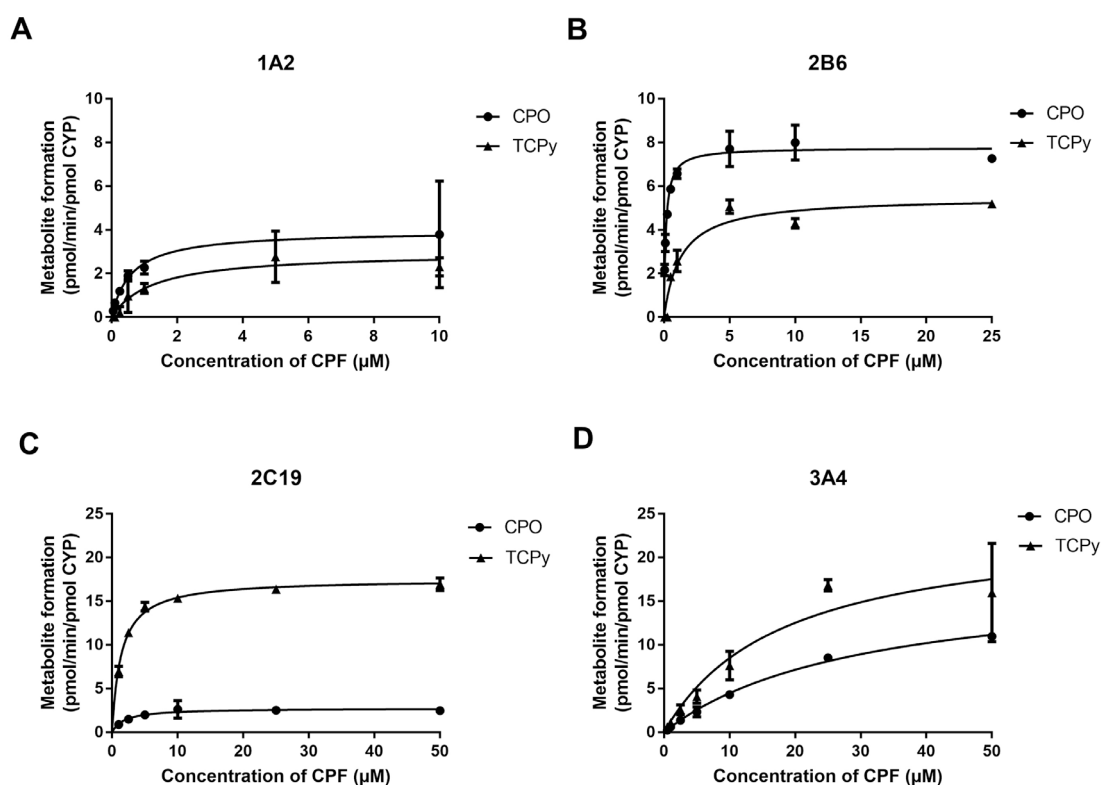
- Venkatakrishnan K, von Moltke LL, Greenblatt DJ (2001) Human drug metabolism and the cytochromes P450: application and relevance of in vitro models *The Journal of Clinical Pharmacology* 41:1149-1179
- Westlind-Johnsson A, Malmebo S, Johansson A, Otter C, Andersson TB, Johansson I, . . . Ingelman-Sundberg M (2003) Comparative analysis of CYP3A expression in human liver suggests only a minor role for CYP3A5 in drug metabolism *Drug Metabolism and Disposition* 31:755-761
- Zhang X, Tsang AM, Okino MS, Power FW, Knaak JB, Harrison LS, Dary CC (2007) A physiologically based pharmacokinetic/pharmacodynamic model for carbofuran in Sprague-Dawley rats using the exposure-related dose estimating model *Toxicological Sciences* 100:345-359
- Zhao S, Kamelia L, Boonpawa R, Wesseling S, Spenkelink B, Rietjens IMCM (2019) Physiologically based kinetic modeling-facilitated reverse dosimetry to predict in vivo red blood cell acetylcholinesterase inhibition following exposure to chlorpyrifos in the Caucasian and Chinese population *Toxicological Sciences* 171:69-83
- Zhao S, Wesseling S, Spenkelink B, Rietjens IMCM (2021) Physiologically based kinetic modelling based prediction of in vivo rat and human acetylcholinesterase (AChE) inhibition upon exposure to diazinon *Archives of Toxicology*:1-21

Supplementary materials

For convenience, **Supplementary material I** can be found at the following link:

https://drive.google.com/file/d/1RizslAUCLgP_Tr8GZ6I9GUAZZYH4rwTK/view?usp=sharing

Supplementary material II

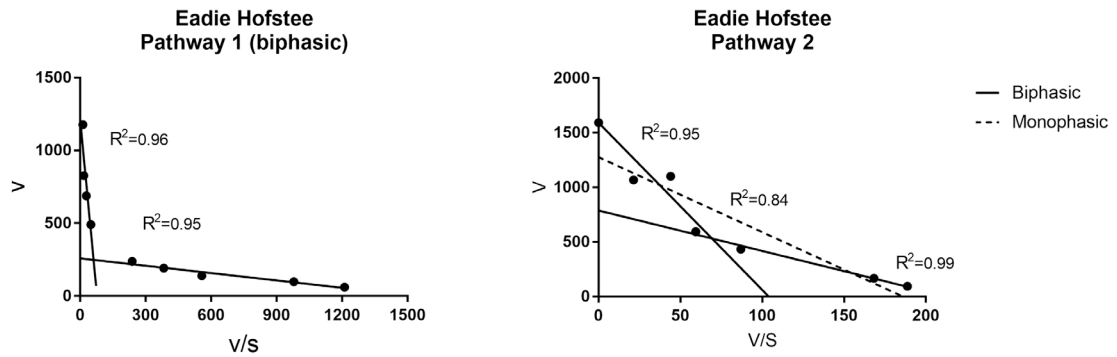


CYP450-mediated CPF concentration-dependent formation of TCPy (filled triangle) and CPO (filled circle) in incubations with human supersomeTM CYP1A2 (A), CYP2B6 (B), CYP 2C19 (C) and CYP3A4 (D). Data points represent mean \pm SD of two experiments for each conversion.



Supplementary material III

Eadie-Hofstee plot



Eadie-Hofstee plot (V_{max} versus V_{max}/CPF concentration (V vs V/S)) for (A) pathway 1 (biphasic) and (B) pathway 2 (for both monophasic and biphasic).

Supplementary material IV

Kinetic parameters (V_{max} and K_m) and catalytic efficiency (CE) (calculated as V_{max}/K_m) for the detoxification of CPO to TCPy in incubations with plasma from 25 Caucasian individuals. Data represent mean of two experiments for each parameter.

Number	Gender	Age	Total protein ^a	$K_{m(app)}$ ^b	$V_{max(app)}$ ^c	V_{max}^d	CE ^e	Scaled V_{max}^f	Scaled CE ^g
1	Male	64	73.3	388.3	21.78	1596	4.1	291247	750.1
2	Male	65	71.2	310.4	17.32	1233	4.0	224952	724.7
3	Male	56	75.9	379.7	32.15	2439	6.4	445176	1172.4
4	Male	52	71.1	317.1	22.39	1591	5.0	290427	915.9
5	Male	51	72.4	637.6	45.36	3284	5.2	599306	939.9
6	Male	57	80.9	327.1	23.22	1878	5.7	342626	1047.5
7	Female	25	80.3	152.3	14.99	1203	7.9	219543	1441.5
8	Female	38	78.0	227.8	21.31	1663	7.3	303506	1332.3
9	Female	38	78.5	282.8	27.46	2157	7.6	393583	1391.7
10	Female	32	82.0	258.7	28.9	2370	9.2	43441	1671.6
11	Female	22	75.4	205.1	17.42	1314	6.4	239710	1168.7
12	Female	46	92.0	299.3	26.75	2461	8.2	449105	1500.5
13	Female	51	72.8	225.7	20.58	1498	6.6	273437	1211.5
14	Female	75	72.8	357.5	28.36	2064	5.8	376692	1053.7
15	Female	55	74.2	187.3	24.79	1840	9.8	335867	1793.2
16	Female	53	80.8	247.7	11.28	912	3.7	166366	671.6
17	Female	50	71.4	282	32.03	2287	8.1	417377	1480.1
18	Female	58	74.6	200.7	15.18	1132	5.6	206569	1029.2
19	Male	48	73.0	249.8	18.21	1329	5.3	242612	971.2
20	Male	49	84.9	307.6	24.85	2111	6.9	385226	1252.4
21	Male	44	79.6	283.4	23.05	1835	6.5	334943	1181.9
22	Male	34	71.8	237.6	24.05	1726	7.3	315041	1325.9
23	Male	47	89.0	373.9	24.05	2141	5.7	390628	1044.7
24	Male	28	82.9	269.7	28.44	2357	8.7	430169	1595.0
25	Male	41	75.7	236.5	22.13	1676	7.1	305884	1293.4

^a mg/ml

^b μ M

^c nmol/min/mg plasma protein

^d V_{max} (nmol/min/ml plasma), calculated by multiplying $V_{max (app)}$ (nmol/min/mg plasma protein) with total protein content (mg/ml)

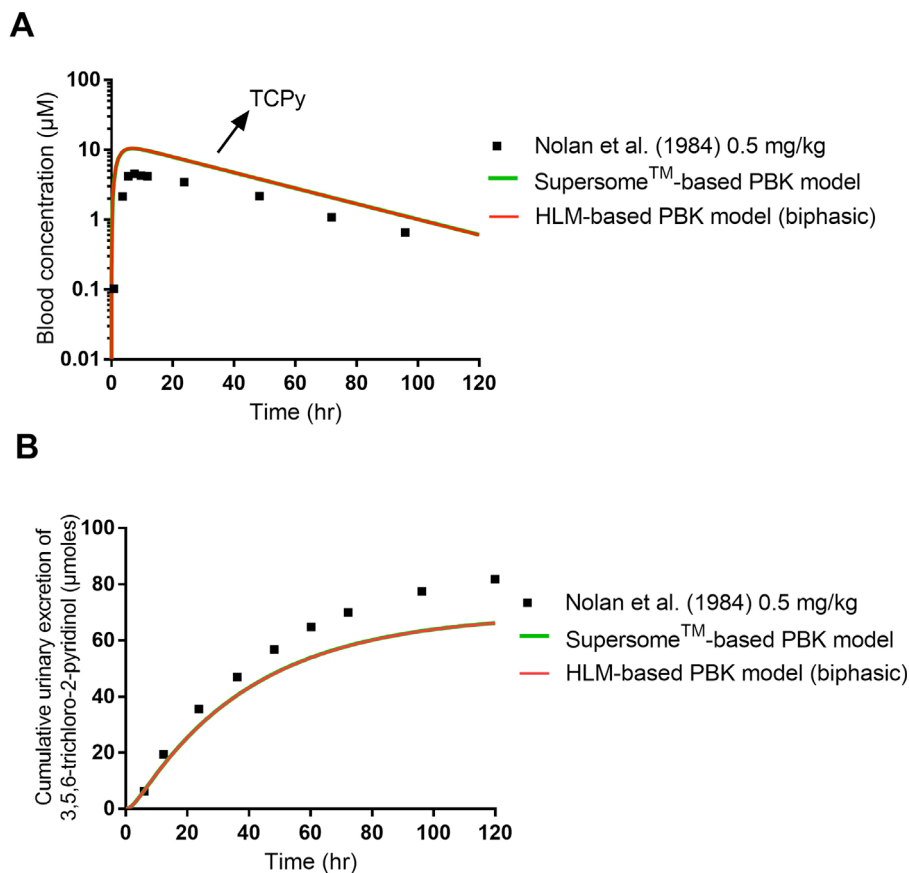
^e CE = catalytic efficiency (ml/min/ ml plasma), calculated as V_{max} (nmol/min/ml plasma) / $K_{m(app)}$ (μ M)

^f Scaled V_{max} (μ mol/hr/plasma), calculated based on Eq 7

^g Scaled CE (l/hr/plasma), calculated as scaled V_{max} (μ mol/hr/plasma) / $K_{m(app)}$ (μ M)



Supplementary material V

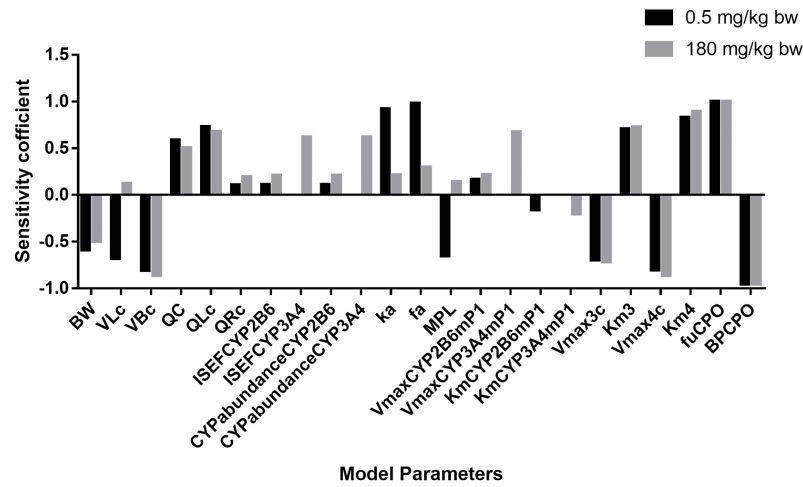


5

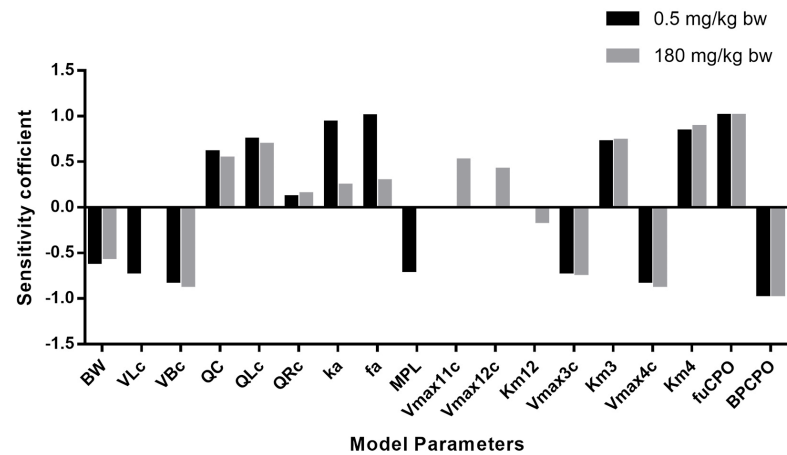
Comparison between reported in vivo data and PBK model predictions for (A) time-dependent blood concentrations of TCPy at a dose of 0.5 mg/kg bw (Nolan et al. 1984), (B) time-dependent urinary TCPy excretion at a dose of 0.5 mg/kg bw (Nolan et al. 1984)

Supplementary material VI

A



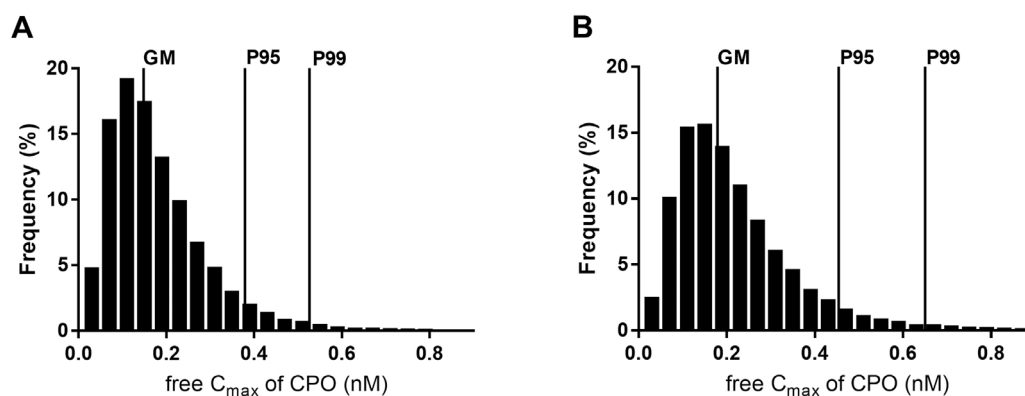
B



Sensitivity analysis for the predicted free blood C_{max} concentration of CPO at a low dose level of CPF of 0.5 mg/kg and a high dose level of 180 mg/kg bw by the Supersome™ CYP-based PBK model (A) and the HLM-based PBK model (biphasic) (B). The parameters represent: BW body weight, VLc fraction of liver tissue, VBc fraction of blood, QC cardiac output, QLc fraction of blood flow to liver, QRc fraction of blood flow to richly perfused tissue, ISEFCYP2B6 intersystem extrapolation factors for CYP2B6, ISEFCYP3A4 intersystem extrapolation factors for CYP3A4, CYPabundance2B6 average endogenous abundance (pmol CYP/mg microsomal protein) of CYP2B6 isoform in human liver microsome, CYPabundance3A4 average endogenous abundance (pmol CYP/mg microsomal) of CYP3A4 isoform in human liver microsome, Ka first-order rate constant for absorption CPF from stomach into liver, fa fractional absorption, MPL liver microsomal protein yield, VmaxCYP2B6mP1 maximum rate for conversion of CPF to CPO by CYP2B6, VmaxCYP3A4mP1 maximum rate for conversion of CPF to CPO by CYP3A4, KmCYP2B6P1 Michaelis Menten constant for conversion of CPF to CPO by CYP2B6, KmCYP3A4P1 Michaelis Menten constant for conversion of CPF to CPO by CYP3A4, Vmax11c maximum rate for conversion of CPF to CPO at low concentration range by HLM, Vmax12c maximum rate for conversion of

CPF to CPO at high concentration range by HLM, K_{m12} Michaelis Menten constant for conversion of CPF to CPO at high concentration range by HLM, V_{max3c} maximum rate for conversion of CPO to TCPy by HLM, K_{m3} Michaelis Menten constant for conversion of CPO to TCPy by HLM, V_{max4c} maximum rate for conversion of CPO to TCPy by HP, K_{m4} Michaelis Menten constant for conversion of CPO to TCPy by HP, f_u CPO free fraction of CPO in vivo, BPCPO blood to plasma ratio of CPO.

Supplementary material VII



Frequency distribution for the predicted blood free maximum concentration (C_{max}) of CPO after a single oral CPF dose of 0.47 mg/kg bw for 58792 individuals using the Supersome™ CYP-based PBK model approach (A), and 9712 individuals using the HLM-based PBK model approach (biphasic) (B), obtained by taking variation in the CYP abundance, V_{max} and K_m into account in the Monte Carlo simulation. The GM, P95 and P99 represent the geometric mean, the 95th and the 99th percentile of the distribution.

Supplementary material VIII

Comparison of predicted BMDL₁₀ values from the present study to the reported BMDL₁₀ value established by USEPA (2014)

	Prediction			Reported
	Supersome™ CYP-based approach	HLM-based approach (non-biphasic)	HLM-based approach (biphasic)	EPA BMDL ₁₀ (derive from human PBK model)
BMDL₁₀ (mg/kg bw)	0.25	1.55	0.26	0.47

Chapter 6

General discussion
and
future perspectives

Overview of main findings

Organophosphate (OP) pesticides make up one of the major groups of pesticides used primarily in agriculture, horticulture, or residential applications to control pests. As neurotoxicants, their potential effects on the human nervous system are of concern. To safeguard public health, numerous risk assessments have been conducted for different OP pesticides, and their corresponding points of departure (PODs) have been derived based on red blood cell (RBC) acetylcholinesterase (AChE) inhibition observed in experimental animals following OP pesticide exposure as the critical endpoint for the adverse effects (EFSA 2006; EFSA 2014a; USEPA 2016b; USEPA 2016c). However, the question may arise as to what extent the POD derived from an *in vivo* animal study, and its downstream health-based guidance value (HBGV) obtained by applying the default uncertainty factor (UF) of 100, provides adequate protection for the human population. Therefore, development of a method that enables predicting the POD based on human data and deriving a chemical-specific adjustment factor (CSAF) for calculating an HBGV is of importance in human risk assessment of OP pesticides. To this end, the aim of the present thesis was to investigate whether new approach methodologies (NAMs) and especially physiologically based kinetic (PBK) model-based reverse dosimetry using *in vitro* and *in silico* data, in combination with Monte Carlo simulations or the toxic equivalency factor (TEF) approach, can be used to derive PODs and CSAF values for characterizing inter-ethnic (**Chapter 2**), inter-species (**Chapter 3 and 4**) and inter-individual (**Chapter 5**) differences in toxicokinetics and RBC AChE inhibition following OP pesticide single acute oral exposure.

6

In **Chapter 2**, PBK models for one of the most widely used OP pesticides, namely chlorpyrifos (CPF) were developed for both the Chinese and Caucasian population. To do so, reported ethnicity-specific anatomical and physiological parameters (Brown et al. 1997; NHFPC 2007a; NHFPC 2007b; NHFPC 2014), *in silico* calculated physico-chemical parameters (DeJongh et al. 1997), and experimentally derived ethnicity-specific kinetic parameters determined by *in vitro* incubations with relevant tissue fractions of the two populations, were incorporated into corresponding PBK models. These PBK models were subsequently used to convert concentration-response curves for human RBC AChE inhibition reported by Eyer et al. (2009) to the corresponding *in vivo* dose-response curves by reverse dosimetry. The results obtained revealed a marked inter-ethnic difference in toxicokinetics of CPF, with a slower CPF bioactivation and faster detoxification of its active metabolite chlorpyrifos-oxon (CPO) in the

Chinese than in Caucasian population. These differences could be explained by the inter-ethnic variation in enzyme profiles and enzyme activities involved in biotransformation of CPF and CPO. The differences resulted in 5- to 6-fold lower POD values for the Caucasian than the Chinese population. The difference in POD values between the two populations reflects a lower risk of CPF for the Chinese than the Caucasian population at similar levels of exposure. The inter-ethnic variation in toxicokinetics of CPF, also resulted in 2-fold lower cumulative urinary levels of 3,5,6-trichloro-2-pyridinol (TCPy), used as a biomarker for CPF exposure, in Chinese compared to Caucasians at the same dose levels, implying the importance of taking possible inter-ethnic differences into account when characterizing CPF exposure for different ethnic groups on the basis of their urinary biomarker levels.

To further explore whether the PBK-based reverse dosimetry could also be successfully applied for establishment of PODs for other OP pesticides, a study was performed for another OP pesticide, profenofos (PFF), which is described in **Chapter 3**. In this study the possible inter-species differences between rat and human in PFF-related RBC AChE inhibition were assessed. The PBK models for the two species were developed using a similar strategy as applied in **Chapter 2**. The concentration-dependent inhibition of rat and human RBC AChE was determined in vitro using recombinant human AChE enzyme (rhAChE) and rat AChE enzyme extracted from RBC. The concentration-response curves thus obtained were translated using PBK model-based reverse dosimetry to predicted dose-dependent RBC AChE inhibition curves for rat and human in vivo. From the predicted dose-response curves, the benchmark dose lower confidence limits for 10% inhibition (BMDL₁₀) values were derived by benchmark dose (BMD) analysis as PODs. The obtained results show that the predicted POD value derived from the human data was 45-fold lower than that derived from the rat data, indicating human to be more sensitive than rat. Such differences appeared mainly due to marked inter-species differences in toxicokinetics of PFF, with rat being more efficient in hepatic and plasma detoxification of PFF than human, while the difference in toxicodynamics appeared limited as reflected by similar in vitro concentration-response curves for RBC AChE inhibition in the two species. In conclusion, **Chapter 3** demonstrated the applicability of PBK-model based reverse dosimetry to predict in vivo RBC AChE inhibition by PFF, providing another proof-of-principle that integrating in vitro toxicity data and PBK model-based reverse dosimetry is a promising strategy for non-animal-based safety assessment of OP pesticides.

Chapter 4 further challenged the applicability of PBK-based reverse dosimetry, by investigating the possibility of using this approach to predict the inhibitory effect on RBC

AChE for an OP pesticide for which both the parent OP pesticide and its metabolite are active AChE inhibitors. This required integrating the TEF methodology into the PBK model. Diazinon (DZN) was selected as model compound based on the fact that both DZN and its bioactive metabolite diazoxon (DZO) are able to inhibit AChE. Similar as in **Chapter 3**, the possible inter-species differences in sensitivity for RBC AChE inhibition of rat and human following DZN exposure were characterized and used to derive a POD. To enable definition of the required TEF values, in vitro concentration-dependent inhibition curves of rat and human RBC AChE by DZN and DZO were defined. The TEF values were calculated based on the ratio of the half maximal inhibitory concentration (IC₅₀) derived from these in vitro concentration-RBC AChE inhibition curves. Moreover, the PBK models and their input parameters for the two species were defined using in silico and in vitro methods. To further describe the combined free blood concentration of DZN plus DZO at the target site (RBC AChE), the free effective blood maximum concentration of DZN plus DZO was expressed in DZO equivalents by multiplying the respective concentrations with the corresponding TEF values, and adding up the resulting DZO equivalent values. Use of the TEF coded PBK model enabled calculation of the external exposure dose of DZN that would produce a defined combined free DZN plus DZO concentration expressed in DZO equivalents in human/rat blood, and to translate the observed inhibition effects of DZO in the in vitro concentration-response curve expressed in free in vitro DZO equivalents to the in vivo situation. From the predicted in vivo dose-response curves, the POD (BMDL₁₀) values were derived using a BMD analysis. The obtained results show that the free blood concentration of DZN contributes substantially to the DZO equivalents, indicating it is of critical importance to take internal free DZN concentrations into account in addition to the concentrations of its active oxon metabolite DZO when conducting a risk assessment for DZN. Besides, although no inter-species difference was observed in the in vitro concentration-response curves for rat or human RBC AChE inhibition, marked inter-species differences in toxicokinetics were observed, as rat displayed a faster metabolic rate for bioactivation and detoxification of DZN and/or DZO than human, resulting in a 6-fold lower POD in human than in rat. Altogether, this chapter demonstrated that use of the TEF coded PBK model-based reverse dosimetry can predict combined effect of DZN and DZO on RBC AChE inhibition, providing a proof-of-principle for derivation of a point of departure (POD) in risk assessment for an OP pesticide for which both the parent OP and its oxon metabolite have the ability to contribute substantially to RBC AChE inhibition.

In **Chapter 5**, the inter-individual variation in metabolism of CPF and its resulting RBC AChE inhibition was studied in further detail. A CSAF for inter-individual differences in kinetics (HK_{AF}) was quantified on the basis of the PBK model for CPF developed for Caucasians (**Chapter 2**), in combination with Monte Carlo simulation. To define the metabolic variation in the PBK model, two different approaches were developed and compared, namely a SupersomeTM cytochrome P450 (CYP)-based PBK model approach and a human liver microsome (HLM)-based PBK model approach. SupersomeTM CYP-derived kinetic data revealed that bioactivation of CPF exhibits biphasic kinetics due to distinct differences in the K_m value for CYPs involved. Therefore, to accurately predict the toxicokinetics of CPF, the HLM-based PBK model was refined to include biphasic kinetics in the bioactivation of CPF. In the SupersomeTM CYP-based approach, the variation in conversion was calculated using SupersomeTM CYP-derived kinetic data together with reported values for the coefficients of variation (CVs) in CYP abundance together with applying the intersystem extrapolation factors (ISEFs) to scale CYP isoform activity in the SupersomeTM to HLM and eventually to the in vivo situation. In the HLM-based approach, the variation was described by the reported CV of HLM-related kinetic data for CPF in 30 individuals (Smith et al. 2011). In the subsequent step, Monte Carlo simulations were performed to generate a population distribution of maximum free blood concentrations (C_{max}) of CPO (the active metabolite of CPF). No substantial difference was found in the predicted C_{max} of CPO in the two approaches, implying that there is a good match between the two procedures. From the concentration distributions obtained, the HK_{AF} values were calculated by dividing the tail (95th or 99th) of the distribution by its corresponding geometric mean (GM) at an oral dose of 0.47 mg/kg bw, which represents the BMDL₁₀, and is used as a POD by the United States Environmental Protection Agency (USEPA) for setting a health based guidance value for CPF (USEPA 2014a). Comparison of the HK_{AF} derived by the two approaches indicates no difference, with both values at the 99th percentile being slightly higher than the default UF of 3.16, reflecting possible inadequate protection for extreme sensitive adult individuals by this default UF. To further evaluate the performance of the two approaches, the in vitro CPO induced concentration-dependent rhAChE inhibition curve was extrapolated to its corresponding in vivo dose-response curves, also taking the inter-individual differences into account, resulting in comparable predictions when using the two approaches with an only 1.04-fold difference in the BMDL₁₀ values obtained. Altogether, the results presented in **Chapter 5** demonstrated that use of either a SupersomeTM CYP-based approach or an HLM-based approach, together with Monte Carlo simulations and PBK model-based reverse dosimetry provide a promising tool for

characterization of inter-individual variation in metabolism and sensitivity toward RBC AChE inhibition following CPF exposure. Given that the Supersome™ CYP-based approach was able to identify the biphasic kinetics, which appeared to be less evident when using the HLM-based approach, it is concluded that the Supersome™ CYP-based approach seems to be the preferred option for defining inter-individual differences in CYP-mediated kinetics.

In the following sections, the results of the present thesis, the possibilities and limitations of using of the NAM based on PBK model-based reverse dosimetry of in vitro data to predict in vivo dose response curves for risk assessment are discussed, and some future perspectives are provided.

General discussion and future perspectives

Regarding the results obtained and approaches applied in the present thesis, several topics can be considered that may be of relevance for further research on the use of NAMs in the risk assessment of OP pesticides.

These topics include:

- The in vitro system selected for studying AChE inhibition
- The dose metric selected for performing reverse dosimetry based quantitative in vitro to in vivo extrapolation (QIVIVE)
- The application of PBK models for assessing inter-ethnic variation
- The possibility of using TEF coded PBK models for predicting combined inhibitory effects of an OP pesticide and its bioactive metabolite
- The comparison of Supersome™ CYP-based and HLM-based approaches for assessing inter-individual variation
- The comparison of in vitro and in vivo results
- The implications for risk assessment
- The future perspectives

The in vitro system selected for studying AChE inhibition

The present thesis applied the in vitro AChE inhibition assay to study inhibitory effects of OP pesticides and/or their metabolites on RBC AChE activity, which was further translated to

describe *in vivo* RBC AChE inhibition in target groups by PBK model-facilitated reverse dosimetry based QIVIVE. AChE inhibition in RBC has been widely used as a surrogate biomarker for AChE inhibition in the nervous system to derive PODs for human risk assessment for OP pesticides (EFSA 2014a; USEPA 2011; USEPA 2014a; USEPA 2016b; USEPA 2016c). This is based on the fact that the measurement of AChE inhibition in the nervous system (e.g. brain) is not easily experimentally accessible, and that AChE in RBC has a high functional similarity (e.g. activity) to that in the nervous system, so that changes in RBC AChE activity may reflect changes in brain AChE activity (King and Aaron 2015; Worek et al. 2012). To investigate the inhibitory potency of OP pesticides and/or their metabolites on RBC AChE, relevant tissue fractions such as whole blood, isolated RBC or extracted RBC AChE enzyme were often used (Das et al. 2006; Eyer et al. 2009; Fakhri-Bafghi et al. 2016; Kasteel et al. 2020). It is important to mention that, in addition to these tissue fractions, rhAChE can also be used to investigate the inhibitory potency of OP pesticides and/or their metabolites on human RBC AChE activity. Use of rhAChE is considered simple (easy to use because no lysing, washing and extracting steps are required) and stable (the measurement of enzyme activity will not be affected by hemoglobin which can be, in case of the human whole blood, RBC or extracted RBC AChE enzyme) (Assis et al. 2018; George and Abernethy 1983). Besides, only a very low level of albumin (0.1 mg/ml) was required to be added to the *in vitro* medium to stabilize the rhAChE when performing the assay, which was found to have no substantial influence on the effective concentration of OP pesticides and/or metabolites (**Chapter 3, 4 and 5**), therefore minimizing the potential effect of protein binding on the intrinsic inhibitory potency results. The low disturbance by protein binding in the AChE inhibition assay using rhAChE is also reflected by the observation that the inhibitory potency of OP pesticides measured using whole blood (Kasteel et al. 2020) is lower than what is observed when using rhAChE (**Chapter 3, 4 and 5**). Such difference in potency can be offset by taking protein binding of OP pesticides in blood into account, as demonstrated by the comparable IC₅₀ of different OP pesticides in incubations with rhAChE (**Chapter 3, 4 and 5**) to their IC₅₀s in human whole blood (Kasteel et al. 2020). This comparison indicates that rhAChE and native human RBC have a comparable *in vitro* sensitivity towards OP pesticides. Hence, use of rhAChE is considered to be adequate for investigating and representing the *in vitro* intrinsic inhibitory profile of OP pesticides on native human RBC AChE. For assessing RBC AChE inhibition in rat, extracted rat RBC AChE was used in the present thesis because at the time of the study, recombinant rat AChE was not commercially available. Use of extracted rat RBC AChE is expected to have a similar effect on the concentration of test compounds in the assay

as rhAChE, since there are no blood protein components, except RBC AChE being present in the final extracted enzyme sample. As mentioned above, the presence of hemoglobin in extracted RBC AChE enzyme may hinder the measurement of AChE activity, but this appeared not relevant for the rat RBC preparation applied, since no reddish color was observed in the final obtained rat RBC AChE sample, and the background absorption in the measurement was corrected by the absorbance value in the test samples with that of the positive control (in which the enzyme activity was totally inhibited) during data analysis. Thus, use of extracted rat RBC AChE in the present study was regarded as adequate.

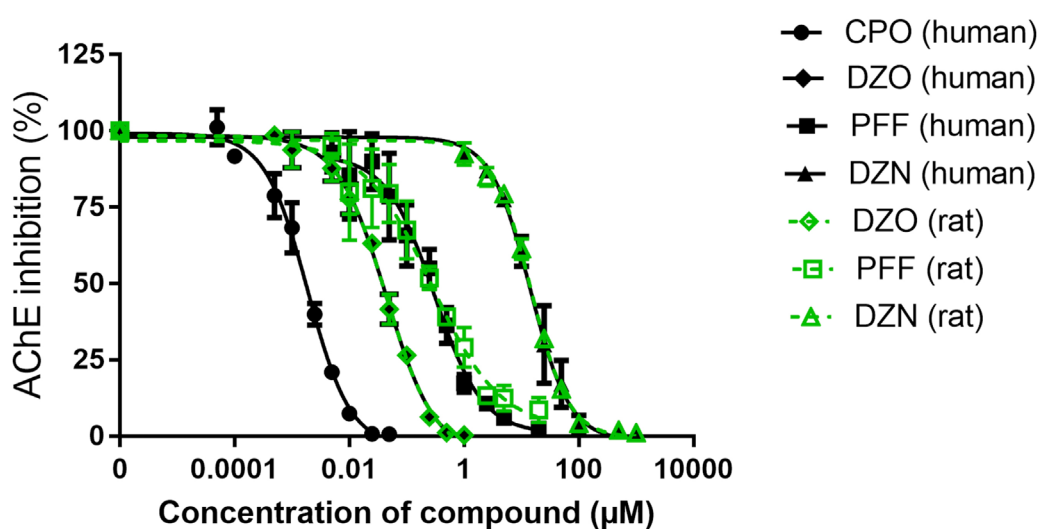


Fig 1. Inhibitory effect of increasing concentration of CPO (circle), DZO (diamond), PFF (square) and DZN (triangles) on activity of rat RBC AChE (green) or rhAChE (black) at 37 °C.

6

To obtain an overview of the intrinsic inhibitory potency of the different OP pesticides and their active oxon metabolites on rat RBC AChE and rhAChE, the relevant results obtained in the present thesis (**Chapter 3, 4 and 5**) were summarized in Figure 1. The overview thus obtained corroborates that the oxon metabolite (containing a P=O moiety) formed metabolically by CYPs is more potent than the parent OP pesticide (containing a P=S moiety), with the IC₅₀ values of DZO being around 300-fold lower than that of its parent OP pesticide DZN in both rat and human. Although PFF is also a parent OP pesticide, due to the presence of a P=O moiety in its chemical structure, a higher inhibitory potency (47-fold in both rat and human) was observed for PFF compared to DZN. Although not tested in the present thesis, CPF is expected to be less potent than its metabolite CPO, while having similar potency as DZN in human (Li et al. 2019b). Based on previous rhAChE inhibition data (Li et al. 2019b),

CPF can be regarded as equally potent as DZN, and CPO to be more than three orders of magnitude more potent than its parent OP pesticide CPF. The overview also illustrates that generally no inter-species differences in *in vitro* RBC AChE inhibition for rat and human were observed for the different OPs and their metabolites (Figure 1). Altogether, these results indicate that the *in vitro* intrinsic potency for RBC AChE inhibition decreases in the order CPO>DZO>PFF>DZN=CPF in human and rat, and that the presence of a P=O moiety in the chemical structure markedly increases the inhibitory ability towards RBC AChE *in vitro*. The lower potency of OPs with a P=S moiety than those with a P=O moiety can be explained by the lower electronegativity of sulfur compared to oxygen, which results in a lower polarization of the P=S moiety than the P=O moiety, thus leading to a lower reactivity of the P=S containing OPs with the serine hydroxyl group at the active site of AChE (Fukuto 1990). These observations are in line with available knowledge on the structure activity characteristics of OP pesticides (King and Aaron 2015).

As stated above, there was no inter-species difference in the *in vitro* concentration-response curves for OP induced RBC AChE inhibition between rat and human (Figure 1). A similar conclusion has been previously reported for dichlorvos, another OP pesticide (MacGregor et al. 2005). This observation suggests that, when POD values in risk assessment for these OP pesticides were derived using data from an *in vivo* rat study or *in vitro* rat RBC AChE inhibition, the default UF of 2.5 for inter-species differences in toxicodynamics might be reconsidered and/or eliminated. However, this may not hold when other species would be used for characterizing the RBC AChE inhibitory potency of OP pesticides, for example electric eel AChE, which was found to be more sensitive than human RBC AChE toward OP exposure (Kasteel et al. 2020). Therefore, the CSAF for inter-species differences in toxicodynamics (AD_{AF}) should be defined case by case to account for the differences in sensitivity toward OP pesticides mediated RBC AChE inhibition between the species used and human RBC AChE, to prevent under- or over-estimation of the toxicity of OP pesticides in human.

It is important to realize that the rhAChE-based *in vitro* inhibition assay used in the present thesis does not reflect potential human inter-individual variability in RBC AChE inhibition (toxicodynamics) (**Chapter 5**), as the rhAChE is produced by transfecting a specific human AChE gene in human HEK293 cells (Sigma-Aldrich). Such inter-individual differences in toxicodynamics of RBC AChE inhibition by OP pesticides might be limited, since only 2.2-fold and 1.4-fold inter-individual toxicodynamics variability in RBC AChE inhibition were observed for CPO and DZO, respectively, when using whole blood samples from 20

individuals (12 male and 8 female between 24 to 68 year) (Kasteel et al. 2020). Although this suggests that the inter-individual variability in toxicodynamics can be well covered by the default UF of 3.16, it is also important to note that these studies relate to a relatively small number of subjects, and did not include potentially sensitive subpopulations like for example children. Thus, such inter-individual variability in dynamics provide an important topic for future studies, with the in vitro assay for AChE inhibition in RBC or blood samples providing a suitable model to quantify this variability.

Another aspect that needs to be considered is the inter-ethnic difference in RBC AChE inhibition (toxicodynamics). In the present thesis (**Chapter 2**), the inhibition was assumed to be the same for different ethnicities, because of the absence of commercial Chinese RBC AChE relevant tissue fractions. Characterizing potential ethnic differences in RBC AChE inhibition seems a valid topic for the future research which would require use of ethnicity-specific blood or RBC samples.

Another factor that needs to be considered when using the in vitro AChE inhibition assay to define the in vitro concentration-response curves for reverse dosimetry is the temperature used for carrying out the in vitro AChE inhibition assay, as this may have a direct impact on the results. Such potential impact can be illustrated by the results presented in Figure 2. For all three tested OP pesticides or metabolites (Figure 2), the IC₅₀ values obtained at 37 °C were found to be approximately 2-fold lower than those obtained at room temperature, in line with general observations on the effect of temperature on reaction rates (LibreTexts™ 2020; Robinson 2015), indicating the need to use 37 °C as incubation temperature to match the human in vivo body temperature when performing the in vitro AChE inhibition assay, as done in the present thesis.

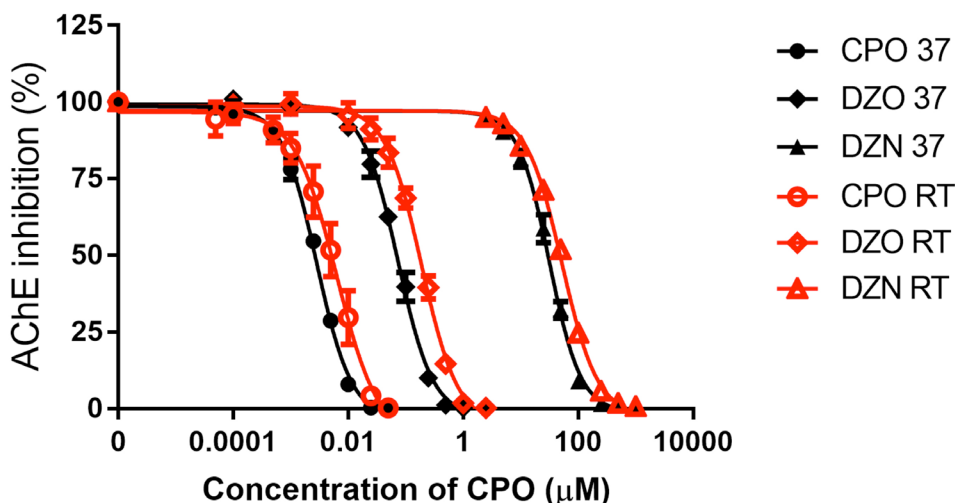


Fig 2. Inhibitory effect of increasing concentration of CPO (circle), DZO (diamond) and DZN (triangle) on activity of rhAChE at room temperature (open symbols) or 37 °C (closed symbols).

Furthermore, the AChE inhibition assay used in the present thesis is an endpoint static assay, in which the concentration-response curve is determined using a fixed incubation time, during which the inhibitory reaction between AChE and the inhibitor (e.g. CPO, DZO) takes place. Available studies (Colovic et al. 2013; Krstić et al. 2008) show that the irreversible inhibition of RBC AChE by OP pesticides is time-dependent, with the amount of inhibited enzyme at a test concentration of OP pesticides being dependent on how long the enzyme is incubated with the OP pesticides, and the time required to reach the maximum inhibition varying with the OP pesticide test concentration. In the present study, 15 min was used as incubation time. One may expect the inhibition level may increase with longer incubation times, potentially resulting in lower inhibitory potency. However, based on the data reported by Colovic et al. (2013) for DZO, this effect appeared limited. For DZO, the inhibition was about 1.1-fold, 1.2-fold and 1.4-fold more at test concentrations of 20 nM, 30 nM and 50 nM, respectively (similar to the concentrations used in the present study that cause approximately 30%, 40% and 50% inhibition of enzyme), when incubated time was increased from 15 to 25 min. An even smaller difference would be expected at the lower concentrations that would induce 10% inhibition, the level of inhibition at which the benchmark response and POD were defined. In addition, the adequacy of the estimation of the inhibition level for different OP pesticides obtained under the conditions used in the present study is supported by the comparable POD values predicted in the present thesis (**Chapter 2, 3, 4 and 5**) and presented in the relevant risk assessment documents (EFSA 2006; EFSA 2014a; JMPR 2007; JMPR 2016; USEPA 2006b; USEPA 2011; USEPA 2014a; USEPA 2016b; USEPA 2016c).

In the present study, inhibition of RBC AChE enzyme activity was used as the endpoint in the *in vitro* assay. Therefore, this does not account for dynamic changes over time in AChE activity including for example AChE synthesis and degradation, implying that the *in vitro* data obtained by the present thesis can be used to predict AChE inhibition following a single external dose level but may be less appropriate for prediction of dynamic influences on the inhibition of AChE activity over time upon repeated exposure. Given that the POD derived in the present thesis is used to set an HBGV for acute exposure, the application of the *in vitro* assay used in the present thesis is considered valid. For investigating possible dynamic aspects influencing the AChE activity and its inhibition upon repeated exposure, other type of methods would be required. One possible approach would be to build an *in silico* pharmacodynamic model, which includes a batch of enzyme related parameters (e.g. synthesis rate, degradation rate, etc) to describe dynamic changes of RBC AChE activity over time following repeated exposure (Westerink 2013). However, use of such an *in silico* dynamic model is often challenged by the availability and reliability of the parameters used in the model. As a result, such models are not yet common practice for most OP pesticides though they have been applied for CPF and DZN previously (Poet et al. 2004; Poet et al. 2017; Timchalk et al. 2002).

In recent years, available studies have raised the concern that neurodevelopmental toxicity (e.g. deficits in working memory, cognitive) may happen at concentrations below those required for inhibiting AChE activity following repeated exposure (Burke et al. 2017), although the mode of action and adverse outcome pathway (AOP) for these other neurodevelopmental toxicities have not yet been elucidated. This issue has been highlighted by the European Food Safety Authority (EFSA 2019) and the USEPA (2016a), indicating the potential inadequacy of using RBC AChE as an endpoint to derive a POD for repeated OP exposure. Recent studies show that use of human induced pluripotent stem cell (hiPSC)-derived neural stem cells (NSCs) may enable detection of other endpoints for neurotoxicity and/or key neurodevelopmental processes for human brain development, providing the possibility to elucidate the mechanisms underlying such potential adverse outcomes upon repeated OP exposure (Barenys and Fritsche 2018; Di Consiglio et al. 2020). However, to what extent these hiPSC models may capture the mechanism underlying the different neurodevelopmental toxicity processes remains to be investigated

The dose metric selected for performing reverse dosimetry based QIVIVE

The dose metric used for the PBK model-facilitated reverse dosimetry is another item to discuss to some further extent. The extrapolation of in vitro concentration-response curves to in vivo dose-response curves is often based on dose metrics such as maximum blood or plasma concentration (C_{\max}) or the area under the plasma/blood concentration time curve (AUC). In general, if the effect is expected to accumulate over sub-chronic or chronic exposure, then using the AUC may be the preferred option, while if the effect occurs following acute exposure or when toxicity is related to exceeding an internal concentration threshold, use of C_{\max} may be more appropriate (Rietjens et al. 2019; USEPA 2014b). In the present thesis, the reverse dosimetry based QIVIVE was conducted on the basis of the predicted blood C_{\max} of CPO (**Chapter 2 and 5**), PFF (**Chapter 3**) and DZO equivalents (**Chapter 4**) obtained from the corresponding developed PBK models. Use of C_{\max} was considered an appropriate dose metric in this case, since the in vitro effect was quantified after a fixed incubation time as a function of the concentration tested, and the critical effect measured represented an effect observed upon single acute exposure. The use of this approach was supported by the fact that the POD values derived from the predicted dose-response curves for each OP pesticide (**Chapter 2, 3, 4 and 5**) based on C_{\max} were found to be comparable to their corresponding reported POD values in the risk assessment documents (EFSA 2006; EFSA 2014a; JMPR 2007; JMPR 2016; USEPA 2006b; USEPA 2011; USEPA 2014a; USEPA 2016b; USEPA 2016c). When using the AUC as the dose metric for the conversion, the predicted $BMDL_{10}$ was far lower or higher than the in vivo obtained $BMDL_{10}$ depending on the time taken for quantification of the AUC. For example, the predicted $BMDL_{10}$ of DZN for adult rat was 9-fold lower (based on in vivo $AUC_{0-\infty}$) or 8-fold higher (based on in vivo $AUC_{0-0.25 \text{ hours}}$, which is the AUC for the in vitro assay incubation time) compared to that of in vivo adult rat data, indicating that conversion based on C_{\max} turned out to be more appropriate.

Another important issue to discuss is the correction for protein binding applied during the QIVIVE, since only the unbound concentration of the OP pesticide is assumed to exert the effect. The protein binding of the OP pesticide in the in vitro medium was considered negligible because only a very low level of albumin (0.1 mg/ml) was present in the in vitro medium to stabilize the enzyme. The study of Heilmair et al. (2008) showed that the presence of such a low level of albumin had no substantial effect on the effective concentration of CPO. This was further supported by the data on the unbound fraction obtained in **Chapter 4** of the present thesis using rapid equilibrium dialysis, showing that 96% of DZO in the in vitro incubation

medium was unbound, suggesting the influence of protein binding on the effective unbound concentration of the OP pesticide in the *in vitro* medium of the AChE inhibition assay to be negligible. Rapid equilibrium dialysis can in theory also be used to determine the unbound fraction of the test chemical in plasma. However, this assay failed for determining the unbound fraction of some OP pesticides and their active metabolite in plasma. For example, in case of DZO, only very low levels of DZO were detected in the plasma and buffer chambers. Similar results were also reported for another tested OP pesticide (CPO) by Foxenberg et al. (2011). Because of the high levels of paraoxonase 1 (PON1) in plasma, it might be speculated that DZO was hydrolyzed by PON1 during the DZO equilibrium dialysis. To prevent such hydrolysis, the extra PON1 inhibitor (ethylenediaminetetraacetic acid disodium salt dihydrate (EDTA) at 10 mM (Heilmair et al. 2008)) was added already 2 hours before and during the dialysis to irreversibly inhibit PON1. By doing so, indeed, the levels of DZO were found to be higher in both chambers, although the recovery was still relatively low (45%), hampering use of this method to detect the fraction unbound of the OP pesticide. One of the possible explanations for the low recovery even in the presence of the PON1 inhibitor could be the non-specific binding of the OP to the reaction apparatus. However, it might not be the only reason as the protein binding in the *in vitro* medium was obtained with an average recovery of 74%. Apparently, other unknown interferences may occur, leading to the extra loss of the compound, although no additional experiments were performed to elucidate further reasons underlying the relatively low recovery. Instead, the unbound fraction of the OP pesticides in plasma were obtained from the literature where the fraction of compound bound to plasma protein was calculated based on the decrease of the eel AChE inhibition rate (Heilmair et al. 2008), or using *in silico* prediction software such as Simcyp (Simcyp 2016) and pkCSM (pkCSM n.d.) on the basis of LogP and/or pKa (ChemAxon) and/or the SMILES string of the OP pesticide under study. Such obtained values obviously do not account for possible inter-species, inter-ethnic or inter-individual variation in the protein binding of the OP pesticide. However, the inter-species and inter-ethnic variation may be limited, as the albumin concentration in different species (rat and human), or different ethnic groups (Chinese and Caucasian) is known to be quite conserved (Heilmair et al. 2008; Tarhoni et al. 2008; Zhou et al. 1990). Also inter-individual variation in albumin concentration may be limited with values ranging from 35 g/l to 50 g/l being reported by the study of Weaving et al. (2016). The potential inter-individual differences induced by such differences in plasma protein levels and resulting protein binding could be included in a future study to refine the predictions for inter-individual variability. Despite the fact that the protein binding of OP pesticides is mainly attributable to albumin in plasma (Heilmair et al. 2008),

available studies (Costa 2006; Jokanović 2009) also show that OP pesticides can bind to B-esterases like butyrylcholinesterase (BuChE) and carboxylesterase (CaE), thus reducing the effective concentration of the OP pesticide. Such potential effect of B-esterases may depend on: (1) the affinity between the enzymes and the respective OP (Chanda et al. 2002); (2) the endogenous level of the enzymes (Chanda et al. 2002; Jokanović M 2020); and (3) the genotype of the enzymes (Eaton et al. 2008). In the present thesis, this potential effect of the B-esterases was not specifically considered. Taking this extra binding to B-esterases into account would result in dose-dependent RBC AChE inhibition at dose levels higher than what is now predicted. This indicates the approach now taken is conservative. However, the comparison of predicted dose-response curves for each OP pesticide with the available *in vivo* data showed a good agreement (**Chapter 2, 3, 4**), thus indicating the effect of B-esterases might be limited if any. Nevertheless, it should be noted that the different B-esterase profiles (e.g. affinity, activity, concentration level, genotypes) in different target groups may introduce additional variability in the inter-species, inter-ethnic and inter-individual variation in sensitivity of humans to OP pesticide induced adverse effects, which could be quantified to a further extent in future studies.

The application of PBK models for assessing inter-ethnic variation

PBK models have been applied for different purposes. This includes for example quantification of inter-ethnic differences in the toxicokinetics and resulting toxicity of the pyrrolizidine alkaloids lasiocarpine and riddelliine and the alkenylbenzene estragole (Ning et al. 2019a; Ning et al. 2017). This inspired the study in the present thesis investigating the usefulness of this approach to characterize inter-ethnic differences in the kinetics of OP pesticides as another group of chemicals of interest. To this end, in **Chapter 2**, PBK model-based reverse dosimetry was used to characterize the inter-ethnic variation in CPF-induced RBC AChE inhibition upon acute single dose exposure of the average Caucasian and Chinese individuals. The inter-ethnic variation in the PBK models was introduced by using ethnicity-specific physiological and kinetic parameters. The anatomical and physiological parameters were obtained from the literature (Brown et al. 1997; NHFPC 2007a; NHFPC 2007b; NHFPC 2014), accounting for ethnicity-specific differences in body weight, cardiac output, tissue volumes and tissue blood flows. Kinetic parameters were obtained using either Chinese or Caucasian pooled liver microsomes, characterizing the possible ethnic difference in hepatic toxicokinetics of CPF. To scale hepatic apparent kinetic data from the microsomal level to the whole liver, the scaling

factor for mg of microsomal protein per gram of liver (MPL) obtained from Caucasian (Barter et al. 2007) was used for both ethnicities, because of the limited information on scaling factors for the Chinese population at that time. Recently a study reported by Li et al. (2019a) compared the MPL values between Chinese and Caucasian, showing no difference in MPL values between Chinese and Caucasian at age 20 to 40. However, an inter-ethnic difference was found at ages above 40 which further increased at older age with the MPL in Caucasian being up to approximately 1.3-fold lower than that for the Chinese. This observation was due to the age-independent MPL values in Chinese and an age-dependent decrease at age >40 years of the MPL values in Caucasian, which theoretically may result in an age-dependent decrease in the maximum velocity (V_{max}) value for bioactivation of CPF and detoxification of CPO for Caucasians, leading to an even larger difference between Chinese and Caucasian at older age than what was predicted in **Chapter 2**.

It is of importance to notice as well that in the PBK model the kinetic data for detoxification of CPO by PON1 in plasma for the Chinese were assumed to be equal to those of Caucasian, due to the lack of commercial Chinese plasma samples. One study (Zhang et al. 2014) pointed out that there is an inter-ethnic difference in allele (L and R genotype) frequencies for the plasma PON1 coding regions L55M and Q192R, with the frequency of L and R being higher in Chinese than Caucasian, providing a potential basis for a higher PON1 activity in the Chinese population, although so far no further comparisons were made of the consequences of these polymorphisms for the endogenous PON1 level and activity. Such a difference however would probably be consistent with the inter-ethnic variation observed in hepatic PON1-mediated CPO detoxification in **Chapter 2**, for which the activity was higher in Chinese than in Caucasian. This observation could be due to a relatively higher frequency of the L and R genotype in the Chinese than Caucasian, provided these isotypes result in higher PON1 activity. Therefore, future studies could focus on this data gap to better understand the inter-ethnic difference in PON1 activity and its consequences for the toxicokinetics of CPF, since an accurate description of the potential differences in detoxification of CPO are of critical importance for the sensitivity of Chinese individuals to the OP-induced adverse effects. Such information can aid in the risk assessment and definition of HBGV values for the Chinese population, especially given that CPF is still being used in China.

Other parameters that were not yet taken into account but could in theory contribute to the ethnic disparities are the absorption related parameters (e.g. fraction absorbed, absorption rate

constant). This is especially of interest given that greater ethnic differences were observed in the responses upon oral administration than upon intravenous administration for some drugs (Chen 2006). In **Chapter 2**, the effect of the fraction absorbed on the CPF exposure-induced RBC AChE has been well defined by including different absorption fraction scenarios (0.224, 0.462, 0.7) based on the reported in vivo data in Caucasian (Nolan et al. 1984; Timchalk et al. 2002). Due to lack of relevant information on Chinese, the same scenarios were applied for this population. Since the different scenarios applied reflect possible scenarios that could occur in real-life, comparison of these different scenarios for both ethnicities can provide insight in possible inter-ethnic differences introduced by potential differences in the fraction absorbed. For the absorption rate constant, the Caucasian in vivo data were applied for both ethnicities due to the absence of the relevant information in Chinese, and this limitation might be overcome in future studies by using ethnicity-specific intestinal cell models if such cell lines would become commercially available.

In spite of the intrinsic factors (e.g. genetic variability, physiological condition), as addressed in the International Council for Harmonisation of Technical Requirements for Pharmaceuticals for Human Use (ICH) Harmonized Guideline (ICH 1998), the ethnic disparities can also be caused by extrinsic factors like diet and lifestyle. It is well known that Chinese and Caucasian historically have a marked difference in food types and cooking culture. Such differences may affect the activity or endogenous level of enzymes (e.g. CYPs) (Harris et al. 2003) in these populations, thus potentially contributing to the varied ethnic metabolism profile of OPs. Apart from that, due to economic developments, differences in food availability, food habits and lifestyle may introduce variation within and between the two populations, and overweight as well as obesity could also be a factor of influence. The WHO (2020) reported that in 2016, 39% of adults aged 18 years and over (39% of men and 40% of women) were overweight around the world. Overweight and obesity can affect the physiological conditions (e.g. body weight, metabolism rate, etc.) of people, thus ultimately introducing new uncertainties in characterization of inter-ethnic variation, indicating that it is necessary to consider and include such up to date variabilities in the future risk assessment to better protect public health.

The possibility of using TEF coded PBK models for predicting combined inhibitory effects of an OP pesticide and its bioactive metabolite

In **Chapter 4**, the PBK model-facilitated reverse dosimetry approach included TEF values to address the combined effect of the parent OP pesticide DZN and its metabolites DZO, which are both able to inhibit AChE. The use of the TEF approach is based on the fact that (1) DZN and DZO initiate toxicity via the same mode of toxic action (AChE inhibition); (2) their concentration–response curves are parallel; and (3) their toxicity is additive (Starr et al. 1999; Watt et al. 2016). The combined free blood C_{\max} concentration of DZN and DZO in the PBK model was expressed in free blood DZO equivalents. The TEF values of DZO and DZN were obtained based on the IC_{50} values derived from concentration-response curves for RBC AChE inhibition characterized using the *in vitro* AChE inhibition assay. Calculation of TEF values in this way is possible because the *in vitro* concentration-dependent RBC AChE inhibition curves of DZN and DZO are parallel reflecting that DZN and DZO only differ in potency, and that the potency difference between DZN and DZO will always be the same no matter at what inhibition level it is defined. Under this condition, IC_{50} values can be used, because these represent the most widely used and informative measure of potency of compounds, and have been used before to provide information on the potency of DZN and DZO in *in vitro* AChE inhibition studies (Colovic et al. 2013; Li et al. 2019a). Therefore, in the present thesis, quantification of the TEF value using the IC_{50} was considered appropriate.

Since DZN and CPF have a similar *in vitro* inhibitory potency on RBC AChE, similar chemical structure (contains P=S moiety), and similar biotransformation pathways, in theory CPF could also be expected to contribute to the RBC AChE inhibition in addition to CPO upon CPF exposure. However, in the present thesis, the inhibitory effect upon CPF exposure was ascribed to CPO solely. This was considered adequate because the *in vitro* intrinsic inhibitory potency of CPO was reported to be at least three orders of magnitude higher than that of CPF (Li et al. 2019b), and the *in vivo* effective concentration of CPF is not substantially different compared to that of CPO, thus resulting in a limited contribution of CPF (up to 0.2%) to the total inhibition at target site. This observation indicates that when assessing the combined inhibitory effect of an OP pesticide and its bioactive metabolites, their relative contributions to the *in vivo* RBC AChE inhibition is dependent on the difference in their intrinsic inhibitory potency as reflected by the TEF value, and their relative *in vivo* effective concentrations. Therefore, the effect of the parent OP pesticide and its metabolite on RBC AChE activity has to be assessed case by case, and when the differences in inhibitory potency of parent and metabolites appears to be

substantial, while their relative internal effective concentrations are not substantially different, the contribution of the parent OP might be negligible and can thus be considered less relevant.

It is important to notice that no inter-species differences in the TEF values for DZN relative to DZO between rat and human were observed (only a 1.1-fold difference). This observation is in line with the earlier conclusion that rat and human RBC AChE appear to show comparable sensitivity towards in vitro inhibition following DZO and DZN exposure.

The comparison of the Supersome™ CYP-based and the HLM-based approaches for assessing inter-individual variation

In **Chapter 5**, a Supersome™ CYP-based PBK and an HLM-based PBK facilitated QIVIVE approach was employed to characterize the possible inter-individual toxicokinetic variability and its consequence for inhibition of RBC AChE. The HLM-based PBK QIVIVE approach has been used previously to evaluate inter-individual toxicokinetic variability in different studies (Ning et al. 2019b; Strikwold et al. 2017). However, by comparing it with a Supersome™ CYP-based PBK QIVIVE approach, as done in the present thesis, some limitations of the HLM-based approach were elucidated. Firstly, when two or more CYP isoforms with distinct affinities toward CPF are involved in the same metabolic conversion, use of Supersome™ CYP-derived kinetic parameters together with corresponding CYP abundances to describe inter-individual variability in toxicokinetics enable the identification of the different kinetic affinity components of the CYP-mediated metabolism. It was shown that the conversion rates especially at low dose levels may be substantially under-estimated when not taking the contribution of high affinity CYPs at low concentration into account. When using HLM, identification of the kinetics at low substrate concentrations was hampered by the experimental detection limits and the relatively low conversion rates in incubations with HLM at these low concentrations compared to Supersome™ CYP, because of the lower activity of the respective CYPs in HLM than in Supersome™ CYP. Additionally, Supersome™ CYP can provide detailed information on the kinetic parameters for each relevant individual CYP toward the compound of interest, while HLM represent the overall metabolic consequence of all relevant CYPs. Moreover, the Supersome™ CYP-based approach makes it possible to take the different CYP phenotypes and their corresponding frequency in the general population into account when a Monte Carlo simulation is conducted, while this frequency is less likely to be

adequately defined when using the HLM-based approach, as it would require large numbers of different individual HLM samples to obtain the variation that can (sufficiently) represent the whole population. On the other hand, it should be noted that the use of the Supersome™ CYP-based approach might be hindered by the fact that different uncertainties may be involved in the definition of the ISEF values. ISEF values are known to be dependent on the substrate probe used, the laboratory conducting the experiment and the commercially supplied Supersome™ CYP and HLM used (Proctor et al. 2004), leading to uncertainty in the ISEF values. Therefore, derivation of an appropriate ISEF is of critical importance as it is functioning as a normalizer to correct for the differences in intrinsic activity between Supersome™ CYP and HLM. In the present thesis, an effort was made to minimize the possible variation in ISEF determination by using a probe substrate for the relevant CYPs in both enzyme systems to derive the ISEFs (instead of using default ISEF values), and using the same batch of Supersome™ CYP and HLM for all ISEF determinations in the same laboratory. The ISEF values thus obtained were considered appropriate.

The comparison of in vitro and in vivo results

In the present thesis, PBK model-based reverse dosimetry was employed to predict the RBC AChE inhibition induced by CPF, DZN or PFF acute single oral exposure in human and rat.

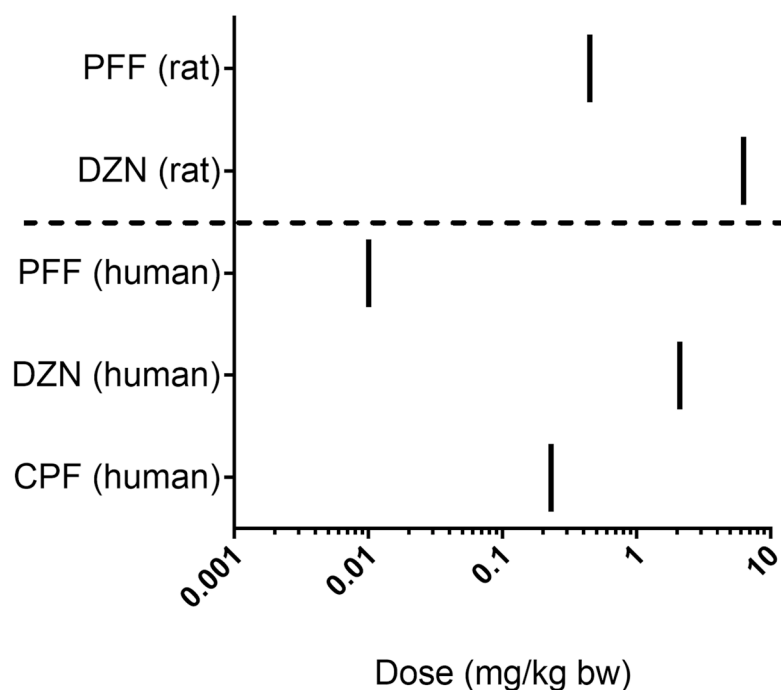


Fig 3. Comparison of predicted POD (BMDL₁₀) values of different OP pesticides derived from their corresponding predicted dose-response curves that were extrapolated from their in vitro concentration-response curves by PBK model-based reverse dosimetry. PFF, DZN and CPF are profenofos, diazinon and chlorpyrifos.

Figure 3 presents an overview of the predicted POD (BMDL₁₀) values of the OP pesticides studied for rat and human RBC AChE inhibition, as obtained in the present thesis (**Chapter 3, 4 and 5**). Furthermore, to gain insight into the extent to which the absorption, distribution, metabolism and excretion (ADME) of OP pesticides in vivo can alter the OP pesticide toxicity, the potency of each tested OP pesticide in vivo (Figure 3) can be compared to the in vitro potency (Figure 1). As indicated earlier, comparing the in vitro potency of each OP pesticide for inhibition on RBC AChE in rat to that in human reveals the absence of an inter-species difference (Figure 1). However, upon the QIVIVE conversion, a clear inter-species difference in in vivo RBC AChE inhibition by PFF and DZN was observed, with human being predicted to be more sensitive than rat (Figure 3). This comparison highlights the impact of the ADME

characteristics on the *in vivo* potency of OP pesticides studied, and provides an insight into how OP pesticide toxicity can be affected by *in vivo* kinetics. The results also show that *in vivo*, PFF is predicted to be more potent than DZN and CPF, indicating that exposure to the OP pesticide containing the P=O moiety may induce toxicity at lower dose levels than exposure to the ones requiring bioactivation to a P=O containing metabolite. The potency ranking of the OP pesticides predicted in rat (PFF>DZN) is in line with that reported in risk assessment documents on the basis of *in vivo* rat data (PFF>DZN) (EFSA 2006; EFSA 2014a; JMPR 2007; USEPA 2011; USEPA 2014a; USEPA 2016b; USEPA 2016c), indicating that the PBK model-based QIVIVE approach applied in the present thesis adequately assessed the relative *in vivo* potency of the respective OP pesticides in rat. However, Figure 3 also shows that the predicted potency difference between PFF and DZN in rats (14-fold) is substantially smaller than what is predicted for human (210-fold), reflecting the concerns related to the use of animal derived PODs to set HBGV for human safety evaluation, and meanwhile indicating the added value of the application of PBK models for the extrapolation of *in vitro* toxicity data to the *in vivo* situation. Moreover, considering the consistency of the predicted *in vivo* dose-response curves and PODs for RBC AChE inhibition by PFF and DZN in rat (**Chapter 3, 4**) with reported *in vivo* data points and PODs (JMPR 2007; JMPR 2016; USEPA 2016b; USEPA 2016c), using PBK model-facilitated reverse dosimetry based on *in vitro* and *in silico* data for predicting the potency of OP pesticides *in vivo* appears to be valid and applicable, supporting the derivation of PODs for human using this NAM.

6

The implications for risk assessment

Given that the European Union (EU) is dedicated to promote the 3Rs (replacement, reduction, and refinement) in animal testing, and the fact that traditional risk assessment approaches using animal data may not adequately identify and evaluate human risks, the development of NAMs, such as *in silico* and *in vitro* testing in combination with PBK model-based reverse dosimetry to translate *in vitro* data to the *in vivo* situation, becomes increasingly important. The present thesis provides several proofs-of-principle that the combination of *in vitro* concentration-response curves with PBK model-based reverse dosimetry can support the application of the 3R principles in risk assessment for this group of substances, and even enable predictions for the human situation using *in vitro* models mainly based on human enzymes and/or cell models and human PBK models.

In addition to the PBK model-based reverse dosimetry for QIVIVE, in the present thesis, an effort has also been made to study inter-species, inter-ethnic and inter-individual differences for OP pesticide-induced RBC AChE inhibition. This provided information for the refinement of the default UF to a CSAF. In case of CPF, the obtained CSAF for inter-individual variation in toxicokinetics ($HK_{AF}=3.6$) for Caucasians (**Chapter 5**) was slightly higher than the default UF of 3.16, indicating this default UF may not provide adequate protection for extreme sensitive individuals. However, combination of the derived HK_{AF} with the reported (Kasteel et al. 2020) inter-individual differences in toxicodynamics for CPO (HD_{AF}) of 2.2 results in an UF of 7.9 ($=3.6 \times 2.2$). This value is lower than the default UF of 10 for inter-individual differences, indicating the default UF of 10 might be somewhat overprotective. This is in line with the CSAF value of 3.4, reported by Poet et al. (2017) to account for both kinetic and dynamic interspecies differences, which is also lower than the default UF of 10. This factor of 3.4 was derived based on kinetic and dynamic modeling. However, it should be noted that the HK_{AF} of 3.6 defined in **Chapter 5** may still have to include other parameters that have a substantial impact on the predicted output such as body weight, absorption rate and fractional absorption. Additionally, the HK_{AF} obtained in the present study only relates to the general adult population, since kinetic parameters and CV values defined did not yet relate to other potentially sensitive sub-populations (e.g. pregnant women, infants and children). Some data suggest that there is a different capacity for CPO detoxification between these sub-groups and general adults. For example, there is an age-dependent increase of PON1 levels and its activity (Huen et al. 2010), or pregnancy can lead to an approximately 30% reduction in PON1 activity (Ferré et al. 2006). Therefore, the HK_{AF} derived in the present study may not provide a fully adequate protection for these sensitive sub-group. In further research, the Supersome™ CYP-based approach could be extended to also include these sub-populations, allowing definition of a HK_{AF} that covers the different sub-groups within the population. Furthermore, given that the POD derived for CPF in **Chapter 5** is based on a human PBK model and rhAChE derived in vitro data, which account for human specific physiology, metabolism and inhibitory effect, the UF of 10 for inter-species differences would no longer be required. However, when taking a POD derived using this in vitro in silico NAM approach for calculation of an HBGV, an extra uncertainty factor may be considered to account for the fact that the in vitro in-silico QIVIVE approach brings other uncertainties. Nevertheless, these results together provide another possibility for the definition of UFs for deriving an HBGV.

Regarding the inter-ethnic differences in toxicokinetics and the resulting prediction for toxicity of CPF reported in **Chapter 2**, Chinese were found to be less sensitive than Caucasians (5 to 6-fold), suggesting that for CPF exposure-induced toxicity, there is a relatively lower risk for the Chinese population. Given that Chinese are less sensitive than Caucasians, use of a POD derived based on Caucasian RBC AChE inhibition as starting point to calculate an HBGV for the Chinese seems more than sufficiently protective for the Chinese. However, due to the inter-individual variation for the Chinese population remains to be quantified, use of a Chinese specific CSAF is not indicated, and the default UF of 10 for inter-individual differences should remain. While for reasons already indicated above, an extra uncertainty factor may be considered to cover the potential uncertainties of the in vitro in-silico QIVIVE approach.

For the inter-species differences studied in **Chapter 3** for PFF and **Chapter 4** for DZN, human was found to be 45-fold and 6-fold more sensitive than rat, respectively. These data indicate that the default UF of 10 adequately protects the inter-species differences for DZN but not for PFF. Thus, use of the default UF of 10 to calculate an HBGV might not cover the inter-species differences for all OP pesticides, indicating that it is necessary to study the inter-species differences on a case-by-case basis when defining an HBGV based on a POD value derived from rat RBC AChE inhibition data.

Given the widespread occurrence of OP pesticide mixture residues in food (EFSA 2020; Omwenga et al. 2020), while risk assessments of OP pesticides in human are still often performed for individual compounds, developing a methodology that allows to evaluate the combined effects of OP pesticides is of high relevance. To address this issue, different international institutions (e.g. EFSA and USEPA) have made an effort to develop frameworks for a cumulative risk assessment of pesticide mixtures by grouping different pesticides into cumulative assessment groups (CAGs) on the basis of inducing similar toxicological effects (e.g. acute effects on the nervous system (brain and/or RBC AChE inhibition)) or sharing an identified common mechanism of toxicity (same toxic effect occurs in the same organ or tissue by essentially the same sequence of major biochemical events) (EFSA et al. 2020; USEPA 2006a). However, a harmonized methodology for addressing the cumulative risk of combined exposures to multiple pesticides for human health has not yet been implemented. To contribute to that, the project European Test and Risk Assessment Strategies for Mixtures (EuroMix) was launched to develop internationally harmonized new approaches and testing strategies for the risk assessment of multiple chemical mixtures (including pesticide mixtures) on the basis of the AOP concept, which was implemented in a web model and data toolbox called Monte Carlo

Risk Assessment (MCRA) (Van der Voet et al. 2020). This approach enables the integration of *in silico* and *in vitro* data in PBK model-facilitated combined risk assessment of mixtures. The results from the present thesis might add valuable information to this test strategy, as it demonstrates the applicability of PBK model-based reverse dosimetry for assessing toxicokinetics of OP pesticides and for translating the *in vitro* data for their target effect to the *in vivo* situation and external exposure levels, thus bridging the gap between external dose and internal dose and effects. Moreover, results of the present thesis also confirm the ability of such a PBK model-based approach for identifying the *in vivo* potency of different OP pesticides in a target group of interest, and for predicting the combined effect of parent OP pesticides and their active metabolites on target sites, while also illustrating its further possibilities for including TEF or relative potency factors (RPF) values for the analysis of combined effects of OP pesticide mixture exposures.

The future perspectives

The present thesis demonstrated the applicability of the use of PBK model-based reverse dosimetry for the translation of *in vitro* concentration-response curves to *in vivo* dose-response curves for *in vivo* RBC AChE inhibition following CPF, PFF and DZN exposure. However, it remains necessary to evaluate more OP pesticides to increase the confidence and broaden the applicability domain of such an approach. When the toxicity of more OP pesticides would be assessed by this approach and would provide additional proofs-of-principle, this approach can be considered for use as a regular method for OP pesticide risk assessment.

Another point that can be considered in the future is to extend the application of Supersome™ CYP for characterizing the biotransformation of different OP pesticides. In the present thesis, Supersome™ CYP have been successfully applied to assess the metabolism of CPF. Use of Supersome™ CYP allows quantification of the intrinsic activity and kinetic constants of individual CYP enzymes for the conversion of the OP pesticide under study. Supersome™ CYP also enable investigation of the role of individual CYP enzyme in catalyzing a specific metabolic conversion. All the more, it enabled capturing not only the low affinity kinetic components but also the high affinity kinetic components of CPF bioactivation, which were shown to be a dominant factor at CPF concentrations lower than 1 μM , a concentration that is considered physiologically relevant. Regarding the advantage of using Supersome™ CYP, it may be of interest to develop and include other Supersome™ enzyme models for

characterization of biotransformation reactions. As more human enzyme abundance data in different population groups become available in the future, such Supersome™ enzymes (e.g. CYP isoforms, paraoxonase 1 (PON1), UDP-glucuronosyl transferases (UGTs), flavin-containing monooxygenases (FMOs), monoamine oxidases (MAOs), sulfotransferases (SULT), human aldehyde oxidase (AOs), soluble N-acetyltransferases (NATs), and carboxylesterases (CESs)) would be extremely valuable for studying inter-individual, inter-ethnic, and age-dependent variation in relation to different chemical exposures and toxicological outcomes, and establishment of safe levels of exposure using the methods applied and shown valid in the present thesis for the OP pesticide model compounds

To date, most regulators seem still hesitant to use NAMs to support regulatory decision-making, due to uncertainties underlying model development and evaluation. To evaluate such uncertainties and provide a better framework for evaluating predictive toxicity models, in recent years, various international organizations, such as EFSA, the World Health Organization (WHO) International Programme of Chemical Safety (IPCS), and the Organization for Economic Cooperation and Development (OECD), have published different guidance documents on application of PBK models using alternative data (in vitro and in silico) for a regulatory risk assessment purpose (EFSA 2014b; IPCS 2010; OECD 2021). Despite the fact that it might still take time to widely implement NAMs for regulatory decision-making, it can be expected that this may gradually change when more data and proofs-of-principle for different types of chemicals and toxicity endpoints become available, and a more harmonized and completed framework for characterizing and validating PBK models will be generated. An increase in the acceptance of such approaches in regulatory safety decision making would be expected and seems essential to contribute to what is often referred to as next generation risk assessment.

6

Conclusion

To conclude, the present thesis generated proofs-of-principle for the use of PBK model-facilitated reverse dosimetry based on in vitro assays and in silico data, in combination with Monte Carlo simulations or TEF methodology, to derive PODs and CSAF values for defining inter-ethnic, inter-species and inter-individual differences in toxicokinetics and the resulting RBC AChE inhibition following an OP pesticide acute single oral exposure. The data obtained in the present thesis may assist in the application of such NAM in ongoing and future next

generation human health risk assessments for OP pesticides, allowing prediction directly applicable for the human situation on the basis of in vitro and in silico data, eliminating the need for in vivo animal studies. Altogether, the current work supports the application of such a NAM in regulatory safety decision making, and contributes to the implementation of the 3Rs principle, ultimately promoting the development and use of next generation risk assessment.

References

- Assis CR, Linhares AG, Cabrera MP, Oliveira VM, Silva KC, Marcuschi M, . . . Carvalho LB (2018) Erythrocyte acetylcholinesterase as biomarker of pesticide exposure: new and forgotten insights *Environmental Science and Pollution Research* 25:18364-18376
- Barenys M, Fritsche E (2018) A historical perspective on the use of stem/progenitor cell-based in vitro methods for neurodevelopmental toxicity testing *Toxicological Sciences* 165:10-13
- Barter ZE, Bayliss MK, Beaune PH, Boobis AR, Carlile DJ, Edwards RJ, . . . Pelkonen OR (2007) Scaling factors for the extrapolation of in vivo metabolic drug clearance from in vitro data: reaching a consensus on values of human micro-somal protein and hepatocellularity per gram of liver *Current drug metabolism* 8:33-45
- Brown RP, Delp MD, Lindstedt SL, Rhomberg LR, Beliles RP (1997) Physiological parameter values for physiologically based pharmacokinetic models *Toxicology and industrial health* 13:407-484
- Burke RD, Todd SW, Lumsden E, Mullins RJ, Mamczarz J, Fawcett WP, . . . Albuquerque EX (2017) Developmental neurotoxicity of the organophosphorus insecticide chlorpyrifos: from clinical findings to preclinical models and potential mechanisms *Journal of neurochemistry* 142:162-177
- Chanda S, Lassiter T, Moser V, Barone S, Padilla S (2002) Tissue carboxylesterases and chlorpyrifos toxicity in the developing rat *Human and Ecological Risk Assessment* 8:75-90
- ChemAxon Chemicalize. <https://chemaxon.com/products/chemicalize>. Accessed 21 February 2021
- Chen M-L (2006) Ethnic or racial differences revisited *Clinical pharmacokinetics* 45:957-964
- Colovic MB, Krstic DZ, Lazarevic-Pasti TD, Bondzic AM, Vasic VM (2013) Acetylcholinesterase inhibitors: pharmacology and toxicology *Current neuropharmacology* 11:315-335
- Costa LG (2006) Current issues in organophosphate toxicology *Clinica chimica acta* 366:1-13
- Das GP, Jamil K, Rahman M (2006) Effect of four organophosphorus compounds on human blood acetylcholinesterase: in vitro studies *Toxicology mechanisms and methods* 16:455-459
- DeJongh J, Verhaar HJ, Hermens JL (1997) A quantitative property-property relationship (QPPR) approach to estimate in vitro tissue-blood partition coefficients of organic chemicals in rats and humans *Archives of Toxicology* 72:17-25
- Di Consiglio E, Pistollato F, Mendoza-De Gyves E, Bal-Price A, Testai E (2020) Integrating biokinetics and in vitro studies to evaluate developmental neurotoxicity induced by chlorpyrifos in human iPSC-derived neural stem cells undergoing differentiation towards neuronal and glial cells *Reproductive Toxicology* 98:174-188
- Eaton DL, Daroff RB, Autrup H, Bridges J, Buffler P, Costa LG, . . . Nadel L (2008) Review of the toxicology of chlorpyrifos with an emphasis on human exposure and neurodevelopment *Critical reviews in toxicology* 38:1-125
- EFSA (2006) Conclusion regarding the peer review of the pesticide risk assessment of the active substance diazinon <https://efsa.onlinelibrary.wiley.com/doi/epdf/10.2903/j.efsa.2006.85r>. Accessed 27th January 2021
- EFSA (2014a) Conclusion on the peer review of the pesticide human health risk assessment of the active substance chlorpyrifos *EFSA Journal* 12:3640
- EFSA (2014b) Scientific Opinion on good modelling practice in the context of mechanistic effect models for risk assessment of plant protection products *EFSA Journal* 12:3589
- EFSA (2019) Statement on the available outcomes of the human health assessment in the context of the pesticides peer review of the active substance chlorpyrifos *EFSA Journal* 17:e05809
- EFSA (2020) The 2018 European Union report on pesticide residues in food *EFSA Journal* 18:e06057
- EFSA, Craig PS, Dujardin B, Hart A, Hernández-Jerez AF, Hougaard Bennekou S, . . . Wolterink G (2020) Cumulative dietary risk characterisation of pesticides that have acute effects on the nervous system *EFSA Journal* 18:e06087
- Eyer F, Roberts DM, Buckley NA, Eddleston M, Thiermann H, Worek F, Eyer P (2009) Extreme variability in the formation of chlorpyrifos oxon (CPO) in patients poisoned by chlorpyrifos (CPF) *Biochemical pharmacology* 78:531-537

- Fakhri-Bafghi MS, Ghasemi-Niri SF, Mostafalou S, Navaei-Nigjeh M, Baeeri M, Mohammadirad A, Abdollahi M (2016) Protective effect of selenium-based medicines on toxicity of three common organophosphorus compounds in human erythrocytes in vitro *Cell Journal (Yakhteh)* 17:740
- Ferré N, Camps J, Fernández-Ballart J, Arijá V, Murphy MM, Marsillach J, Joven J (2006) Longitudinal changes in serum paraoxonase-1 activity throughout normal pregnancy *Clinical Chemistry and Laboratory Medicine (CCLM)* 44:880-882
- Foxenberg RJ, Ellison CA, Knaak JB, Ma C, Olson JR (2011) Cytochrome P450-specific human PBPK/PD models for the organophosphorus pesticides: chlorpyrifos and parathion *Toxicology* 285:57-66
- Fukuto TR (1990) Mechanism of action of organophosphorus and carbamate insecticides *Environmental health perspectives* 87:245-254
- George P, Abernethy M (1983) Improved Ellman procedure for erythrocyte cholinesterase *Clinical chemistry* 29:365-368
- Harris RZ, Jang GR, Tsunoda S (2003) Dietary effects on drug metabolism and transport *Clinical pharmacokinetics* 42:1071-1088
- Heilmair R, Eyer F, Eyer P (2008) Enzyme-based assay for quantification of chlorpyrifos oxon in human plasma *Toxicology letters* 181:19-24
- Huen K, Harley K, Bradman A, Eskenazi B, Holland N (2010) Longitudinal changes in PON1 enzymatic activities in Mexican–American mothers and children with different genotypes and haplotypes *Toxicology and applied pharmacology* 244:181-189
- ICH (1998) E5(R1) Ethnic Factors in the Acceptability of Foreign Clinical Data https://www.ema.europa.eu/en/documents/scientific-guideline/ich-e-5-r1-ethnic-factors-acceptability-foreign-clinical-data-step-5_en.pdf. Accessed 1st May 2021
- IPCS Wa (2010) Characterization and application of physiologically based pharmacokinetic models in risk assessment. International Programme on Chemical Safety. https://www.who.int/ipcs/methods/harmonization/areas/pbpc_models.pdf?ua=1. Accessed 9 May 2021
- JMPR (2007) Pesticide residue in food-2007. <http://www.inchem.org/documents/jmpr/jmpmono/v2007pr01.pdf>. Accessed 1st February 2021
- JMPR (2016) Pesticide residues in food 2016. <http://www.fao.org/3/a-i5693e.pdf>. Accessed 26 January 2021
- Jokanović M (2009) Current understanding of the mechanisms involved in metabolic detoxification of warfare nerve agents *Toxicology letters* 188:1-10
- Jokanović M RD, Kovač B, Stojiljković MP (2020) Handbook of Toxicology of Chemical Warfare Agents. Elsevier Inc. doi:<https://doi.org/10.1016/C2018-0-04837-9>
- Kasteel EE, Nijmeijer SM, Darney K, Lautz LS, Dorne JLC, Kramer NI, Westerink RH (2020) Acetylcholinesterase inhibition in electric eel and human donor blood: an in vitro approach to investigate interspecies differences and human variability in toxicodynamics *Archives of toxicology* 94:4055-4065
- King AM, Aaron CK (2015) Organophosphate and carbamate poisoning *Emergency Medicine Clinics* 33:133-151
- Krstić DZ, Čolović M, Bavcon kralj M, Franko M, Krinulović K, Trebše P, Vasić V (2008) Inhibition of AChE by malathion and some structurally similar compounds *Journal of enzyme inhibition and medicinal chemistry* 23:562-573
- Li G-F, Zheng Q-S, Yu Y, Zhong W, Zhou H-H, Qiu F, . . . Derendorf H (2019a) Impact of ethnicity-specific hepatic microsomal scaling factor, liver weight, and cytochrome P450 (CYP) 1A2 content on physiologically based prediction of CYP1A2-mediated pharmacokinetics in young and elderly Chinese adults *Clinical pharmacokinetics* 58:927-941
- Li S, Zhao J, Huang R, Santillo MF, Houck KA, Xia M (2019b) Use of high-throughput enzyme-based assay with xenobiotic metabolic capability to evaluate the inhibition of acetylcholinesterase activity by organophosphorous pesticides *Toxicology in Vitro* 56:93-100
- LibreTexts™ (2020) Temperature, pH, and enzyme concentration on the rate of a reaction. https://chem.libretexts.org/Courses/University_of_Arkansas_Little_Rock/CHEM_4320_5320%3A_Biochemistry_1/05%3A_Michaelis-

- [Menten Enzyme Kinetics/5.5%3A Temperature%2C pH%2C and enzyme concentration on the rate of a reaction](#). Accessed 10 June 2021
- NHFPC (2007a) Reference individuals for use in radiation protection—Part 1: Physique parameters. <http://www.nirp.cn/userfiles/file/GBZT200.1-2007.pdf>. Accessed 30 April 2021
- NHFPC (2007b) Reference individuals for use in radiation protection—Part 2: Masses of main organs and tissues. <http://www.nirp.cn/userfiles/file/GBZT200.2-2007.pdf>. Accessed 30 April 2021
- NHFPC (2014) Reference individuals for use in radiation protection—Part 3: Main physiological parameters. <http://www.nirp.cn/userfiles/file/GBZT200.3-2014.pdf>. Accessed 22 April 2021
- Ning J, Chen L, Strikwold M, Louisse J, Wesseling S, Rietjens IMCM (2019a) Use of an in vitro–in silico testing strategy to predict inter-species and inter-ethnic human differences in liver toxicity of the pyrrolizidine alkaloids lasiocarpine and riddelliine Archives of toxicology 93:801-818
- Ning J, Louisse J, Spenkeliink B, Wesseling S, Rietjens IMCM (2017) Study on inter-ethnic human differences in bioactivation and detoxification of estragole using physiologically based kinetic modeling Archives of toxicology 91:3093-3108
- Ning J, Rietjens IMCM, Strikwold M (2019b) Integrating physiologically based kinetic (PBK) and Monte Carlo modelling to predict inter-individual and inter-ethnic variation in bioactivation and liver toxicity of lasiocarpine Archives of toxicology 93:2943-2960
- Nolan R, Rick D, Freshour N, Saunders J (1984) Chlorpyrifos: pharmacokinetics in human volunteers Toxicology and applied pharmacology 73:8-15
- OECD (2021) Guidance document on the characterisation, validation and reporting of Physiologically Based Kinetic (PBK) models for regulatory purposes. <https://www.oecd.org/chemicalsafety/risk-assessment/guidance-document-on-the-characterisation-validation-and-reporting-of-physiologically-based-kinetic-models-for-regulatory-purposes.pdf>. Accessed 9 May 2021
- Omwenga I, Kanja L, Zomer P, Louisse J, Rietjens IMCM, Mol H (2020) Organophosphate and carbamate pesticide residues and accompanying risks in commonly consumed vegetables in Kenya Food Additives & Contaminants: Part B:1-11
- pkCSM (n.d.) prediction tools-distribution-Fraction unbound. <http://biosig.unimelb.edu.au/pkcsml/>. Accessed 18 September 2020
- Poet TS, Kousba AA, Dennison SL, Timchalk C (2004) Physiologically based pharmacokinetic/pharmacodynamic model for the organophosphorus pesticide diazinon Neurotoxicology 25:1013-1030
- Poet TS, Timchalk C, Bartels MJ, Smith JN, McDougal R, Juberg DR, Price PS (2017) Use of a probabilistic PBPK/PD model to calculate Data Derived Extrapolation Factors for chlorpyrifos Regulatory Toxicology and Pharmacology 86:59-73
- Proctor N, Tucker G, Rostami-Hodjegan A (2004) Predicting drug clearance from recombinantly expressed CYPs: intersystem extrapolation factors Xenobiotica 34:151-178
- Rietjens IMCM, Ning J, Chen L, Wesseling S, Strikwold M, Louisse J (2019) Selecting the dose metric in reverse dosimetry based QIVIVE Archives of toxicology 93:1467-1469
- Robinson PK (2015) Enzymes: principles and biotechnological applications Essays in biochemistry 59:1
- Sigma-Aldrich (n.d.) Acetylcholinesterase human. <https://www.sigmaaldrich.com/catalog/product/sigma/c1682?lang=en®ion=NL>. Accessed 13 May 2021
- Simcyp (2016) Blood to Plasma Partition Ratio (B/P). <https://members.simcyp.com/account/tools/BP/>. Accessed 27 March 2021
- Smith JN, Timchalk C, Bartels MJ, Poet TS (2011) In vitro age-dependent enzymatic metabolism of chlorpyrifos and chlorpyrifos-oxon in human hepatic microsomes and chlorpyrifos-oxon in plasma Drug metabolism and disposition 39:1353-1362
- Starr TB, Greenlee WF, Neal RA, Poland A, Sutter TR (1999) The trouble with TEFs Environmental health perspectives 107:A492-A493
- Strikwold M, Spenkeliink B, Woutersen RA, Rietjens IMCM, Punt A (2017) Development of a combined in vitro physiologically based kinetic (PBK) and Monte Carlo modelling approach to predict interindividual human variation in phenol-induced developmental toxicity Toxicological sciences 157:365-376

- Tarhoni MH, Lister T, Ray DE, Carter WG (2008) Albumin binding as a potential biomarker of exposure to moderately low levels of organophosphorus pesticides *Biomarkers* 13:343-363
- Timchalk C, Nolan R, Mendrala A, Dittenber D, Brzak K, Mattsson J (2002) A physiologically based pharmacokinetic and pharmacodynamic (PBPK/PD) model for the organophosphate insecticide chlorpyrifos in rats and humans *Toxicological Sciences* 66:34-53
- USEPA (2006a) Organophosphorus Cumulative Risk Assessment (2006 Update). <https://www.regulations.gov/document/EPA-HQ-OPP-2006-0618-0002>. Accessed 5 May 2021
- USEPA (2006b) Reregistration Eligibility Decision for Diazinon https://www3.epa.gov/pesticides/chem_search/reg_actions/reregistration/red_PC-057801_31-Jul-06.pdf. Accessed 26 January 2021
- USEPA (2011) Preliminary Human Health Risk Assessment. <https://www.regulations.gov/document?D=EPA-HQ-OPP-2008-0850-0025>. Accessed 29th January 2021
- USEPA (2014a) Chlorpyrifos: Revised Human Health Risk Assessment for Registration Review. <https://www.regulations.gov/document?D=EPA-HQ-OPP-2008-0850-0195>. Accessed 30th January 2021
- USEPA Guidance for applying quantitative data to develop data-derived extrapolation factors for interspecies and intraspecies extrapolation. In: Washington, DC: Office of the Science Advisor. Risk Assessment Forum, 2014b.
- USEPA (2016a) Chlorpyrifos: Revised human health risk assessment for registration review Washington, DC, USA
- USEPA (2016b) Diazinon Draft Human Health Risk Assessment for Registration Review. <https://www.regulations.gov/document?D=EPA-HQ-OPP-2008-0351-0093>. Accessed 31st January 2021
- USEPA (2016c) Profenofos: Human Health Draft Risk Assessment (ORA) for Registration Review. https://www3.epa.gov/pesticides/chem_search/cleared_reviews/csr_PC-111401_19-Oct-16.pdf. Accessed 1st February 2021
- Van der Voet H, Kruisselbrink JW, De Boer WJ, Van Lenthe MS, Van den Heuvel JH, Crépet A, . . . Tebby C (2020) The MCRA toolbox of models and data to support chemical mixture risk assessment *Food and Chemical Toxicology* 138:111185
- Watt J, Webster TF, Schlezinger JJ (2016) Generalized concentration addition modeling predicts mixture effects of environmental PPAR γ agonists *Toxicological Sciences* 153:18-27
- Weaving G, Batstone GF, Jones RG (2016) Age and sex variation in serum albumin concentration: an observational study *Annals of clinical biochemistry* 53:106-111
- Westerink RH (2013) Do we really want to REACH out to in vitro? *Neurotoxicology* 39:169-172
- WHO (2020) Obesity and overweight. <https://www.who.int/news-room/fact-sheets/detail/obesity-and-overweight>. Accessed 1st May 2021
- Worek F, Eyer P, Thiermann H (2012) Determination of acetylcholinesterase activity by the Ellman assay: a versatile tool for in vitro research on medical countermeasures against organophosphate poisoning *Drug testing and analysis* 4:282-291
- Zhang X, Sui H, Li H, Zheng J, Wang F, Li B, Zhang Y (2014) Paraoxonase activity and genetic polymorphisms in northern Han Chinese workers exposed to organophosphate pesticides *Experimental Biology and Medicine* 239:232-239
- Zhou HH, Adedoyin A, Wilkinson GR (1990) Differences in plasma binding of drugs between Caucasians and Chinese subjects *Clinical Pharmacology & Therapeutics* 48:10-17

Chapter 7

Summary

The aim of the present thesis was to investigate whether new approach methodologies (NAMs) and especially physiologically based kinetic (PBK) model-based reverse dosimetry using in vitro assays and in silico data, in combination with Monte Carlo simulations or the toxic equivalency factor (TEF) methodology, can be used to derive points of departure (POD) and chemical-specific adjustment factors (CSAFs) for characterizing inter-ethnic, inter-species, and inter-individual differences in toxicokinetics and red blood cell (RBC) acetylcholinesterase (AChE) inhibition by organophosphate (OP) pesticides upon single acute oral exposure.

Chapter 1 provided an overview of relevant background information, including an introduction of chlorpyrifos (CPF), diazinon (DZN), and profenofos (PFF) as model compounds, their absorption, distribution, metabolism and excretion (ADME) and toxicity profiles, as well as their reported PODs and health-based guidance values (HBGVs). The aim of the thesis and the NAMs that were applied in the thesis (PBK model-based reverse dosimetry solely, or combined with Monte Carlo simulations or the TEF methodology) were also presented. At the end, the general outline of the thesis was provided.

Chapter 2 assessed the inter-ethnic differences in toxicokinetics of CPF and its resulting RBC AChE inhibition between the Chinese and Caucasian populations using PBK model-facilitated reverse dosimetry based on in vitro and in silico data. The results obtained revealed a marked inter-ethnic difference in toxicokinetics of CPF, with a slower CPF bioactivation and faster detoxification of its active metabolite chlorpyrifos oxon (CPO) in the Chinese than in the Caucasian population. This could be explained by the inter-ethnic variation in enzyme profiles and enzyme activities involved in biotransformation of CPF and CPO. The differences resulted in 5- to 6-fold lower predicted POD values of CPF for the Caucasian than the Chinese population, reflecting a lower risk of CPF for the Chinese than the Caucasian at similar levels of exposure. Besides, because of inter-ethnic variation in toxicokinetics of CPF, 2-fold lower cumulative urinary 3,5,6-trichloro-2-pyridinol (TCPy) biomarker levels were observed in Chinese than in Caucasian at similar dose levels, implying the importance of taking possible inter-ethnic differences into account when characterizing CPF exposure for different ethnic groups based on their urinary biomarker levels.

Chapter 3 focused on another OP and investigated the inter-species differences between rat and human in PFF-induced RBC AChE inhibition by PBK model-based reverse dosimetry. The obtained results show the predicted POD of human to be 45-fold lower than that of rat, indicating human to be more sensitive than rat to the inhibition from equivalent oral doses of

PFF. Such differences appeared mainly due to marked interspecies differences in toxicokinetics of PFF, with rat being more efficient in hepatic and plasma detoxification of PFF than human, while the difference in toxicodynamics appeared limited as reflected by a similar potency of PFF to inhibit rat RBC AChE and human recombinant AChE in vitro. In conclusion, this chapter provided another proof-of-principle that integrating in vitro toxicity data and PBK model-based reverse dosimetry is a promising strategy for non-animal-based safety assessment of OP pesticides.

Chapter 4 further studied the applicability of PBK model-based reverse dosimetry to predict the combined inhibitory effect of DZN and its active oxon metabolite diazoxon (DZO) on RBC AChE inhibition by integrating the TEF approach into the model. Use of the TEF coded PBK model enabled calculation of the external exposure dose of DZN that would produce a defined combined free DZN plus DZO concentration expressed in DZO equivalents in human/rat blood, and to translate the observed inhibition effects of DZO in the in vitro concentration-response curve expressed in free in vitro DZO equivalents to the in vivo situation. The obtained results show that DZN contributes substantially to the DZO equivalents, indicating it is of critical importance to take DZN into account in addition to the active metabolite DZO when conducting a risk assessment for DZN. Although no inter-species differences were observed in the in vitro concentration-response curves for rat or human RBC AChE inhibition by DZN or DZO, marked inter-species differences in toxicokinetics were observed, as rat displayed a faster metabolic rate for biotransformation of DZN and DZO than human, resulting in a 6-fold lower POD in human than in rat. In conclusion, this chapter provided a proof-of-principle for derivation of a point of departure (POD) in risk assessment for an OP pesticide for which both the parent OP and its oxon metabolite have the ability to contribute to RBC AChE inhibition.

Chapter 5 characterized the inter-individual variation in toxicokinetics of CPF and its resulting RBC AChE inhibition. A CSAF for inter-individual differences in kinetics (HK_{AF}) was quantified on the basis of the PBK model for CPF developed in Caucasian (**Chapter 2**), in combination with Monte Carlo simulations. To define the metabolic variation in the PBK model, two different approaches were developed and compared, namely a Supersome™ cytochrome P450 (CYP)-based PBK model approach and a human liver microsome (HLM)-based PBK model approach. The results revealed that bioactivation of CPF exhibits biphasic kinetics due to distinct differences in K_m values for CYPs involved in the CPF metabolic pathway, and these kinetic characteristics could be best identified by Supersome™ CYP. In general, there is a good match between the two approaches, as no substantial differences were

found in the predicted HK_{AF} values and the $BMDL_{10}$ values obtained by the two procedures. The predicted HK_{AF} values for the 99th percentile obtained by the two approaches were slightly higher than the default uncertainty factor (UF) of 3.16, reflecting possible inadequate protection for extremely sensitive adult individuals by the default UF. Altogether, this chapter provided a proof-of-principle for assessing inter-individual variation in toxicokinetics of OP pesticides and its resulting RBC AChE inhibition, and the SupersomeTM CYP-based approach seems to be the preferred option for defining inter-individual differences in CYP-mediated kinetics.

Chapter 6 provided an overview of the results and main findings of the present thesis, followed by an in-depth discussion of the results obtained, and the future perspectives. It was concluded that the present thesis generated proofs-of-principle for the use of NAM and especially PBK model-facilitated reverse dosimetry based on in vitro assays and in silico data, in combination with Monte Carlo simulations or the TEF methodology, to derive PODs and CSAF values for defining inter-ethnic, inter-species and inter-individual differences in toxicokinetics and the resulting RBC AChE inhibition following an OP pesticide acute single oral exposure. Altogether, the current work supports the application of such a NAM in regulatory safety decision making on compounds, and contributes to the implementation of the 3Rs (replacement, reduction, and refinement of experimental animal studies), thereby promoting the development of next generation risk assessment.

Appendix

Acknowledgements

About the author

List of publications

Overview of completed training activities

Acknowledgements

Throughout my PhD, I have received a great deal of support and assistance.

First, I would like to express my very great appreciation to my promotor Ivonne Rietjens and co-promotor Marije Strikwold for their patient guidance, support, and assistance in keeping my progress on schedule, dankjewel! **Ivonne**, thanks for always being there when I encountered difficulties and guiding me to overcome them. I still remember when I received the feedback from reviewers for my first paper, I was a bit nervous and went to your office at end of the day to ask for advice. No doubt that your support and guidance are what got me through and help me grow into a more independent researcher. I also highly appreciate all efforts you made to my project, especially at the last stage of my thesis. You have tried your best (even work until late at night) to provide feedback promptly, thank you so so so much for that. I have learned so much from you, calmness, the way of thinking, decision making, dedication....., and your involvement has helped me in a variety of ways including but not limited to research. I am truly grateful for the encouragement, advice, support that you've given me not only for the past few years but also for my future career. **Marije**, thank you for all your critical comments, guidance, and being so patient to read and reply to my super long emails. I appreciated and enjoyed the discussions we had along the way, especially when we figured out the reason and find the explanation for “why”. I sincerely thank your wiliness to assist me when I encountered a challenge. I am very grateful for your dedicated support and guidance on modelling. I would say your meticulous and conscientious working style has impressed me a lot and has motivated me to strive harder to fulfill my potential. Thank you for challenging me always to dig a little deeper, learn more, and know more. I truly appreciate you, the time you spent, the effort you made, the encouragement you gave, and the advice you provided.

I would like to extend my sincere gratitude and appreciation to Ans Punt for her valuable advice on my last paper, which has given me a new perspective. **Ans**, I am glad that I got the chance to learn from you, thank you very much for all your contribution, highly appreciated. I would also like to say thanks to Jochem Louisse for his help in the preparations of PhD application. **Jochem**, thank you very much!

I would like to take this opportunity to express my sincere thanks to the **PhD committee**: Prof. Dr B.J. (Bas) Blaauboer, Dr A. Punt, Prof. Dr Martin van den Berg, and Prof. Dr P.J. (Paul) van den Brink. Thank you very much for the time and effort took to review and evaluate this thesis.

I would also like to express my gratitude to the former and current staff members at TOX for their support. **Bert**, I was so lucky to have you around to talk with and to learn from. Your dedicated works have motivated me to learn more and to work harder. Thank you for saving me from the problems of UPLC, helping me to order products. I enjoyed the conversations we had and thank you for sharing your family stories and pictures of grandchildren with me. **Sebas**, thank you so much for your assistance and help in the ordering of products, setting up the methods of UPLC and LC-MS/MS, and being so patient to teach me how to use the machines. I'm so grateful for your time, effort, and positive energy! Also, I would like to say thanks to Hans van den Berg. **Hans**, thank you very much for helping me to order the products. To **Lidy**, **Gerda** and **Carla**, thank you very much for your support and helpful assistance. **Letty**, thanks for helping me arranging PET courses. **Laura**, it is very nice to talk with you from time to time, although I did not get a chance to work with you. **Wouter**, it is my pleasure to work with you during the practical course. Another person I would like to say thanks to is **Nacho**. Although you were not involved in my PhD thesis, I would say without your encouragement, guidance, and help during my master thesis, I do not think I would think of pursuing a PhD. I am truly grateful for all you have done!!

To my former MSc students (**Sujing**, **Wenbo**, and **Zhen**), thank you very much for your hard work, and for the fact that all of you have done a great job! I wish for all of you a bright future.

I'm grateful to all of my former and current office mates for the time we have shared. **Aziza** and **Nacho**, thank you so much for being so cheerful, you brought a lot of fun to this office. Do you still remember the book that you would like to write? Hope it will come true one day! **Menno**, thank you so much for being so patient to teach me one Dutch word per day. Although I have tried to remember them by writing them down and sticking them to my PC, it seems it will still take me some time and effort to let them finally stick to my brain. Also, thanks for coming up with some solutions when I encountered problems. **Diego**, thank you for all your support and chocolate, it has brought a lot of energy to me. **Biyao**, thank you so much for being so warmhearted and helpful. I'm really glad that we could made fundraising together, and the trip we had in Japan has brought a lot of fun (and nice pictures, haha) to me! Also, thank you for taking me home during quarantine :), I would say thank you for everything. **Jin** (靳姐), although you have only been here for a certain period, we really have a lot of nice chats and laughed a lot together in the office, I am really glad that I have met you! **Liang** and **Jiaqi**, I wish all the best to you. I know the two of you are working very hard, but please also be relaxed a bit and enjoy the lives that you have now. I would also like to express my thanks to Rungnapa

Acknowledgements

Boonpawa for her contribution to my first paper. **Rung**, thank you so much for being there for me at the first stage of my PhD, I still remember we were sitting side by side in the office to discuss my model, I sincerely appreciate your generous help. To all TOX PhDs who I have met: **Nacho, Marta, Diego, Lenny, Mebrahtom, Aziza, Pim, Artem, Ashraf, Jia, Lu, Shuo, Mengying, Diana, Annelies, Katja, Qianrui, Felicia, Isaac, Danlei, Menno, Bohan, Suparmi, Miaoying, Biyao, Gogo, Qiuhui, Weija, Jing, Jing, Chen, Merel, Veronique, Edith, Maartje, Akanksha, Frances, Yasser, Jiaqi, Yiming, Merel, Katharina, Tessa, Jingxuan, Nina, Liang, Orsolya, Aafke**, I appreciated the time we shared the fun we had and the songs we sang together. For the PhDs who I haven't got the chance to say hi: **Wisse, Hugo, Aishwarya, Xukun**, I wish you all the best! A special thanks to **Katja, Annelies, Danlei, Diana, Qianrui, Ixchel, Yiming, Shuo, Nina, Weijia**, and **Chen**, I was very lucky to have you around in the UPLC lab. I always enjoyed our catch-up chats. I'm so grateful for your help, suggestions, and support during my challenging time. I also would like to say thanks to our pesticide buddy **Isaac**, thank you for all the enlightening discussions and help. Thank you for sharing different ideas, traditions, and knowledge with me. I cannot wait to see animal migration in Kenya. **Jia**, thank you very much for all your help at the beginning of my PhD, I highly appreciated everything that you have taught me! **Suparmi** and **Gogo**, thank you for all the tips and help that you have given to me! To my colleague & neighbor. **Danlei**, to be your neighbor is a wonderful experience, fish, cake, fried chicken, dumplings... the taste is the best out of the best. **Bohan**, one of my best neighbors, thank you so much for all your help. **Lenny** and **Miaoying**, thank you for the never-ending support, for being there listening to all my troubles and for sharing yours with me, for helping me to be a better person, and for understanding me without being judgmental. Thank you, I know I don't say it enough, but I do appreciate your help and support.

Lei and Jiaqi, thank you so much for willing to be my paronymphs. **Lei**, although I always call you "brother Lei" (磊哥), to be honest, you are the sweetest girl that I have ever met :), thank you for your endless support, being so thoughtful and trying so hard to feed me with different types of nice foods, it is so nice to have you around, toast to our friendship! **Jiaqi**, I had fun talking with you, although we only got to know each other for several months. You are such a pure and humble girl, and I am so grateful for your help. I hope you can keep calm and enjoy your PhD journey!

To my friends **Liyan, Mia, Qiao, Lei**, thank you for being my friend. I'm really glad you girls

are present in my life, we laugh, gossip, make fun of each other, no matter where we are. My friends, best wishes to you! (朋友们, 样样好!) **Laoyanyan** there were so many silly things that happened between us, when I think about it, I cannot stop laughing. Thank you for always taking me in just like I'm part of your family, thank you for visiting my parents when I'm not around, thank you for always checking on me when you sense my sadness, thank you for helping me to design the cover of my PhD thesis, thank you I know you know how grateful I am, thank you for being my BFF. **Yueyue** and **Yingzi**, we came to NL together for our master study, I still remember that day, we said bye to our parents and friend, we hold each other's hands, started our new journey. **Yueyue**, thank you for being such a good friend, someone I can always talk with, no matter if I'm sad, happy, anxious... hahaha, but I have to say, you always bring a lot of fun to me, unexpectedly. I'm just glad I have you with me the whole way. **Yingzi**, thank you for standing by me through good and bad. Thank you for being someone who knows me better than I know myself. Sometimes, we fought over the smallest things, but with you, I can just be me. Nothing I can say, but just thanks, I hope we will always be there for each other's journey. To my lovely sister **Siying**, everyone was surprised when they knew we met each other on the plane. Life is mysterious. I truly appreciated that I could have a young sister like you, an independent, thoughtful, cute girl. Thank you for always standing by my side no matter what, you make me realize what does sister means.

Finally, I heartfelt thanks to my family for motivating me to go further. **Xiao Feng** and **Lao Zhao**, I find myself is so lucky to have you as my parents and friends, someone who can guide me, listen to me, support me, encourage me along the way. Because of you, I can grow without any worry, because of you, I can fight for my own life bravely. Xiao Feng and Lao Zhao, I love you! My best parents! Although it is a pity that you cannot attend my defense in the Aula due to COVID-19, I know you will be with me online, please share the Dr title with me. My lovely **grandmother Huang**, thank you for always thinking of me, no matter how hard I tried to prove to you that I have a good life, you always worried about me. I am the luckiest to have you in my life. My lovely **grandmother Chen**, you have witnessed the start and the end of every different stage of my life, high school, college, Master of Science.... I really appreciate your unreserved support, care and love! And my **grandfather Zhao** and **grandfather Feng**, you have always been there to guide me grow up, thank you! My lovely **granduncle**, thank you very much for your pertinent advice. In the end, I would like to thank all my **family members** (aunt Feng, uncle Yongmin, uncle Feng, aunt Zhu, my cousin...) I love you all! (小冯, 老赵, 我爱你们! 我最棒的老爸老妈! 虽然这次很遗憾因为疫情没办法让你们来荷兰参加

Acknowledgements

我的毕业答辩，但是我知道您们一定会为我加油，等我拿到博士称号，分您们一半可好～哈哈！我亲爱的奶奶，谢谢您总是挂念我。虽然无论我怎么绞尽脑汁想向您证明我过的很好，您都总觉得我一个人外面一定吃不饱穿不暖。不过您的担忧总让我觉得我真的是一个很幸福很幸运的人。还有我可爱的外婆，我坚强有力的后盾，您见证了我每一个不同人生阶段的开始与结束，高中，大学，硕士....我真的很感谢您对我毫无保留的支持，关心和爱护，比心！还有我的外公和爷爷，有您们陪着我成长真好！我最敬爱的二公公，非常感谢您在我面临人生的重要选择的时候总是给予我最中肯的建议。最后的最后，感谢我所有家人（二孃，永敏叔叔，三舅，小祝孃，老龙，老师，姨妈.....）我爱你们！)

About the author

Shensheng Zhao was born on August 24, 1992 in Puer city, Yunnan province, China. She studied biotechnology at Shanghai Ocean University, China for four years. After obtaining her bachelor's degree in 2015, she continued to pursue a master's degree in food safety at Wageningen University & Research in the Netherlands. In her second year of master, she did her thesis at the Division of Toxicology at Wageningen University & Research and her internship at the National Institute for Public Health and Environment (RIVM). In 2017, Shensheng started her PhD at the Division of Toxicology



at Wageningen University & Research under the supervision of Ivonne M.C.M. Rietjens and Marije Strikwold with the financial support of the Chinese Scholarship Council (CSC). During her PhD, she followed a postgraduate education in Toxicology, which enables her to register as a European Toxicologist.

List of publications

Zhao, S., Kamelia, L., Boonpawa, R., Wesseling, S., Spenkelink, B., & Rietjens, I.M.C.M. (2019). Physiologically based kinetic modeling-facilitated reverse dosimetry to predict in vivo red blood cell acetylcholinesterase inhibition following exposure to chlorpyrifos in the Caucasian and Chinese population. *Toxicological sciences*, 171(1), 69-83.

Omwenga, I., Zhao, S., Kanja, L., Mol, H., Rietjens, I.M.C.M. & Louisse, J. (2021). Prediction of dose-dependent in vivo acetylcholinesterase inhibition by profenofos in rats and humans using physiologically based kinetic (PBK) modeling-facilitated reverse dosimetry. *Archives of toxicology*, 95(4), 1287-1301.

Zhao, S., Wesseling, S., Spenkelink, B., & Rietjens, I.M.C.M. (2021). Physiologically based kinetic modelling based prediction of in vivo rat and human acetylcholinesterase (AChE) inhibition upon exposure to diazinon. *Archives of Toxicology*, 95(5), 1573-1593.

Zhao, S., Wesseling, S., Spenkelink, B., Rietjens, I.M.C.M. & Strikwold M. Inter-individual variation in chlorpyrifos toxicokinetics characterized by physiologically based kinetic (PBK) and Monte Carlo simulation comparing human liver microsome and SupersomeTM cytochromes P450 (CYP)-specific kinetic data as model input. (in preparation)

Overview of completed training activities

Discipline specific activities

Molecular toxicology	PET	2018
Cell Toxicology	PET	2019
Pathobiology	PET	2019
Organ Toxicology	PET	2020
Laboratory of animal science	PET	2019
Epidemiology	PET	2018
Immunotoxicology	PET	2018
Mutagenesis and Carcinogenesis	PET	2019

Conferences

55th congress of the European Societies of Toxicology (EUROTOX), Helsinki, Finland, poster, 2019

General courses

VLAG PhD week	WUR	2018
The essentials of scientific writing and presenting	WUR	2018
Philosophy and ethics of food science and technology	WUR	2019
Brain training	WUR	2018
Introduction to R	WUR	2019
Applied statistic	WUR	2020

Other activities

Preparation of research proposal	TOX-WUR	2017
PhD trip to Japan	TOX-WUR	2018
Environmental toxicology	TOX-WUR	2018
General toxicology	TOX-WUR	2018
Scientific presentation at Division of Toxicology	TOX-WUR	2017-2021

Approved by the graduate school VLAG

The research described in this thesis was financially supported by China Scholarship Council (No. 201707720063 to ZHAO SHENSHENG)

Financial support from Wageningen University for printing this thesis is gratefully appreciated.

Cover design by Shensheng Zhao, Yan Zhang.

Printed by ProefschriftMaken || proefschriftmaken.nl

